NUWC-NPT Technical Report 11,369
14 May 2002

Extremely Low Frequency (ELF) Propagation Formulas for Dipole Sources Radiating in a Spherical Earth-Ionosphere Waveguide

John P. Casey
Submarine Electromagnetic Systems Department

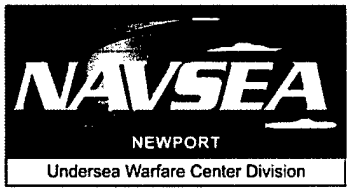

Naval Undersea Warfare Center Division
Newport, Rhode Island

PREFACE

This work was conducted in support of the "ELF Communications Program," program manager Robert J. Aiksnoras (Code 3491). The sponsoring activity is the Space and Naval Warfare Systems Command, Acquisition Program Manager for Strategic Systems, Paul Singer (PMW 173-2).

The technical reviewers for this report were Thomas A. Wettergren (Code 2002) and Peter R. Bannister of Sebastian, FL. The author is grateful to these reviewers for their helpful comments and suggestions.

Reviewed and Approved: 14 May 2002

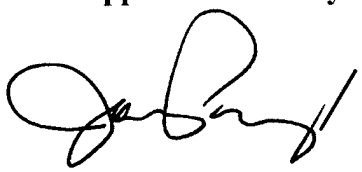

Peter M. Trask
Head, Submarine Electromagnetic Systems Department

REPORT DOCUMENTATION PAGE

Form Approved
OMB No. 0704-0188

1. AGENCY USE ONLY *(Leave blank)*	2. REPORT DATE	3. REPORT TYPE AND DATES COVERED
	14 May 2002	

4. TITLE AND SUBTITLE

Extremely Low Frequency (ELF) Propagation Formulas for Dipole Sources Radiating in a Spherical Earth-Ionosphere Waveguide

5. FUNDING NUMBERS

6. AUTHOR(S)

John P. Casey

7. PERFORMING ORGANIZATION NAME(S) AND ADDRESS(ES)

Naval Undersea Warfare Center Division
1176 Howell Street
Newport, RI 02841-1708

8. PERFORMING ORGANIZATION REPORT NUMBER

TR 11,369

9. SPONSORING/MONITORING AGENCY NAME(S) AND ADDRESS(ES)

Space and Naval Warfare Systems Command (PMW 173)
4301 Pacific Highway (Bldg. OT-4)
San Diego, CA 92110-3127

10. SPONSORING/MONITORING AGENCY REPORT NUMBER

11. SUPPLEMENTARY NOTES

12a. DISTRIBUTION/AVAILABILITY STATEMENT

Approved for public release; distribution is unlimited.

12b. DISTRIBUTION CODE

13. ABSTRACT (Maximum 200 words)

Extremely low frequency (ELF) propagation formulas are derived for dipole sources radiating in a spherical earth-ionosphere waveguide. In these formulas, the earth and ionosphere boundaries are modeled as scalar surface impedances. The spherical waveguide formulas are applied to predict the electromagnetic fields produced by vertical and horizontal electric dipoles (located on the surface of the earth) at antipodal ranges for several frequencies and propagation conditions. These results are used to establish the maximum ranges of validity of ELF propagation formulas that are based on the earth-flattening approximation. Numerous derivations are given in the appendices.

14. SUBJECT TERMS

Electromagnetics Extremely Low Frequency Earth-Ionosphere Waveguide

15. NUMBER OF PAGES

186

16. PRICE CODE

17. SECURITY CLASSIFICATION OF REPORT	18. SECURITY CLASSIFICATION OF THIS PAGE	19. SECURITY CLASSIFICATION OF ABSTRACT	20. LIMITATION OF ABSTRACT
Unclassified	Unclassified	Unclassified	SAR

TABLE OF CONTENTS

TABLE OF CONTENTS (Cont'd)

LIST OF ILLUSTRATIONS (Cont'd)

LIST OF ILLUSTRATIONS (Cont'd)

LIST OF ILLUSTRATIONS (Cont'd)

LIST OF TABLES

LIST OF TABLES (Cont'd)

EXTREMELY LOW FREQUENCY (ELF) PROPAGATION FORMULAS FOR DIPOLE SOURCES RADIATING IN A SPHERICAL EARTH-IONOSPHERE WAVEGUIDE

1. INTRODUCTION

Extremely low frequency (ELF) propagation formulas for dipole sources radiating in a spherical earth-ionosphere waveguide (figure 1-1) have been derived by various authors. Developments of such formulas are provided in the texts written by J. R. Wait (reference 1) and J. Galejs (reference 2). These spherical waveguide formulas have been derived for a uniform earth and ionosphere and, depending on the field component, have a range dependence characterized by either the Legendre function of the first kind of complex degree and order zero or one of its first two derivatives. In the ELF band (defined here as 30 to 300 Hz), because the ionospheric reflection height is less than one-half of a free-space wavelength, the only propagating mode in the earth-ionosphere waveguide is the zeroth-order transverse magnetic (TM) mode, which is commonly referred to as the quasi-transverse electromagnetic (quasi-TEM) mode.

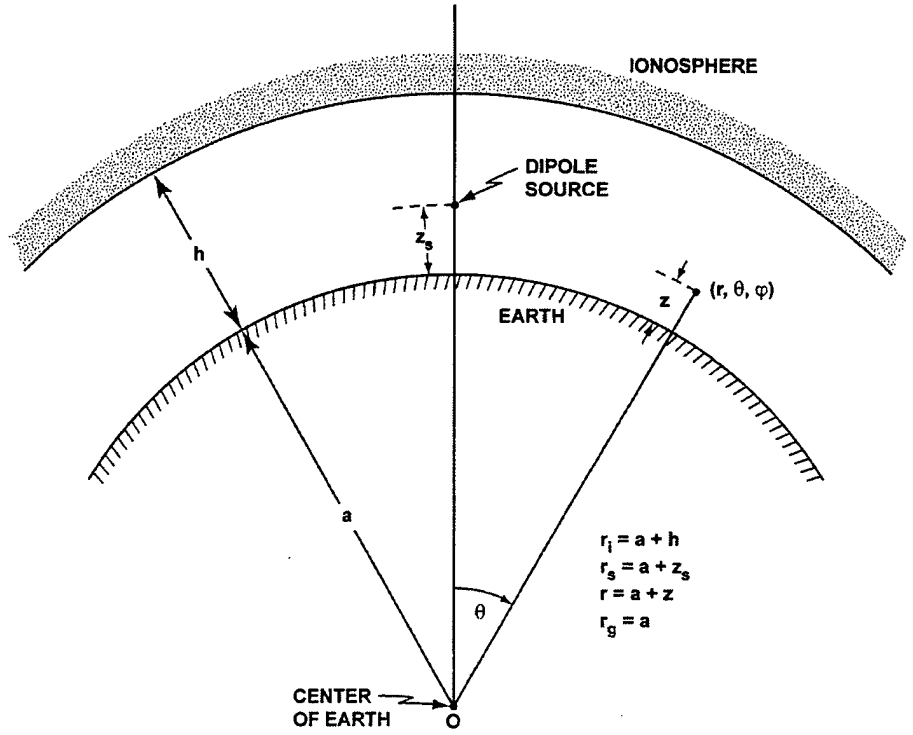

Figure 1-1. Spherical Coordinate System Description of the Earth-Ionosphere Waveguide

To predict the fields more accurately at ranges closer to the source or to account for more complicated boundary conditions, various investigators have incorporated the earth-flattening approximation into their ELF propagation formulas. In this approximation, the Legendre function range dependence is approximated by the product of a Hankel function and a curvature correction term (spherical earth spreading factor). As a result, the fields are derived from a planar earth-ionosphere waveguide model and then multiplied by the curvature correction term. For example, Bannister (reference 3) has derived ELF propagation formulas based on the earth-flattening approximation that extend the results of Wait and Galejs to closer ranges from the source. Whereas the spherical waveguide formulas given by Wait and Galejs are valid for ranges greater than approximately three ionospheric reflection heights from the source, Bannister's formulas are valid in the quasi-nearfield range, which is defined as the range where the measurement distance is greater than an earth wavelength, but much less than a free-space wavelength. However, Bannister's approximate formulas are not valid at field points close to the antipode where the simple spherical focusing factor fails.

To account for the anisotropic surface impedance in the vicinity of a horizontal electric dipole (HED) at ELF, Wolkoff and Kraimer (references 4 and 5) have listed propagation formulas that are modifications of Bannister's HED formulas. Wolkoff and Kraimer's formulas account for the anisotropic ground through the use of two complex-valued antenna pattern factors. These antenna pattern factors are unique for a given HED and must be determined from near-field measurements of the antenna. Wolkoff and Kraimer have determined the antenna pattern factors for each of the U.S. Navy's ELF transmitting antennas (reference 4). Wolkoff and Kraimer's propagation formulas have been formally derived from Bannister's formulas by Casey (reference 6) through use of the reciprocity theorem.

For prediction of the ELF fields from dipole sources at antipodal ranges, propagation formulas that are valid out to approximately 20 Mm from the source must be applied. In a recent report (reference 7), approximate formulas for a HED source that contain the proper range dependence at antipodal ranges in a spherical earth-ionosphere waveguide, referred to as "antipode-centered propagation formulas," were derived. These HED formulas are based on Burrow's simple parallel-plate waveguide approximation of the earth-ionosphere waveguide (reference 8) and include a curvature correction factor. In reference 7, the antipode-centered propagation formulas were compared with Bannister's HED formulas (direct and indirect great-

circle path fields were combined) under various propagation conditions, where both the source and field points are located on the earth's surface. The results showed that Bannister's vertical electric field and radial magnetic field formulas (magnitude only) agree to within 1 dB of the corresponding antipode-centered formulas for ranges greater than 0.97 Mm to 1.13 Mm from the antipode, depending on the propagation conditions. In addition, Bannister's azimuthal magnetic field formula agrees to within 1 dB of the corresponding antipode-centered formula for ranges greater than 3.17 Mm to 3.72 Mm from the antipode, depending on the propagation conditions.

In this report, ELF propagation formulas for dipole sources radiating in a spherical earth-ionosphere waveguide are derived from first principles. These derivations are presented because the developments given by previous authors were found to be difficult to follow. The formulas derived here are based on the assumptions of a homogeneous, isotropic earth and a homogeneous, isotropic ionosphere of constant reflection height. As a result, the earth and ionosphere boundaries are modeled as scalar surface impedances. The spherical waveguide formulas are expressed in terms of series expansions of TM and transverse electric (TE) modes. However, at ELF, the only mode of practical interest is the quasi-TEM mode. The computed results for the spherical waveguide formulas presented in this report are based on an exact hypergeometric series representation of the Legendre function of the first kind. The propagation formulas for a horizontal magnetic dipole (HMD) can be derived from the HED formulas through application of the duality principle (reference 2).

In addition, in this report, through appropriate approximations of the range dependence, it will be shown how the spherical waveguide formulas (for both vertical electric dipole (VED) and HED sources) can reduce to Bannister's formulas or to the antipode-centered formulas. It will also be shown how the quasi-TEM spherical waveguide formulas derived for a HED located at the surface of the earth can be modified to account for the anisotropic surface impedance in the vicinity of the antenna. These modified spherical waveguide formulas will include Wolkoff and Kraimer's antenna pattern factors and will be useful for prediction of the electromagnetic (EM) fields radiated by the U. S. Navy's four transmitting antennas at antipodal ranges. Detailed derivations of approximate formulas for the Legendre function range dependence are given in the appendices. Comparisons of the spherical waveguide propagation formulas with both Bannister's direct great-circle path and total field (direct plus indirect great-circle paths) formulas are presented for the surface magnetic field and vertical electric field components under various propagation conditions. The field comparisons are presented at several frequencies for

both VED and HED sources at ranges that extend from 1 Mm from the source to the antipode, where both the source and field points are located at the earth's surface. These comparisons will help to more accurately establish the maximum ranges over which Bannister's approximate formulas are valid.

2. APPLICATION OF PARALLEL-PLATE WAVEGUIDE MODEL FOR DETERMINATION OF APPROXIMATE MODE CUTOFF FREQUENCIES

To obtain a basic understanding of EM propagation in a spherical earth-ionosphere waveguide in the ELF band, it is helpful to formulate the problem under the assumption of planar boundaries. Such an approach has been applied by Burrows (reference 8) and Budden (reference 9). In the ELF band, both the earth and ionosphere appear as nearly perfect conductors (references 2 and 8). Therefore, in this section, the TEM, TM, and TE modes are derived for a parallel-plate waveguide with perfectly conducting walls.

The analysis of this section will show that, because the ionospheric reflection height is much less than a free-space wavelength at ELF, the TEM mode is the only propagating mode. The TEM mode is characterized by electric and magnetic fields that are oriented perpendicular to the direction of propagation. If the finite conductivity of the earth and ionosphere are considered, the TEM mode configuration is perturbed to the quasi-TEM mode. The quasi-TEM mode includes surface electric- and magnetic-field components that lie along the direction of propagation. Therefore, the quasi-TEM mode is the only mode of practical concern at ELF. The cutoff frequencies for the dominant TE and TM modes are given for several representative ionospheric reflection heights. The propagation formulas for dipole sources radiating in a parallel-plate waveguide with finitely conducting boundaries have been derived by Burrows (reference 8) and will not be presented in this report.

2.1 TEM AND TM MODES

Consider the parallel-plate waveguide model of the earth-ionosphere waveguide, as shown in figure 2-1. In this model, the z-direction is normal to the planar boundaries and the x-direction denotes the direction of propagation. Because the parallel-plate waveguide is a two-dimensional model, it is assumed that there is no variation along the y-direction, i.e., $?/?y = 0$ for all field components. For simplicity, the earth and ionosphere are both assumed to be perfectly conducting.

Appendix A provides a derivation of the EM fields in terms of potentials. These formulas are based on an assumed time-harmonic dependence of $e^{j\omega t}$, where $\omega = 2\pi f$ is the angular frequency (rad/s), f is the frequency in Hertz (Hz), and $j = \sqrt{-1}$. A time-harmonic dependence will be assumed in each of the field expressions presented in this report.

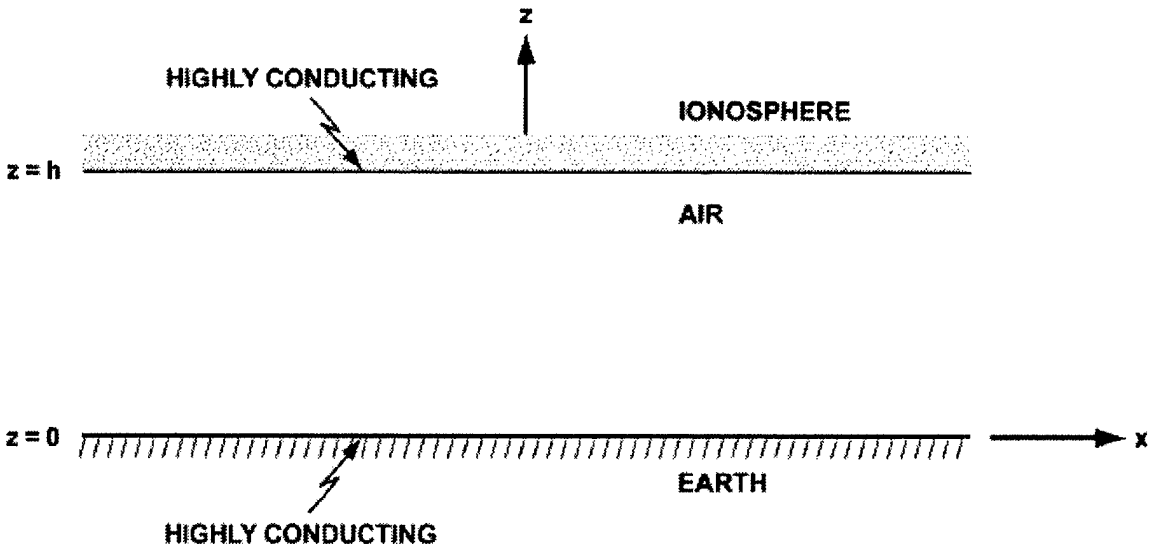

Figure 2-1. Parallel-Plate Model of the Earth-Ionosphere Waveguide

In this section, the TEM and TM modes (with respect to the z-direction) are derived in terms of the z component of the electric Hertz potential π_z^e; and the TE modes (with respect to the z-direction) are derived in terms of the z component of the magnetic Hertz potential π_z^h. The z component of each potential is chosen in order to generate modes that will correspond with the spherical waveguide modes that are derived in appendix C.

To derive the TEM and TM modes in the parallel-plate waveguide, consider the electric Hertz potential $\boldsymbol{\pi}^e$ that is given as

$$\boldsymbol{\pi}^e = \hat{z}\, \pi_z^e(x,z) \ , \tag{2-1}$$

where $\hat{z}$ denotes the unit vector along the z-direction. The electric Hertz vector is defined in terms of the magnetic vector potential $\boldsymbol{A}$ in appendix A, expression (A-26a). The substitution of this definition into the inhomogeneous vector Helmholtz equation for the magnetic vector potential (A-6) yields

$$\nabla \times \nabla \times \boldsymbol{\pi}^e - k_o^2 \boldsymbol{\pi}^e = -\nabla \Phi^e + \frac{1}{j\omega\varepsilon_o} \boldsymbol{J} \ , \tag{2-2}$$

where $k_o = \omega\sqrt{\mu_o \varepsilon_o}$ is the wave number in free space, μ_0 and ε_0 are the permeability and permittivity, respectively, of free space, Φ^e is the electric scalar potential, and $\boldsymbol{J}$ is the electric current density. Note that expression (2-2) applies to a point lying in free space.

To eliminate Φ^e from the above equation, the Lorentz gauge condition (reference 10) is applied, i.e.,

$$\nabla \cdot \boldsymbol{\pi}^e + \Phi^e = 0 \ . \tag{2-3}$$

The substitution of expression (2-3) into (2-2) yields

$$\nabla^2 \boldsymbol{\pi}^e + k_o^2 \boldsymbol{\pi}^e = -\frac{1}{j\omega\varepsilon_o} \boldsymbol{J} . \tag{2-4}$$

To derive the TEM and TM modes, it is assumed that there are no sources so that $\boldsymbol{J} = 0$ in formula (2-4). The following is obtained if expression (2-1) is substituted into equation (2-4):

$$\frac{\partial^2 \pi_z^e}{\partial x^2} + \frac{\partial^2 \pi_z^e}{\partial z^2} + k_o^2 \pi_z^e = 0 \ . \tag{2-5}$$

Because the modes are assumed to propagate along the x-direction in the waveguide, π_z^e can be expressed as

$$\pi_z^e(x,z) = f(z)\, e^{-jkx} \ , \tag{2-6}$$

where k is the wave number (along the direction of propagation) and $f(z)$ is a function to be determined. The substitution of expression (2-6) into (2-5) yields

$$f''(z) + k_c^2 f(z) = 0 , \tag{2-7}$$

where

$$k_c^2 \equiv k_o^2 - k^2 \ . \tag{2-8}$$

In the above formula, k_c is commonly referred to as the cutoff wave number (reference 10).

Expressions for the EM fields in terms of the electric- and magnetic-Hertz vectors are given in formulas (A-27) and (A-28). For the TEM and TM modes, the magnetic-Hertz vector $\boldsymbol{\pi}^h$ is zero. Therefore, the substitution of equation (2-1) into the EM field formulas (A-27) and (A-28) yields the following:

$$E_x = -jk \frac{\partial \pi_z^e}{\partial z} \ , \tag{2-9a}$$

$$E_z = k^2 \pi_z^e \ , \tag{2-9b}$$

and

$$H_y = -\omega\varepsilon_o k \pi_z^e \cdot \tag{2-9c}$$

Note that the x variation defined in expression (2-6) has been accounted for in the above field formulas. The field components listed above are the only nonzero components. Also, note that because the TM modes are "transverse magnetic" with respect to the z-direction, $H_z = 0$.

The solution of the differential equation (2-7) is given as

$$f(z) = c_1 \cos k_c z + c_2 \sin k_c z \ , \tag{2-10}$$

where c_1 and c_2 are arbitrary constants. To determine c_1 and c_2, the boundary conditions at the surfaces of the earth and ionosphere must be applied. Because the earth and ionosphere are assumed to be perfectly conducting, the following boundary conditions apply:

$$E_x(x,0) = 0, \ z = 0, h \ . \tag{2-11}$$

The substitutions of expressions (2-9a) and (2-6) into the boundary conditions above yields

$$f'(0) = f'(h) = 0 \ . \tag{2-12}$$

From formula (2-10), $f'(z)$ is given as

$$f'(z) = -k_c c_1 \sin k_c z + k_c c_2 \cos k_c z \ . \tag{2-13}$$

The application of the boundary condition for f' at $z = 0$ to formula (2-13) gives

$$k_c c_2 = 0 \ . \tag{2-14}$$

Therefore, the solutions of the above equation are $k_c = 0$ or $c_2 = 0$. If $c_2 = 0$, then the boundary condition $f'(h) = 0$ results in

$$k_{cn} = \frac{n\pi}{h} \ , \ n = 0, 1, 2, \ldots \ . \tag{2-15}$$

The index n in the above formula denotes the mode index.

The substitution of the above result for $f(z)$ into expression (2-6) for π_z^e yields

$$\pi_{zn}^e(x,z) = c_1 \cos\left(\frac{n\pi z}{h}\right) e^{-jkx} \ , \ n = 0, 1, 2, \ldots , \tag{2-16}$$

where k is given from formulas (2-8) and (2-15) as

$$k^2 = k_o^2 - \left(\frac{n\pi}{h}\right)^2, \quad n = 0, 1, 2, \ldots . \tag{2-17}$$

A mode is said to be at cutoff when $k = 0$ or equivalently, when $k_c = k_o$. The cutoff wave numbers for the TEM ($n = 0$) and TM modes ($n = 1, 2, \ldots$) are given in formula (2-15). Therefore, the cutoff frequencies for these modes are given by

$$f_{cn} = \frac{c}{2\pi} k_{cn} = \frac{nc}{2h}, \quad n = 0, 1, 2, \ldots , \tag{2-18}$$

where c denotes the speed of light in free space. Table 2-1 lists the cutoff frequencies for the dominant modes in the parallel-plate waveguide as computed from expression (2-18) for several representative ionospheric reflection heights. The table indicates that the TEM mode propagates at all frequencies while the TM_1 mode does not propagate for frequencies below 1.67 kHz. Because the frequency range of interest here lies below 300 Hz, the TM modes are of no concern.

Table 2-1. Cutoff Frequencies for TEM, TM_1, and TM_2 Modes for a Parallel-Plate Waveguide with Perfect Electrically Conducting Boundaries for Several Waveguide Heights

h (km)	f_{c0} (Hz)	f_{c1} (kHz)	f_{c2} (kHz)
50	0	3.00	6.00
75	0	2.00	4.00
90	0	1.67	3.33

The TEM and TM fields are determined through the substitution of expression (2-16) into formulas (2-9) to give the following:

$$E_{xn} = \frac{jn\pi k}{h} \sin\left(\frac{n\pi z}{h}\right) e^{-jkx}, \quad n = 1, 2, 3, \ldots , \tag{2-19a}$$

$$E_{zn} = k^2 \cos\left(\frac{n\pi z}{h}\right) e^{-jkx}, \quad n = 0, 1, 2, \ldots , \tag{2-19b}$$

and

$$H_{yn} = -\omega\varepsilon_o \cos\left(\frac{n\pi z}{h}\right) e^{-jkx}, \quad n = 0, 1, 2, \ldots . \tag{2-19c}$$

In formulas (2-19), note that the arbitrary constant has been suppressed. It should be noted that E_x vanishes for the TEM mode ($n = 0$). This is consistent with the fact that the TEM mode has no field component along the direction of propagation (reference 10). However, for a finitely conducting boundary, E_x does not vanish but is related to the surface magnetic field H_y through the surface impedance of the boundary surface. For example, for a finitely conducting earth with surface impedance η_e, E_x is related to H_y at z = 0 as $E_x = -\eta_e H_y$.

2.2 TE MODES

The derivation of the TE modes in the parallel-plate waveguide are very similar to the derivation of the TM modes. Consider the magnetic Hertz potential $\boldsymbol{\pi}^h$ that is given as

$$\boldsymbol{\pi}^h = \hat{z}\, \pi_z^h(x,z) \ . \tag{2-20}$$

The magnetic Hertz vector is defined in terms of the electric vector potential $\boldsymbol{F}$ in expression (A-26b). The substitution of this definition into the inhomogeneous vector Helmholtz equation for the electric vector potential (A-11) yields

$$\nabla \times \nabla \times \boldsymbol{\pi}^h - k_o^2 \boldsymbol{\pi}^h = -\nabla \Phi^h + \frac{1}{j\omega\mu_o} \boldsymbol{M} , \tag{2-21}$$

where Φ^h is the magnetic scalar potential and $\boldsymbol{M}$ is the magnetic current density. It should be noted that expression (2-21) applies to a point in free space.

To eliminate Φ^h from the above equation, the Lorentz gauge condition (reference 10) is applied, i.e.,

$$\nabla \cdot \boldsymbol{\pi}^h + \Phi^h = 0 \ . \tag{2-22}$$

The substitution of expression (2-22) into (2-21) yields

$$\nabla^2 \boldsymbol{\pi}^h + k_o^2 \boldsymbol{\pi}^h = -\frac{1}{j\omega\mu_o} \boldsymbol{M} \ . \tag{2-23}$$

To derive the TE modes, it is assumed that there are no sources so that $\boldsymbol{M} = 0$ in the above formula. If expression (2-20) is substituted into equation (2-23), the following expression is obtained:

$$\frac{\partial^2 \pi_z^h}{\partial x^2} + \frac{\partial^2 \pi_z^h}{\partial z^2} + k_o^2 \pi_z^h = 0 \ . \tag{2-24}$$

Because the modes are assumed to propagate along the x-direction in the waveguide, π_z^h can be expressed as

$$\boldsymbol{\pi^h} = \hat{\boldsymbol{z}}\, \pi^h(x,z) = \hat{\boldsymbol{z}}\, g(z)\, e^{-jkx}, \tag{2-25}$$

where $g(z)$ is a function to be determined. The substitution of expression (2-25) into (2-24) yields

$$g''(z) + k_c^2 g(z) = 0 \ , \tag{2-26}$$

where the cutoff wave number k_c is defined in formula (2-8).

The TE mode EM fields can be obtained through the substitution of expression (2-20) into formulas (A-27) and (A-28) with the electric Hertz vector $\boldsymbol{\pi^e}$ set to zero to yield the following:

$$E_y = \omega \mu_o k \pi_z^h \ , \tag{2-27a}$$

$$H_x = -jk \frac{\partial \pi_z^h}{\partial z}, \tag{2-27b}$$

and

$$H_z = k^2 \pi_z^h \ . \tag{2-27c}$$

Note that the x variation defined in expression (2-25) has been accounted for in the above field formulas. The field components listed above are the only the nonzero components. Also, note that because the TE modes are transverse electric with respect to the z-direction, we have $E_z = 0$.

The solution of the differential equation (2-26) is given as

$$g(z) = c_3 \cos k_c z + c_4 \sin k_c z \ , \tag{2-28}$$

where c_3 and c_4 are arbitrary constants. To determine c_3 and c_4, the boundary conditions at the surfaces of the earth and ionosphere must be applied. Because the earth and ionosphere are assumed to be perfectly conducting, the following boundary conditions exist:

$$E_y(x,0) = 0, \ z = 0, h \ . \tag{2-29}$$

The substitutions of expressions (2-27a) and (2-25) into the boundary conditions above yields

$$g(0) = g(h) = 0 \cdot \tag{2-30}$$

The substitution of the boundary conditions (2-30) into expression (2-28) results in the following solution:

$$g_m(z) = c_4 \sin\left(\frac{m\pi z}{h}\right), m = 1, 2, 3, \ldots . \tag{2-31}$$

A comparison of formulas (2-28) and (2-31) shows that the cutoff wave number k_{cm} for the *mth* TE mode is given as

$$k_{cm} = \frac{m\pi}{h}, \ m = 1, 2, 3, \ldots \cdot \tag{2-32}$$

The substitution of the above result for $g_m(z)$ into formula (2-25) for π_z^h followed by another substitution into the TE field expressions (2-27) yields

$$E_{ym} = \omega\mu_o k \sin\left(\frac{m\pi z}{h}\right) e^{-jkx}, \ m = 1, 2, 3, \ldots, \tag{2-33a}$$

$$H_{xm} = -\frac{jkm\pi}{h} \cos\left(\frac{m\pi z}{h}\right) e^{-jkx}, \ m = 1, 2, 3, \ldots, \tag{2-33b}$$

and

$$H_{zm} = k^2 \sin\left(\frac{m\pi z}{h}\right) e^{-jkx}, \ m = 1, 2, 3, \ldots, \tag{2-33c}$$

where the wave number k is given from formulas (2-8) and (2-32) as

$$k^2 = k_o^2 - \left(\frac{m\pi}{h}\right)^2, \ m = 1,2,3, \ldots . \tag{2-34}$$

The cutoff frequencies for the TE modes are given by

$$f_{cm} = \frac{c}{2\pi} k_{cm} = \frac{mc}{2h}, \ m = 1, 2, 3, \ldots . \tag{2-35}$$

A comparison of formula (2-18) with (2-35) indicates that the cutoff frequencies of the TM_n and TE_m modes are the same provided $n = m$. Therefore, the cutoff frequencies for the TE_1 and TE_2 are the same as those of the TM_1 and TM_2 modes, respectively, given in table 2-1. Thus, because the frequency range of interest here lies below 300 Hz, the TE modes are also of no concern in this report.

3. ELF PROPAGATION FORMULAS BASED ON THE EARTH-FLATTENING APPROXIMATION

To reduce the mathematical complexities associated with the problem of the propagation of radio waves over a spherical earth, Pryce (reference 11) introduced the earth-flattening approximation in which the problem reduces to the propagation over a planar earth with an atmosphere having a modified refractive index. In his investigation of the accuracy of the earth-flattening approximation, Pekeris (reference 12) assumed that the range-dependence function can be expanded in an asymptotic series involving increasing negative powers of the earth's radius. In Pekeris' asymptotic series (for the range dependence), the first term corresponds to the model of a flat earth and the succeeding terms are corrections for curvature. Koo and Katzin (reference 13) extended the work of Pryce and Pekeris to obtain exact differential equations for the spherical geometry in terms of equations of planar earth type, resulting in solutions that are applicable for arbitrary ranges and heights. Wait (reference 1) has applied the earth-flattening approximation to obtain an approximate range dependence in the ELF band.

In this section, the earth-flattening approximation as applied to the range dependence of the fields is presented. Bannister's ELF propagation formulas, which incorporate the earth-flattening approximation, are presented for VED and HED antennas located on the surface of the earth. In addition, Wolkoff and Kraimer's HED propagation formulas, which are modifications of Bannister's formulas to account for the anisotropic surface impedance in the vicinity of the source, are also presented. For each set of formulas presented in this section, both the direct and indirect great-circle path fields are given because both fields must be combined in order to predict the propagation at antipodal ranges. In section 5 of this report, Bannister's formulas are compared with the spherical waveguide formulas to determine the maximum ranges of validity of Bannister's formulas.

3.1 EARTH-FLATTENING APPROXIMATION TO THE LEGENDRE FUNCTION OF THE FIRST KIND

As shown in appendices F, G, and H, the range dependencies of the EM fields in the earth-ionosphere waveguide are expressed in terms of the Legendre function of the first kind, $P_\nu(-\cos\theta)$, or one of its first two derivatives. From appendix J, the complex degree ν of the Legendre function is related to the wave number k in the waveguide as

$$k \equiv \beta - j\alpha = \frac{\nu + 1/2}{a} , \tag{3-1}$$

where $\beta = 2\pi/\lambda$ and α are the phase and attenuation constants, respectively, and λ is the wavelength. It should be mentioned that k corresponds to the quasi-TEM mode, the only propagating mode in the spherical waveguide at ELF.

A mathematical development of the earth flattening approximation is given in appendix K. From expression (K-33), the Legendre function is approximated as

$$\frac{P_\nu(-\cos\theta)}{j\sin\nu\pi} \cong H_o^{(2)}(k\rho)\sqrt{\frac{\rho/a}{\sin\rho/a}}\ ,\ |\nu| \gg 1, |k\rho| \gg 1\ , \tag{3-2}$$

where $\rho = a\theta$ is the great-circle path distance along the earth from the source point to the field point and $H_o^{(2)}$ denotes the Hankel function of the second kind with order 0. In the above approximation, $H_o^{(2)}(k\rho)$ corresponds to the range dependence for a flat earth and the square-root term is the correction for curvature. Expression (3-2) is sometimes referred to as the earth-flattening approximation with curvature correction. It should be noted that expression (3-2) differs by a factor of j with the one given by Wait (reference 1). The propagation formulas presented in the remainder of this section each incorporate approximation (3-2).

3.2 BANNISTER'S FORMULAS

As mentioned in section 1, Bannister (reference 3) has derived ELF propagation formulas for dipole sources that incorporate the earth-flattening approximation. These formulas are valid in the quasi-near field range, which corresponds to measurement distances that are greater than an earth wavelength. Although only Bannister's formulas for VED and HED sources are presented here, the field expressions for an HMD source can be readily obtained from the HED formulas (reference 14) through replacement of the electric dipole moment p with $jk_e m$, where m is the current moment (current-area product) of the HMD, and k_e is the wave number in the earth. It should be added that the equivalent HMD is oriented perpendicular to the HED, i.e., a y-directed HMD is equivalent to an x-directed HED located on the surface of the earth, where the z direction points radially outward from the earth's surface.

It should be mentioned that Bannister's formulas presented here have been slightly modified in order to compute the phase as well as the magnitude of the field. The same formula modifications were used by Wolkoff and Kraimer (references 4 and 5) in their HED formulas.

3.2.1 VED

Consider a VED located on the earth's surface and oriented along the positive z direction in the coordinate system defined in figure 3-1. Under the assumption of a scalar earth conductivity σ_e, Bannister (reference 3) has derived propagation formulas that are valid at the earth's surface ($z = 0$) for ranges greater than an earth's wavelength (i.e., $\rho > \lambda_e$). These formulas are given as

$$E_z^d = \frac{j\eta_o p}{2\pi k_o \rho^3}\left[V_h(t)\, e^{-\alpha\rho} + j\frac{\pi}{2}\, G_h(u)\,(k\rho)^2\, H_0^{(2)}(k\rho)\right]\left[\frac{\rho/a}{\sin(\rho/a)}\right]^{1/2}, \tag{3-3a}$$

$$E_\rho^d = \frac{j\eta_e kp}{4\rho}\, G_h(u)\, H_1^{(2)}(k\rho)\left[\frac{\rho/a}{\sin(\rho/a)}\right]^{1/2}, \tag{3-3b}$$

and

$$H_\varphi^d = -\frac{jkp}{4\rho}\, G_h(u)\, H_1^{(2)}(k\rho)\left[\frac{\rho/a}{\sin(\rho/a)}\right]^{1/2}, \tag{3-3c}$$

where

$$G_h(u) = \frac{2u}{\pi}\coth(u) + \left(1 - \frac{2}{\pi}\right)u^2 \operatorname{csch}^2(u), \tag{3-4}$$

$$V_h(t) = t^3 \coth(t)\, \operatorname{csch}^2(t), \tag{3-5}$$

and

$p = I\,dl$ (electric dipole moment),

$k_o = \frac{\omega}{c} = \frac{2\pi}{\lambda_o}$ (wave number in free space),

$k = \frac{\omega}{v} - j\alpha$ (wave number in the earth-ionosphere waveguide),

$S = \frac{k}{k_o} = \frac{c}{v} - j\frac{\alpha}{k_o}$ (normalized wave number),

$\eta_e = \sqrt{\frac{j\omega\mu_o}{\sigma_e + j\omega\varepsilon_e}}$ (intrinsic impedance of the earth),

$u = \frac{\pi\rho}{2h}$,

and

$$t = \frac{u}{S^2} = \frac{\pi\rho}{2h}\left(\frac{k_o}{k}\right)^2 .$$

The superscript d in the field components refers to the direct great-circle path contribution. In the above formulas, I denotes the antenna current, dl is the effective length of the antenna, a is the radius of the earth, λ_o is the wavelength in free space, ε_e is the permittivity of the earth, v is the speed of propagation in the earth-ionosphere waveguide, α is the attenuation constant in Np/m, h is the ionospheric reflection height, and $\rho = a\theta$ is the direct great-circle path distance from the source to the field point. Note that a time-harmonic dependence of $e^{j\omega t}$ is assumed in expressions (3-3), where $\omega = 2\pi f$ is the angular frequency (rad/s), and f is the frequency in Hertz.

The functions G_h and V_h were included by Bannister to extend the range of the previous ELF formulas down to the quasi-nearfield range (i.e., $\rho > \lambda_e$ and $\rho \ll \lambda_o$). Therefore, for an earth conductivity $\sigma_e = 2 \times 10^{-4}$ S/m and frequency $f = 76$ Hz, Bannister's formulas are valid for ranges greater than 30 km from the source. Bannister has noted that for $u < 0.5$, $G_h(u) \cong 1$; for $t < 0.5$, $G_h(t) \cong V_h(t) \cong 1$; for $u > 2.5$, $G_h(u) \cong \frac{2u}{\pi} = \frac{\rho}{h}$; for $t > 4.5$, $V_h(t) \cong 0$. Note that the spherical earth spreading (curvature) factor $\left[(\rho/a) / \sin(\rho/a)\right]^{1/2}$ appears in each VED field component expression.

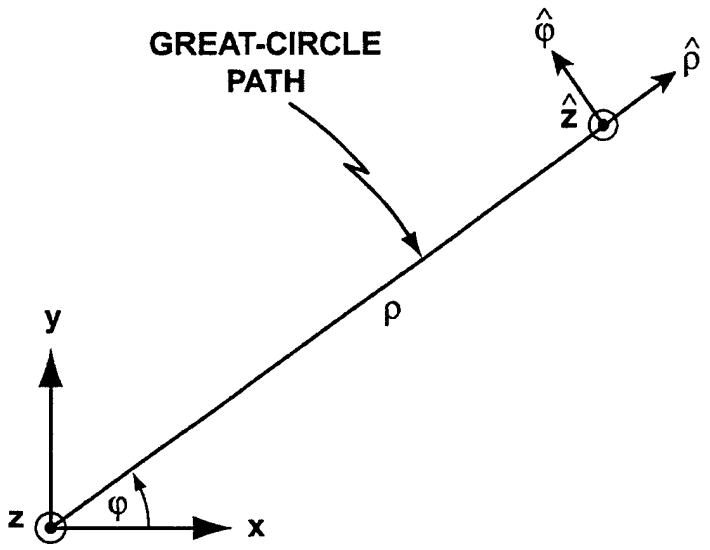

Figure 3-1. Coordinate System Used by Bannister (Reference 3)
(The VED and HED sources are each located at the origin with the VED oriented along the positive z-direction and the HED along the positive x-direction.)

The VED field expressions given above are associated with the fields that propagate along the direct great-circle path that connects the source and field points (figure 3-2). At antipodal ranges, the contribution from the indirect great-circle path field must be included in order to account for the interference produced by the two paths. The indirect great-circle path field components for the VED can be obtained from the direct great-circle path fields in equations (3-3) through replacement of the range ρ with the indirect great-circle path range $\rho_i = 2\pi a - \rho$ (figure 3-2) and with the inclusion of the appropriate phase shift as obtained from table J-1 in appendix J. As explained in appendix J, this added phase shift of $\pm j$ depends on the primary range dependence of the field and therefore varies with each field component. Therefore, the indirect great-circle path VED fields are given as follows:

$$E_z^i = -\frac{\eta_o p}{2\pi k_o \rho_i^3}\left[V_h(t_i)\, e^{-\alpha\rho_i} + j\,\frac{\pi}{2}\, G_h(u_i)\,(k\rho_i)^2\, H_0^{(2)}(k\rho_i)\right]\left[\frac{\rho_i / a}{\sin(\rho / a)}\right]^{1/2}, \tag{3-6a}$$

$$E_\rho^i = \frac{\eta_e kp}{4\rho_i}\, G_h(u_i)\, H_1^{(2)}(k\rho_i)\left[\frac{\rho_i / a}{\sin(\rho / a)}\right]^{1/2}, \tag{3-6b}$$

and

$$H_\varphi^i = -\frac{kp}{4\rho_i}\, G_h(u_i)\, H_1^{(2)}(k\rho_i)\left[\frac{\rho_i / a}{\sin(\rho / a)}\right]^{1/2}, \tag{3-6c}$$

where $u_i = \frac{\pi\rho_i}{2h}$ and $t_i = \frac{\pi\rho_i}{2h}\frac{1}{S^2}$. The superscript i in the field components refers to the indirect great-circle path contribution. For each component, the total field is obtained through addition of the direct and indirect great-circle path contributions, i.e.,

$$E_z = E_z^d + E_z^i, \tag{3-7a}$$

$$E_\rho = E_\rho^d + E_\rho^i, \tag{3-7b}$$

and

$$H_\varphi = H_\varphi^d + H_\varphi^i. \tag{3-7c}$$

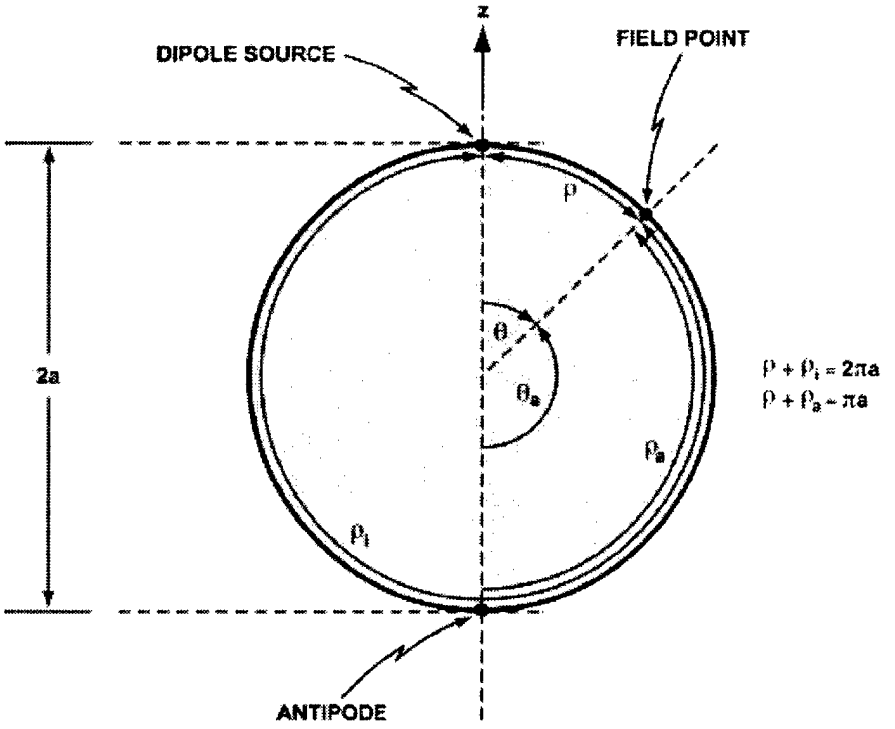

Figure 3-2. The Earth and the Two Great-Circle Paths to the Field Point

3.2.2 Horizontal Electric Dipole

Consider a HED located on the earth's surface and oriented along the positive x direction of the coordinate system defined in figure 3-1. Under the same assumptions given for the VED, the HED propagation formulas are given as follows:

$$E_z^d = \frac{-j\eta_e kp}{4\rho} G_h(u)\, H_1^{(2)}(k\rho) \left[\frac{\rho / a}{\sin(\rho / a)}\right]^{1/2} \cos\varphi \ , \tag{3-8a}$$

$$E_\rho^d = \frac{\eta_e^2 k^2 p G_h(t)}{4\omega\mu_o\rho} \left[H_0^{(2)}(k\rho) - \frac{1}{k\rho} H_1^{(2)}(k\rho)\right] \left[\frac{\rho / a}{\sin(\rho / a)}\right]^{1/2} \cos\varphi \ , \tag{3-8b}$$

$$E_\varphi^d = -\frac{\eta_e^2 kpH_h(t)}{4\omega\mu_o\rho^2} H_1^{(2)}(k\rho) \left[\frac{\rho / a}{\sin(\rho / a)}\right]^{3/2} \sin\varphi \ , \tag{3-8c}$$

$$H_\rho^d = -\frac{\eta_e kpH_h(t)}{4\omega\mu_o\rho^2} H_1^{(2)}(k\rho) \left[\frac{\rho / a}{\sin(\rho / a)}\right]^{3/2} \sin\varphi \ , \tag{3-8d}$$

and

$$H_{\varphi}^{d} = -\frac{\eta_e k^2 p G_h(t)}{4\omega\mu_o\rho}\left[H_0^{(2)}(k\rho) - \frac{1}{k\rho}H_1^{(2)}(k\rho)\right]\left[\frac{\rho/a}{\sin(\rho/a)}\right]^{1/2}\cos\varphi\ , \tag{3-8e}$$

where

$$H_h(t) = G_h(t) + V_h(t)\ . \tag{3-9}$$

Bannister has noted that for $t > 2.5$, $G_h(t) \cong \frac{2t}{\pi} = \frac{\rho}{h}\left(\frac{k_o}{k}\right)^2$ and for $t > 4.5$, $V_h(t) \cong 0$ and $H_h(t) \cong G_h(t) \cong \frac{2t}{\pi} = \frac{\rho}{h}\left(\frac{k_o}{k}\right)^2$. Note that the spherical earth spreading factor $\left[(\rho/a) / \sin(\rho/a)\right]^{1/2}$ appears in each HED field component expression along with an additional factor of $\left[(\rho/a) / \sin(\rho/a)\right]$ appearing in the E_{φ}^{d} and H_{ρ}^{d} formulas. This factor of $\left[(\rho/a) / \sin(\rho/a)\right]$ also appears in the corresponding HED spherical waveguide formulas derived in the appendix H. Note that the surface electric field components E_{ρ}^{d} and E_{φ}^{d} are related to the surface magnetic field components H_{φ}^{d} and H_{ρ}^{d}, respectively, through the impedance of the earth η_e.

As previously mentioned, at antipodal ranges, the contribution from the indirect great-circle path field must be included in order to predict the interference produced by the two paths. The indirect great-circle path field components for the HED can be obtained from the direct great-circle path fields in equations (3-8) through replacement of the range ρ with the indirect great-circle path range ρ_i and with the inclusion of the appropriate phase shift as obtained from table J-1 in appendix J. As mentioned earlier in this section, the added phase shift of $\pm j$ depends on the primary range dependence of the field and therefore varies with each field component. Thus, the indirect great-circle path HED fields are given as follows:

$$E_z^i = \frac{-\eta_e k p G_h(u_i)}{4\rho_i}H_1^{(2)}(k\rho_i)\left[\frac{\rho_i/a}{\sin(\rho/a)}\right]^{1/2}\cos\varphi\ , \tag{3-10a}$$

$$E_{\rho}^i = \frac{j\eta_e^2 k^2 p G_h(t_i)}{4\omega\mu_o\rho_i}\left[H_0^{(2)}(k\rho_i) - \frac{1}{k\rho_i}H_1^{(2)}(k\rho_i)\right]\left[\frac{\rho_i/a}{\sin(\rho/a)}\right]^{1/2}\cos\varphi\ , \tag{3-10b}$$

$$E_{\varphi}^i = \frac{j\eta_e^2 k p H_h(t_i)}{4\omega\mu_o\rho_i^2}H_1^{(2)}(k\rho_i)\left[\frac{\rho_i/a}{\sin(\rho/a)}\right]^{3/2}\sin\varphi\ , \tag{3-10c}$$

$$H_{\rho}^{i} = \frac{j\eta_e kp}{4\omega\mu_o} \frac{1}{\rho_i^2} H_h(t_i) H_1^{(2)}(k\rho_i) \left[\frac{\rho_i / a}{\sin(\rho / a)} \right]^{3/2} \sin\varphi \,, \qquad \text{(3-10d)}$$

and

$$H_{\varphi}^{i} = -\frac{j\eta_e k^2 p}{4\omega\mu_o} \frac{1}{\rho_i} G_h(t_i) \left[H_0^{(2)}(k\rho_i) - \frac{1}{k\rho_i} H_1^{(2)}(k\rho_i) \right] \left[\frac{\rho_i / a}{\sin(\rho / a)} \right]^{1/2} \cos\varphi \,, \qquad \text{(3-10e)}$$

where ρ_i, u_i, and t_i were previously defined for the VED. For each field component, the total field is obtained through addition of the direct and indirect great-circle path contributions as is shown for the VED fields in expressions (3-7).

3.3 FORMULAS FOR A HED ABOVE AN ANISOTROPIC GROUND

To account for the anisotropic earth conductivity beneath a HED antenna, Wolkoff and Kraimer (references 4 and 5) have extended Bannister's formulas (3-8). Wolkoff and Kraimer's formulas have been formally derived by Casey (reference 6). The coordinate system used by Wolkoff and Kraimer to describe the EM field radiated by a HED at a given point on the surface of the earth is described in figure 3-3. In this illustration, E_t and N_t refer to the geometric (or true) east and north directions, respectively, at the transmitter location, while E_r and N_r refer to the geometric east and north directions, respectively, at the receiver location (or field point). Note that the geometric east and north directions vary as functions of location along the earth's surface and lie on the tangent plane to the spherical earth. In addition, E and N correspond to the x and y directions, respectively, in the local rectangular coordinate system at each point on the spherical earth, and the vertical direction z points radially outward from the center of the earth at each point as illustrated in figure 3-4.

In figure 3-3, the range ρ is the direct great-circle path distance from the HED center to the field point, φ is the azimuthal angle measured counterclockwise from true east at the transmitter, and φ_n is the azimuthal angle measured clockwise from true north at the transmitter. The unit vectors $(\hat{\rho}, \hat{\varphi}, \hat{z})$ form a right-handed cylindrical coordinate system in which $\hat{z}$ is directed radially outward from the center of the earth. This cylindrical coordinate system differs from the convention used by Bannister and others (compare with figure 3-1), who define the azimuthal angle φ to be measured counterclockwise with respect to the electrical axis of the HED. Wolkoff and Kraimer (references 4 and 5) use the revised coordinate system described here because their antenna pattern factors are determined from magnetic field measurements that are referenced with respect to the local north and east directions.

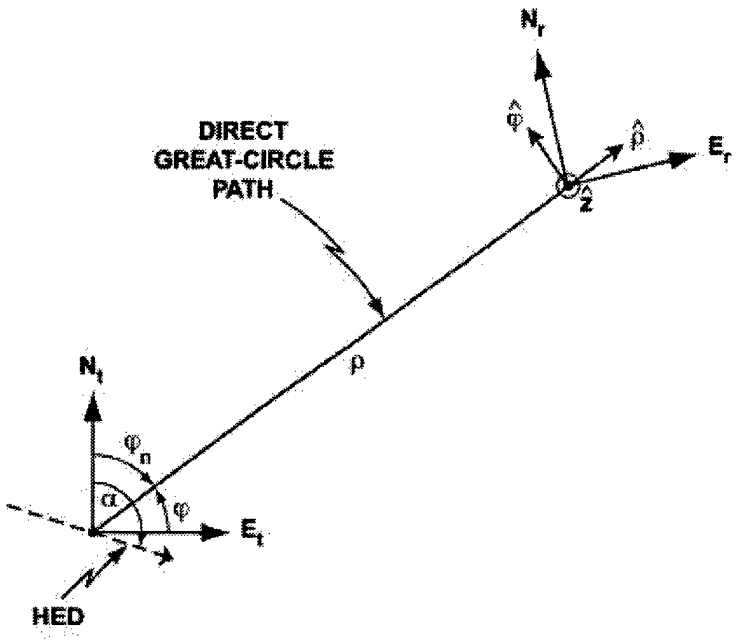

Figure 3-3. Coordinate Systems at the Transmitter and Receiver Locations Used by Wolkoff and Kraimer (References 4 and 5)

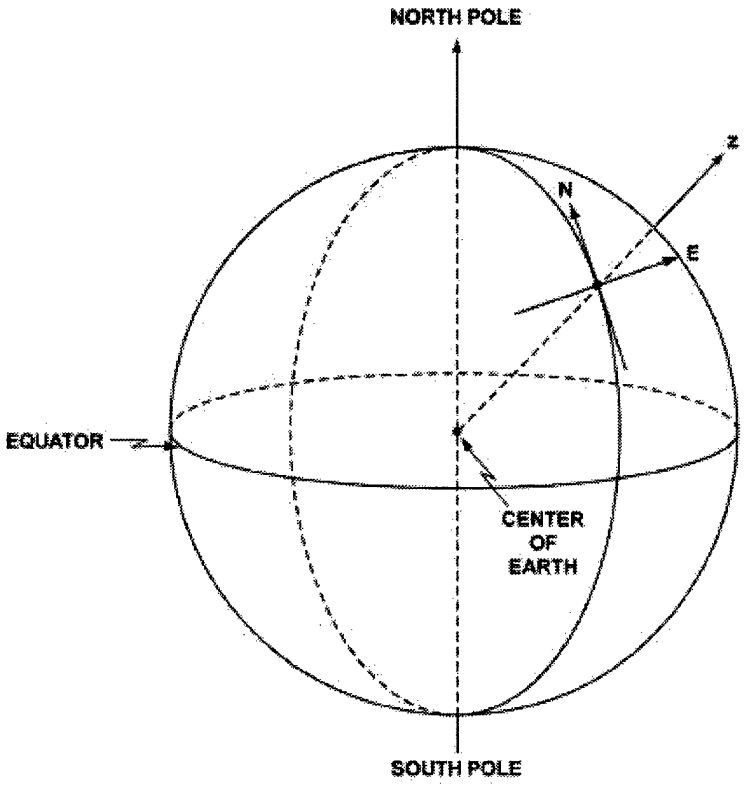

Figure 3-4. Local Rectangular Coordinate System (E, N, z) at a Given Point on a Spherical Earth

Wolkoff and Kraimer's propagation formulas for the direct wave fields from a HED are given as follows:

$$E_z^d = \frac{jkIG_h(u)}{4\rho} H_1^{(2)}(k\rho) \left[\frac{\rho / a}{\sin(\rho / a)} \right]^{1/2} \left[T_e \sin \varphi_n - T_n \cos \varphi_n \right], \tag{3-11a}$$

$$H_\rho^d = \frac{kIH_h(t)}{4\omega\mu_o\rho^2} H_1^{(2)}(k\rho) \left[\frac{\rho / a}{\sin(\rho / a)} \right]^{3/2} \left[T_e \cos \varphi_n + T_n \sin \varphi_n \right], \tag{3-11b}$$

and

$$H_\varphi^d = \frac{k^2 IG_h(t)}{4\omega\mu_o\rho} \left[H_0^{(2)}(k\rho) - \frac{1}{k\rho} H_1^{(2)}(k\rho) \right] \left[\frac{\rho / a}{\sin(\rho / a)} \right]^{1/2} \left[T_e \sin \varphi_n - T_n \cos \varphi_n \right]. \tag{3-11c}$$

In the above formulas, T_e and T_n denote the antenna pattern factors in the east and north directions, respectively. These complex-valued quantities account for the antenna length as well as the anisotropic ground conductivity beneath the antenna. For a given HED, T_e and T_n are determined through measurement of the surface magnetic field at a location lying in the near field of the antenna (reference 4). It should be noted that in the above formulas, T_e and T_n have been interchanged from their original definitions given in reference 6. A detailed discussion of the antenna pattern factors is given in a technical report that is still in preparation (reference 15).

Wolkoff and Kraimer's propagation formulas for the indirect-wave fields from a HED are obtained from the direct great-circle path fields in equations (3-11) through replacement of the range ρ with the indirect great-circle path range ρ_i and with the inclusion of the appropriate phase shift of $\pm j$ for each field component as obtained from table J-1 in appendix J. Thus, Wolkoff and Kraimer's HED indirect wave formulas are given as follows:

$$E_z^i = \frac{kIG_h(u_i)}{4\rho_i} H_1^{(2)}(k\rho_i) \left[\frac{\rho_i / a}{\sin(\rho / a)} \right]^{1/2} \left[T_e \sin \varphi_n - T_n \cos \varphi_n \right], \tag{3-12a}$$

$$H_\rho^i = -\frac{jkIH_h(t_i)}{4\omega\mu_o\rho_i^2} H_1^{(2)}(k\rho_i) \left[\frac{\rho_i / a}{\sin(\rho / a)} \right]^{3/2} \left[T_e \cos \varphi_n + T_n \sin \varphi_n \right], \tag{3-12b}$$

and

$$H_\varphi^i = \frac{jk^2 IG_h(t_i)}{4\omega\mu_o\rho_i} \left[H_0^{(2)}(k\rho_i) - \frac{1}{k\rho_i} H_1^{(2)}(k\rho_i) \right] \left[\frac{\rho_i / a}{\sin(\rho / a)} \right]^{1/2} \left[T_e \sin \varphi_n - T_n \cos \varphi_n \right], \tag{3-12c}$$

where ρ_i is defined in figure 3-2 and u_i and t_i are defined in section 3.2.1. For each field component, the total field is obtained through addition of the direct and indirect great-circle path contributions as is shown for the VED fields in expressions (3-7).

A comparison of Wolkoff and Kraimer's HED formulas (3-11) with Bannister's formulas (3-8) yields the conversions in table 3-1.

Table 3-1. Conversion Table Relating Bannister's HED Propagation Formulas with Those of Wolkoff and Kraimer

Field Component	Bannister	Wolkoff and Kraimer
E_z, H_φ	$-\eta_e\, dl \cos\varphi$	$T_e \sin\varphi_n - T_n \cos\varphi_n$
H_ρ	$-\eta_e\, dl \sin\varphi$	$T_e \cos\varphi_n + T_n \sin\varphi_n$

To convert from one of Bannister's HED formulas to the corresponding Wolkoff and Kraimer formula, the quantity in the second column of table 3-1 is replaced by the corresponding quantity given in the third column. Table 3-1 is a revision of a similar table originally presented by Casey (reference 7). A comparison of columns two and three above shows that the antenna length *dl* in Bannister's formulas is absorbed into the antenna pattern factors.

Numerical results based on Wolkoff and Kraimer's HED formulas will not be presented in this report. For results based on these formulas, the reader is referred to a forthcoming report (reference 15).

4. SPHERICAL WAVEGUIDE PROPAGATION FORMULAS

ELF propagation formulas for VED and HED sources that radiate in a spherical earth-ionosphere waveguide have been derived in appendices F and H, respectively. These spherical waveguide formulas are based on the assumptions of a uniform isotropic earth and a uniform isotropic ionosphere of constant height, where the waveguide boundaries are represented by scalar surface impedances. Through use of the thin-shell approximation derived in appendix I, it is shown that only the quasi-TEM mode can propagate in the 30-Hz to 300-Hz frequency band. In this section, the quasi-TEM spherical waveguide formulas for VED and HED sources are presented, where the source and observation points are located on the surface of the earth. From the series approximation of the Legendre function of the first kind (see appendix J, section J.2), it is shown that the HED spherical waveguide formulas reduce to expressions that are closely related to the antipode-centered formulas that were previously derived (reference 7) for antipodal ranges. In addition, through use of the earth-flattening approximation derived in appendix K, it is shown that the spherical waveguide formulas reduce to Bannister's formulas given in section 3.2. Finally, through use of table 3-1, spherical waveguide formulas for a HED above an anisotropic ground are presented.

4.1 PROPAGATION PARAMETERS FOR TM AND TE MODES AT ELF

The radial wave numbers for the quasi-TEM, TM, and TE modes in the spherical earth-ionosphere waveguide at ELF are derived in appendix I. These formulas are based on the thin-shell approximation that has been shown (reference 2) to be suitable in the ELF band. The radial wave number k_{rv} has been defined in terms of the free-space wave number k_o and the wave number k in the direction of propagation as

$$k_{rv} \equiv \left(k_o^2 - k^2\right)^{1/2}. \tag{4-1}$$

From appendix I, approximate formulas for the radial wave number k_{rv_o} for the quasi-TEM mode and the radial wave numbers k_{rv_n} for the TM modes are given as

$$k_{rv_o} \cong (1+j)\left[\frac{(\Delta_g + \Delta_e)k_o}{2h}\right]^{1/2}, \quad |\Delta_g| \ll |\Delta_e|, |\Delta_e k_o h| \ll 1, \tag{4-2}$$

and

$$k_{r\nu_n} \cong \frac{n\pi}{h} + \frac{j(\Delta_g+\Delta_e)k_o}{n\pi}, \quad |\Delta_e k_o h| \ll 1 \; ; \; n = 1, 2, 3, \ldots . \tag{4-3}$$

Similarly, approximate formulas for the radial wave numbers $k_{r\bar{\nu}_m}$ for the TE modes are given by

$$k_{r\bar{\nu}_m} \cong \frac{m\pi}{h}\left[1 - \frac{j(\Delta_g + \Delta_h)}{k_o h}\right]^{-1} \; ; \; m = 1, 2, 3, \ldots . \tag{4-4}$$

In the above approximations, it is assumed that the spherical waveguide boundaries appear as nearly perfect conductors. Therefore, in formulas (4-2) and (4-3), $|\Delta_g| \ll 1$ and $|\Delta_e| \ll 1$, where Δ_g denotes the normalized surface impedance of the earth and Δ_e denotes the normalized surface impedance of the ionosphere for the quasi-TEM and TM modes. Similarly, in formula (4-4), $|\Delta_g| \ll 1$ and $|\Delta_h| \ll 1$, where Δ_h denotes the normalized surface impedance of the ionosphere for the TE modes.

For a given mode, the wave number k in the direction of propagation is given from formula (4-1) as

$$k \equiv \beta - j\alpha = \left(k_o^2 - k_{r\nu}^2\right)^{1/2}, \tag{4-5}$$

where $\beta = 2\pi/\lambda$ and α are the phase and attenuation constants, respectively, and λ is the wavelength. In the above formula, note that the radial wave number $k_{r\nu}$ corresponds to a particular mode and is given by one of the approximations (4-2), (4-3), or (4-4). A subscript or superscript has not been included with k because only quasi-TEM mode propagation formulas are referred to in the remainder of section 4. In the ELF propagation literature, the mode propagation parameters are given by c/v, α, and h, where c is the speed of light in free space, v is the phase velocity of the mode, and h is the ionospheric reflection height. The mode parameter c/v is expressed in terms of the wave number k as

$$\frac{c}{v} = \frac{\mathrm{Re}\{k\}}{k_o} = \frac{\beta}{k_o} . \tag{4-6}$$

Tables 4-1a and 4-1b provide a listing of the phase velocity ratio (c/v) and attenuation α, respectively, for equally spaced frequencies across the 30-Hz to 300-Hz frequency band under daytime propagation conditions with h = 50 km, earth conductivity $\sigma_g = 10^{-3}$ S/m, and ionospheric conductivity $\sigma_i = 10^{-5}$ S/m. These tables are based on the thin-shell approximation

and are computed from formulas (4-2) to (4-6). Note that the attenuation, expressed in decibels per megameter (dB/Mm), can be obtained from α(Np/m) through the relation 1 Np = 20 $\log_{10}$(e) dB = 8.686 dB.

Table 4-1a. Phase Velocity Ratio c/v for the Dominant Modes in a Spherical Earth-Ionosphere Waveguide at ELF Frequencies Under Daytime Conditions with h = 50 km, $\sigma_g = 10^{-3}$ S/m, and $\sigma_i = 10^{-5}$ S/m

Frequency (Hz)	Quasi-TEM	TM_1	TM_2	TE_1	TE_2
30	1.157	3.199×10^{-3}	1.599×10^{-3}	17.33	34.65
60	1.112	4.524×10^{-3}	2.262×10^{-3}	7.268	14.53
90	1.092	5.542×10^{-3}	2.770×10^{-3}	4.280	8.556
120	1.079	6.402×10^{-3}	3.199×10^{-3}	2.916	5.827
150	1.071	7.161×10^{-3}	3.577×10^{-3}	2.157	4.308
180	1.065	7.849×10^{-3}	3.919×10^{-3}	1.682	3.358
210	1.060	8.483×10^{-3}	4.234×10^{-3}	1.361	2.716
240	1.056	9.075×10^{-3}	4.527×10^{-3}	1.132	2.258
270	1.053	9.635×10^{-3}	4.803×10^{-3}	0.9621	1.917
300	1.050	1.017×10^{-2}	5.064×10^{-3}	0.8313	1.655

Table 4-1b shows that the quasi-TEM mode is the only propagating mode in the ELF band with an attenuation rate of approximately 0.75 dB/Mm at 30 Hz that increases with frequency to 2.63 dB/Mm at 300 Hz. Table 4-1b also shows that the attenuation rates of the TM and TE modes are too high to be of any practical concern across the 30-Hz to 300-Hz frequency band. Note that the attenuation increases with the order of the mode. In addition, the attenuation rates of the TE_1 and TE_2 modes are less than those of the TM_1 and TM_2 modes, respectively. Table 4-1a indicates that the phase velocity of the quasi-TEM mode monotonically increases with frequency over the 30-Hz to 300-Hz band.

Table 4-1b. Attenuation α in dB/Mm for the Dominant Modes in a Spherical Earth-Ionosphere Waveguide at ELF Frequencies Under Daytime Conditions with $h = 50$ km, $\sigma_g = 10^{-3}$ S/m, and $\sigma_i = 10^{-5}$ S/m

Frequency (Hz)	Quasi-TEM	TM_1	TM_2	TE_1	TE_2
30	0.7543	545.7	1091	390.6	781.3
60	1.110	545.6	1091	430.4	861.0
90	1.385	545.4	1091	449.5	899.5
120	1.617	545.2	1091	461.3	923.3
150	1.822	544.9	1091	469.4	939.9
180	2.007	544.5	1091	475.3	952.3
210	2.178	544.1	1091	479.8	961.9
240	2.337	543.6	1090	483.4	969.7
270	2.486	543.1	1090	486.2	976.1
300	2.628	542.5	1090	488.5	981.5

Tables 4-2a and 4-2b list the phase velocity ratio and attenuation rate, respectively, for equally spaced frequencies across the 30-Hz to 300-Hz ELF band under nighttime propagation conditions with $h = 75$ km, $\sigma_g = 10^{-3}$ S/m, and $\sigma_i = 10^{-5}$ S/m. The numbers in these tables are also based on the thin-shell approximation. Table 4-2b shows that the quasi-TEM mode is the only propagating mode in the ELF band at nighttime with an attenuation rate of approximately 0.53 dB/Mm at 30 Hz that monotonically increases with frequency to 1.78 dB/Mm at 300 Hz . Note that the attenuation rates of the TM and TE modes are again too high to be of any practical concern. Table 4-2a indicates that the phase velocity of the quasi-TEM mode monotonically increases with frequency over the tabulated frequency band.

A comparison of tables 4-1 with tables 4-2 shows that the mode attenuation rates are less at nighttime. In addition, the phase velocity of the quasi-TEM mode is greater at nighttime. Because the quasi-TEM mode is the only propagating mode in the 30-Hz to 300-Hz band, the remainder of this report will focus on the quasi-TEM mode.

Table 4-2a. Phase Velocity Ratio c/v for the Dominant Modes in a Spherical Earth-Ionosphere Waveguide at ELF Frequencies Under Nighttime Conditions with h = 75 km, $\sigma_g = 10^{-3}$ S/m, and $\sigma_i = 10^{-5}$ S/m

Frequency (Hz)	Quasi-TEM	TM_1	TM_2	TE_1	TE_2
30	1.106	3.199×10^{-3}	1.599×10^{-3}	9.360	18.72
60	1.075	4.525×10^{-3}	2.262×10^{-3}	3.729	7.455
90	1.061	5.546×10^{-3}	2.771×10^{-3}	2.143	4.283
120	1.053	6.409×10^{-3}	3.200×10^{-3}	1.439	2.873
150	1.048	7.172×10^{-3}	3.579×10^{-3}	1.054	2.103
180	1.043	7.867×10^{-3}	3.921×10^{-3}	0.8163	1.627
210	1.040	8.510×10^{-3}	4.237×10^{-3}	0.6572	1.308
240	1.038	9.113×10^{-3}	4.532×10^{-3}	0.5445	1.082
270	1.035	9.685×10^{-3}	4.809×10^{-3}	0.4612	0.9151
300	1.037	1.023×10^{-2}	5.072×10^{-3}	0.3976	0.7875

Table 4-2b. Attenuation α in dB/Mm for the Dominant Modes in a Spherical Earth-Ionosphere Waveguide at ELF Frequencies Under Nighttime Conditions with $h = 75$ km, $\sigma_g = 10^{-3}$ S/m, and $\sigma_i = 10^{-5}$ S/m

Frequency (Hz)	Quasi-TEM	TM_1	TM_2	TE_1	TE_2
30	0.5263	363.8	727.6	290.9	581.9
60	0.7655	363.6	727.6	310.7	621.6
90	0.9496	363.4	727.4	319.7	640.0
120	1.105	363.0	727.3	325.1	651.2
150	1.242	362.6	727.1	328.6	658.8
180	1.366	362.1	726.8	331.0	664.4
210	1.480	361.5	726.5	332.7	668.6
240	1.586	360.8	726.2	333.9	672.0
270	1.686	360.0	725.8	334.6	674.7
300	1.780	359.2	725.3	335.1	676.8

4.2 QUASI-TEM FIELDS

4.2.1 VED

The spherical waveguide propagation formulas for a VED located at an arbitrary height above the surface of the earth are derived in appendix F. These formulas simplify considerably for the case when both the source and observation points are located on the surface of the earth. Under this assumption, from appendix F, section F.2, the quasi-TEM fields for a VED are given as follows:

$$E_r^{ve} = \frac{j\eta_o p}{4k_o h a^2} \frac{\nu_o(\nu_o + 1)}{\sin \nu_o \pi} P_{\nu_o}(-\cos\theta) \ , \tag{4-7a}$$

$$E_\theta^{ve} = -\frac{\eta_o p \Delta_g}{4ha} \frac{1}{\sin \nu_o \pi} \frac{\partial}{\partial \theta} P_{\nu_o}(-\cos\theta) \ , \tag{4-7b}$$

and

$$H_\varphi^{ve} = \frac{p}{4ha} \frac{1}{\sin \nu_o \pi} \frac{\partial}{\partial \theta} P_{\nu_o}(-\cos\theta) \ . \tag{4-7c}$$

The reader is referred to the spherical coordinate system (r, θ, φ) described in figure 1-1 with unit vectors $(\hat{r},\hat{\theta},\hat{\varphi})$ illustrated in figure 4-1. In these formulas, the VED is located at $(r, \theta) = (a, 0)$ and the observation point is at $(r, \theta, \varphi) = (a, \theta, \varphi)$. Note that because of azimuthal symmetry, the above formulas are independent of φ. In addition, the excitation factor Λ_o^e has been replaced by 0.5, a suitable approximation at ELF, as is shown in appendix I, section I.2. In the above formulas, Δ_g denotes the normalized surface impedance of the earth and P_{ν_o} is the Legendre function of the first kind of degree ν_0 and order zero, where ν_0 is the $n = 0$ solution of the TM-mode characteristic equation.

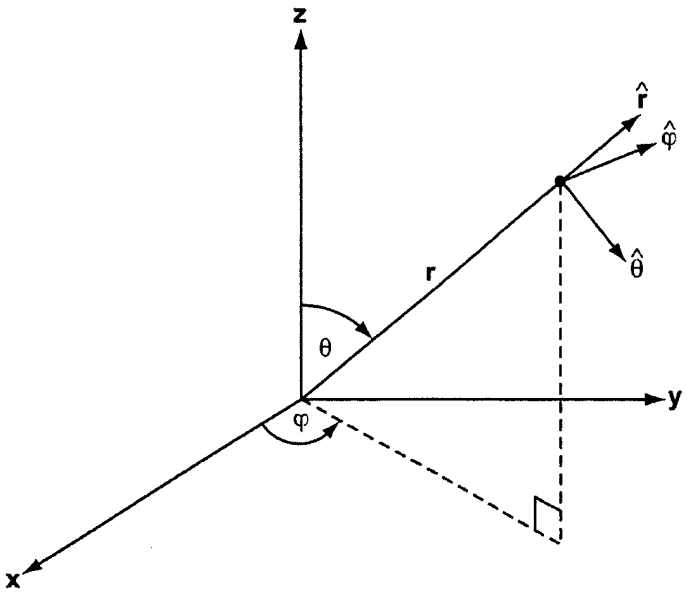

Figure 4-1. Spherical Coordinate System

From appendix J, section J.1, ν_0 is related to the quasi-TEM wave number k as

$$k = \frac{\nu_o + 1/2}{a} \quad . \tag{4-8}$$

As discussed in appendix K, if $|\nu_0| \gg 1$, then

$$\nu_o + 1/2 \cong \left[\nu_o(\nu_o + 1)\right]^{1/2} \quad . \tag{4-9}$$

The above result is generally valid in the ELF band. Therefore, under this condition, the wave number k can be approximated as

$$k \cong \frac{\left[\nu_o(\nu_o+1)\right]^{1/2}}{a} \quad . \tag{4-10}$$

For a homogeneous and isotropic earth, the normalized surface impedance Δ_g is given by

$$\Delta_g = \frac{\eta_e}{\eta_o} \quad , \tag{4-11}$$

where the intrinsic impedance of the earth η_e is given in section 3.2.1.

4.2.2 Horizontal Electric Dipole

The spherical waveguide propagation formulas for a HED located at an arbitrary height above the surface of the earth are derived in appendix H. As with the VED formulas, the HED formulas simplify considerably for the case when both the source and observation points are located on the surface of the earth. Under this assumption, from appendix H, section H.2, the quasi-TEM fields for a HED are given as follows:

$$E_r^{he} = -\frac{\eta_o \Delta_g p}{4ha} \frac{1}{\sin \nu_o \pi} \frac{\partial}{\partial \theta} P_{\nu_o}(-\cos\theta) \cos\varphi \quad , \tag{4-12a}$$

$$E_\theta^{he} = -\frac{jk_o \eta_o \Delta_g^2 p}{4h} \frac{1}{\nu_o(\nu_o+1)} \frac{1}{\sin \nu_o \pi} \frac{\partial^2}{\partial \theta^2} P_{\nu_o}(-\cos\theta) \cos\varphi, \tag{4-12b}$$

$$E_\varphi^{he} = \frac{j\omega\mu_o \Delta_g^2 p}{4h} \frac{1}{\nu_o(\nu_o+1)} \frac{1}{\sin \nu_o \pi} \frac{1}{\sin\theta} \frac{\partial}{\partial \theta} P_{\nu_o}(-\cos\theta) \sin\varphi, \tag{4-12c}$$

$$H_\theta^{he} = \frac{jk_o \Delta_g p}{4h} \frac{1}{\nu_o(\nu_o+1)} \frac{1}{\sin \nu_o \pi} \frac{1}{\sin\theta} \frac{\partial}{\partial \theta} P_{\nu_o}(-\cos\theta) \sin\varphi, \tag{4-12d}$$

and

$$H_\varphi^{he} = \frac{jk_o \Delta_g p}{4h} \frac{1}{\nu_o(\nu_o+1)} \frac{1}{\sin \nu_o \pi} \frac{\partial^2}{\partial \theta^2} P_{\nu_o}(-\cos\theta) \cos\varphi \quad . \tag{4-12e}$$

The reader is again referred to the spherical coordinate system (r, θ, φ) described in figure 1-1. In these formulas, the HED is located at $(r, \theta) = (a, 0)$ and the observation point is at $(r, \theta, \varphi) = (a, \theta, \varphi)$. Note that the above formulas have the same azimuthal dependencies as Bannister's HED formulas that are listed in section 3.2.2. As in the VED case, the excitation factor Λ_o^e has been approximated by 0.5. The complex degree ν_0 in the above HED formulas corresponds to the $n = 0$ solution of the TM-mode characteristic equation.

4.3 ANTIPODE-CENTERED FORMULAS

In order to predict the EM fields produced by a HED at antipodal ranges, the author (reference 7) derived some simple approximate formulas that are based on an earth-flattening type of approximation that has the proper range dependence in the vicinity of the antipode and accounts for spherical curvature at further distances from the antipode. The resulting "antipode-centered" formulas have range dependencies that are similar in form to the corresponding ones that incorporate the earth-flattening approximation except that the Hankel function is replaced by a Bessel function of the first kind and the range argument is replaced by ρ_a, where $\rho_a = a(\pi - \theta)$ is the great-circle path distance from the antipode to the field point (figure 3-2). The range dependencies in the antipode-centered formulas are derived from an approximate series representation of $P_\nu(-\cos\theta)$ that is suitable in the vicinity of the antipode ($\theta = \pi$). From the primary terms in this series, approximate formulas for $P_\nu(-\cos\theta)$ and its first two derivatives with respect to θ are derived in appendix J, section J.2. These formulas are given as follows:

$$P_\nu(-\cos\theta) \cong J_0(k\rho_a)\left[\frac{\rho_a/a}{\sin\rho_a/a}\right]^{1/2}, \tag{4-13a}$$

$$\frac{d}{d\theta}P_\nu(-\cos\theta) \cong ka\,J_1(k\rho_a)\left[\frac{\rho_a/a}{\sin\rho_a/a}\right]^{1/2}, \tag{4-13b}$$

and

$$\frac{d^2}{d\theta^2}P_\nu(-\cos\theta) \cong -(ka)^2\left[J_0(k\rho_a) - \frac{1}{k\rho_a}J_1(k\rho_a)\right]\left[\frac{\rho_a/a}{\sin\rho_a/a}\right]^{1/2}. \tag{4-13c}$$

Through use of the above approximations, antipode-centered formulas for both VED and HED sources are derived from the spherical waveguide formulas presented in section 4.2. The resulting HED formulas are then compared with the corresponding formulas derived in reference 7.

4.3.1 VED

The application of the approximate formulas (4-13) and (I-7) to the spherical waveguide formulas for a VED source given in expressions (4-7) yields the following field approximations:

$$E_r^{ve} \cong \frac{j\eta_o k^2 p}{4k_o h}\frac{1}{\sin\nu_o\pi}J_0(k\rho_a)\left[\frac{\rho_a/a}{\sin\rho_a/a}\right]^{1/2}, \tag{4-14a}$$

$$E_{\theta}^{ve} \cong -\frac{\eta_o k p \Delta_g}{4h} \frac{1}{\sin \nu_o \pi} J_1(k\rho_a) \left[\frac{\rho_a/a}{\sin \rho_a/a}\right]^{1/2}, \tag{4-14b}$$

and

$$H_{\varphi}^{ve} \cong \frac{kp}{4h} \frac{1}{\sin \nu_o \pi} J_1(k\rho_a) \left[\frac{\rho_a/a}{\sin \rho_a/a}\right]^{1/2}, \tag{4-14c}$$

where $\rho_a = a(\pi - \theta)$ is the great-circle path distance from the antipode to the field point (figure 3-2). In the above formulas, note that $\sin \theta = \sin (\rho/a) = \sin (\rho_a/a)$ and $\rho + \rho_a = \pi a$.

4.3.2 Horizontal Electric Dipole

The application of the approximate formulas (4-13) and (I-7) to the spherical waveguide formulas for a HED source given in expressions (4-12) results in the following field approximations:

$$E_r^{he} \cong -\frac{\eta_o k \Delta_g p}{4h} \frac{1}{\sin \nu_o \pi} J_1(k\rho_a) \left[\frac{\rho_a/a}{\sin \rho_a/a}\right]^{1/2} \cos \varphi, \tag{4-15a}$$

$$E_{\theta}^{he} \cong \frac{j\omega\mu_o \Delta_g^2 p}{4h} \frac{1}{\sin \nu_o \pi} \left[J_0(k\rho_a) - \frac{1}{k\rho_a} J_1(k\rho_a)\right] \left[\frac{\rho_a/a}{\sin \rho_a/a}\right]^{1/2} \cos \varphi, \tag{4-15b}$$

$$E_{\varphi}^{he} \cong \frac{j\omega\mu_o \Delta_g^2 p}{4kh\rho_a} \frac{1}{\sin \nu_o \pi} J_1(k\rho_a) \left[\frac{\rho_a/a}{\sin \rho_a/a}\right]^{3/2} \sin \varphi, \tag{4-15c}$$

$$H_{\theta}^{he} \cong \frac{jk_o \Delta_g p}{4kh\rho_a} \frac{1}{\sin \nu_o \pi} J_1(k\rho_a) \left[\frac{\rho_a/a}{\sin \rho_a/a}\right]^{3/2} \sin \varphi, \tag{4-15d}$$

and

$$H_{\varphi}^{he} \cong -\frac{jk_o \Delta_g p}{4h} \frac{1}{\sin \nu_o \pi} \left[J_0(k\rho_a) - \frac{1}{k\rho_a} J_1(k\rho_a)\right] \left[\frac{\rho_a/a}{\sin \rho_a/a}\right]^{1/2} \cos \varphi. \tag{4-15e}$$

A comparison of expressions (4-15a), (4-15d), and (4-15e) with the corresponding formulas given in reference 7 shows that the above formulas differ by a factor C that is defined as

$$C \equiv \frac{e^{jk\pi a}}{2 \sin \nu_o \pi} = \frac{j}{2} \frac{e^{j\nu_o \pi}}{\sin \nu_o \pi} \quad . \tag{4-16}$$

Note that the final expression in formula (4-16) was obtained through use of equation (4-8).

Table 4-3 lists the magnitude and phase of C for several frequencies in the ELF band. The magnitude of C is tabulated to three significant figures while the phase of C is given to the nearest thousandth of a degree. Because the antipode-centered propagation formulas in reference 7 were derived via Bannister's HED formulas and because there is a sign difference between Bannister's HED formulas and the spherical waveguide formulas (see section 4.4), C has been multiplied by –1 in table 4-3. The results show that C is very small in magnitude and phase over the ELF band, indicating that the HED antipode-centered propagation formulas of reference 7 are sufficiently accurate to be used in place of expressions (4-15a), (4-15d), and (4-15e).

Table 4-3. Magnitude and Phase of Difference Factor C in HED Antipode-Centered ELF Propagation Formulas at Several Frequencies under Daytime Conditions

Frequency (Hz)	ν_o	$\lvert C \rvert$ **(dB)**	**Phase{-C} (deg)**
30	4.75 - j 0.440	- 2.56 x 10^{-2}	3.599
76	11.7 - j 0.880	- 1.52 x 10^{-2}	0.204
100	15.9 - j 1.32	1.92 x 10^{-3}	0.007
300	46.4 - j 3.67	- 5.73 x 10^{-10}	0.000

The suitability of the antipode-centered ELF propagation listed in formulas (4-14) and (4-15) depends entirely on the accuracy of the approximations for $P_\nu(-\cos\theta)$ and its first two derivatives with respect to θ as given in expressions (4-13). Comparison plots of the exact series formulas for $P_\nu(-\cos\theta)$ (and its first two derivatives with respect to θ) and the approximate formulas (4-13) are given in appendix J, section J.3, for frequencies of 30 Hz and 76 Hz. The plots show that the approximate formulas are in close agreement with the corresponding exact formulas. This comparison improves with increasing frequency and degrades with increasing derivative order. (For more details regarding this comparison, refer to appendix J, section J.3.) In summary, the antipode-centered propagation formulas (4-14) and (4-15) are suitable substitutes for the spherical waveguide formulas presented in section 4.2.

4.4 REDUCTION TO BANNISTER'S FORMULAS VIA THE EARTH-FLATTENING APPROXIMATION

The earth-flattening approximation to the Legendre function of the first kind is derived in appendix K. Earlier in this report, it was mentioned that this approximation has been incorporated into Bannister's VED and HED formulas given in section 3.2. Through use of the earth-flattening approximation, it is shown that the VED and HED spherical waveguide formulas can reduce to Bannister's formulas.

4.4.1 VED

From expression (K-33) in appendix K, the Legendre function of the first kind and degree ν is approximated as

$$P_\nu(-\cos\theta) \cong j \sin \nu\pi \, H_o^{(2)}(k\rho) \left[\frac{\rho / a}{\sin(\rho / a)}\right]^{1/2}, \tag{4-17}$$

where $\rho = a\theta$ is the great-circle path distance along the earth from the source point to the field point (figure 3-1) and $H_o^{(2)}$ denotes the Hankel function of the second kind with order 0. As discussed in section 3.1, $H_o^{(2)}(k\rho)$ corresponds to the range dependence for a flat earth and the square-root term is the correction for curvature. The spherical waveguide propagation formulas for a VED are given in expressions (4-7). In these formulas, the range dependencies are expressed in terms of either $P_\nu(-\cos\theta)$ or its first derivative. From the approximation (4-17), the derivative of $P_\nu(-\cos\theta)$ with respect to θ is given by

$$\frac{\partial}{\partial\theta} P_{\nu_o}(-\cos\theta) \cong -jka \sin \nu_o\pi \, H_1^{(2)}(k\rho) \left[\frac{\rho / a}{\sin(\rho / a)}\right]^{1/2}, \tag{4-18}$$

where the θ-derivative of $H_o^{(2)}(k\rho)$ is given by

$$\frac{\partial}{\partial\theta} H_0^{(2)}(k\rho) = ka \, H_0^{(2)'}(k\rho) = -ka \, H_1^{(2)}(k\rho) \; . \tag{4-19}$$

In the approximation (4-18), note that the θ derivative was applied only to the Hankel function term because it varies more rapidly than the curvature correction term.

The substitution of the approximations (4-10), (4-17) and (4-18) along with expression (4-11) into the VED formulas (4-7) yields

$$E_z^{ve} \cong -\frac{\eta_o k^2 p}{4k_o h} H_o^{(2)}(k\rho) \left[\frac{\rho/a}{\sin(\rho/a)}\right]^{1/2}, \tag{4-20a}$$

$$E_\rho^{ve} \cong \frac{j\eta_e kp}{4h} H_1^{(2)}(k\rho) \left[\frac{\rho/a}{\sin(\rho/a)}\right]^{1/2}, \tag{4-20b}$$

and

$$H_\varphi^{ve} \cong -\frac{jkp}{4h} H_1^{(2)}(k\rho) \left[\frac{\rho/a}{\sin(\rho/a)}\right]^{1/2}. \tag{4-20c}$$

In the above formulas, note that the spherical components r and θ have been replaced by the equivalent cylindrical components z and ρ, respectively. The above formulas are generally valid for ranges greater than three ionospheric reflection heights, i.e., $\rho > 3h$. In order to show that the above VED formulas are equivalent to those of Bannister given in section 3.2.1, the functions G_h and V_h must be replaced by their approximate forms. For $\rho > 3h$, these functions can be approximated as

$$G_h(u) \cong \frac{2u}{\pi} = \frac{\rho}{h}, \tag{4-21}$$

and

$$V_h(t) \cong 0. \tag{4-22}$$

The substitutions of the above approximations into Bannister's VED formulas (3-3) yields

$$E_z^d \cong -\frac{\eta_o k^2 p}{4k_o h} H_0^{(2)}(k\rho) \left[\frac{\rho/a}{\sin(\rho/a)}\right]^{1/2}, \tag{4-23a}$$

$$E_\rho^d \cong \frac{j\eta_e kp}{4h} H_1^{(2)}(k\rho) \left[\frac{\rho/a}{\sin(\rho/a)}\right]^{1/2}, \tag{4-23b}$$

and

$$H_\varphi^d \cong -\frac{jkp}{4h} H_1^{(2)}(k\rho) \left[\frac{\rho/a}{\sin(\rho/a)}\right]^{1/2}. \tag{4-23c}$$

A comparison of formulas (4-20) with (4-23) shows that the VED spherical waveguide formulas reduce to Bannister's formulas for $\rho > 3h$.

4.4.2 Horizontal Electric Dipole

The spherical waveguide propagation formulas for a HED are given in expressions (4-12). In these formulas, the range dependencies are expressed in terms of either the first or second derivatives of $P_\nu(-\cos\theta)$. An approximation for the first derivative of $P_\nu(-\cos\theta)$ with respect to θ is given in formula (4-18). From this approximation, the second derivative of $P_\nu(-\cos\theta)$ is given as

$$\frac{\partial^2}{\partial\theta^2} P_{\nu_o}(-\cos\theta) \cong -jka \sin \nu_o\pi \frac{\partial}{\partial\theta} \left\{ H_1^{(2)}(k\rho) \left[\frac{\rho/a}{\sin(\rho/a)} \right]^{1/2} \right\}$$

$$\cong -j(ka)^2 \sin \nu_o\pi \left[H_0^{(2)}(k\rho) - \frac{1}{k\rho} H_1^{(2)}(k\rho) \right] \left[\frac{\rho/a}{\sin(\rho/a)} \right]^{1/2} . \qquad (4\text{-}24)$$

In the above approximation, note that the θ derivative was only applied to the Hankel function term because it varies more rapidly than the curvature correction term.

The substitution of the approximations (4-10), (4-17), (4-18), and (4-24), along with expression (4-11), into the HED formulas (4-12) yields

$$E_z^{he} \cong \frac{j\eta_e kp}{4h} H_1^{(2)}(k\rho) \left[\frac{\rho/a}{\sin(\rho/a)} \right]^{1/2} \cos\varphi , \qquad (4\text{-}25a)$$

$$E_\rho^{he} \cong -\frac{k_o\eta_e^2 p}{4\eta_o h} \left[H_0^{(2)}(k\rho) - \frac{1}{k\rho} H_1^{(2)}(k\rho) \right] \left[\frac{\rho/a}{\sin(\rho/a)} \right]^{1/2} \cos\varphi , \qquad (4\text{-}25b)$$

$$E_\varphi^{he} \cong \frac{k_o\eta_e^2 p}{4\eta_o kh\rho} H_1^{(2)}(k\rho) \left[\frac{\rho/a}{\sin(\rho/a)} \right]^{3/2} \sin\varphi , \qquad (4\text{-}25c)$$

$$H_\rho^{he} \cong \frac{k_o\eta_e p}{4\eta_o kh\rho} H_1^{(2)}(k\rho) \left[\frac{\rho/a}{\sin(\rho/a)} \right]^{3/2} \sin\varphi , \qquad (4\text{-}25d)$$

and

$$H_\varphi^{he} \cong \frac{k_o\eta_e p}{4\eta_o h} \left[H_0^{(2)}(k\rho) - \frac{1}{k\rho} H_1^{(2)}(k\rho) \right] \left[\frac{\rho/a}{\sin(\rho/a)} \right]^{1/2} \cos\varphi . \qquad (4\text{-}25e)$$

In the above formulas, note that the spherical components r and θ have again been replaced by the equivalent cylindrical components z and ρ, respectively. The above formulas are generally valid for $\rho > 3h$. In order to show that the above HED formulas are equivalent to those of Bannister given in section 3.2.2, the functions G_h, V_h, and H_h must be replaced by their approximate forms. Approximations for $G_h(u)$ and $V_h(t)$ are given in expressions (4-21) and (4-22), respectively. For $\rho > 3h$, $G_h(t)$ and $H_h(t)$ can be approximated as follows:

$$G_h(t) \cong \frac{2t}{\pi} = \frac{\rho}{h}\left(\frac{k_o}{k}\right)^2, \tag{4-26}$$

and

$$H_h(t) \cong G_h(t) \cong \frac{\rho}{h}\left(\frac{k_o}{k}\right)^2. \tag{4-27}$$

The substitutions of the approximations (4-21), (4-26), and (4-27) into Bannister's HED formulas (3-8) yields

$$E_z^d \cong \frac{-j\eta_e kp}{4h} H_1^{(2)}(k\rho)\left[\frac{\rho/a}{\sin(\rho/a)}\right]^{1/2}\cos\varphi\ , \tag{4-28a}$$

$$E_\rho^d \cong \frac{k_o\eta_e^2 p}{4\eta_o h}\left[H_0^{(2)}(k\rho) - \frac{1}{k\rho}H_1^{(2)}(k\rho)\right]\left[\frac{\rho/a}{\sin(\rho/a)}\right]^{1/2}\cos\varphi\,, \tag{4-28b}$$

$$E_\varphi^d \cong -\frac{k_o\eta_e^2 p}{4\eta_o kh\rho} H_1^{(2)}(k\rho)\left[\frac{\rho/a}{\sin(\rho/a)}\right]^{3/2}\sin\varphi\,, \tag{4-28c}$$

$$H_\rho^d \cong -\frac{k_o\eta_e p}{4\eta_o kh\rho} H_1^{(2)}(k\rho)\left[\frac{\rho/a}{\sin(\rho/a)}\right]^{3/2}\sin\varphi\ , \tag{4-28d}$$

and

$$H_\varphi^d \cong -\frac{k_o\eta_e p}{4\eta_o h}\left[H_0^{(2)}(k\rho) - \frac{1}{k\rho}H_1^{(2)}(k\rho)\right]\left[\frac{\rho/a}{\sin(\rho/a)}\right]^{1/2}\cos\varphi\ . \tag{4-28e}$$

A comparison of formulas (4-25) with (4-28) indicates that each of the HED spherical waveguide formulas reduces to within a factor of -1 of Bannister's formulas for $\rho > 3h$. At this time, there is no explanation for the sign difference.

4.5 MODIFICATION OF HED SPHERICAL WAVEGUIDE FORMULAS TO ACCOUNT FOR AN ANISOTROPIC GROUND

The HED spherical waveguide formulas (4-12) are based on the assumption of a homogeneous, isotropic earth. These formulas can be modified to account for an anisotropic-ground conductivity in the vicinity of the HED through use of the reciprocity theorem. The derivations of the modified HED spherical waveguide formulas follow that given by the author (reference 6) for Bannister's HED formulas and will not be presented here. In addition, the conversion (table 3-1) may be applied to the spherical waveguide formulas if E_z and H_ρ are replaced by E_r and H_θ, respectively. Therefore, the modified HED spherical waveguide formulas are

$$E_r^{he} = \frac{I}{4ha} \frac{1}{\sin \nu_o \pi} \frac{\partial}{\partial \theta} P_{\nu_o}(-\cos\theta) \left[T_e \sin \varphi_n - T_n \cos \varphi_n \right], \tag{4-29a}$$

$$H_\theta^{he} = -\frac{jk_o I}{4\eta_o h} \frac{1}{\nu_o(\nu_o+1)} \frac{1}{\sin \nu_o \pi} \frac{1}{\sin\theta} \frac{\partial}{\partial \theta} P_{\nu_o}(-\cos\theta) \left[T_e \cos \varphi_n + T_n \sin \varphi_n \right], \tag{4-29b}$$

and

$$H_\varphi^{he} = -\frac{jk_o I}{4\eta_o h} \frac{1}{\nu_o(\nu_o+1)} \frac{1}{\sin \nu_o \pi} \frac{\partial^2}{\partial \theta^2} P_{\nu_o}(-\cos\theta) \left[T_e \sin \varphi_n - T_n \cos \varphi_n \right]. \tag{4-29c}$$

In the above formulas, T_e and T_n are the antenna pattern factors in the east and north directions, respectively, and φ_n is defined in figure 3-3. As with Wolkoff and Kraimer's formulas given in section 3.3, only the field components of practical interest are listed above.

5. COMPARISONS OF PROPAGATION FORMULAS

In section 3, Bannister's ELF propagation formulas were presented for both VED and HED sources radiating in a spherical earth-ionosphere waveguide, where both the source and field points are located on the earth's surface. In section 4, spherical waveguide formulas for VED and HED sources were given. The spherical waveguide formulas are expected to be more accurate at antipodal ranges because they have a range dependence that is more accurate than Bannister's formulas, which are based on the earth-flattening approximation with curvature correction.

In this section, plots of the spherical waveguide and Bannister's ELF propagation formulas are presented as functions of range for both daytime and nighttime propagation conditions at several frequencies in the ELF band. Results are presented for VED and HED sources, where both the source and field points are located on the surface of the earth. In the plots of Bannister's formulas, separate graphs of the direct great-circle path field and the summation of the direct and indirect great-circle path fields are given. The comparisons presented here will help to more accurately establish the maximum ranges of validity of Bannister's formulas. Plots of only the dominant field components are presented, i.e., E_z^{ve}, H_φ^{ve}, E_z^{he}, H_ρ^{he}, and H_φ^{he}.

For a HED source, the plots presented in this report are at the azimuth angle φ in which the magnitude of the field component is a maximum. In particular, the plots of E_z^{he} and H_φ^{he} are given for $\varphi = 0°$ and the plots of H_ρ^{he} are given for $\varphi = 90°$. In addition, for the spherical waveguide formulas, the spherical coordinates r and θ are replaced by the cylindrical coordinates z and ρ, respectively, where $z = r - a$, $\rho = a\theta$, and a is the earth's mean radius. The unit vectors in these coordinate systems are related as follows: $\hat{z} = \hat{r}$ and $\hat{\rho} = \hat{\theta}$.

Table 5-1 is a list of the propagation parameters at several ELF frequencies under typical daytime and nighttime conditions. The propagation parameters c/v, α, and h were obtained from Bannister (reference 16) and are based on an exponential conductivity profile of the ionosphere (reference 17). The degrees of the Legendre function ν_o in the spherical waveguide formulas that are listed in this table are computed from formula (4-8). It should be mentioned that the 76-Hz parameters listed in this table are different from those obtained from Wolkoff (reference 18) for use in an earlier investigation (reference 7). In that study, Wolkoff determined the 76-Hz propagation parameters from the measured data listed by Bannister (reference 17). The 76-Hz

frequency is of particular interest in applications because it is the center frequency of the U.S. Navy Submarine ELF Communications System.

Table 5-1. Propagation Parameters for Typical Daytime and Nighttime Conditions at Several Frequencies as Obtained from Bannister (Reference 16)

Frequency (Hz)	Propagation Condition	c/v	α (dB/Mm)	h (km)	ν_o
30	Daytime	1.31	0.60	51	$4.75 - j\ 0.440$
30	Nighttime	1.14	0.70	73	$4.07 - j\ 0.513$
76	Daytime	1.25	1.4	53.5	$12.2 - j\ 1.03$
76	Nighttime	1.12	0.90	77	$10.9 - j\ 0.660$
100	Daytime	1.23	1.8	55	$15.9 - j\ 1.32$
100	Nighttime	1.12	1.15	77	$14.5 - j\ 0.844$
300	Daytime	1.17	5.0	59	$46.4 - j\ 3.67$
300	Nighttime	1.10	2.7	81	$43.6 - j\ 1.98$

5.1 RESULTS AT 76 HZ

Plots of the computed magnitude and phase of the vertical electric field produced by a VED under daytime propagation conditions at 76 Hz are given in figures 5-1a and 5-1b, respectively. In addition, plots of the magnitude and phase of the azimuthal magnetic field from a VED source are presented for the same propagation conditions in figures 5-2a and 5-2b, respectively. Each of these graphs are given as a function of the distance measured from the antipode ρ_a, which is defined in terms of the direct great-circle path distance ρ measured from the source as $\rho_a \equiv \pi a - \rho$ and illustrated in figure 3-2. Figures 5-1a and 5-2a show an interference pattern that is greatest in the vicinity of the antipode and slowly diminishes with increasing distance from the antipode. The interference is caused by the combination of the direct and indirect great-circle path fields. In figures 5-1a and 5-2a, note that Bannister's direct great-circle path field components do not show an interference pattern because they do not include the indirect great-circle path contribution.

In figure 5-1a, Bannister's total field (direct plus indirect great-circle path formulas) result for E_z^{ve} shows good agreement with the spherical waveguide formula for all ranges except those that are very close to the antipode. In particular, Bannister's total field result for E_z^{ve} agrees to within 1 dB of the spherical waveguide formula for ρ_a = 1.15 Mm or, equivalently, ρ = 18.87 Mm. In comparison, Bannister's direct great-circle path formula for E_z^{ve} agrees to within 1 dB of the spherical waveguide formula for ρ_a = 6.09 Mm or, equivalently, ρ = 13.93 Mm. Clearly, under these propagation conditions, Bannister's total field results are much more accurate than Bannister's direct great-circle path results at antipodal ranges.

A comparison of figures 5-1a and 5-2a indicates that Bannister's total field result for H_φ^{ve} does not agree as closely with the corresponding spherical waveguide formula as E_z^{ve}. In figure 5-2a, Bannister's total field result for H_φ^{ve} agrees to within 1 dB of the spherical waveguide formula for ρ_a = 1.89 Mm or equivalently, ρ = 18.13 Mm. In addition, Bannister's direct great-circle path formula for H_φ^{ve} agrees to within 1 dB of the spherical waveguide formula for ρ_a = 6.78 Mm or equivalently, ρ = 13.24 Mm. The poorer agreement in Bannister's total field result for H_φ^{ve} is because its range dependence is proportional to the first derivative of $P_\nu(-\cos\theta)$ as compared with E_z^{ve}, which has a range dependence that is directly proportional to $P_\nu(-\cos\theta)$. This observation is attributed to the fact that in the earth-flattening approximation for $P_\nu(-\cos\theta)$, each successive derivative introduces additional error into the approximation.

The phase plots for E_z^{ve} and H_φ^{ve}, given in figures 5-1b and 5-2b, respectively, show a similar comparison of Bannister's results with the spherical waveguide formulas as was observed for the field magnitudes. In figure 5-1b, Bannister's total field result for E_z^{ve} agrees to within 5° in phase of the spherical waveguide formula result for ρ_a = 1.35 Mm or, equivalently, ρ = 18.67 Mm. In figure 5-2b, Bannister's total field result for H_φ^{ve} agrees to within 5° in phase of the spherical waveguide formula result for ρ_a = 3.67 Mm or, equivalently, ρ = 16.35 Mm. Bannister's direct great-circle path formulas for E_z^{ve} and H_φ^{ve} agree to within 5° in phase of the corresponding spherical waveguide formula results for ρ_a = 7.29 Mm and ρ_a = 7.30 Mm, respectively. As expected, the phase results computed from Bannister's total field formulas agree more closely with the spherical waveguide formulas than do Bannister's direct great-circle path formulas.

Plots of the computed magnitudes and phases of the HED field components E_z^{he}, H_ρ^{he}, and H_φ^{he} under daytime propagation conditions at 76 Hz are given in figures 5-3, 5-4, and 5-5, respectively. The magnitude plots show that Bannister's total field results for E_z^{he}, H_ρ^{he}, and H_φ^{he} agree to within 1 dB of the corresponding spherical waveguide formula results for ρ_a = 1.89 Mm, ρ_a = 2.12 Mm, and ρ_a = 2.67 Mm, respectively. Note that the ranges of agreement for H_φ^{ve} and E_z^{he} are the same. This observation is not surprising because the range dependencies of these field components are each proportional to the first derivative of $P_\nu(-\cos\theta)$. The poorer agreement for H_φ^{he} is because its range dependence is proportional to the second derivative of $P_\nu(-\cos\theta)$, resulting in additional error in the earth-flattening approximation.

In figures 5-3a, 5-4a, and 5-5a, Bannister's direct great-circle path results for E_z^{he}, H_ρ^{he}, and H_φ^{he} agree to within 1 dB of the corresponding spherical waveguide formula results for ρ_a = 6.78 Mm, ρ_a = 6.77 Mm, and ρ_a = 6.08 Mm, respectively. Note that the ranges of agreement for H_φ^{ve}, E_z^{he}, and H_ρ^{he} are nearly identical because the formulas have the same range dependence. Surprisingly, H_φ^{he} shows a better agreement with the spherical waveguide formulas than the other direct great-circle path field components.

The phase plots for E_z^{he}, H_ρ^{he}, and H_φ^{he}, given in figures 5-3b, 5-4b, and 5-5b, respectively, show a similar comparison of Bannister's results with the spherical waveguide formulas as was observed for the field magnitudes. In these plots, Bannister's total field results for E_z^{he}, H_ρ^{he}, and H_φ^{he} agree to within 5° in phase of the corresponding spherical waveguide formula results for ρ_a = 3.67 Mm, ρ_a = 3.67 Mm, and ρ_a = 6.14 Mm, respectively. Based on these comparisons, the phase agreement for each of these field components is worse than observed in the corresponding magnitude comparisons. Bannister's direct great-circle path formulas for E_z^{he}, H_ρ^{he}, and H_φ^{he} agree to within 5° in phase of the corresponding spherical waveguide formula results for ρ_a = 7.30 Mm, ρ_a = 7.31 Mm, and ρ_a = 9.56 Mm, respectively. As was observed for the VED fields, the phase results computed from Bannister's total field HED formulas agree more closely with the spherical waveguide formulas than do Bannister's direct great-circle path formulas.

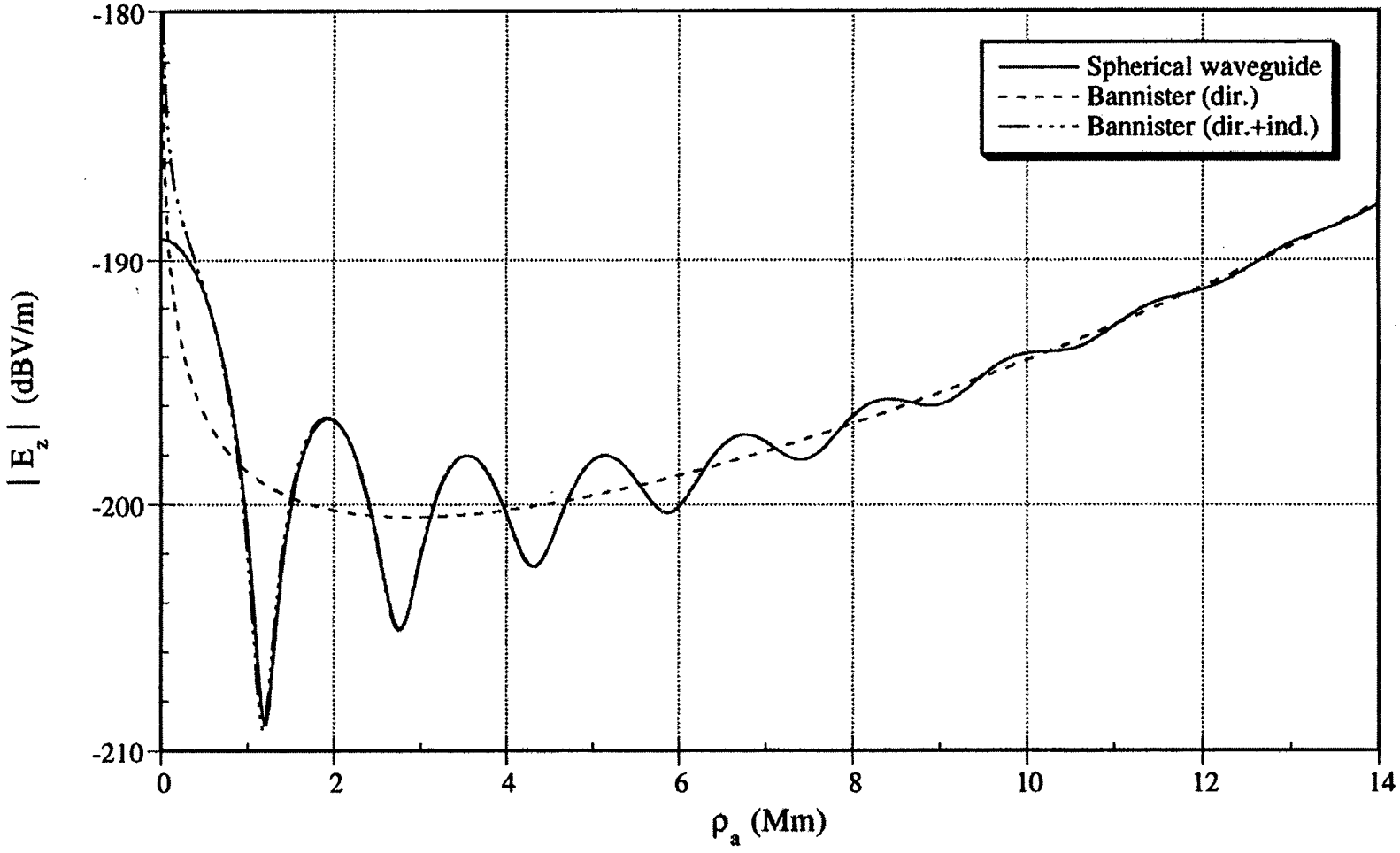

Figure 5-1a. Comparison of Spherical Waveguide and Bannister's ELF Propagation Formulas for the Magnitude of the Vertical Electric Field Produced by a VED Under Typical Daytime Propagation Conditions at 76 Hz

(The propagation parameters are c/v = 1.25, α = 1.4 dB/Mm, h = 53.5 km, and the dipole moment is p = 1 Am.)

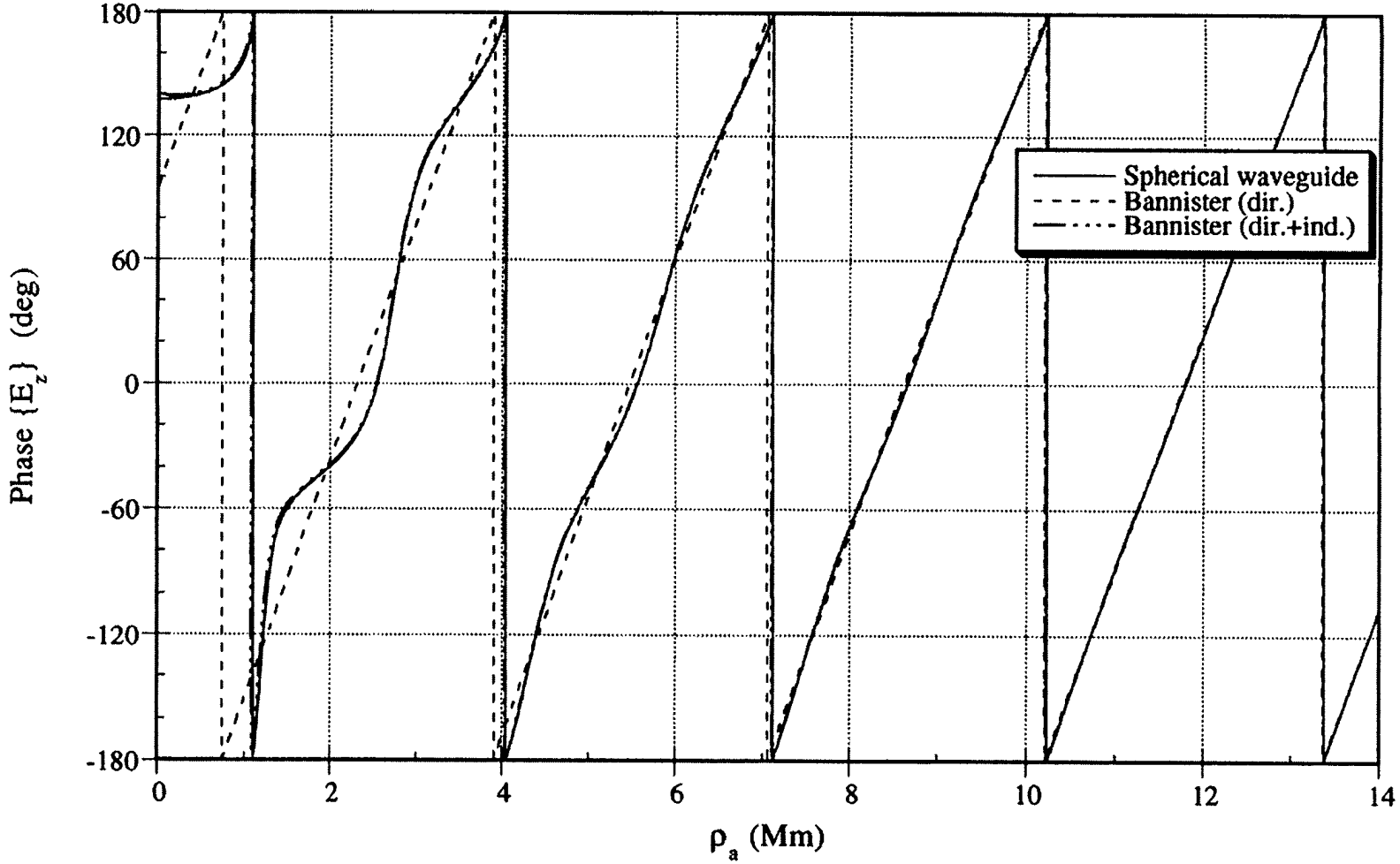

Figure 5-1b. Comparison of Spherical Waveguide and Bannister's ELF Propagation Formulas for the Phase of the Vertical Electric Field Produced by a VED Under Typical Daytime Propagation Conditions at 76 Hz

(The propagation parameters are $c/v = 1.25$, $\alpha = 1.4$ dB/Mm, $h = 53.5$ km, and the dipole moment is $p = 1$ Am.)

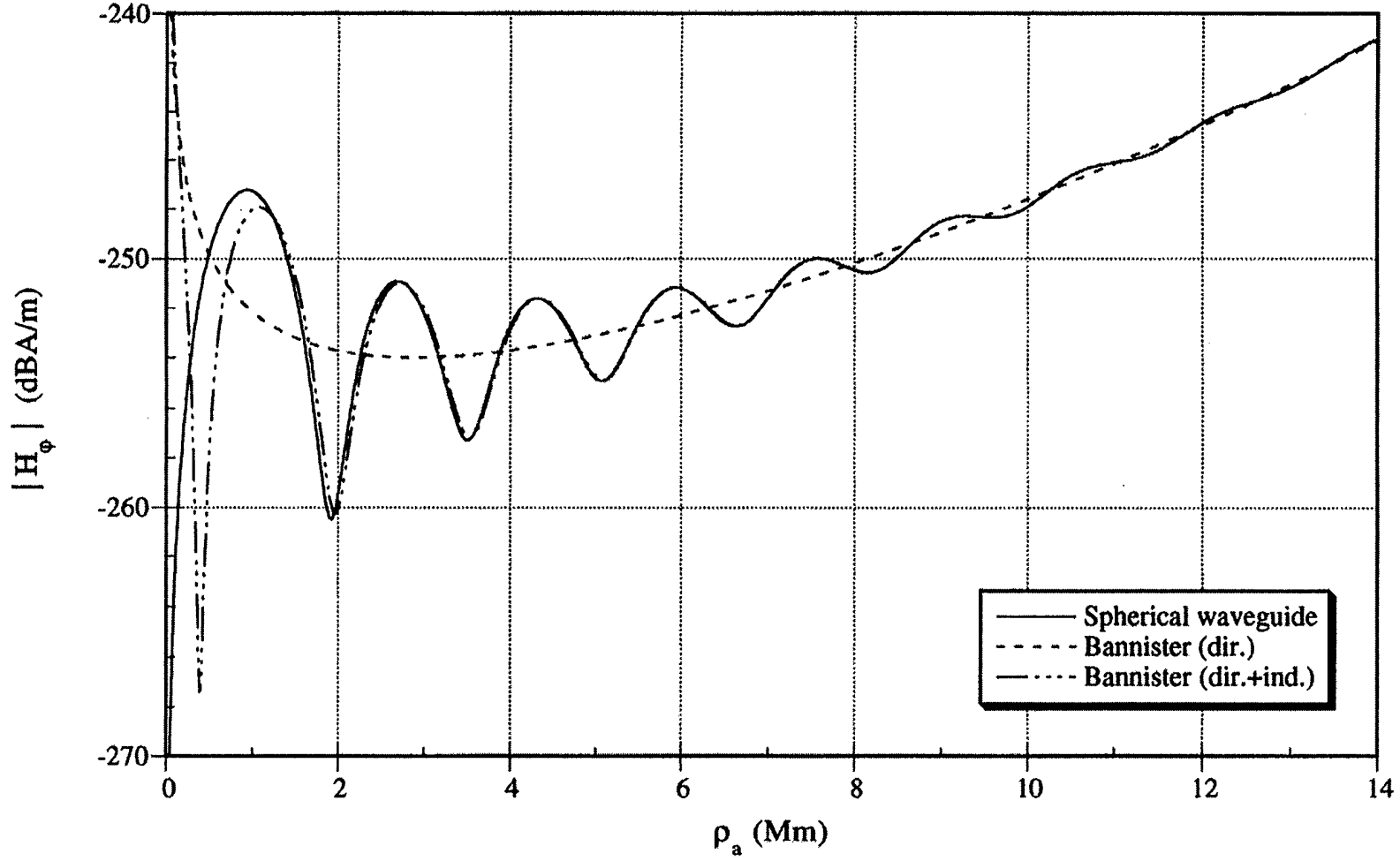

Figure 5-2a. Comparison of Spherical Waveguide and Bannister's ELF Propagation Formulas for the Magnitude of the Azimuthal Magnetic Field Produced by a VED Under Typical Daytime Propagation Conditions at 76 Hz

(The propagation parameters are $c/v = 1.25$, $\alpha = 1.4$ dB/Mm, $h = 53.5$ km, and the dipole moment is $p = 1$ Am.)

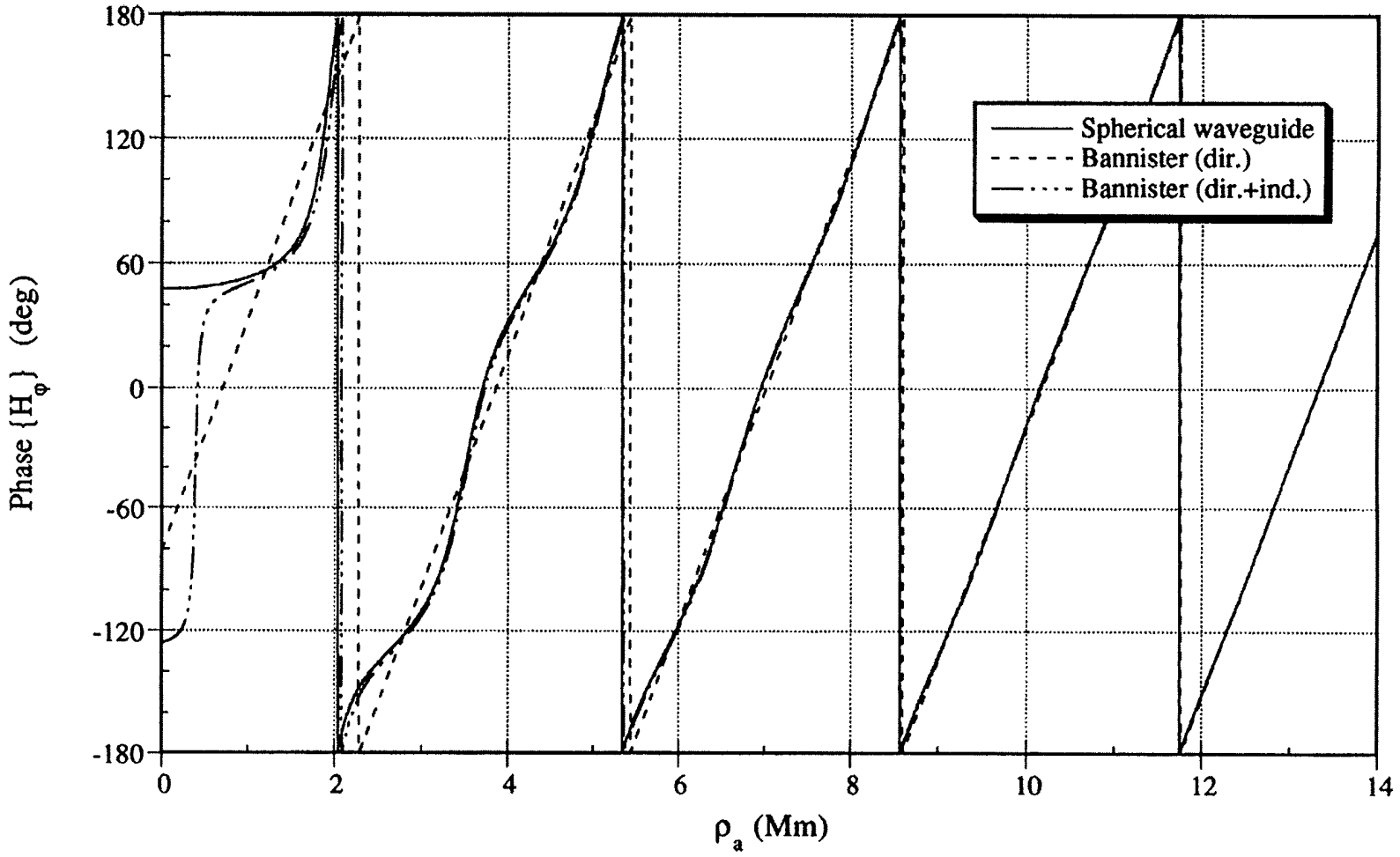

Figure 5-2b. Comparison of Spherical Waveguide and Bannister's ELF Propagation Formulas for the Phase of the Azimuthal Magnetic Field Produced by a VED Under Typical Daytime Propagation Conditions at 76 Hz

(The propagation parameters are $c/v = 1.25$, $\alpha = 1.4$ dB/Mm, $h = 53.5$ km, and the dipole moment is $p = 1$ Am.)

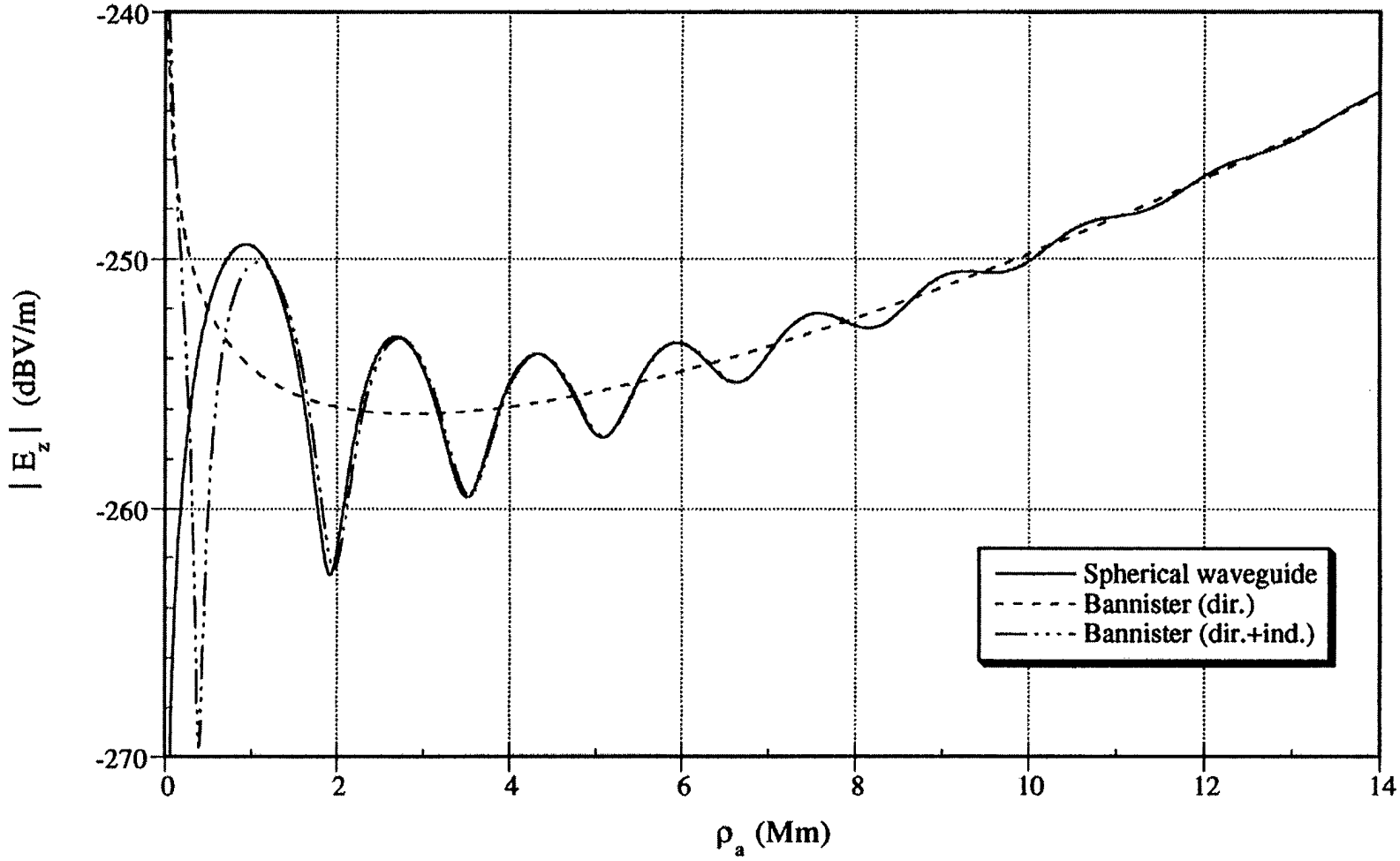

Figure 5-3a. Comparison of Spherical Waveguide and Bannister's ELF Propagation Formulas for the Magnitude of the Vertical Electric Field Produced by a HED Under Typical Daytime Propagation Conditions at 76 Hz

(The propagation parameters are $c/v = 1.25$, $\alpha = 1.4$ dB/Mm, $h = 53.5$ km; the azimuthal angle is $\varphi = 0°$; and the dipole moment is $p = 1$ Am.)

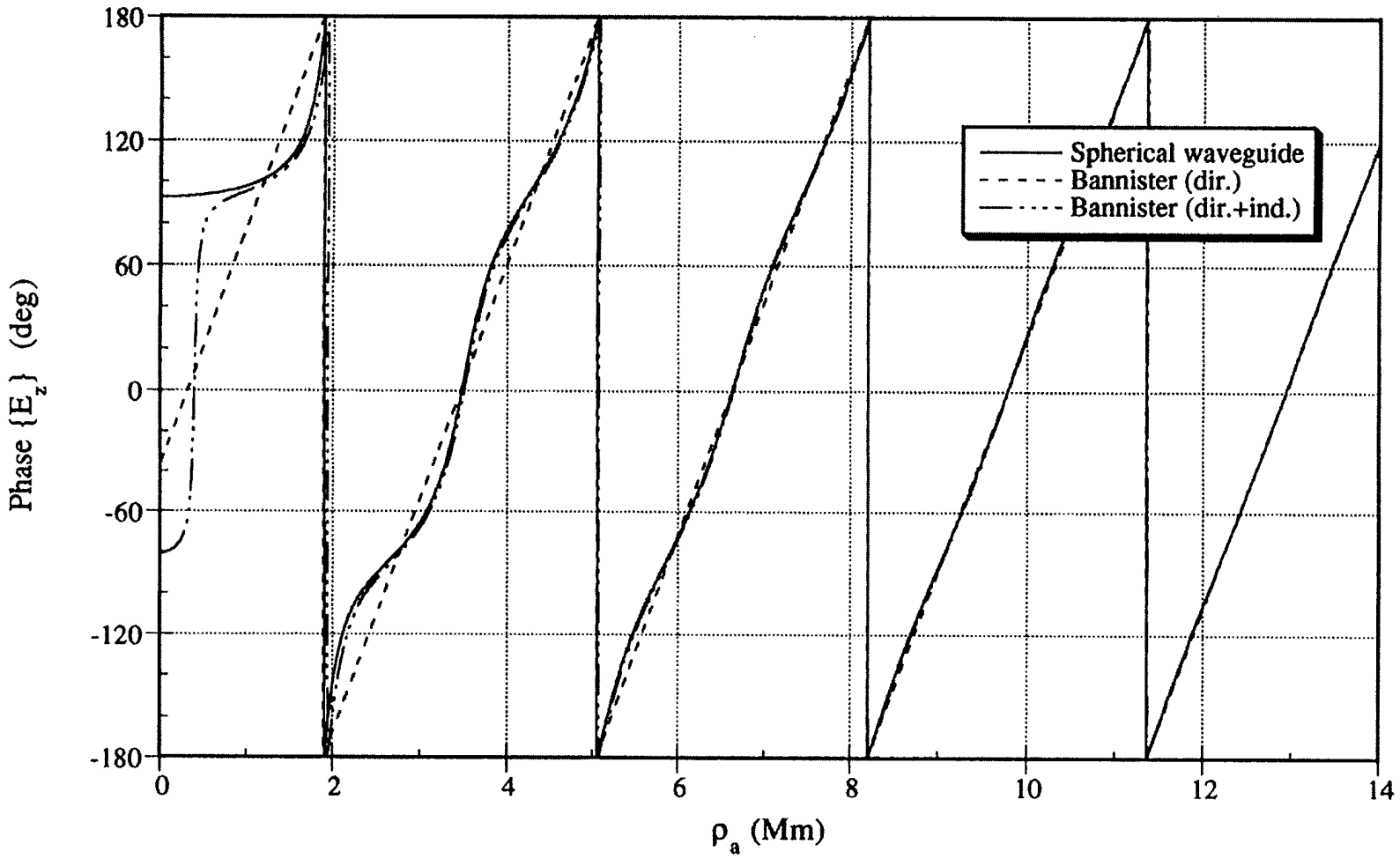

Figure 5-3b. Comparison of Spherical Waveguide and Bannister's ELF Propagation Formulas for the Phase of the Vertical Electric Field Produced by a HED Under Typical Daytime Propagation Conditions at 76 Hz

(The propagation parameters are $c/v = 1.25$, $\alpha = 1.4$ dB/Mm, $h = 53.5$ km; the azimuthal angle is $\varphi = 0°$; and the dipole moment is $p = 1$ Am.)

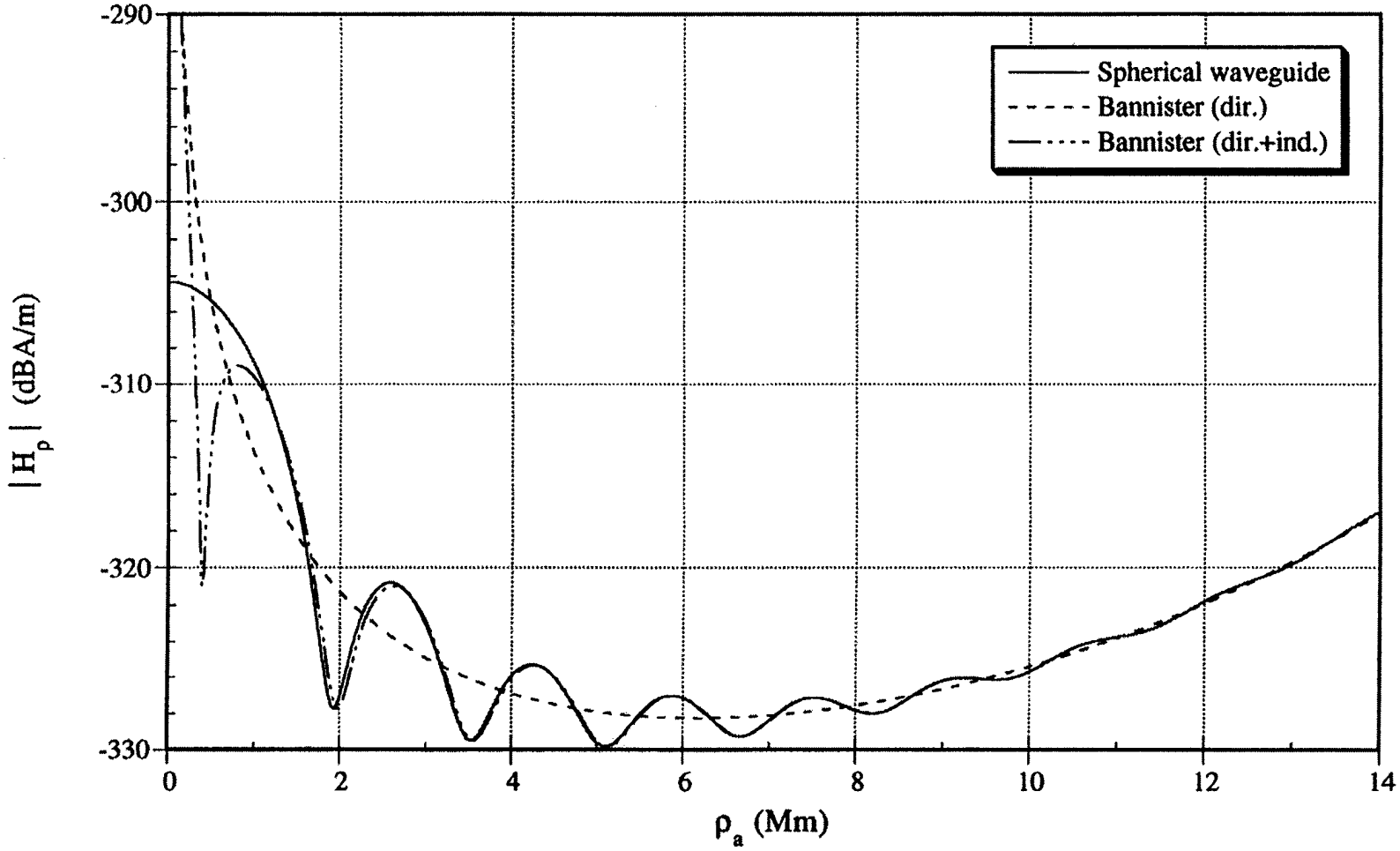

Figure 5-4a. Comparison of Spherical Waveguide and Bannister's ELF Propagation Formulas for the Magnitude of the Radial Magnetic Field Produced by a HED Under Typical Daytime Propagation Conditions at 76 Hz

(The propagation parameters are $c/v = 1.25$, $\alpha = 1.4$ dB/Mm, $h = 53.5$ km; the azimuthal angle is $\varphi = 90°$; and the dipole moment is $p = 1$ Am.)

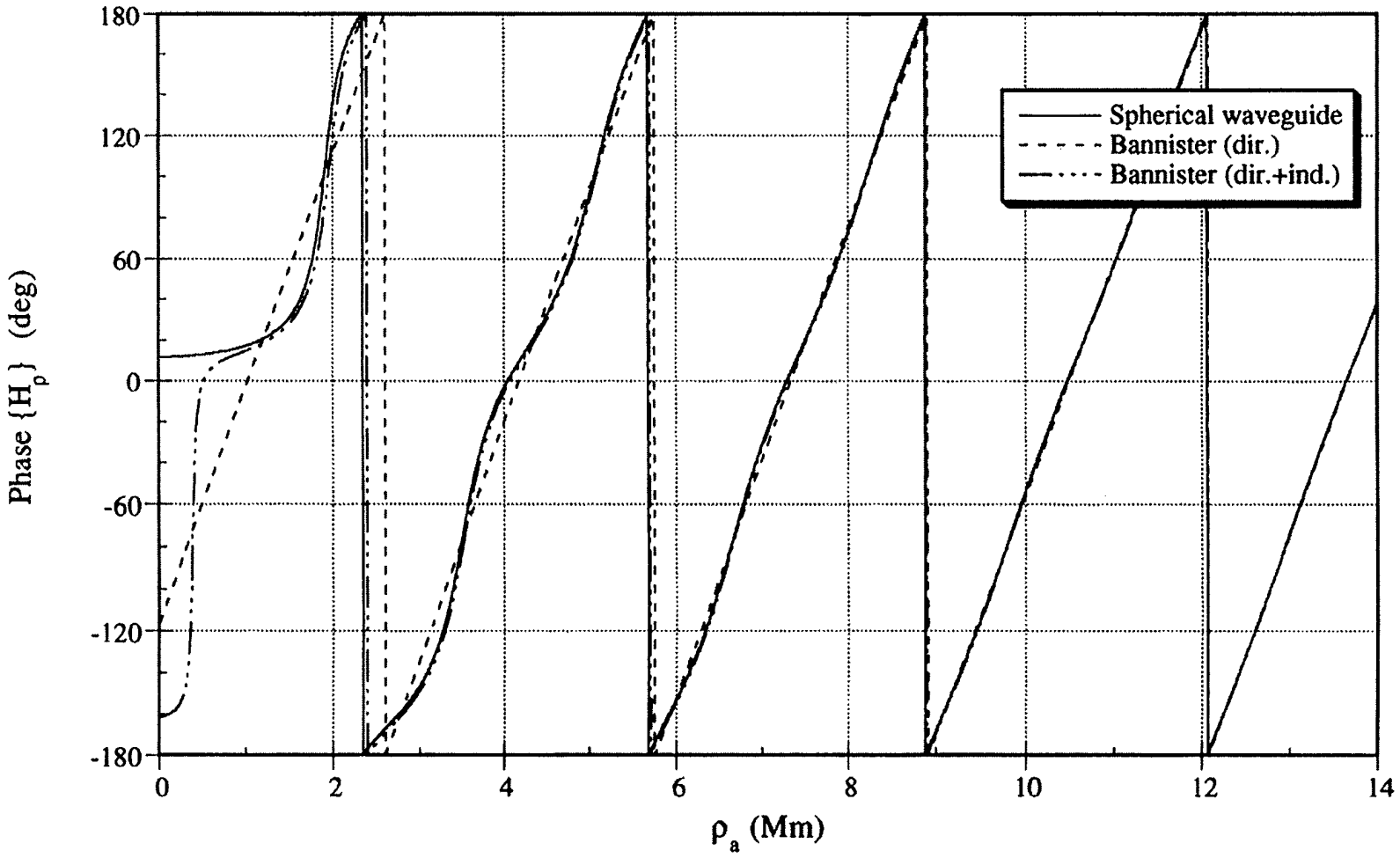

Figure 5-4b. Comparison of Spherical Waveguide and Bannister's ELF Propagation Formulas for the Phase of the Radial Magnetic Field Produced by a HED Under Typical Daytime Propagation Conditions at 76 Hz

(The propagation parameters are $c/v = 1.25$, $\alpha = 1.4$ dB/Mm, $h = 53.5$ km; the azimuthal angle is $\varphi = 90°$; and the dipole moment is $p = 1$ Am.)

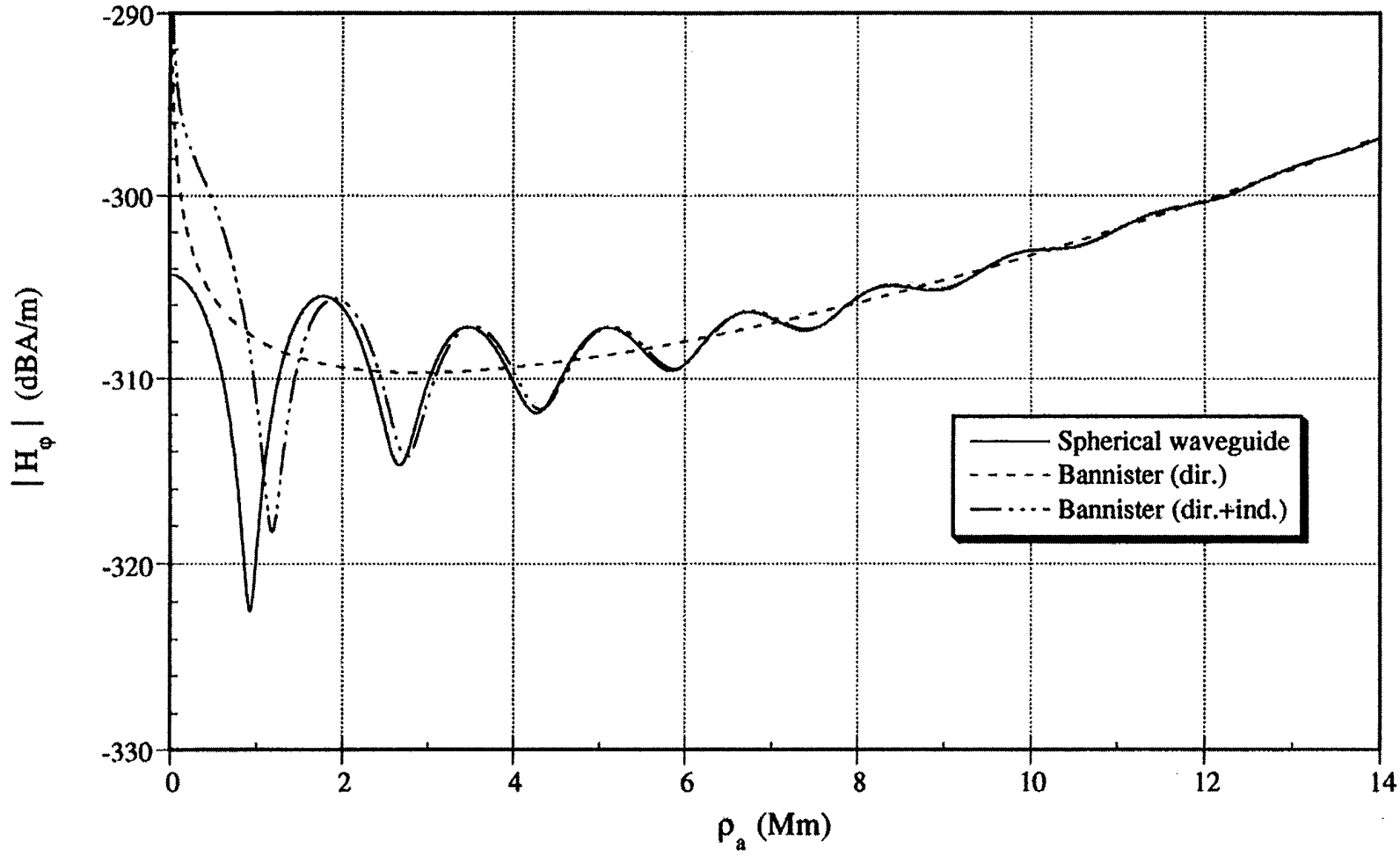

Figure 5-5a. Comparison of Spherical Waveguide and Bannister's ELF Propagation Formulas for the Magnitude of the Azimuthal Magnetic Field Produced by a HED Under Typical Daytime Propagation Conditions at 76 Hz

(The propagation parameters are $c/v = 1.25$, $\alpha = 1.4$ dB/Mm, $h = 53.5$ km; the azimuthal angle is $\varphi = 0°$; and the dipole moment is $p = 1$ Am.)

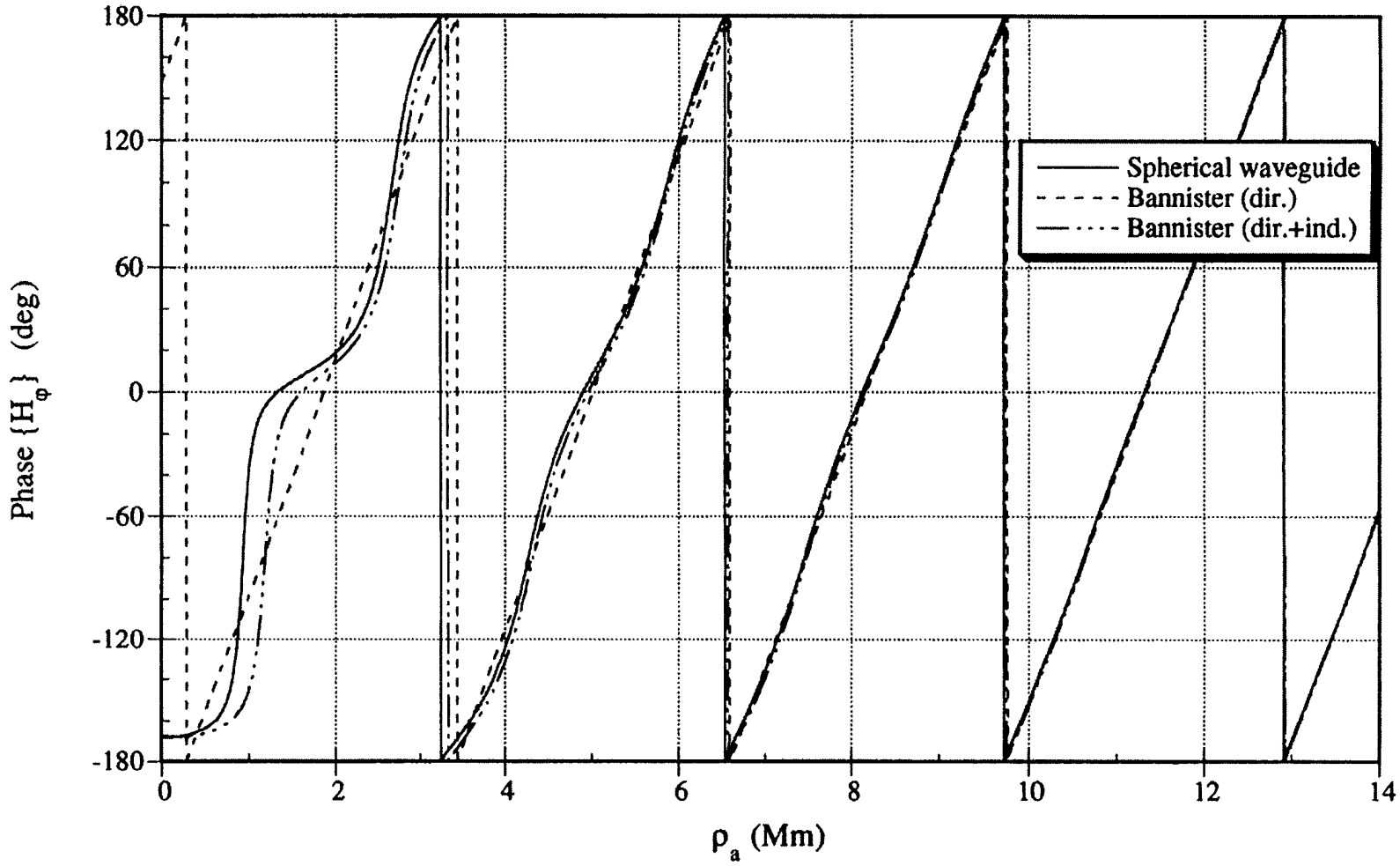

Figure 5-5b. Comparison of Spherical Waveguide and Bannister's ELF Propagation Formulas for the Phase of the Azimuthal Magnetic Field Produced by a HED Under Typical Daytime Propagation Conditions at 76 Hz

(The propagation parameters are $c/v = 1.25$, $\alpha = 1.4$ dB/Mm, $h = 53.5$ km; the azimuthal angle is $\varphi = 0°$; and the dipole moment is $p = 1$ Am.)

Plots of the computed magnitudes of the VED field components E_z^{ve} and H_φ^{ve} under typical nighttime propagation conditions at 76 Hz are given in figures 5-6a and 5-6b, respectively. Similar plots of the computed magnitudes of the HED field components E_z^{he}, H_ρ^{he}, and H_φ^{he} under typical nighttime propagation conditions at 76 Hz are given in figures 5-7a, 5-7b, and 5-7c, respectively. In these plots, Bannister's total field results for E_z^{ve}, H_φ^{ve}, E_z^{he}, H_ρ^{he}, and H_φ^{he} agree to within 1 dB of the corresponding spherical waveguide formula results for $\rho_a \geq 1.49$ Mm, $\rho_a \geq 2.50$ Mm, $\rho_a \geq 2.50$ Mm, $\rho_a \geq 2.51$ Mm, and $\rho_a \geq 3.47$ Mm, respectively. Although these agreements are not quite as good as the corresponding daytime propagation results, they follow the same trend. In comparison, Bannister's direct great-circle path field results for E_z^{ve}, H_φ^{ve}, E_z^{he}, H_ρ^{he}, and H_φ^{he} agree to within 1 dB of the corresponding spherical waveguide formula results for $\rho_a \geq 10.20$ Mm, $\rho_a \geq 10.24$ Mm, $\rho_a \geq 10.24$ Mm, $\rho_a \geq 10.25$ Mm, and $\rho_a \geq 10.21$ Mm, respectively. These ranges of agreement are considerably worse than what was observed for the direct great-circle path field results under daytime conditions. This observation is attributed to the lower attenuation at nighttime which results in an interference pattern from the two great-circle path fields that extends to greater distances from the antipode.

A summary listing of the ranges over which Bannister's direct great-circle path and total field formulas agree to within 1 dB in magnitude of the corresponding spherical waveguide formulas are given in tables 5-2a and 5-2b, respectively, for both typical daytime and nighttime propagation conditions at 76 Hz. In these tables, the normalized range $\beta\rho_a$ is included in parentheses, where $\beta = \mathrm{Re}\{k\} = 2\pi/\lambda$ is the phase constant of the quasi-TEM wave and λ is the corresponding wavelength. (Normalized ranges will be discussed later in this section.)

A comparison of these tables clearly shows that Bannister's total field formulas have a much greater range of agreement with the spherical waveguide formulas than do Bannister's direct great-circle path formulas. From table 5-2a, the ranges of satisfactory agreement for Bannister's direct great-circle path formulas extend from $\rho_a \geq 6.08$ Mm to $\rho_a \geq 10.25$ Mm, depending on the field component and propagation condition. In comparison, from table 5-2b, the ranges of satisfactory agreement for Bannister's total field formulas extend from $\rho_a \geq 1.15$ Mm to $\rho_a \geq 3.47$ Mm. As previously mentioned, the poorer agreement observed for Bannister's direct great-circle path formulas is attributed to their inability to predict the interference produced by the superposition of the direct and indirect great-circle path fields.

Table 5-2a. Ranges Over Which Bannister's Direct Great-Circle Path Field Formulas Agree to Within 1 dB in Magnitude of the Spherical Waveguide Formulas at 76 Hz

Field Component	Propagation Condition	Range
E_z^{ve}	Daytime	$\rho_a \geq 6.09$ Mm $(\beta\rho_a \geq 12.13)$
	Nighttime	$\rho_a \geq 10.20$ Mm $(\beta\rho_a \geq 18.20)$
H_φ^{ve}	Daytime	$\rho_a \geq 6.78$ Mm $(\beta\rho_a \geq 13.50)$
	Nighttime	$\rho_a \geq 10.24$ Mm $(\beta\rho_a \geq 18.27)$
E_z^{he}	Daytime	$\rho_a \geq 6.78$ Mm $(\beta\rho_a \geq 13.50)$
	Nighttime	$\rho_a \geq 10.24$ Mm $(\beta\rho_a \geq 18.27)$
H_ρ^{he}	Daytime	$\rho_a \geq 6.77$ Mm $(\beta\rho_a \geq 13.48)$
	Nighttime	$\rho_a \geq 10.25$ Mm $(\beta\rho_a \geq 18.29)$
H_φ^{he}	Daytime	$\rho_a \geq 6.08$ Mm $(\beta\rho_a \geq 12.11)$
	Nighttime	$\rho_a \geq 10.21$ Mm $(\beta\rho_a \geq 18.21)$

Table 5-2b. Ranges Over Which Bannister's Total Field Formulas Agree to Within 1 dB in Magnitude of the Spherical Waveguide Formulas at 76 Hz

Field Component	Propagation Condition	Range
E_z^{ve}	Daytime	$\rho_a \geq 1.15$ Mm $(\beta\rho_a \geq 2.29)$
	Nighttime	$\rho_a \geq 1.49$ Mm $(\beta\rho_a \geq 2.66)$
H_φ^{ve}	Daytime	$\rho_a \geq 1.89$ Mm $(\beta\rho_a \geq 3.76)$
	Nighttime	$\rho_a \geq 2.50$ Mm $(\beta\rho_a \geq 4.46)$
E_z^{he}	Daytime	$\rho_a \geq 1.89$ Mm $(\beta\rho_a \geq 3.76)$
	Nighttime	$\rho_a \geq 2.50$ Mm $(\beta\rho_a \geq 4.46)$
H_ρ^{he}	Daytime	$\rho_a \geq 2.12$ Mm $(\beta\rho_a \geq 4.22)$
	Nighttime	$\rho_a \geq 2.51$ Mm $(\beta\rho_a \geq 4.48)$
H_φ^{he}	Daytime	$\rho_a \geq 2.67$ Mm $(\beta\rho_a \geq 5.32)$
	Nighttime	$\rho_a \geq 3.47$ Mm $(\beta\rho_a \geq 6.19)$

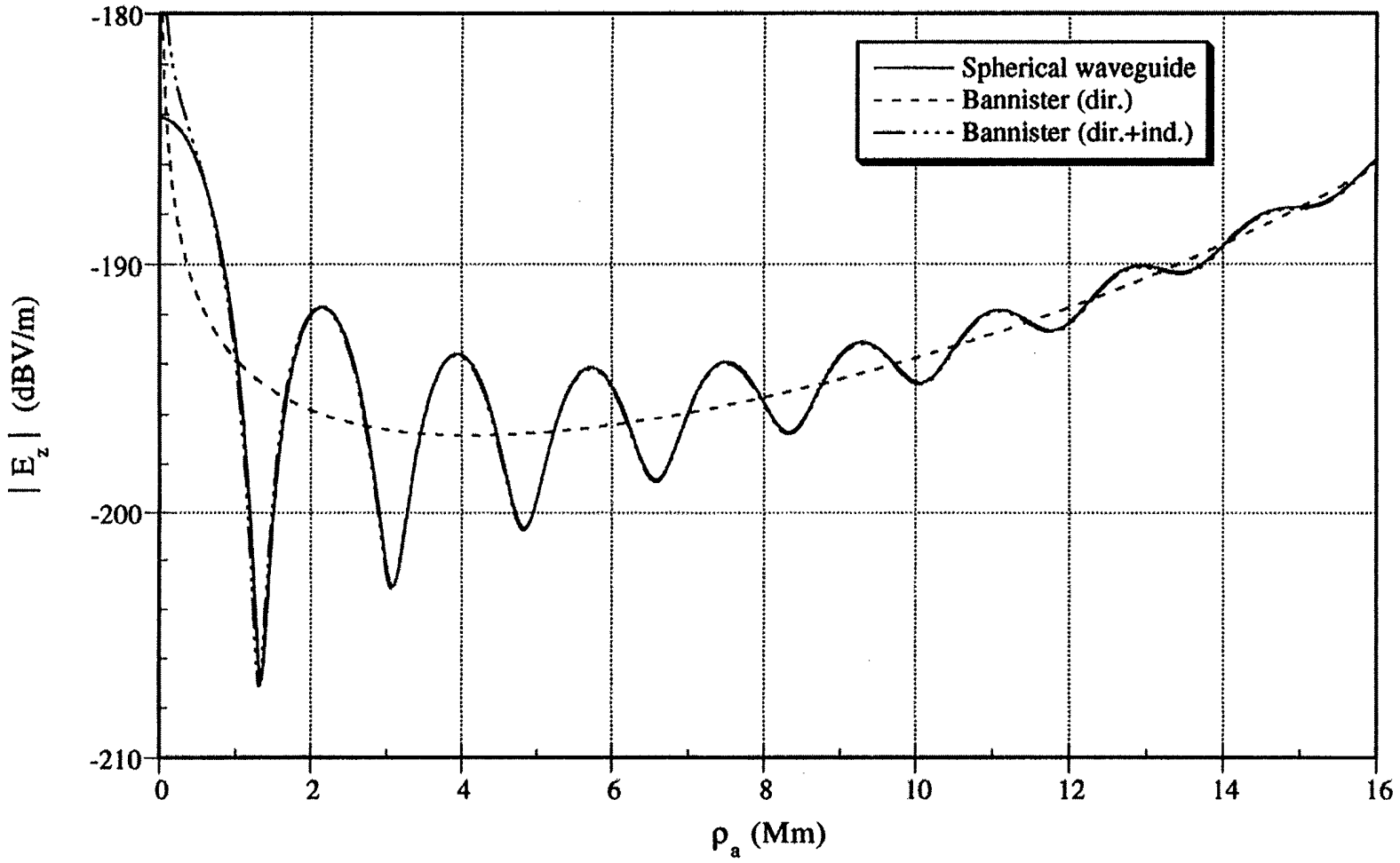

Figure 5-6a. Comparison of Spherical Waveguide and Bannister's ELF Propagation Formulas for the Magnitude of the Vertical Electric Field Produced by a VED Under Typical Nighttime Propagation Conditions at 76 Hz

(The propagation parameters are $c/v = 1.12$, $\alpha = 0.9$ dB/Mm, $h = 77$ km, and the dipole moment is $p = 1$ Am.)

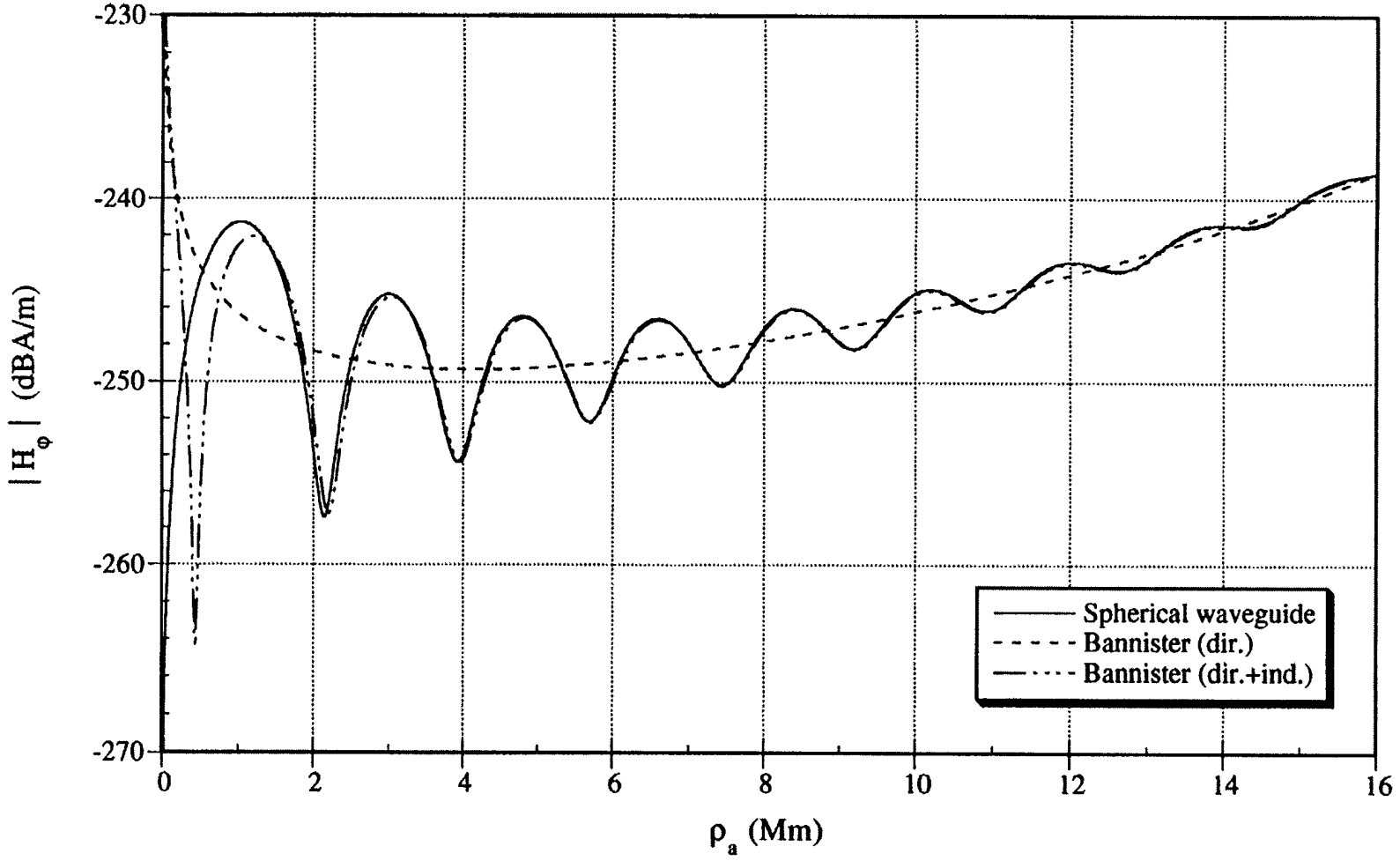

Figure 5-6b. Comparison of Spherical Waveguide and Bannister's ELF Propagation Formulas for the Magnitude of the Azimuthal Magnetic Field Produced by a VED Under Typical Nighttime Propagation Conditions at 76 Hz

(The propagation parameters are $c/v = 1.12$, $\alpha = 0.9$ dB/Mm, $h = 77$ km, and the dipole moment is $p = 1$ Am.)

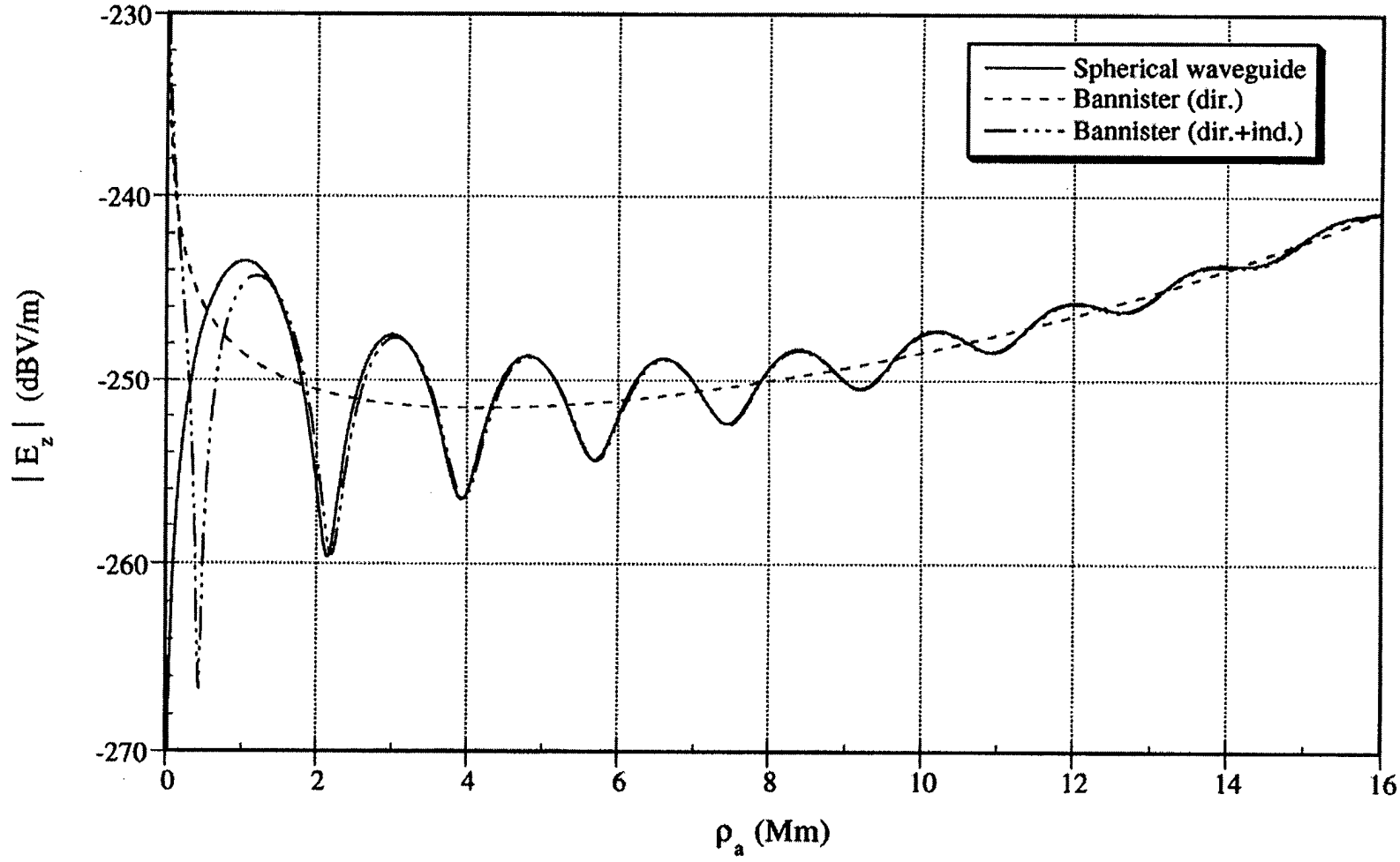

Figure 5-7a. Comparison of Spherical Waveguide and Bannister's ELF Propagation Formulas for the Magnitude of the Vertical Electric Field Produced by a HED Under Typical Nighttime Propagation Conditions at 76 Hz

(The propagation parameters are $c/v = 1.12$, $\alpha = 0.9$ dB/Mm, $h = 77$ km; the azimuthal angle is $\varphi = 0°$; and the dipole moment is $p = 1$ Am.)

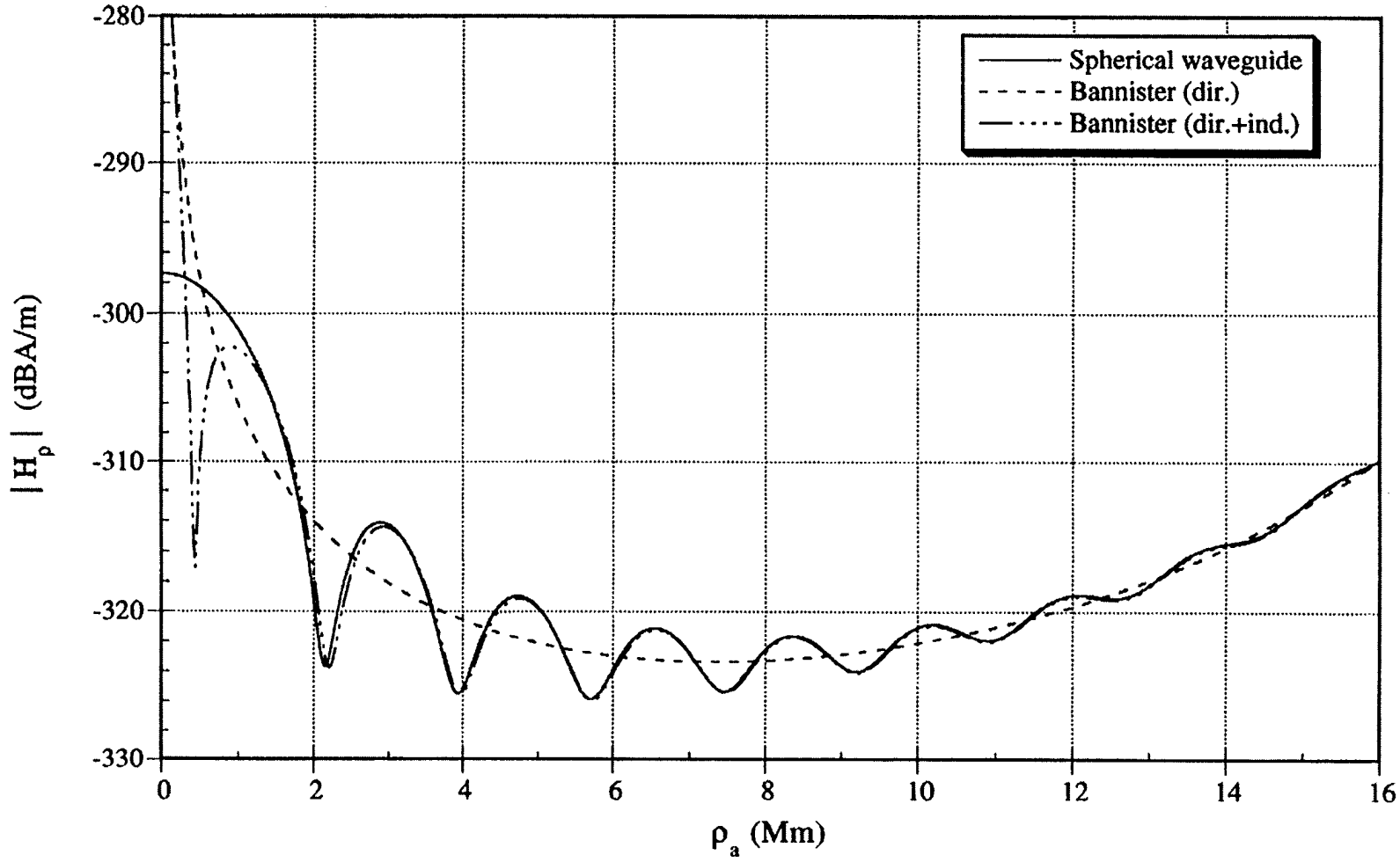

Figure 5-7b. Comparison of Spherical Waveguide and Bannister's ELF Propagation Formulas for the Magnitude of the Radial Magnetic Field Produced by a HED Under Typical Nighttime Propagation Conditions at 76 Hz

(The propagation parameters are $c/v = 1.12$, $\alpha = 0.9$ dB/Mm, $h = 77$ km; the azimuthal angle is $\varphi = 90°$; and the dipole moment is $p = 1$ Am.)

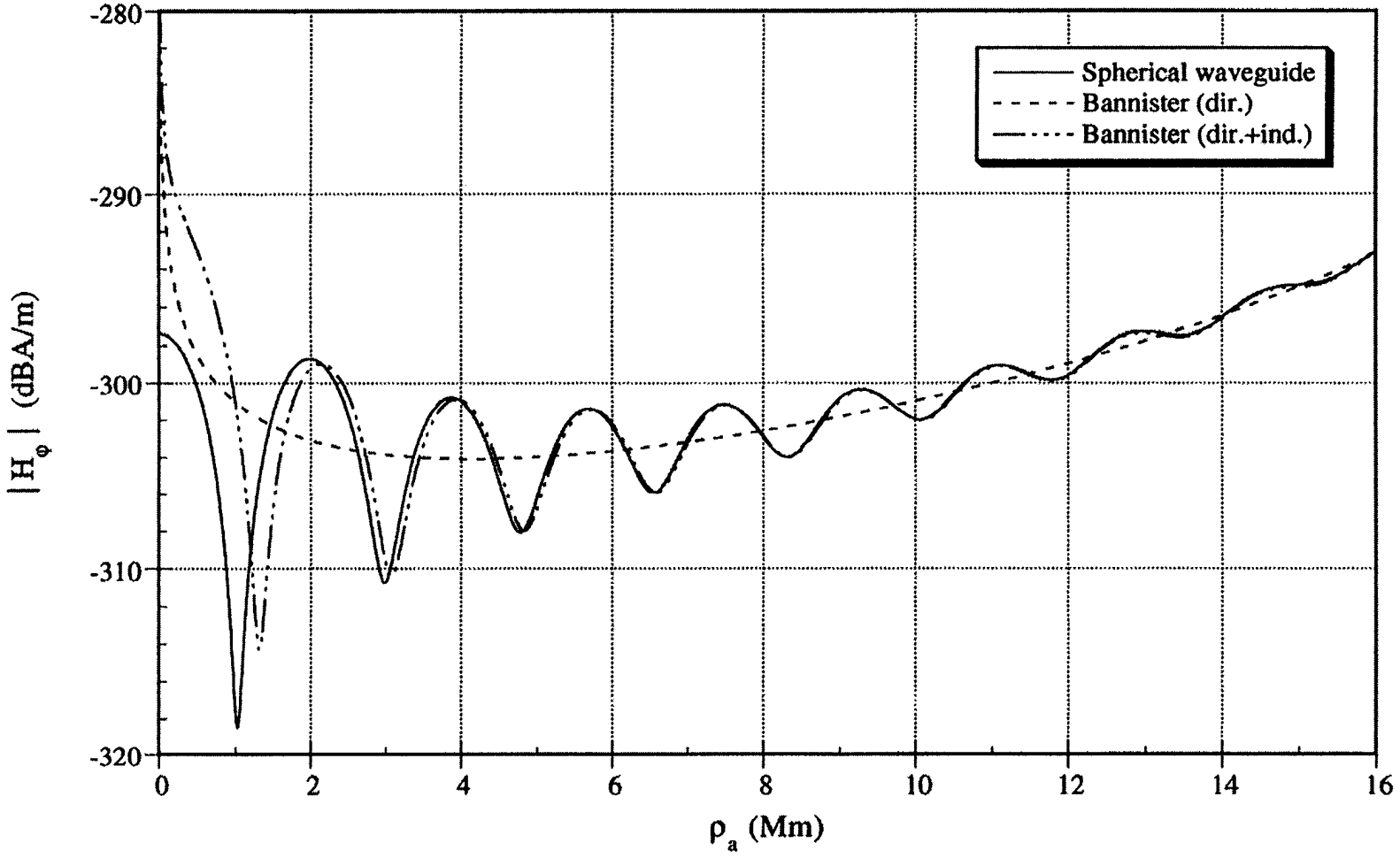

Figure 5-7c. Comparison of Spherical Waveguide and Ban`nister's ELF Propagation Formulas for the Magnitude of the Azimuthal Magnetic Field Produced by a HED Under Typical Nighttime Propagation Conditions at 76 Hz

(The propagation parameters are $c/v = 1.12$, $\alpha = 0.9$ dB/Mm, $h = 77$ km; the azimuthal angle is $\varphi = 0°$; and the dipole moment is $p = 1$ Am.)

5.2 RESULTS AT OTHER FREQUENCIES

In order to obtain a better assessment of the maximum ranges of validity of Bannister's propagation formulas, it is necessary to compare them with the spherical waveguide formulas at additional frequencies across the ELF band. Plots of the computed magnitudes and phases of the VED field components E_z^{ve} and H_φ^{ve} under typical daytime propagation conditions at 30 Hz are given in figures 5-8 and 5-9, respectively. Similar plots of the HED field components E_z^{he}, H_ρ^{he}, and H_φ^{he} under typical daytime propagation conditions at 30 Hz are given in figures 5-10, 5-11, and 5-12, respectively. A comparison of these plots with the corresponding 76-Hz graphs indicates that the 30-Hz field values are generally larger in magnitude, and the interference produced by the two great-circle path fields at 30 Hz extends to much greater distances from the antipode. These observations are the result of the lower attenuation at 30 Hz, which allows the indirect great-circle path fields to propagate over greater ranges from the source. At 30 Hz, Bannister's total field results for E_z^{ve}, H_φ^{ve}, E_z^{he}, H_ρ^{he}, and H_φ^{he} agree to within 1 dB of the corresponding spherical waveguide formula results for $\rho_a \geq 2.71$ Mm, $\rho_a \geq 4.55$ Mm, $\rho_a \geq 4.55$ Mm, $\rho_a \geq 4.52$ Mm, and $\rho_a \geq 6.44$ Mm, respectively. These results indicate that Bannister's total field formulas show a poorer agreement with the spherical waveguide formulas than the 76-Hz results. Similarly, Bannister's direct great-circle path formulas do not agree as well with the spherical waveguide formulas as at 76 Hz.

Magnitude plots of the HED field components E_z^{he}, H_ρ^{he}, and H_φ^{he} under typical nighttime propagation conditions at 30 Hz are given in figures 5-13a, 5-13b, and 5-13c, respectively. In these plots, Bannister's total field formulas for E_z^{he}, H_ρ^{he}, and H_φ^{he} agree to within 1 dB of the corresponding spherical waveguide formula results for $\rho_a \geq 2.76$ Mm, $\rho_a \geq 2.83$ Mm, and $\rho_a \geq 4.69$ Mm, respectively. Unlike the 76-Hz results, the 30-Hz data show that Bannister's total field formulas produce a better agreement with the spherical waveguide formulas at nighttime than in the daytime. The one exception to this observation is E_z^{ve}, which shows a worse agreement at nighttime. The general improvement in the nighttime results at 30 Hz is probably attributed to the larger nighttime attenuation as indicated in table 5-1.

Table 5-3 is a summary list of the ranges over which Bannister's total field formulas agree to within 1 dB in magnitude of the corresponding spherical waveguide formulas for both daytime and nighttime propagation conditions at 30 Hz. A comparison of tables 5-2b and 5-3 clearly shows that Bannister's total field results improve at the higher frequency.

Table 5-3. Ranges Over Which Bannister's Total Field Formulas Agree to Within 1 dB in Magnitude of the Spherical Waveguide Formulas at 30 Hz

Field Component	Propagation Condition	Range
E_z^{ve}	Daytime	$\rho_a \geq 2.71$ Mm $(\beta\rho_a \geq 2.23)$
	Nighttime	$\rho_a \geq 3.10$ Mm $(\beta\rho_a \geq 2.22)$
H_φ^{ve}	Daytime	$\rho_a \geq 4.55$ Mm $(\beta\rho_a \geq 3.75)$
	Nighttime	$\rho_a \geq 2.76$ Mm $(\beta\rho_a \geq 1.98)$
E_z^{he}	Daytime	$\rho_a \geq 4.55$ Mm $(\beta\rho_a \geq 3.75)$
	Nighttime	$\rho_a \geq 2.76$ Mm $(\beta\rho_a \geq 1.98)$
H_ρ^{he}	Daytime	$\rho_a \geq 4.52$ Mm $(\beta\rho_a \geq 3.72)$
	Nighttime	$\rho_a \geq 2.83$ Mm $(\beta\rho_a \geq 2.03)$
H_φ^{he}	Daytime	$\rho_a \geq 6.44$ Mm $(\beta\rho_a \geq 5.30)$
	Nighttime	$\rho_a \geq 4.69$ Mm $(\beta\rho_a \geq 3.36)$

Plots of the computed magnitudes of the field components E_z^{ve}, H_φ^{ve}, E_z^{he}, H_ρ^{he}, and H_φ^{he} under typical daytime propagation conditions at 300 Hz are given in figures 5-14a, 5-14b, 5-15a, 5-15b, and 5-15c, respectively. The plots show that the interference pattern produced by the superposition of the two great-circle path fields attenuates rapidly with distance from the antipode. This observation is the result of the large value of attenuation at this higher frequency. The plots also show that Bannister's formulas produce a better agreement with the corresponding spherical waveguide formulas than at the lower frequencies. In particular, Bannister's total field results for E_z^{ve}, H_φ^{ve}, E_z^{he}, H_ρ^{he}, and H_φ^{he} agree to within 1 dB of the corresponding spherical waveguide formula results for $\rho_a \geq 0.32$ Mm, $\rho_a \geq 0.59$ Mm, $\rho_a \geq 0.59$ Mm, $\rho_a \geq 0.59$ Mm, and $\rho_a \geq 0.82$ Mm, respectively. Bannister's direct great-circle path formulas also produce a better agreement with the spherical waveguide formulas at 300 Hz than at 30 Hz and 76 Hz because the interference pattern does not extend to as great of a distance from the antipode as at the lower frequencies.

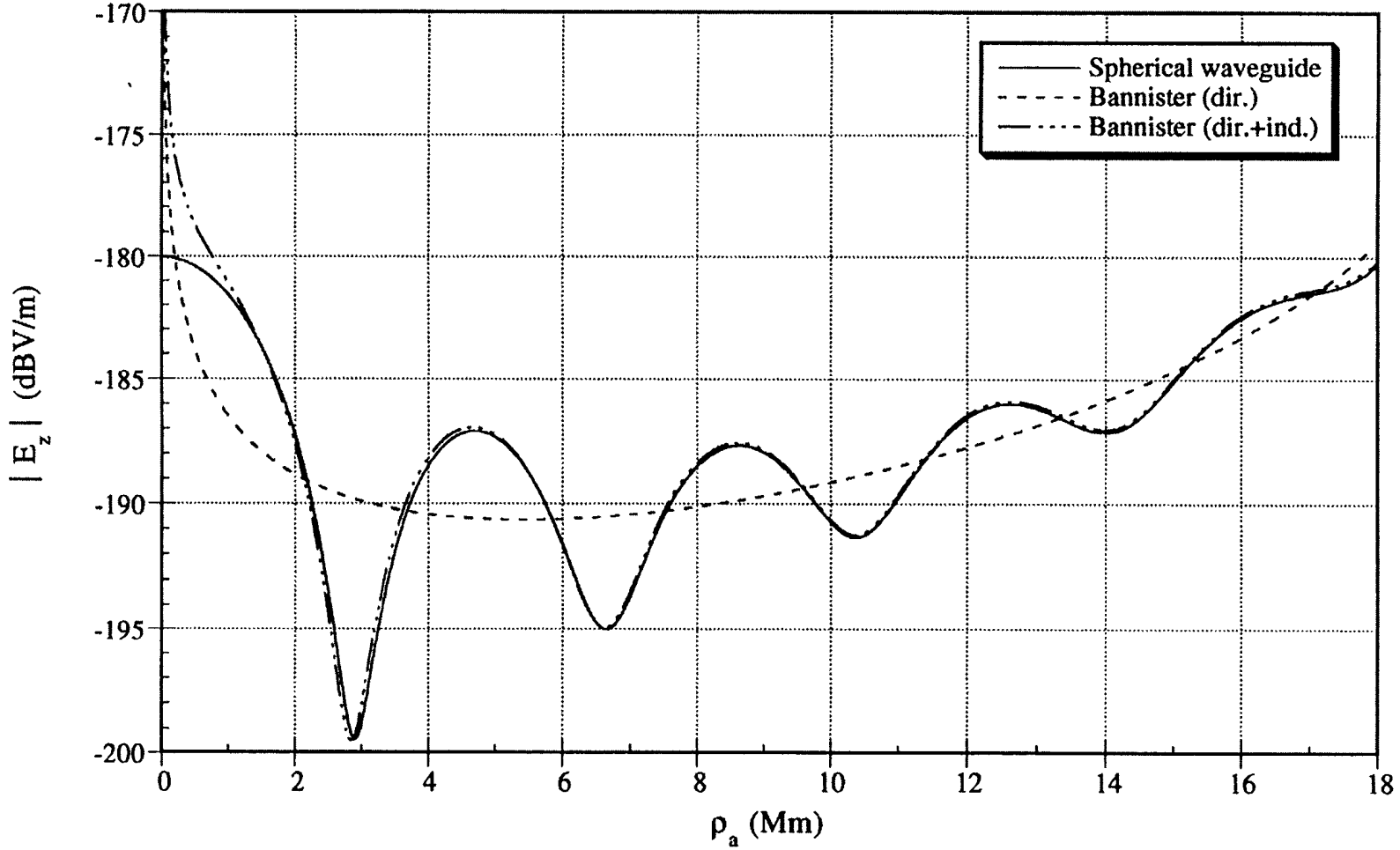

Figure 5-8a. Comparison of Spherical Waveguide and Bannister's ELF Propagation Formulas for the Magnitude of the Vertical Electric Field Produced by a VED Under Typical Daytime Propagation Conditions at 30 Hz

(The propagation parameters are $c/v = 1.31$, $\alpha = 0.6$ dB/Mm, $h = 51$ km, and the dipole moment is $p = 1$ Am.)

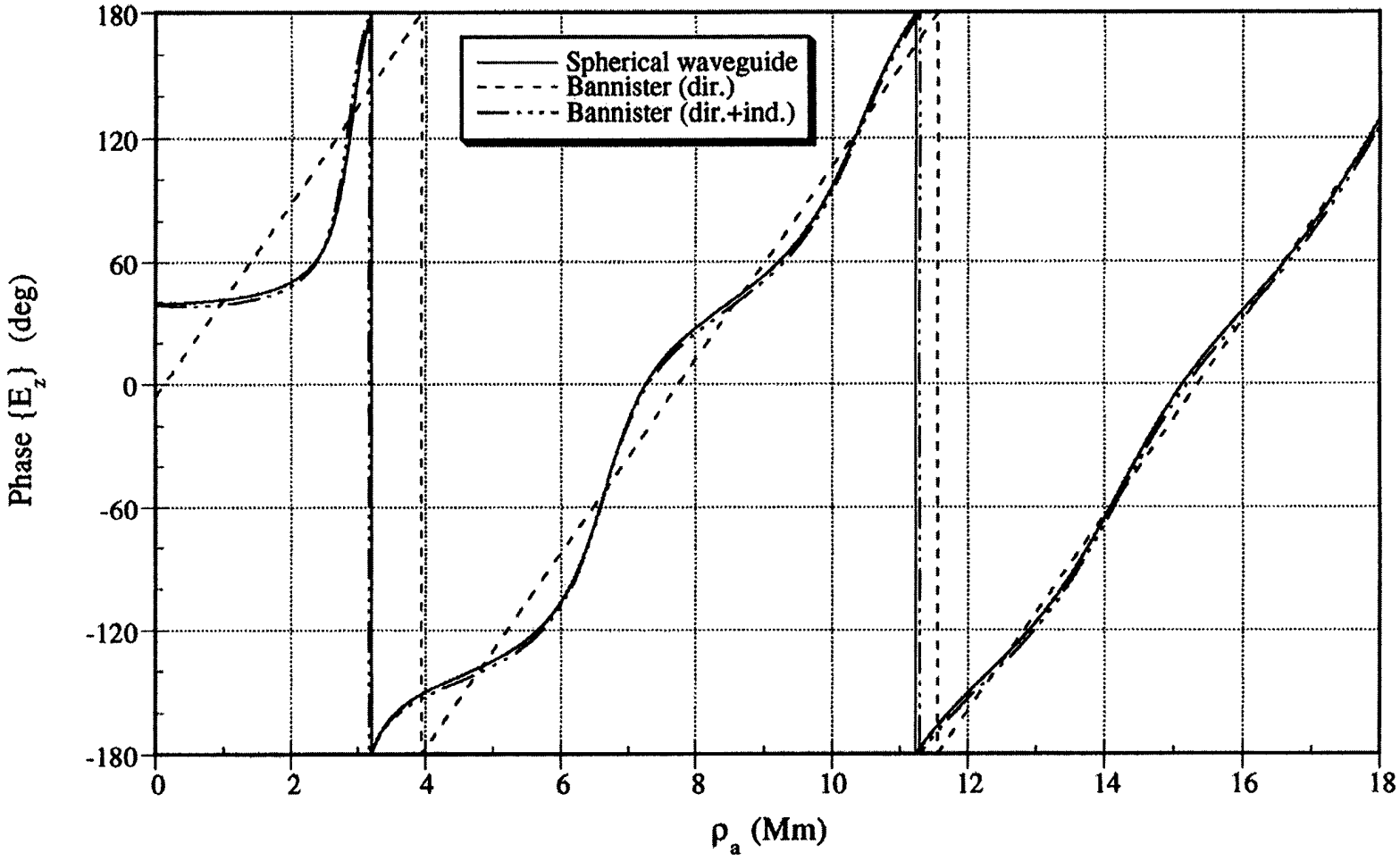

Figure 5-8b. Comparison of Spherical Waveguide and Bannister's ELF Propagation Formulas for the Phase of the Vertical Electric Field Produced by a VED Under Typical Daytime Propagation Conditions at 30 Hz

(The propagation parameters are $c/v = 1.31$, $\alpha = 0.6$ dB/Mm, $h = 51$ km, and the dipole moment is $p = 1$ Am.)

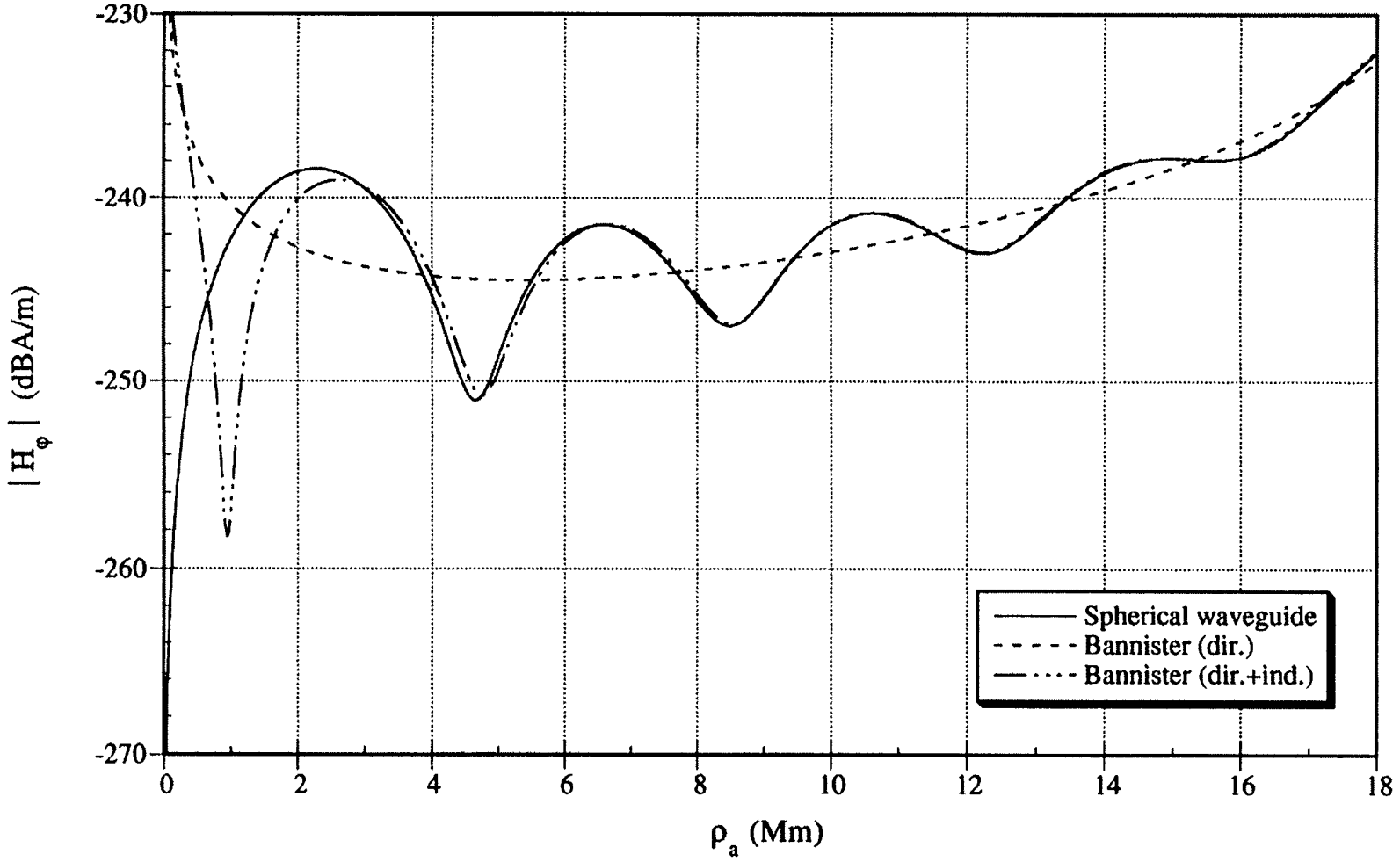

Figure 5-9a. Comparison of Spherical Waveguide and Bannister's ELF Propagation Formulas for the Magnitude of the Azimuthal Magnetic Field Produced by a VED Under Typical Daytime Propagation Conditions at 30 Hz

(The propagation parameters are $c/v = 1.31$, $\alpha = 0.6$ dB/Mm, $h = 51$ km, and the dipole moment is $p = 1$ Am.)

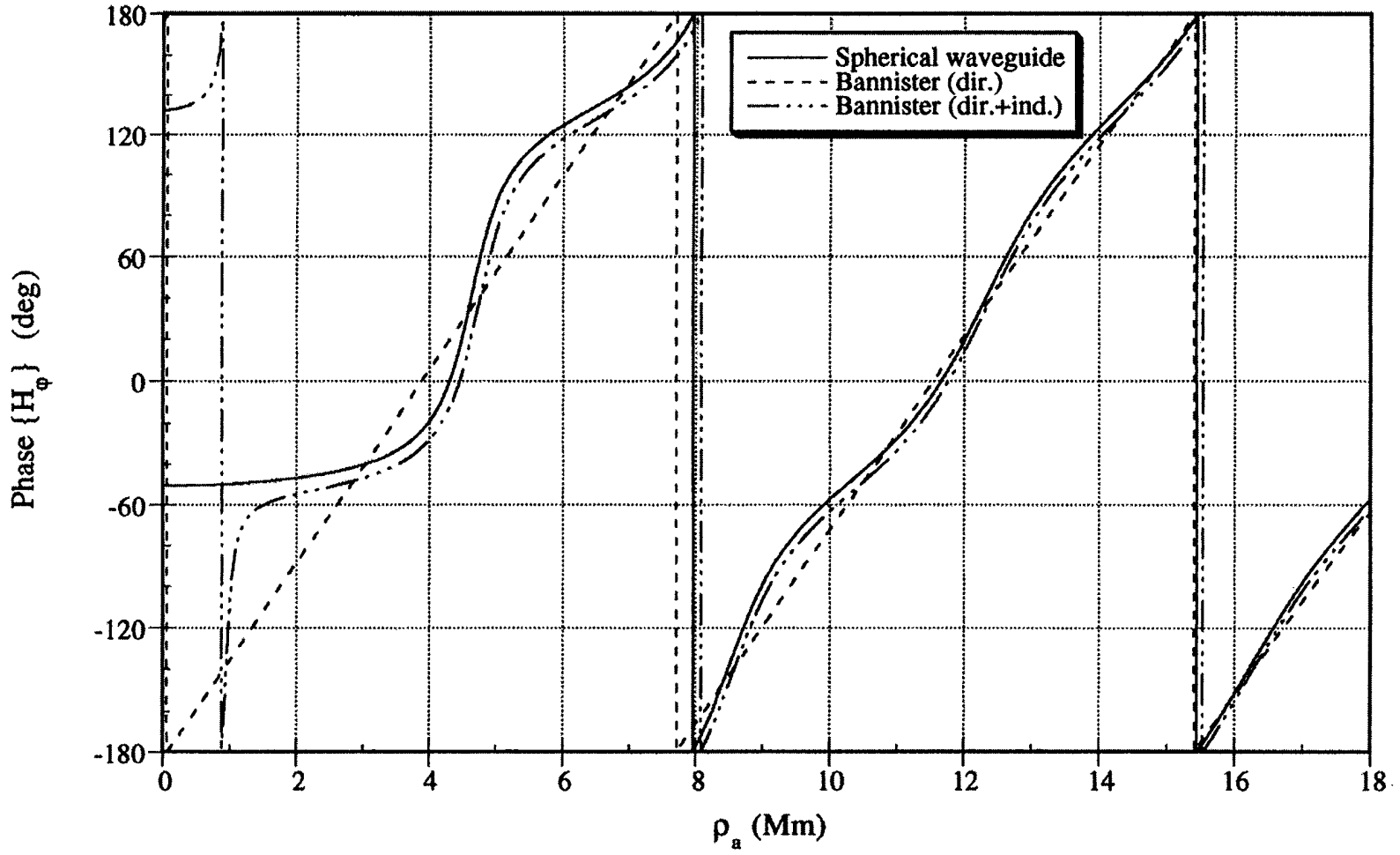

Figure 5-9b. Comparison of Spherical Waveguide and Bannister's ELF Propagation Formulas for the Phase of the Azimuthal Magnetic Field Produced by a VED Under Typical Daytime Propagation Conditions at 30 Hz

(The propagation parameters are $c/v = 1.31$, $\alpha = 0.6$ dB/Mm, $h = 51$ km, and the dipole moment is $p = 1$ Am.)

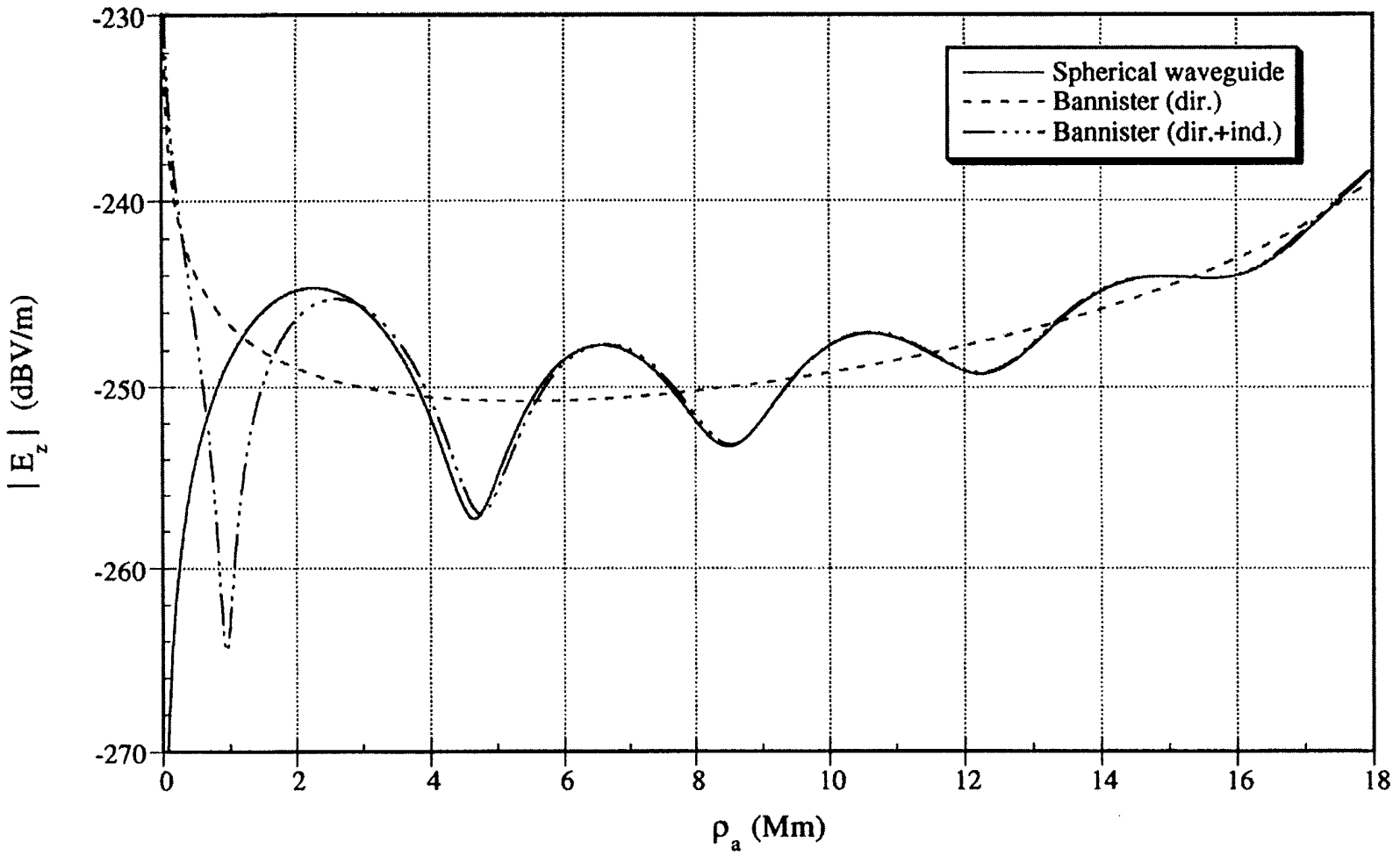

Figure 5-10a. Comparison of Spherical Waveguide and Bannister's ELF Propagation Formulas for the Magnitude of the Vertical Electric Field Produced by a HED Under Typical Daytime Propagation Conditions at 30 Hz

(The propagation parameters are $c/v = 1.31$, $\alpha = 0.6$ dB/Mm, $h = 51$ km; the azimuthal angle is $\varphi = 0°$; and the dipole moment is $p = 1$ Am.)

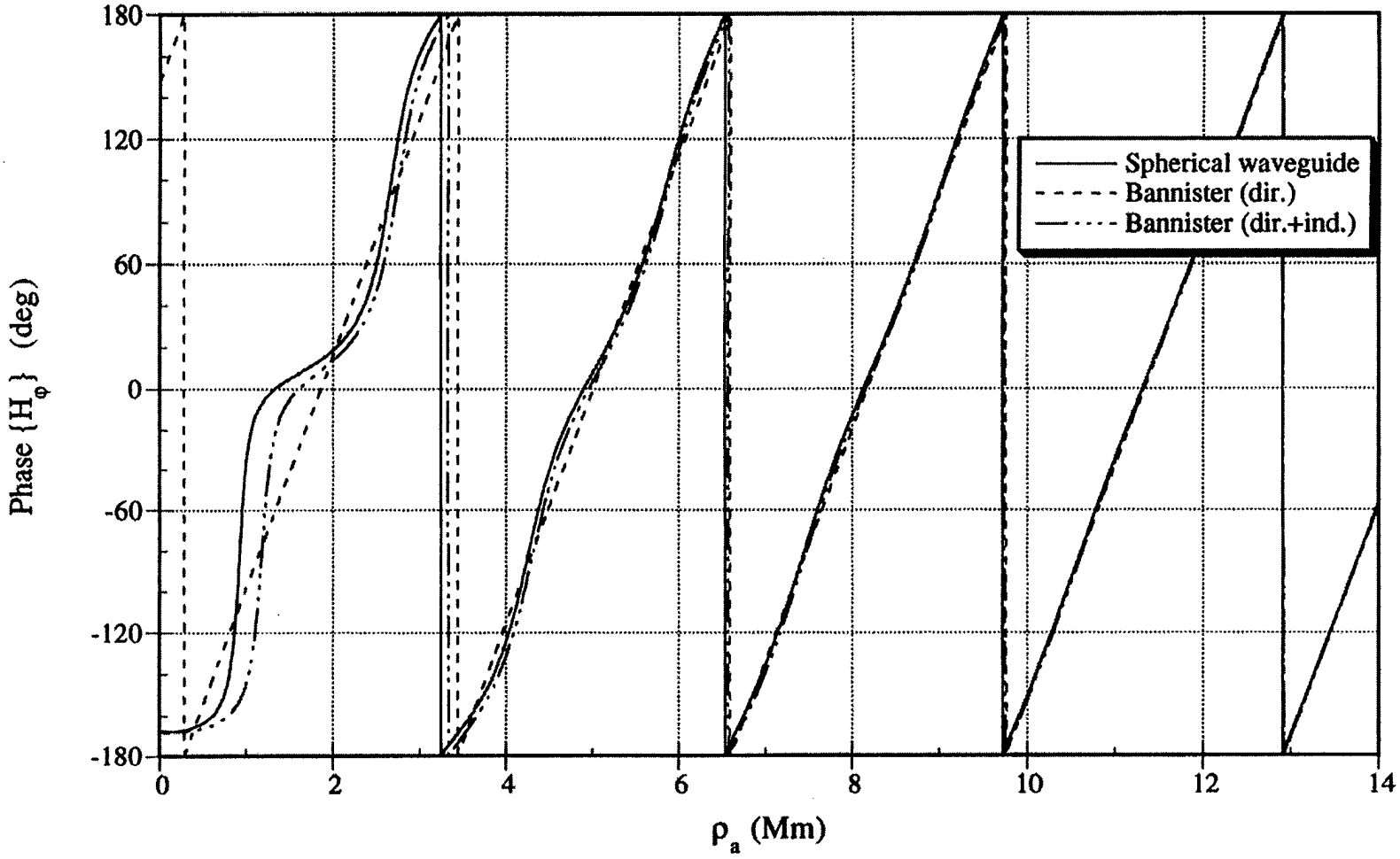

Figure 5-10b. Comparison of Spherical Waveguide and Bannister's ELF Propagation Formulas for the Phase of the Vertical Electric Field Produced by a HED Under Typical Daytime Propagation Conditions at 30 Hz

(The propagation parameters are $c/v = 1.31$, $\alpha = 0.6$ dB/Mm, $h = 51$ km;, the azimuthal angle is $\varphi = 0°$; and the dipole moment is $p = 1$ Am.)

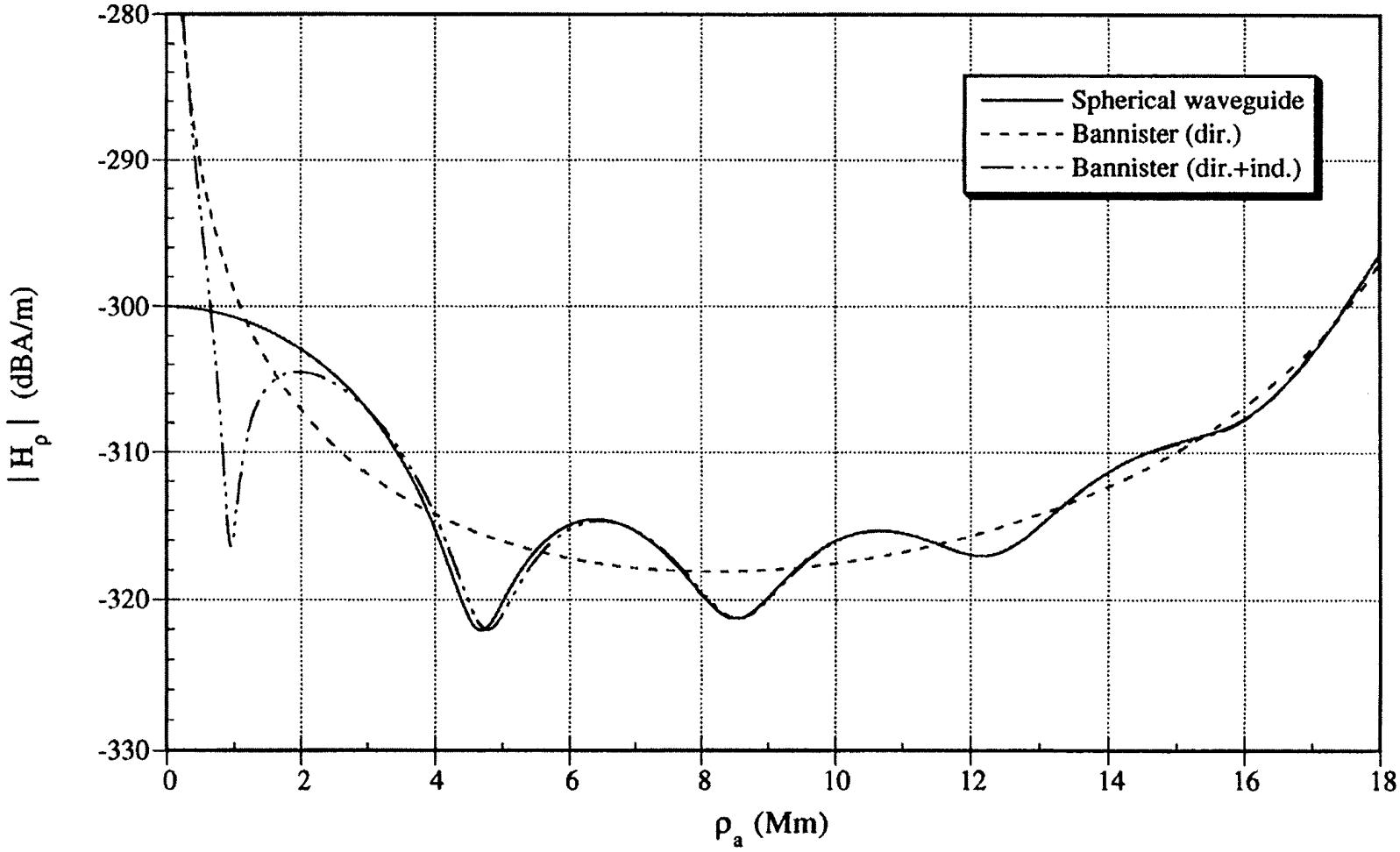

Figure 5-11a. Comparison of Spherical Waveguide and Bannister's ELF Propagation Formulas for the Magnitude of the Radial Magnetic Field Produced by a HED Under Typical Daytime Propagation Conditions at 30 Hz

(The propagation parameters are $c/v = 1.31$, $\alpha = 0.6$ dB/Mm, $h = 51$ km; the azimuthal angle is $\varphi = 90°$; and the dipole moment is $p = 1$ Am.)

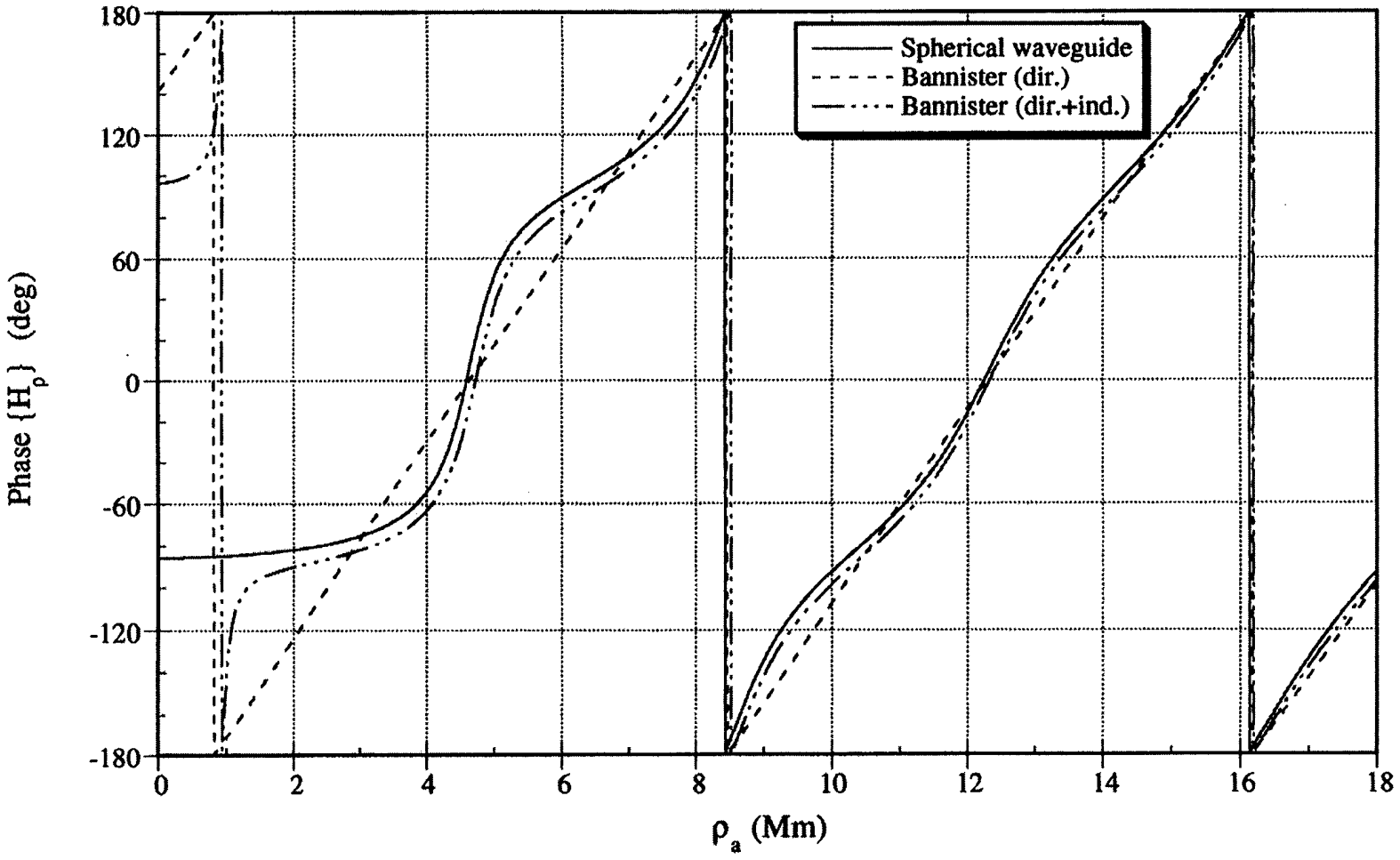

Figure 5-11b. Comparison of Spherical Waveguide and Bannister's ELF Propagation Formulas for the Phase of the Radial Magnetic Field Produced by a HED Under Typical Daytime Propagation Conditions at 30 Hz

(The propagation parameters are $c/v = 1.31$, $\alpha = 0.6$ dB/Mm, $h = 51$ km; the azimuthal angle is $\varphi = 90°$; and the dipole moment is $p = 1$ Am.)

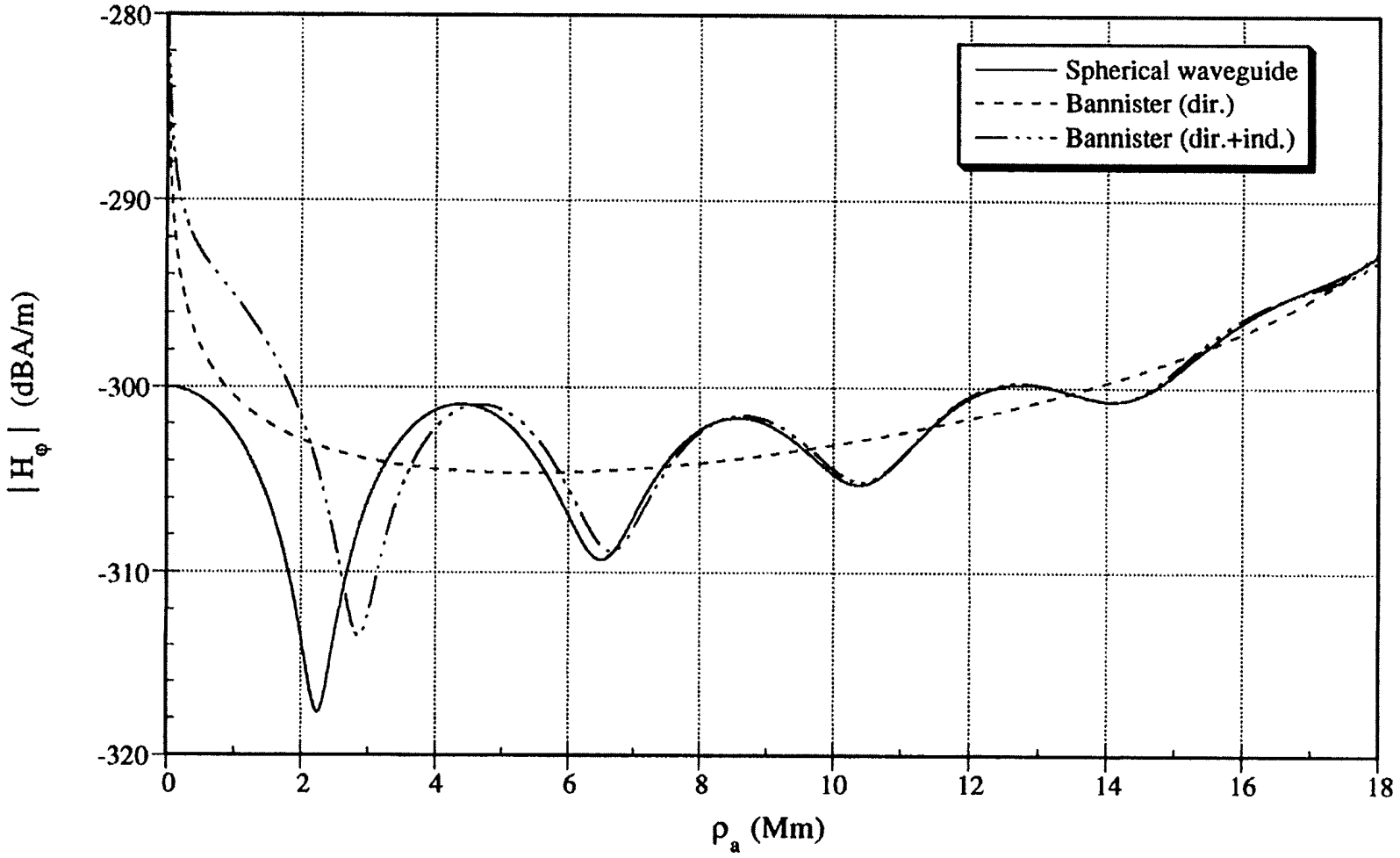

Figure 5-12a. Comparison of Spherical Waveguide and Bannister's ELF Propagation Formulas for the Magnitude of the Azimuthal Magnetic Field Produced by a HED Under Typical Daytime Propagation Conditions at 30 Hz

(The propagation parameters are $c/v = 1.31$, $\alpha = 0.6$ dB/Mm, $h = 51$ km; the azimuthal angle is $\varphi = 0°$; and the dipole moment is $p = 1$ Am.)

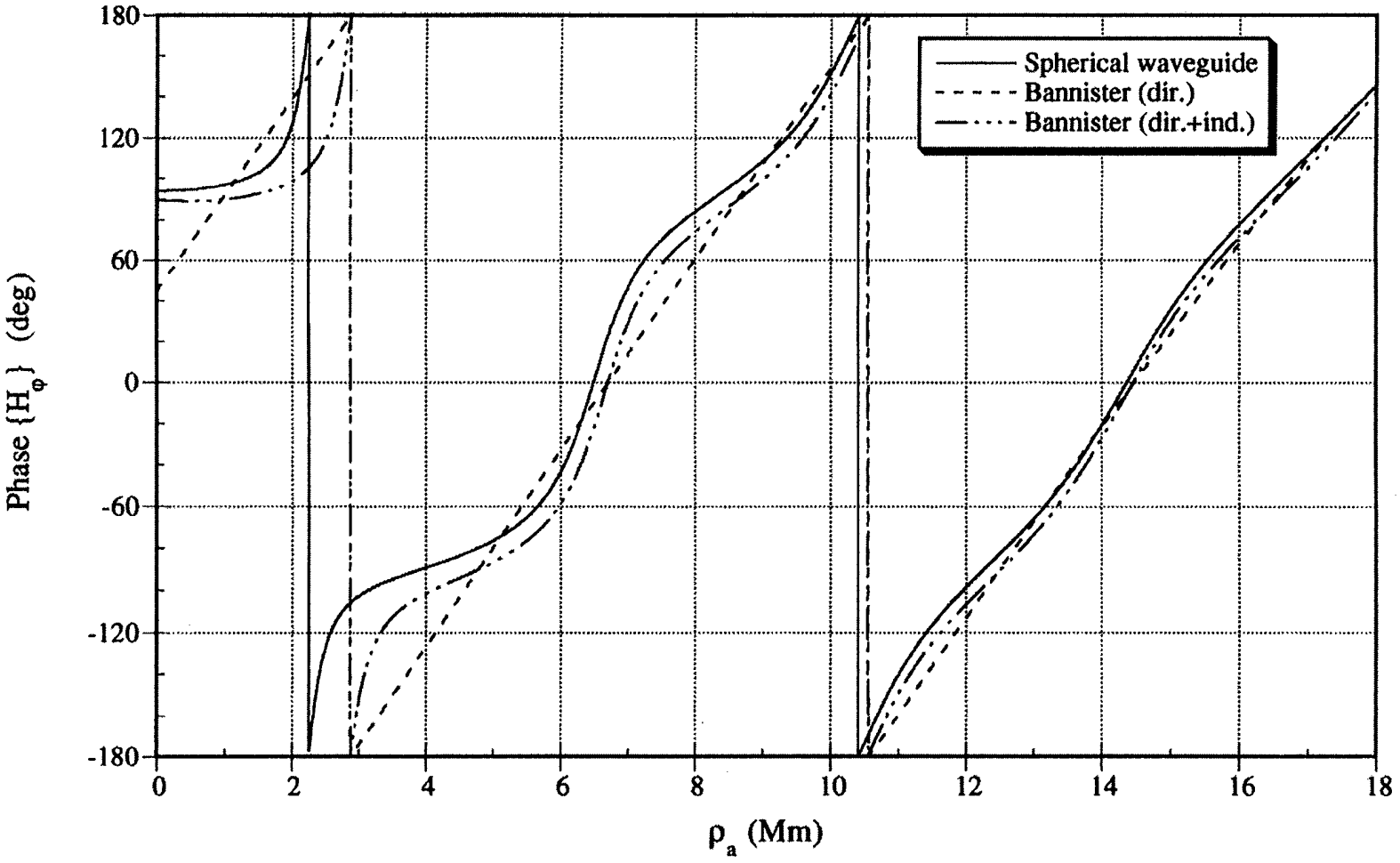

Figure 5-12b. Comparison of Spherical Waveguide and Bannister's ELF Propagation Formulas for the Phase of the Azimuthal Magnetic Field Produced by a HED Under Typical Daytime Propagation Conditions at 30 Hz

(The propagation parameters are $c/v = 1.31$, $\alpha = 0.6$ dB/Mm, $h = 51$ km; the azimuthal angle is $\varphi = 0°$; and the dipole moment is $p = 1$ Am.)

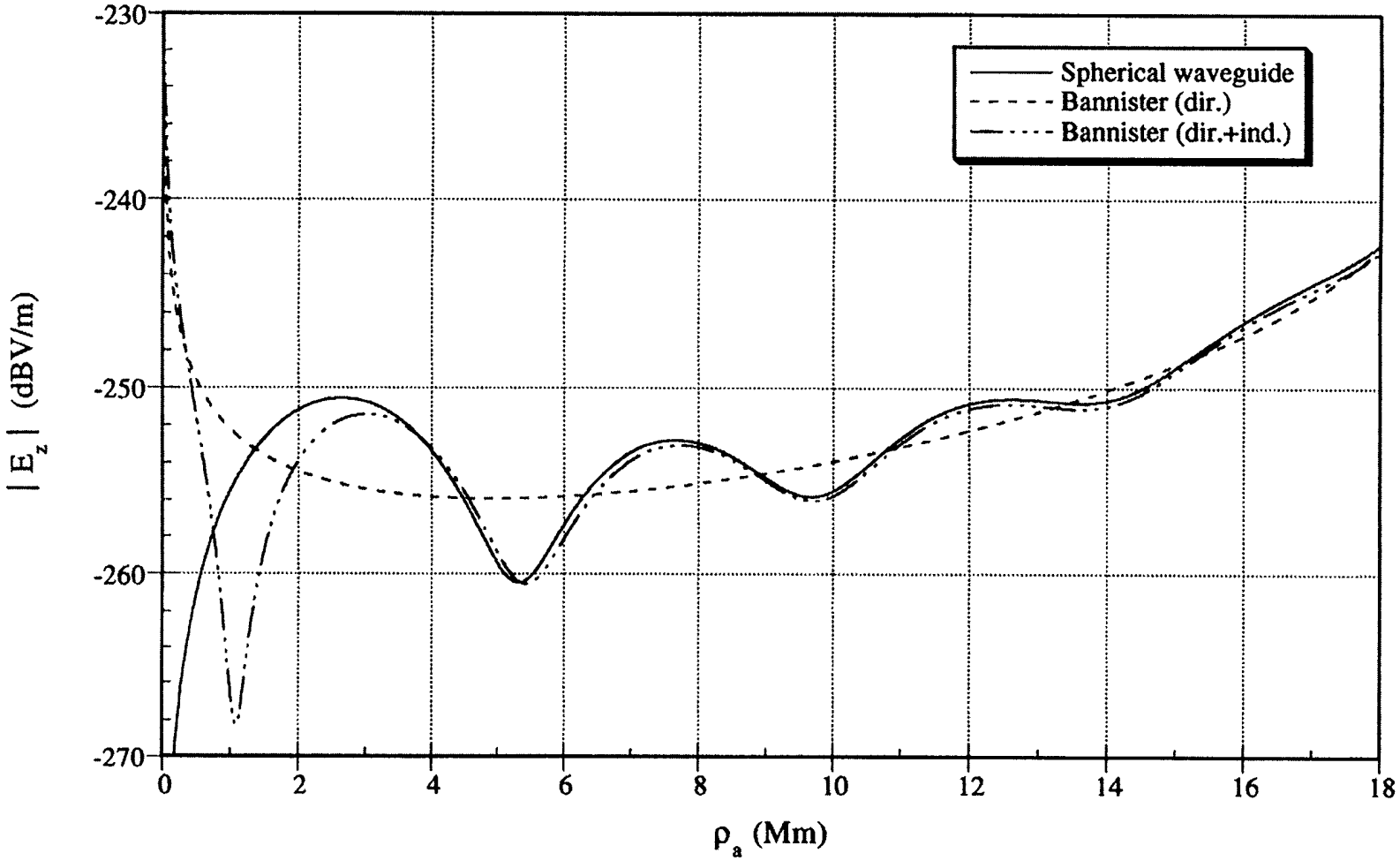

Figure 5-13a. Comparison of Spherical Waveguide and Bannister's ELF Propagation Formulas for the Magnitude of the Vertical Electric Field Produced by a HED Under Typical Nighttime Propagation Conditions at 30 Hz

(The propagation parameters are $c/v = 1.14$, $\alpha = 0.7$ dB/Mm, $h = 73$ km; the azimuthal angle is $\varphi = 0°$; and the dipole moment is $p = 1$ Am.)

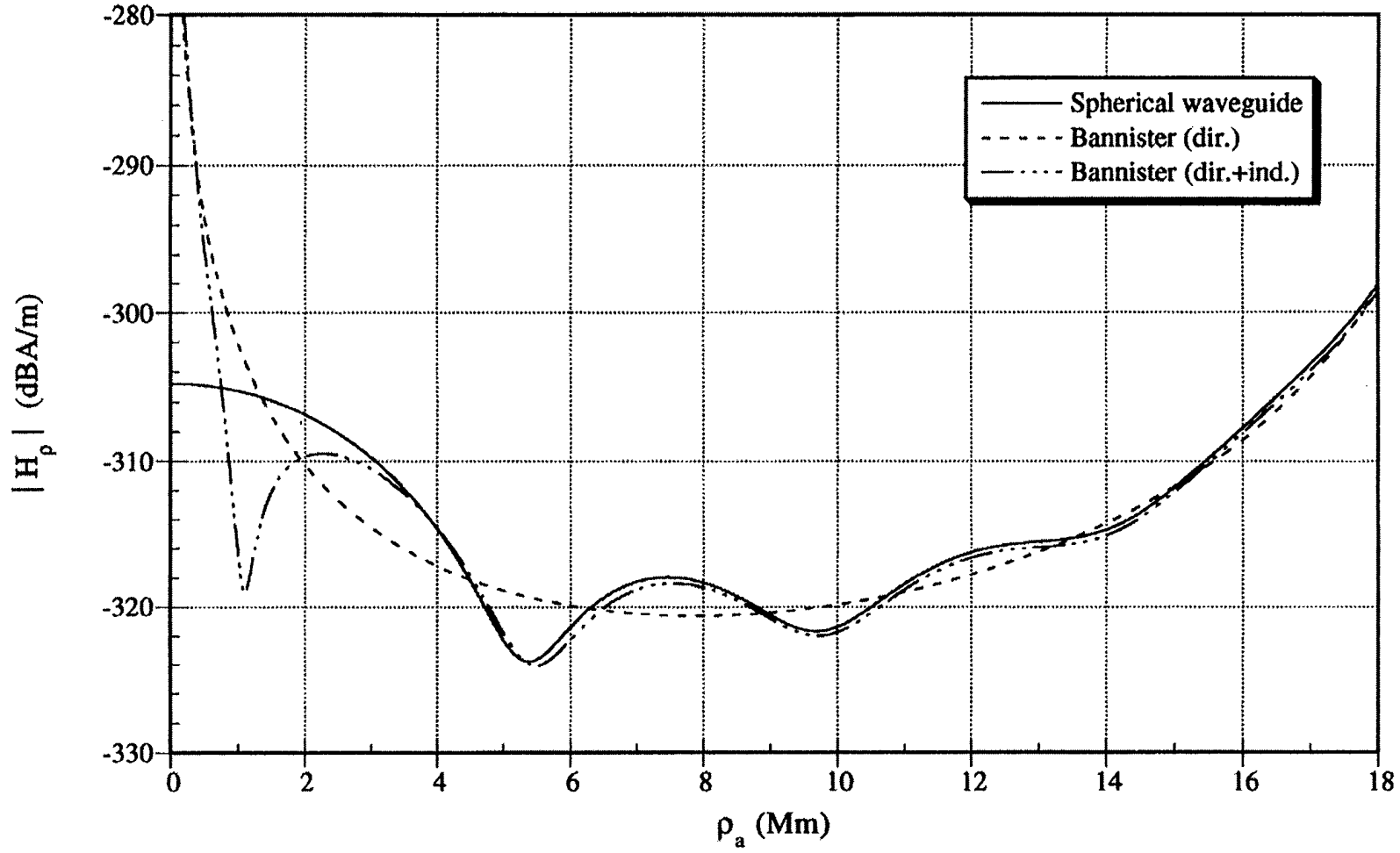

Figure 5-13b. Comparison of Spherical Waveguide and Bannister's ELF Propagation Formulas for the Magnitude of the Radial Magnetic Field Produced by a HED Under Typical Nighttime Propagation Conditions at 30 Hz

(The propagation parameters are $c/v = 1.14$, $\alpha = 0.7$ dB/Mm, $h = 73$ km; the azimuthal angle is $\varphi = 90°$; and the dipole moment is $p = 1$ Am.)

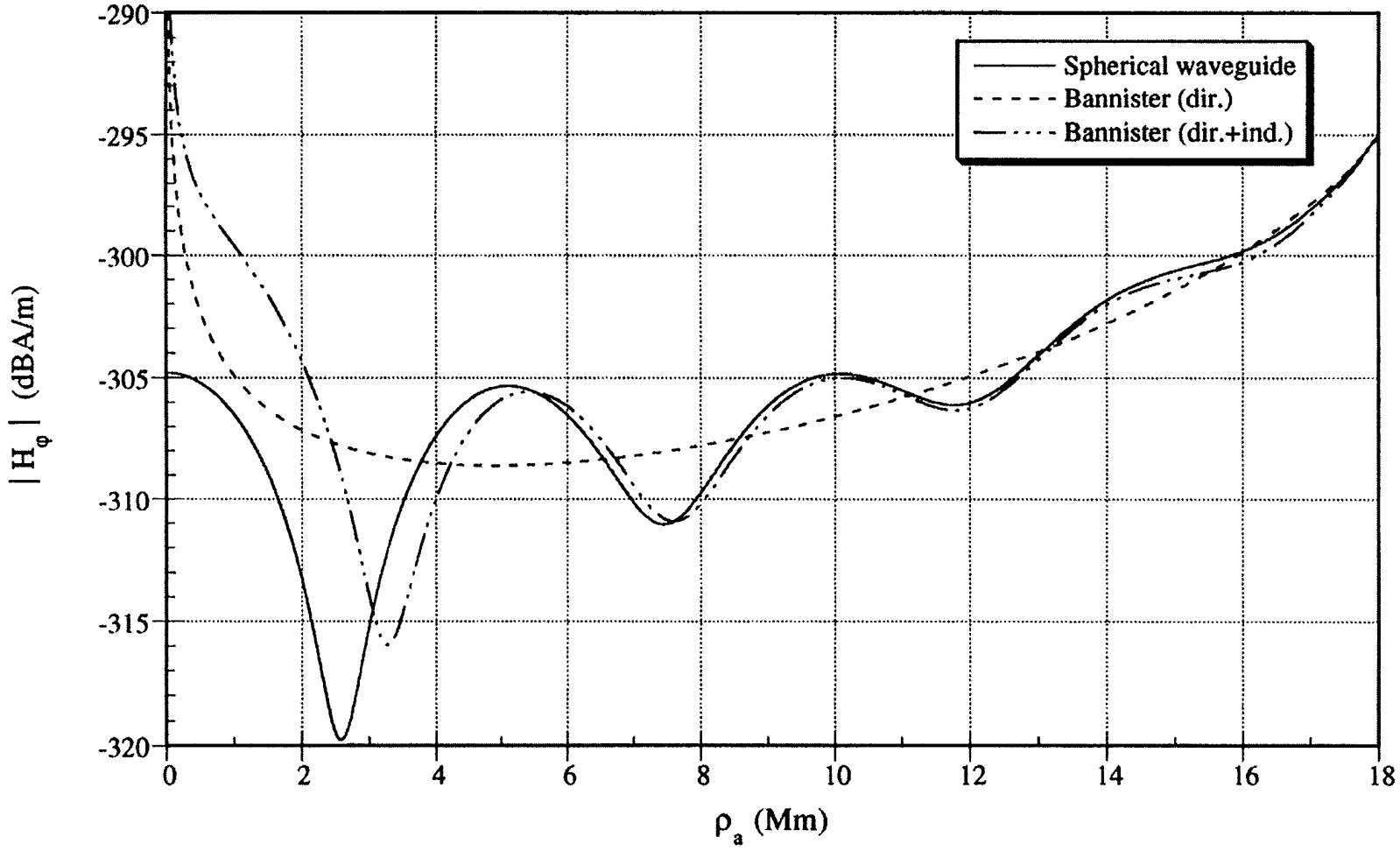

Figure 5-13c. Comparison of Spherical Waveguide and Bannister's ELF Propagation Formulas for the Magnitude of the Azimuthal Magnetic Field Produced by a HED Under Typical Nighttime Propagation Conditions at 30 Hz

(The propagation parameters are $c/v = 1.14$, $\alpha = 0.7$ dB/Mm, $h = 73$ km; the azimuthal angle is $\varphi = 0°$; and the dipole moment is $p = 1$ Am.)

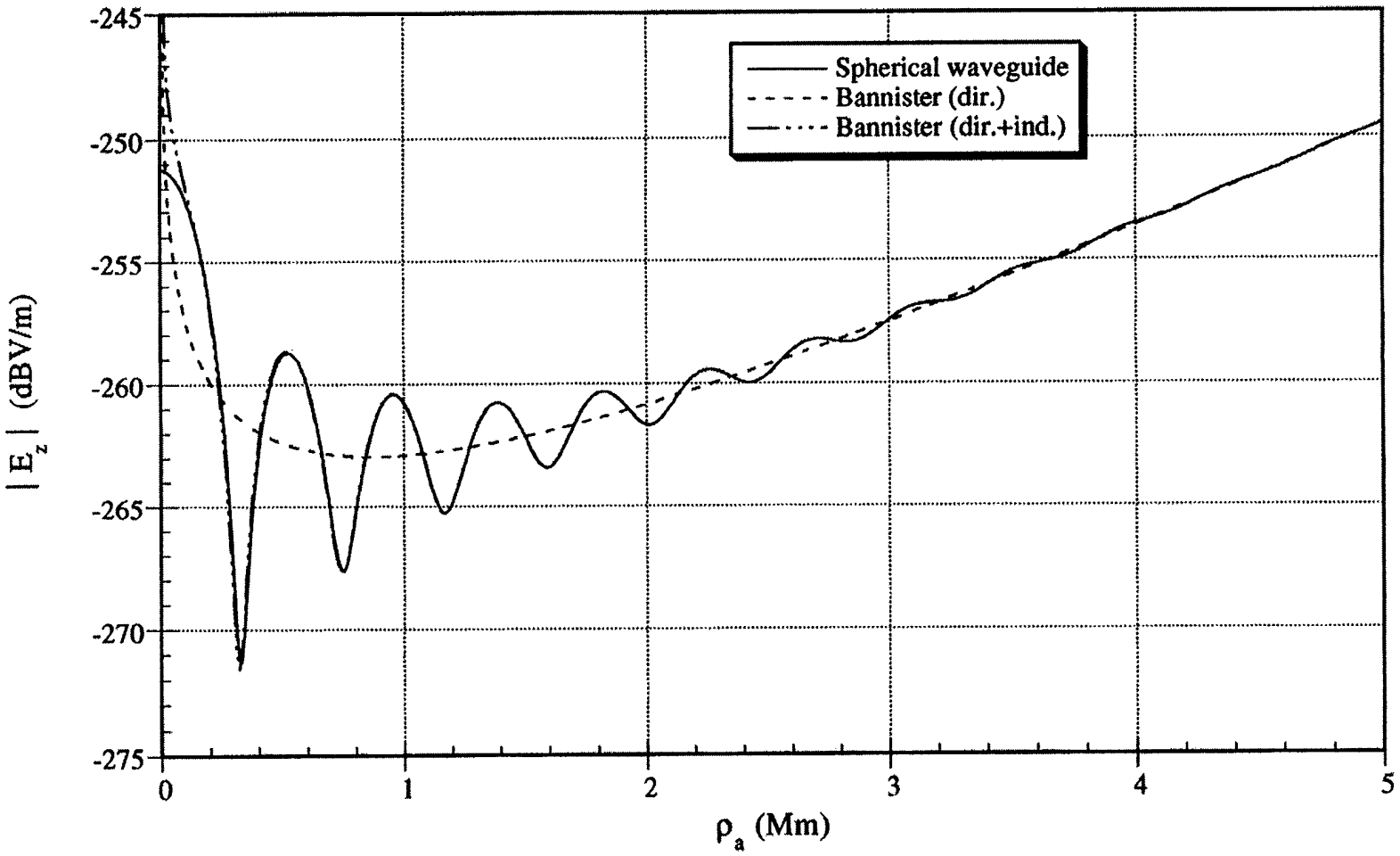

Figure 5-14a. Comparison of Spherical Waveguide and Bannister's ELF Propagation Formulas for the Magnitude of the Vertical Electric Field Produced by a VED Under Typical Daytime Propagation Conditions at 300 Hz

(The propagation parameters are $c/v = 1.17$, $\alpha = 5.0$ dB/Mm, $h = 59$ km, and the dipole moment is $p = 1$ Am.)

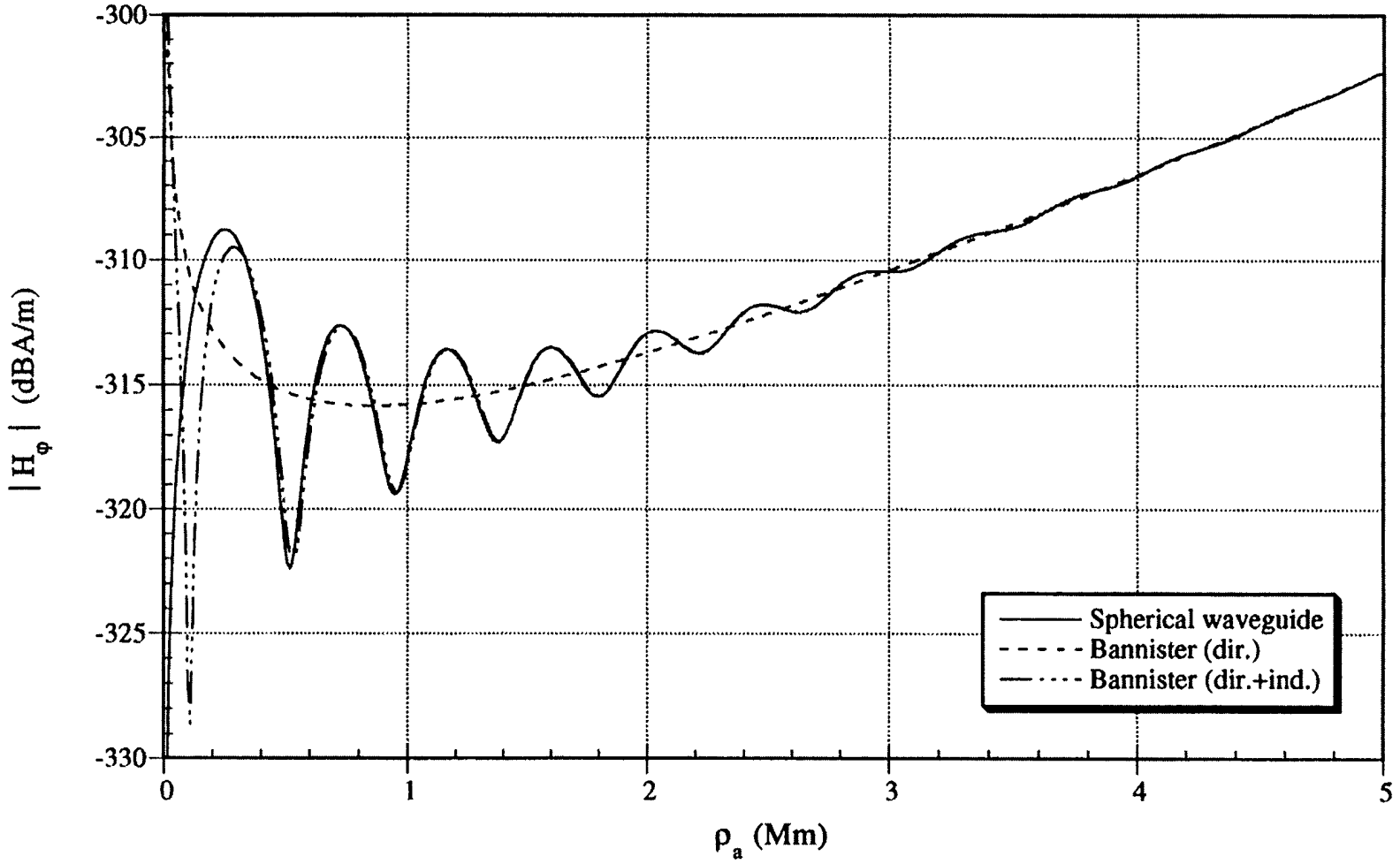

Figure 5-14b. Comparison of Spherical Waveguide and Bannister's ELF Propagation Formulas for the Magnitude of the Azimuthal Magnetic Field Produced by a VED Under Typical Daytime Propagation Conditions at 300 Hz

(The propagation parameters are $c/v = 1.17$, $\alpha = 5.0$ dB/Mm, $h = 59$ km, and the dipole moment is $p = 1$ Am.)

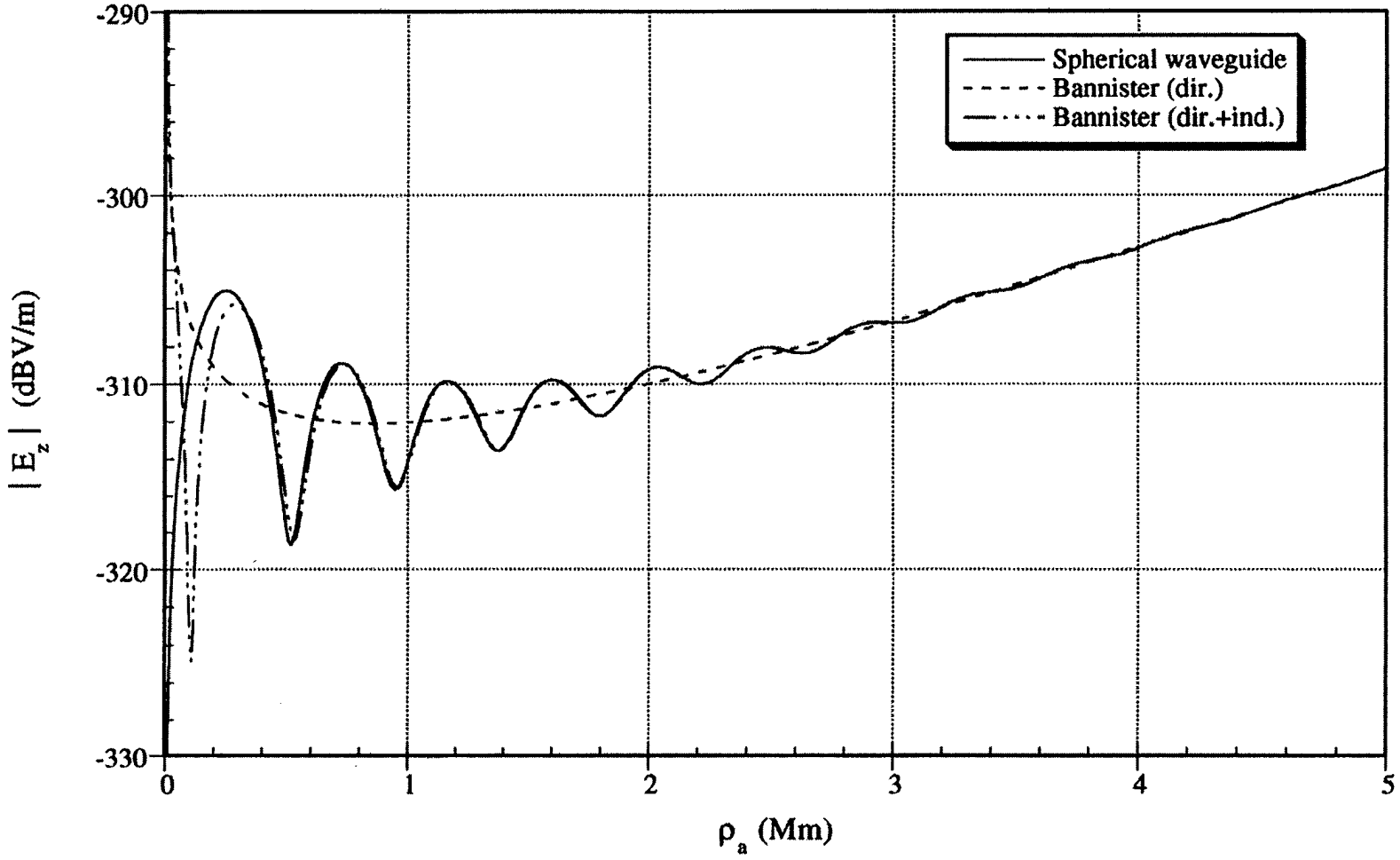

Figure 5-15a. Comparison of Spherical Waveguide and Bannister's ELF Propagation Formulas for the Magnitude of the Vertical Electric Field Produced by a HED Under Typical Daytime Propagation Conditions at 300 Hz

(The propagation parameters are $c/v = 1.17$, $\alpha = 5.0$ dB/Mm, $h = 59$ km; the azimuthal angle is $\varphi = 0°$; and the dipole moment is $p = 1$ Am.)

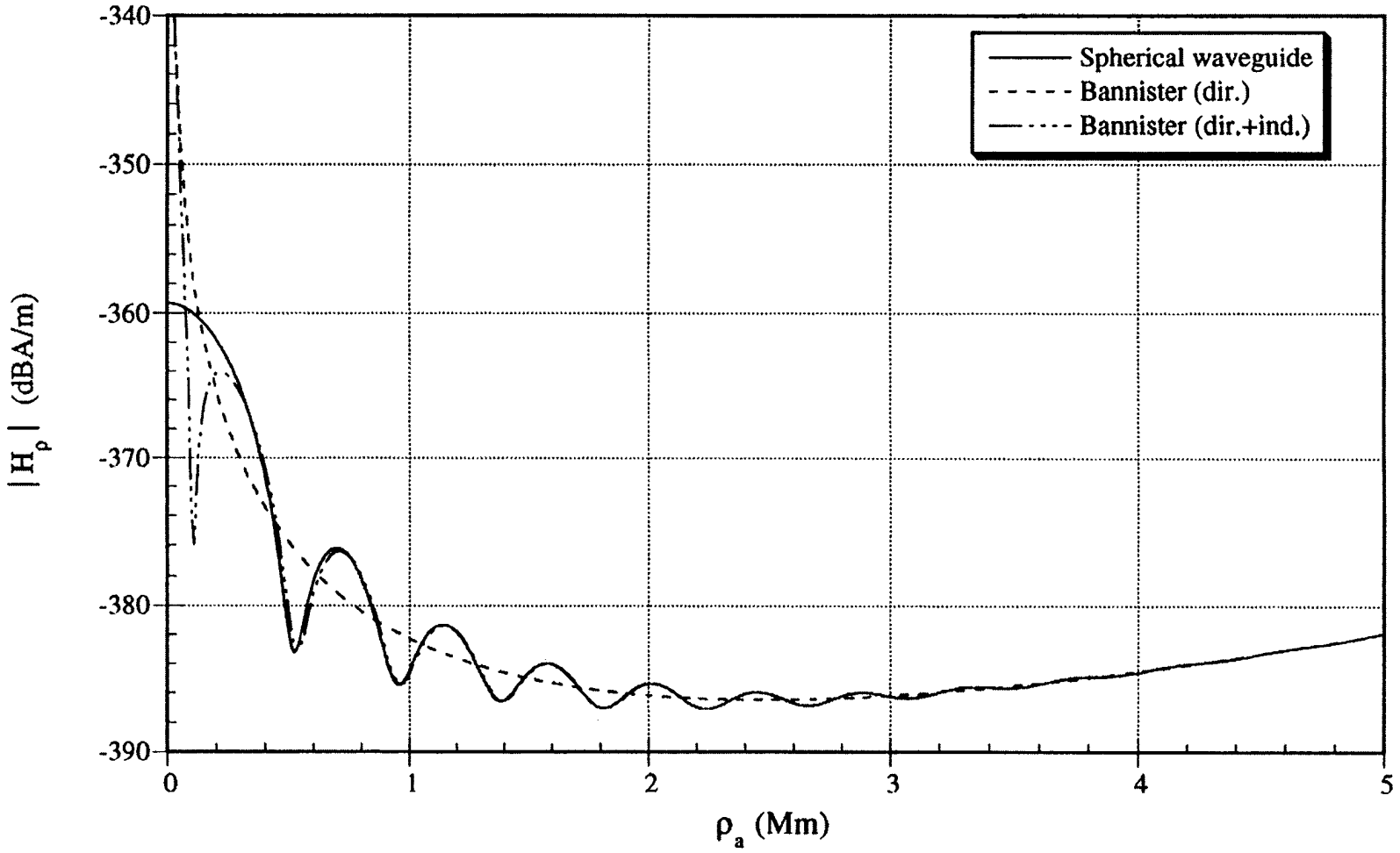

Figure 5-15b. Comparison of Spherical Waveguide and Bannister's ELF Propagation Formulas for the Magnitude of the Radial Magnetic Field Produced by a HED Under Typical Daytime Propagation Conditions at 300 Hz

(The propagation parameters are $c/v = 1.17$, $\alpha = 5.0$ dB/Mm, $h = 59$ km; the azimuthal angle is $\varphi = 90°$; and the dipole moment is $p = 1$ Am.)

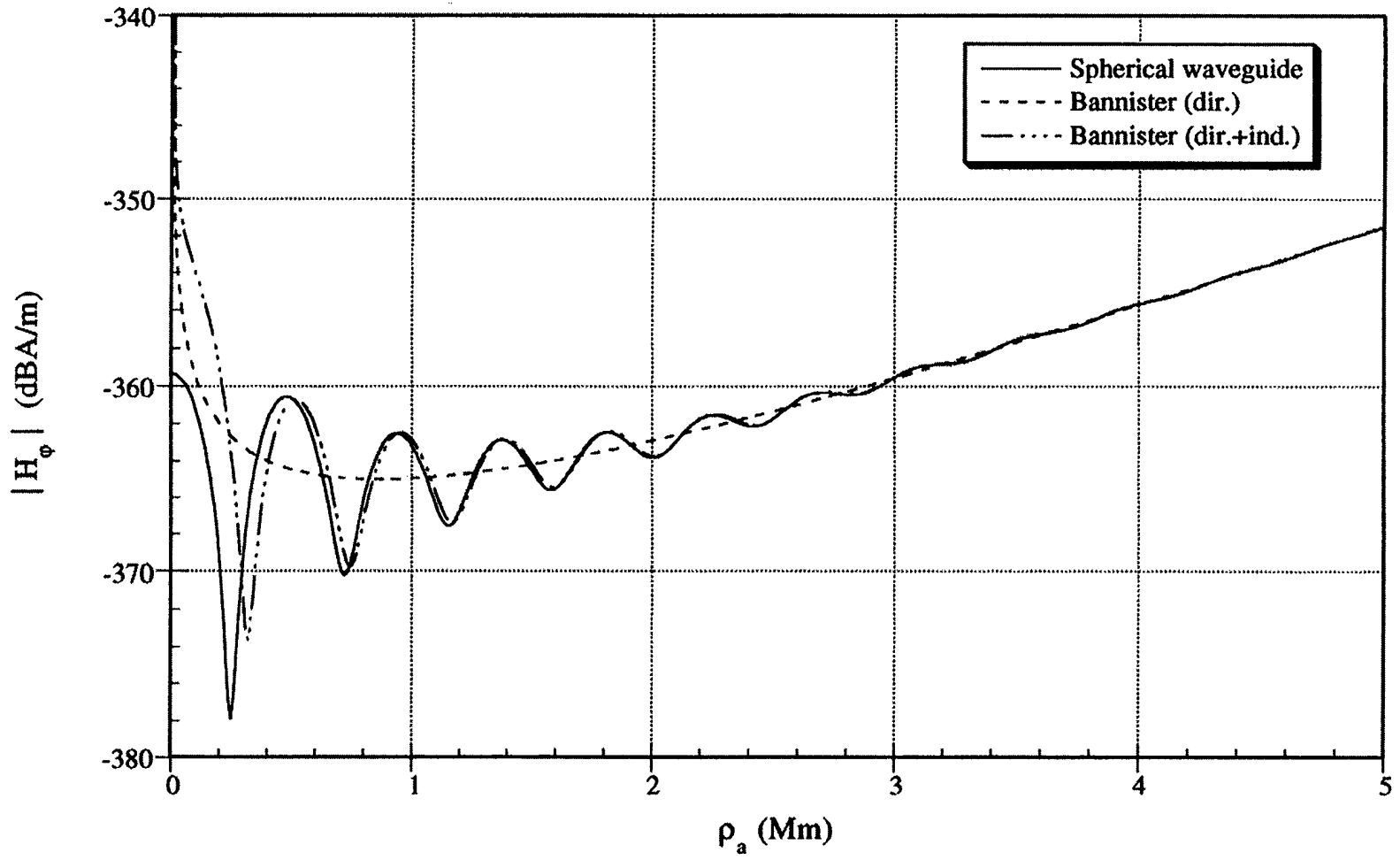

Figure 5-15c. Comparison of Spherical Waveguide and Bannister's ELF Propagation Formulas for the Magnitude of the Azimuthal Magnetic Field Produced by a HED Under Typical Daytime Propagation Conditions at 300 Hz

(The propagation parameters are $c/v = 1.17$, $\alpha = 5.0$ dB/Mm, $h = 59$ km;, the azimuthal angle is $\varphi = 0°$; and the dipole moment is $p = 1$ Am.)

Magnitude plots of the HED field components E_z^{he}, H_ρ^{he}, and H_φ^{he} under typical nighttime propagation conditions at 300 Hz are given in figures 5-16a, 5-16b, and 5-16c, respectively. Because of the lower attenuation at nighttime, the interference pattern produced by the two great-circle path fields extends to greater distances from the antipode. As a result, at nighttime, Bannister's total field results at 300 Hz do not compare as well with the spherical waveguide formulas as under daytime conditions. A similar observation was made at 76 Hz. In the 300-Hz plots, Bannister's total field formulas for E_z^{he}, H_ρ^{he}, and H_φ^{he} agree to within 1 dB of the corresponding spherical waveguide formula results for $\rho_a \geq 0.65$ Mm, $\rho_a \geq 0.65$ Mm, and $\rho_a \geq 1.22$ Mm, respectively.

Table 5-4 is a list of the ranges over which Bannister's total field formulas agree to within 1 dB in magnitude of the corresponding spherical waveguide formulas for both typical daytime and nighttime propagation conditions at 300 Hz. A comparison of tables 5-2b, 5-3, and 5-4 indicates that Bannister's total field results improve with increasing frequency.

Table 5-4. Ranges Over Which Bannister's Total Field Formulas Agree to Within 1 dB in Magnitude of the Spherical Waveguide Formulas at 300 Hz

Field Component	Propagation Condition	Range
E_z^{ve}	Daytime	$\rho_a \geq 0.32$ Mm $(\beta\rho_a \geq 2.35)$
	Nighttime	$\rho_a \geq 0.40$ Mm $(\beta\rho_a \geq 2.77)$
H_φ^{ve}	Daytime	$\rho_a \geq 0.59$ Mm $(\beta\rho_a \geq 4.34)$
	Nighttime	$\rho_a \geq 0.65$ Mm $(\beta\rho_a \geq 4.50)$
E_z^{he}	Daytime	$\rho_a \geq 0.59$ Mm $(\beta\rho_a \geq 4.34)$
	Nighttime	$\rho_a \geq 0.65$ Mm $(\beta\rho_a \geq 4.50)$
H_ρ^{he}	Daytime	$\rho_a \geq 0.59$ Mm $(\beta\rho_a \geq 4.34)$
	nighttime	$\rho_a \geq 0.65$ Mm $(\beta\rho_a \geq 4.50)$
H_φ^{he}	Daytime	$\rho_a \geq 0.82$ Mm $(\beta\rho_a \geq 6.03)$
	Nighttime	$\rho_a \geq 1.22$ Mm $(\beta\rho_a \geq 8.44)$

Table 5-5 is a list of the average normalized ranges (expressed in terms of $\beta\rho_a$) over which Bannister's total field formulas agree to within 1 dB in magnitude of the corresponding spherical waveguide formulas. The ranges have been normalized in order to scale them with respect to a wavelength in the waveguide. The ranges are averaged over the three frequencies discussed in this report, namely, 30 Hz, 76 Hz, and 300 Hz. The third column in the table lists the average

ranges for each field component under typical daytime and nighttime propagation conditions. The fourth row in the table lists the ranges averaged over daytime and nighttime propagation conditions for each field component.

The third column of table 5-5 indicates, on the average, that Bannister's total field formulas for E_z^{ve} and H_φ^{he} produce better agreement with the spherical waveguide formulas at daytime than at nighttime. The opposite result is true for the other field components, H_φ^{ve}, E_z^{he}, H_ρ^{he}. Note that the better agreement in the field components at nighttime was only observed at 30 Hz, where the nighttime attenuation is greater than in the daytime. The results in the fourth column of table 5-5 show that Bannister's total field formula for E_z^{ve} provides the best agreement with the spherical waveguide formula and H_φ^{he} produces the worst agreement. As mentioned, this observation is attributed to the fact that in the earth-flattening approximation for $P_\nu(-\cos\theta)$, each successive derivative introduces additional error into the approximation. Also note in the fourth column of table 5-5 that H_φ^{ve}, E_z^{he}, and H_ρ^{he} each produce a similar average agreement with the corresponding spherical waveguide formulas. This result is attributed to the fact that the range dependence of each of these components is proportional to the first derivative of $P_\nu(-\cos\theta)$. In summary, table 5-5 clearly shows that the spherical waveguide propagation formulas are necessary for prediction of the ELF fields for ranges that are close to the antipode.

Table 5-5. Average Normalized Ranges Over Which Bannister's Total Field Formulas Agree to Within 1 dB in Magnitude of the Spherical Waveguide Formulas (Averages Are Taken Over 30, 76, and 300 Hz)

Field Component	Propagation Condition	Average Normalized Range	Avg Norm. Range (Day and Night)
E_z^{ve}	Daytime	$\beta\rho_a \geq 2.29$	$\beta\rho_a \geq 2.42$
	Nighttime	$\beta\rho_a \geq 2.55$	
H_φ^{ve}	Daytime	$\beta\rho_a \geq 3.95$	$\beta\rho_a \geq 3.80$
	Nighttime	$\beta\rho_a \geq 3.65$	
E_z^{he}	Daytime	$\beta\rho_a \geq 3.95$	$\beta\rho_a \geq 3.80$
	Nighttime	$\beta\rho_a \geq 3.65$	
H_ρ^{he}	Daytime	$\beta\rho_a \geq 4.09$	$\beta\rho_a \geq 3.88$
	Nighttime	$\beta\rho_a \geq 3.67$	
H_φ^{he}	Daytime	$\beta\rho_a \geq 5.55$	$\beta\rho_a \geq 5.77$
	Nighttime	$\beta\rho_a \geq 6.00$	

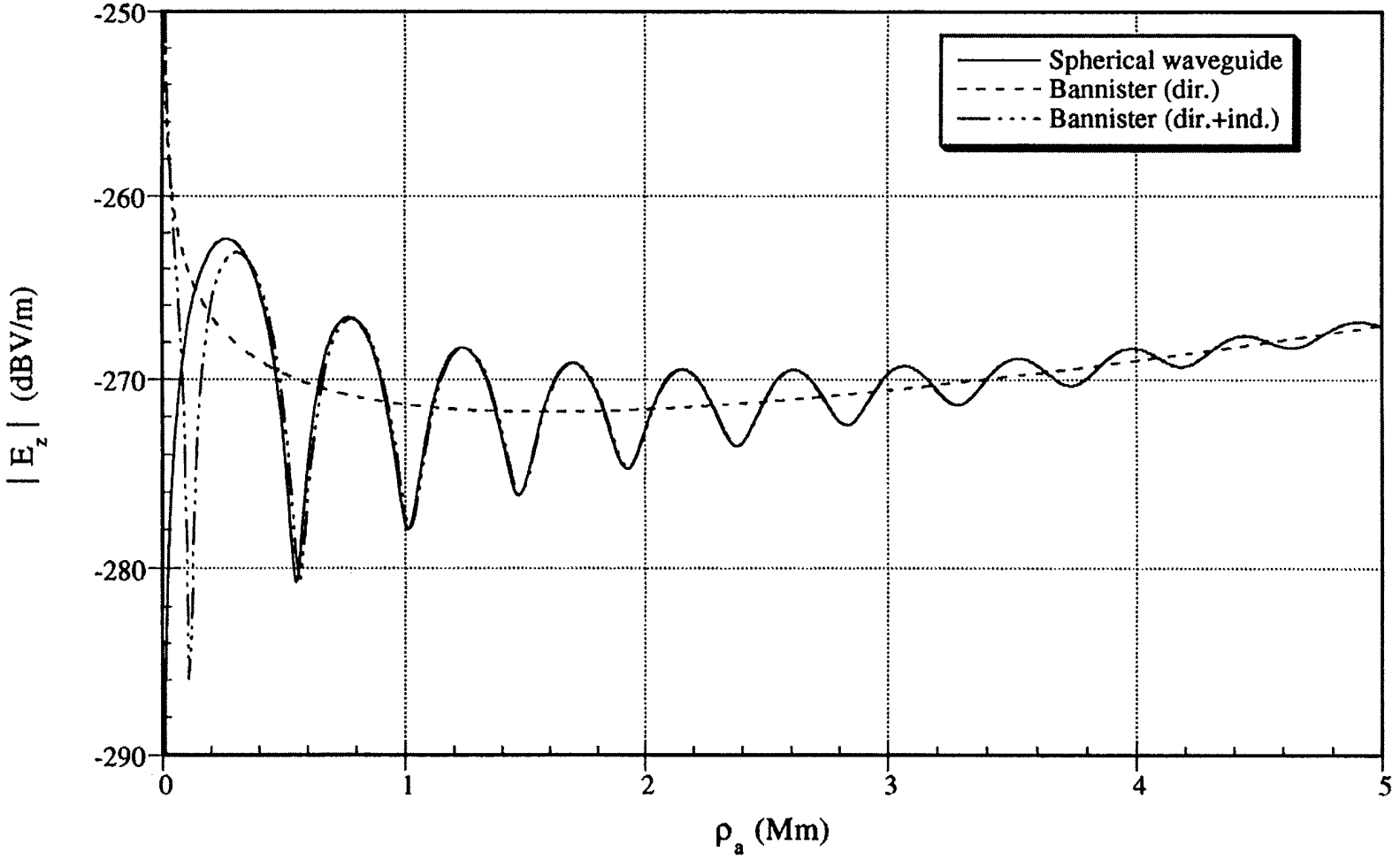

Figure 5-16a. Comparison of Spherical Waveguide and Bannister's ELF Propagation Formulas for the Magnitude of the Vertical Electric Field Produced by a HED Under Typical Nighttime Propagation Conditions at 300 Hz

(The propagation parameters are $c/v = 1.1$, $\alpha = 2.7$ dB/Mm, $h = 81$ km; the azimuthal angle is $\varphi = 0°$; and the dipole moment is $p = 1$ Am.)

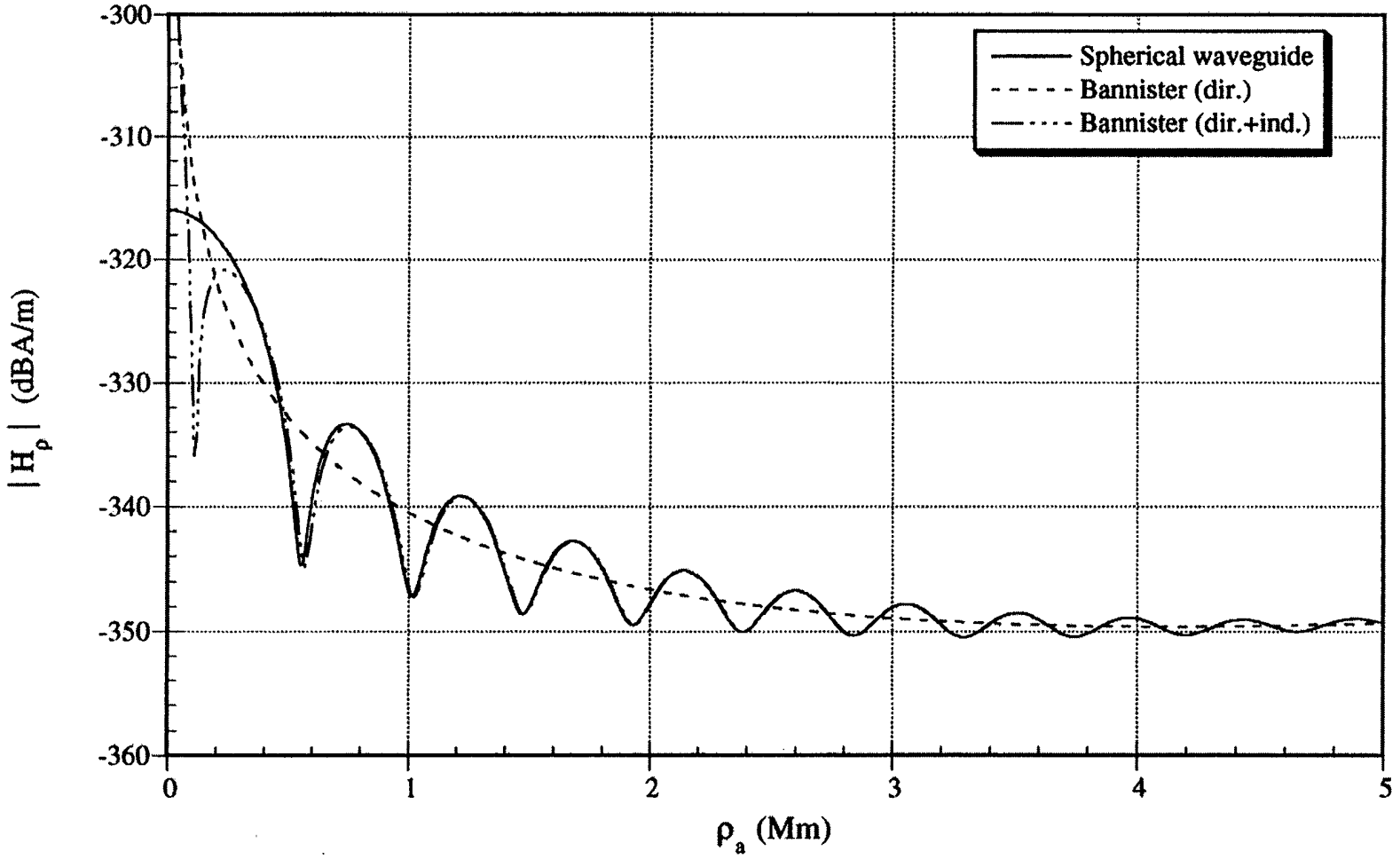

Figure 5-16b. Comparison of Spherical Waveguide and Bannister's ELF Propagation Formulas for the Magnitude of the Radial Magnetic Field Produced by a HED Under Typical Nighttime Propagation Conditions at 300 Hz

(The propagation parameters are $c/v = 1.1$, $\alpha = 2.7$ dB/Mm, $h = 81$ km; the azimuthal angle is $\varphi = 90°$; and the dipole moment is $p = 1$ Am.)

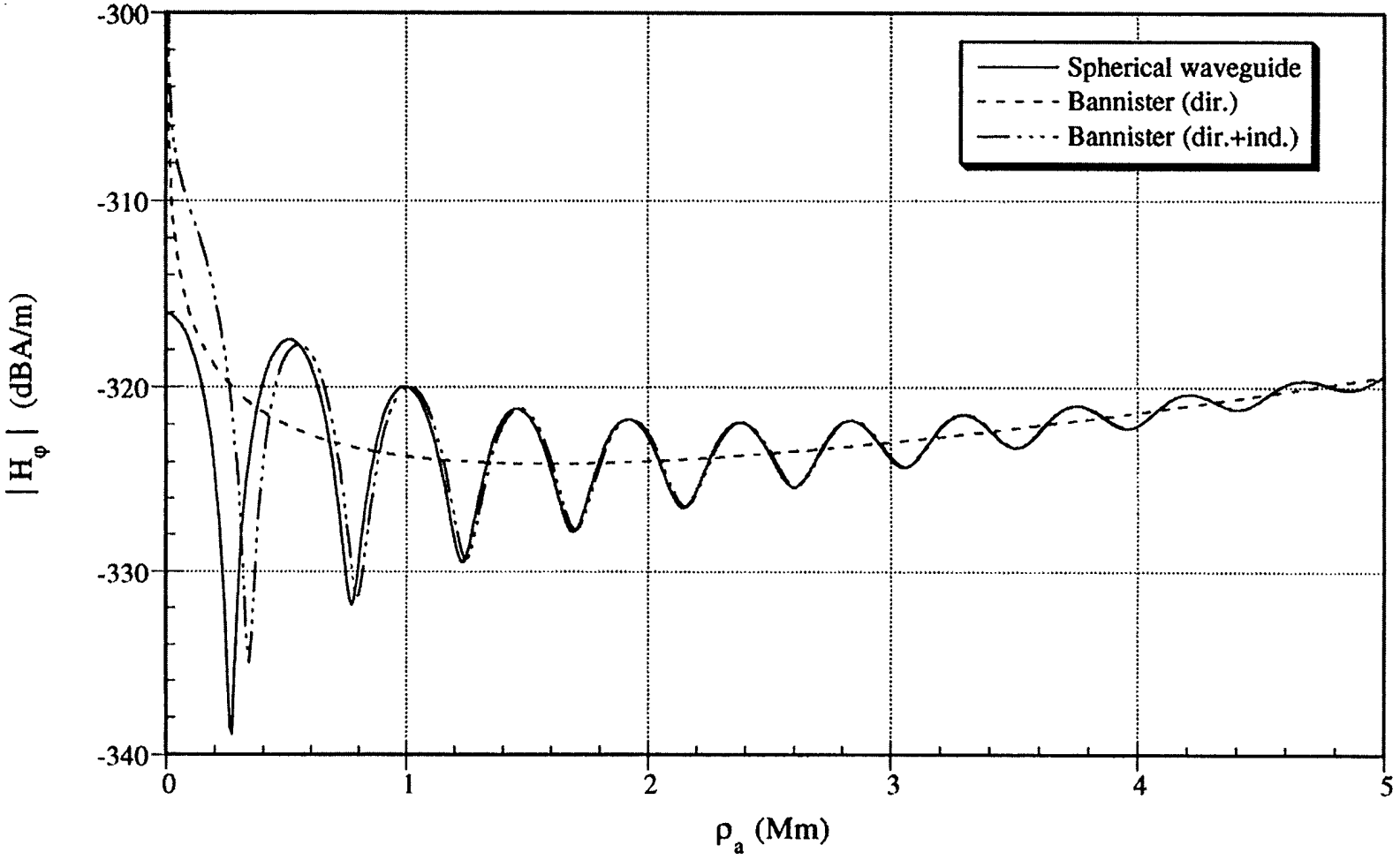

Figure 5-16c. Comparison of Spherical Waveguide and Bannister's ELF Propagation Formulas for the Magnitude of the Azimuthal Magnetic Field Produced by a HED Under Typical Nighttime Propagation Conditions at 300 Hz

(The propagation parameters are $c/v = 1.1$, $\alpha = 2.7$ dB/Mm, $h = 81$ km; the azimuthal angle is $\varphi = 0°$; and the dipole moment is $p = 1$ Am.)

6. SUMMARY AND CONCLUSIONS

ELF propagation formulas have been derived for dipole sources radiating in a spherical earth-ionosphere waveguide, where the waveguide boundaries are approximated as scalar surface impedances. The range dependencies in these formulas involve the Legendre function of the first kind of complex degree and order zero or one of its first two derivatives. Several approximations to the Legendre function were derived. Through use of the earth-flattening approximation to the Legendre function, it was shown how the spherical waveguide formulas reduce to Bannister's simplified propagation formulas. In addition, through use of another approximation to the Legendre function that is suitable for antipodal ranges, it was also shown how the spherical waveguide formulas reduce to formulas that are similar to the antipode-centered formulas that were previously derived by the author. Numerical results focused on the quasi-TEM mode, the only propagating mode in the 30-Hz to 300-Hz band.

Comparisons of Bannister's formulas with the spherical waveguide formulas were made for VED and HED sources for the case where both the source and field points are located along the surface of the earth. The 300-Hz results have shown that Bannister's total field formulas produce a good agreement with the spherical waveguide formulas to distances within less than 1 Mm from the antipode. This agreement degrades with decreasing frequency because of lower attenuation. It was also found that the agreement between the formulas is worse for the field components proportional to the derivatives of the Legendre function. Bannister's direct great-circle path formulas do not agree as closely with the spherical waveguide formulas because they do not account for the interference produced by the indirect great-circle path contribution in the vicinity of the antipode.

This report also presented derivations of the quasi-TEM spherical waveguide formulas for a HED located above an anisotropic surface impedance. These modified spherical waveguide formulas are extensions of Wolkoff and Kraimer's formulas (references 4 and 5) and include the antenna pattern factors that were previously derived in reference 6. These formulas will be useful for the prediction of the EM fields radiated by the U. S. Navy's four transmitting antennas at antipodal ranges.

At antipodal ranges, the spherical model of the earth-ionosphere waveguide may not be suitable because of the variation in the ionospheric reflection height along the great-circle paths. As a result, the spherical waveguide formulas need to be modified in order to account for the

variations in the propagation parameters along the direct and indirect great-circle paths as functions of solar elevation. Wolkoff and Casey (reference 15) present formulas for the effective propagation parameters along a nonuniform earth-ionosphere waveguide. A development of ELF propagation formulas for a nonspherical earth-ionosphere waveguide will be the subject of a future investigation.

APPENDIX A
ELECTROMAGNETIC FIELDS IN TERMS OF POTENTIALS IN SPHERICAL COORDINATES

A.1 ELECTRIC AND MAGNETIC VECTOR POTENTIALS

Consider a homogeneous, isotropic medium of permittivity ε, permeability μ, and conductivity σ. In this medium, there exist electric current and charge distributions $\boldsymbol{J}$ and ρ, respectively, and fictitious magnetic current and charge distributions $\boldsymbol{M}$ and ρ_m, respectively. For a time-harmonic dependence $e^{j\omega t}$, Maxwell's equations are written as follows (references 19, 20, and 21):

$$\nabla \times \boldsymbol{E} = -j\omega\mu\boldsymbol{H} - \boldsymbol{M}, \tag{A-1a}$$

$$\nabla \times \boldsymbol{H} = j\omega\tilde{\varepsilon}\boldsymbol{E} + \boldsymbol{J}, \tag{A-1b}$$

$$\nabla \cdot \boldsymbol{E} = \frac{\rho}{\varepsilon}, \tag{A-1c}$$

$$\nabla \cdot \boldsymbol{H} = \frac{\rho_m}{\mu}. \tag{A-1d}$$

In the above expressions, $\boldsymbol{E}$ and $\boldsymbol{H}$ denote the electric and magnetic fields, respectively, $\omega = 2\pi f$ is the angular frequency, and $\tilde{\varepsilon} = \varepsilon - j\sigma/\omega$ is the effective permeability of the medium. The electric and magnetic fields can each be expressed in terms of a pair of vector potentials. The pair of vector potentials that are most commonly used are the magnetic vector potential $\boldsymbol{A}$ and the electric vector potential $\boldsymbol{F}$. The magnetic vector potential is associated with electric sources ($\boldsymbol{M} = 0$, $\rho_m = 0$) and the electric vector potential is associated with magnetic sources ($\boldsymbol{J} = 0$, $\rho = 0$).

Consider the case when only electric sources exist ($\boldsymbol{M} = 0$, $\rho_m = 0$). From equation (A-1d), the magnetic field is solenoidal and can be represented as the curl of another vector $\boldsymbol{A}$,

$$\boldsymbol{H} = \frac{1}{\mu} \nabla \times \boldsymbol{A}. \tag{A-2}$$

The multiplicative factor $1/\mu$ has been included to conform with the conventional definition. The substitution of equation (A-2) into (A-1a) yields

$$\nabla \times \left(\boldsymbol{E} + j\omega \boldsymbol{A} \right) = 0 . \tag{A-3}$$

In expression (A-3), the term within the parentheses is irrotational and is, therefore, equal to the gradient of a scalar potential Φ^e. Thus,

$$\boldsymbol{E} = -j\omega \boldsymbol{A} - \nabla \Phi^e . \tag{A-4}$$

A negative sign in front of the potential has been included to conform with the convention. An alternate expression for the electric field can be obtained from expressions (A-1a) and (A-2) as

$$\boldsymbol{E} = \frac{1}{j\omega\mu\tilde{\varepsilon}} \left(\nabla \times \nabla \times \boldsymbol{A} - \mu \boldsymbol{J} \right) . \tag{A-5}$$

The substitution of equations (A-2) and (A-4) into (A-1b) yields the general equation for the magnetic vector potential, i.e.,

$$\nabla \times \nabla \times \boldsymbol{A} - k^2 \boldsymbol{A} = - j\omega\mu\tilde{\varepsilon} \nabla \Phi^e + \mu \boldsymbol{J} \ , \tag{A-6}$$

where $k = \omega\sqrt{\mu\tilde{\varepsilon}}$ is the wave number of the medium. From a theorem in vector calculus (reference 22), a vector is uniquely specified by giving its divergence and curl within a given region and its normal component over the boundary. Therefore, in the definition of the magnetic vector potential in (A-2), $\boldsymbol{A}$ is underdetermined because its divergence has not been specified. The specification of the divergence of $\boldsymbol{A}$ is referred to as the gauge condition (reference 23). The gauge condition chosen usually removes the scalar potential term from equation (A-6), thereby simplifying the equation. For the problems of interest in this report, spherical coordinates (r, θ, φ) are used and only radially-directed current sources are of interest.

Consider the case when only magnetic sources exist ($\boldsymbol{J} = 0$, $\rho = 0$). From equation (A-1c), the electric field is solenoidal and can be represented as the curl of another vector $\boldsymbol{F}$, i.e.,

$$\boldsymbol{E} = -\frac{1}{\tilde{\varepsilon}} \nabla \times \boldsymbol{F} . \tag{A-7}$$

The multiplicative factor $-1/\tilde{\varepsilon}$ has been included to conform with the conventional expression. The substitution of expression (A-7) into (A-1b) yields

$$\nabla \times \left(\boldsymbol{H} + j\omega \boldsymbol{F} \right) = 0 . \tag{A-8}$$

In equation (A-8), the term within the parentheses is irrotational and is therefore equal to the gradient of a scalar potential Φ^h. Thus,

$$\boldsymbol{H} = -j\omega\boldsymbol{F} - \nabla\Phi^h \ . \tag{A-9}$$

A negative sign in front of the scalar potential has been included to conform to the convention. An alternate expression for the magnetic field can be obtained from expressions (A-1a) and (A-7) as

$$\boldsymbol{H} = \frac{1}{j\omega\mu\tilde{\varepsilon}}\left(\nabla\times\nabla\times\boldsymbol{F} - \tilde{\varepsilon}\boldsymbol{M}\right). \tag{A-10}$$

The substitution of equations (A-7) and (A-9) into (A-1a) yields the general equation for the electric vector potential, thus,

$$\nabla\times\nabla\times\boldsymbol{F} - k^2\boldsymbol{F} = -j\omega\mu\tilde{\varepsilon}\nabla\Phi^h + \tilde{\varepsilon}\boldsymbol{M}. \tag{A-11}$$

In a homogeneous source-free region (i.e., $\boldsymbol{J} = \boldsymbol{M} = 0$), the electromagnetic (EM) fields can be expressed in terms of both vector potentials. From expressions (A-5) and (A-7), the electric field is given by

$$\boldsymbol{E} = \frac{1}{j\omega\mu\tilde{\varepsilon}}\nabla\times\nabla\times\boldsymbol{A} - \frac{1}{\tilde{\varepsilon}}\nabla\times\boldsymbol{F}. \tag{A-12}$$

From formulas (A-2) and (A-10), the magnetic field is given by

$$\boldsymbol{H} = \frac{1}{\mu}\nabla\times\boldsymbol{A} + \frac{1}{j\omega\mu\tilde{\varepsilon}}\nabla\times\nabla\times\boldsymbol{F}. \tag{A-13}$$

Equations (A-12) and (A-13) are the general formulas for the EM fields in terms of the vector potentials in a source-free region.

In the representation of the EM fields in terms of potentials, suitable expressions can be obtained from only one scalar component of both $\boldsymbol{A}$ and $\boldsymbol{F}$. In spherical coordinates, suitable choices for $\boldsymbol{A}$ and $\boldsymbol{F}$ are given in terms of their radial components as

$$\boldsymbol{A} = \hat{\boldsymbol{r}}\,A_r, \tag{A-14a}$$

and

$$\boldsymbol{F} = \hat{\boldsymbol{r}}\,F_r, \tag{A-14b}$$

where $\hat{\boldsymbol{r}}$ denotes the unit vector along the radial direction (see figure 4-1), and the radial components A_r and F_r are scalars. The substitution of equation (A-14a) into (A-6) with $\boldsymbol{J} = 0$ yields

$$\nabla \times \nabla \times (\hat{\boldsymbol{r}} A_r) - k^2(\hat{\boldsymbol{r}} A_r) = - j\omega\mu\tilde{\varepsilon}\nabla\Phi^e \ . \tag{A-15}$$

Similarly, the substitution of (A-14b) into (A-11) with $\boldsymbol{M} = 0$ results in

$$\nabla \times \nabla \times (\hat{\boldsymbol{r}} F_r) - k^2(\hat{\boldsymbol{r}} F_r) = - j\omega\mu\tilde{\varepsilon}\nabla\Phi^h \ . \tag{A-16}$$

To eliminate the scalar functions Φ^e and Φ^h in equations (A-15) and (A-16), respectively, gauge conditions for $\boldsymbol{A}$ and $\boldsymbol{F}$ must be defined. To obtain the appropriate gauge condition for each vector potential, one must first look at the three spherical components of each vector potential equation. For example, in equation (A-15), the r, θ, and φ components are

$$\frac{1}{r^2 \sin\theta}\frac{\partial}{\partial\theta}\left(\sin\theta \frac{\partial A_r}{\partial\theta}\right) + \frac{1}{r^2 \sin^2\theta}\frac{\partial^2 A_r}{\partial\varphi^2} + k^2 A_r = j\omega\mu\tilde{\varepsilon}\frac{\partial\Phi^e}{\partial r}, \tag{A-17a}$$

$$\frac{\partial^2 A_r}{\partial r\partial\theta} = -j\omega\mu\tilde{\varepsilon}\frac{\partial\Phi^e}{\partial\theta}, \tag{A-17b}$$

and

$$\frac{\partial^2 A_r}{\partial r\partial\varphi} = -j\omega\mu\tilde{\varepsilon}\frac{\partial\Phi^e}{\partial\varphi} \ . \tag{A-17c}$$

The θ and φ components of equation (A-15), given by expressions (A-17b) and (A-17c), respectively, are satisfied identically under the following gauge condition:

$$\frac{\partial A_r}{\partial r} = -j\omega\mu\tilde{\varepsilon}\Phi^e \ . \tag{A-18}$$

The substitution of the above gauge condition into the radial component equation (A-17a) yields

$$\frac{\partial^2 A_r}{\partial r^2} + \frac{1}{r^2 \sin\theta}\frac{\partial}{\partial\theta}\left(\sin\theta \frac{\partial A_r}{\partial\theta}\right) + \frac{1}{r^2 \sin^2\theta}\frac{\partial^2 A_r}{\partial\varphi^2} + k^2 A_r = 0 \ . \tag{A-19}$$

The first term in the above expression can be rewritten as

$$\frac{\partial^2 A_r}{\partial r^2} = \frac{1}{r}\frac{\partial}{\partial r}\left[r^2 \frac{\partial}{\partial r}\left(\frac{A_r}{r}\right)\right] \ . \tag{A-20}$$

The substitution of (A-20) into (A-19) followed by multiplication by $1/r$ yields

$$\frac{1}{r^2}\frac{\partial}{\partial r}\left[r^2\frac{\partial}{\partial r}\left(\frac{A_r}{r}\right)\right]+\frac{1}{r^2\sin\theta}\frac{\partial}{\partial\theta}\left[\sin\theta\frac{\partial}{\partial\theta}\left(\frac{A_r}{r}\right)\right]+\frac{1}{r^2\sin^2\theta}\left[\frac{\partial^2}{\partial\varphi^2}\left(\frac{A_r}{r}\right)\right]+k^2\left(\frac{A_r}{r}\right)=0\,. \quad \text{(A-21)}$$

The above equation may be written more concisely as

$$\left(\nabla^2+k^2\right)\frac{A_r}{r}=0\,. \quad \text{(A-22)}$$

Therefore, A_r/r is a solution of the scalar Helmholtz equation. Following a similar procedure for equation (A-16) in spherical coordinates results in

$$\left(\nabla^2+k^2\right)\frac{F_r}{r}=0 \quad \text{(A-23)}$$

provided that the following gauge condition is satisfied:

$$\frac{\partial F_r}{\partial r}=-j\omega\mu\tilde{\varepsilon}\Phi^h\,. \quad \text{(A-24)}$$

Formulas for the EM field components in terms of A_r and F_r can be obtained through substitution of expressions (A-14a) and (A-14b) into (A-12) and (A-13). In spherical coordinates, the field components are given as follows:

$$E_r=\frac{1}{j\omega\mu\tilde{\varepsilon}}\left(\frac{\partial^2}{\partial r^2}+k^2\right)A_r, \quad \text{(A-25a)}$$

$$E_\theta=\frac{1}{j\omega\mu\tilde{\varepsilon}}\frac{1}{r}\frac{\partial^2 A_r}{\partial r\partial\theta}-\frac{1}{\tilde{\varepsilon}}\frac{1}{r\sin\theta}\frac{\partial F_r}{\partial\varphi}, \quad \text{(A-25b)}$$

$$E_\varphi=\frac{1}{j\omega\mu\tilde{\varepsilon}}\frac{1}{r\sin\theta}\frac{\partial^2 A_r}{\partial r\partial\varphi}+\frac{1}{\tilde{\varepsilon}r}\frac{\partial F_r}{\partial\theta}, \quad \text{(A-25c)}$$

$$H_r=\frac{1}{j\omega\mu\tilde{\varepsilon}}\left(\frac{\partial^2}{\partial r^2}+k^2\right)F_r, \quad \text{(A-25d)}$$

$$H_\theta=\frac{1}{\mu}\frac{1}{r\sin\theta}\frac{\partial A_r}{\partial\varphi}+\frac{1}{j\omega\mu\tilde{\varepsilon}}\frac{1}{r}\frac{\partial^2 F_r}{\partial r\partial\theta}, \quad \text{(A-25e)}$$

and

$$H_\varphi = -\frac{1}{\mu r}\frac{\partial A_r}{\partial \theta} + \frac{1}{j\omega\mu\tilde{\varepsilon}}\frac{1}{r\sin\theta}\frac{\partial^2 F_r}{\partial r \partial \varphi} \ . \qquad \text{(A-25f)}$$

When $F_r = 0$, then $H_r = 0$, and the fields are referred to as transverse magnetic (TM) with respect to the radial direction. Similarly, when $A_r = 0$, then $E_r = 0$ and the fields are referred to as transverse electric (TE) with respect to the radial direction.

A.2 HERTZ VECTOR POTENTIALS

An alternate set of vector potentials that are frequently used in EMs are the electric- and magnetic-Hertz vectors $\boldsymbol{\pi}^e$ and $\boldsymbol{\pi}^h$, respectively. These vectors are defined in terms of the magnetic- and electric-vector potentials as follows (reference 20)

$$\boldsymbol{A} \equiv j\omega\mu\tilde{\varepsilon}\boldsymbol{\pi}^e, \qquad \text{(A-26a)}$$

and

$$\boldsymbol{F} \equiv j\omega\mu\tilde{\varepsilon}\boldsymbol{\pi}^h \ . \qquad \text{(A-26b)}$$

Therefore, in the frequency domain, the replacement of $\boldsymbol{A}$ and $\boldsymbol{F}$ by the Hertz vectors amounts to nothing more than the inclusion of a complex constant factor. The substitution of the above definitions into equations (A-12) and (A-13) yields

$$\boldsymbol{E} = \nabla\times\nabla\times\boldsymbol{\pi}^e - j\omega\mu\,\nabla\times\boldsymbol{\pi}^h, \qquad \text{(A-27)}$$

and

$$\boldsymbol{H} = j\omega\tilde{\varepsilon}\,\nabla\times\boldsymbol{\pi}^e + \nabla\times\nabla\times\boldsymbol{\pi}^h \ . \qquad \text{(A-28)}$$

The above formulas are the EM fields in a homogeneous source-free region in terms of the Hertz vectors.

To represent the EM fields in spherical coordinates in terms of the Hertz vectors, suitable expressions can be obtained from only one scalar component of both $\boldsymbol{A}$ and $\boldsymbol{F}$. Following expressions (A-14a) and (A-14b), the following are defined:

$$\boldsymbol{\pi}^e = \hat{\boldsymbol{r}}\,\pi_r^e \equiv \hat{\boldsymbol{r}}\,r\Psi^e, \qquad \text{(A-29a)}$$

and

$$\pi^h = \hat{r}\,\pi_r^h \equiv \hat{r}\,r\Psi^h \ . \tag{A-29b}$$

With the above definitions, the same procedure after expressions (A-14a) and (A-14b) is followed, resulting in

$$\nabla^2\Psi^e + k^2\Psi^e = 0\,, \tag{A-30a}$$

and

$$\nabla^2\Psi^h + k^2\Psi^h = 0\ . \tag{A-30b}$$

The terms Ψ^e and Ψ^h are sometimes referred to as the Debye potentials (reference 23).

Formulas for the EM field components in terms of Ψ^e and Ψ^h can be obtained through the substitution of expressions (A-29a) and (A-29b) into (A-27) and (A-28). In spherical coordinates, the field components are given as follows:

$$E_r = \left(\frac{\partial^2}{\partial r^2} + k^2\right)(r\Psi^e)\,, \tag{A-31a}$$

$$E_\theta = \frac{1}{r}\frac{\partial^2(r\Psi^e)}{\partial r\partial\theta} - \frac{j\omega\mu}{\sin\theta}\frac{\partial\Psi^h}{\partial\varphi}\,, \tag{A-31b}$$

$$E_\varphi = \frac{1}{r\sin\theta}\frac{\partial^2(r\Psi^e)}{\partial r\partial\varphi} + j\omega\mu\frac{\partial\Psi^h}{\partial\theta}\,, \tag{A-31c}$$

$$H_r = \left(\frac{\partial^2}{\partial r^2} + k^2\right)(r\Psi^h)\,, \tag{A-31d}$$

$$H_\theta = \frac{j\omega\tilde{\varepsilon}}{\sin\theta}\frac{\partial\Psi^e}{\partial\varphi} + \frac{1}{r}\frac{\partial(r\Psi^h)}{\partial r\partial\theta}\,, \tag{A-31e}$$

and

$$H_\varphi = -j\omega\tilde{\varepsilon}\frac{\partial\Psi^e}{\partial\theta} + \frac{1}{r\sin\theta}\frac{\partial^2(r\Psi^h)}{\partial r\partial\varphi}\ . \tag{A-31f}$$

In the above formulas, $\pi_r^e = r\ \Psi^e$ and $\pi_r^h = r\ \Psi^h$. When $\pi_r^e = 0$, the fields are TM with respect to the radial direction. Similarly, when $\pi_r^h = 0$, the fields are TE with respect to the radial direction.

APPENDIX B
SOLUTION OF THE HELMHOLTZ EQUATION IN SPHERICAL COORDINATES

In spherical coordinates, it is shown in appendix A that the electromagnetic (EM) fields can be expressed in terms of the two Debye potentials, Ψ^e and Ψ^h. In addition, at a source-free point, it was shown that these two scalar functions each satisfy the Helmholtz equation, namely

$$\nabla^2\Psi + k^2\Psi = 0 \ . \tag{B-1}$$

In this report, because the transverse magnetic (TM) and transverse electric (TE) fields are derived for axisymmetric sources, the Debye potentials are determined under axisymmetric conditions. Therefore, under axisymmetric conditions, the Helmholtz equation is expressed in spherical coordinates as

$$\frac{1}{r^2}\frac{\partial}{\partial r}\left(r^2\frac{\partial\Psi}{\partial r}\right) + \frac{1}{r^2\sin\theta}\frac{\partial}{\partial\theta}\left(\sin\theta\,\frac{\partial\Psi}{\partial\theta}\right) + k^2\Psi = 0 \ , \tag{B-2}$$

where $\Psi = \Psi(r,\theta)$.

To solve equation (B-2), the separation of variables method is applied. In this method, let

$$\Psi(r,\theta) = R(r)\,T(\theta) \ . \tag{B-3}$$

The substitution of expression (B-3) into (B-2) followed with the multiplication of each side of the equation by r^2/RT yields

$$\frac{1}{R}\frac{d}{dr}\left(r^2\frac{dR}{dr}\right) + \frac{1}{T\sin\theta}\frac{d}{d\theta}\left(\sin\theta\,\frac{dT}{d\theta}\right) + k^2r^2 = 0 \ . \tag{B-4}$$

The above equation can be rewritten as an r-dependent part on one side and a θ-dependent part on the other side, each of which can be set equal to an arbitrary constant $\nu(\nu+1)$ resulting in

$$\frac{1}{R}\frac{d}{dr}\left(r^2\frac{dR}{dr}\right) + k^2r^2 = \frac{-1}{T\sin\theta}\frac{d}{d\theta}\left(\sin\theta\,\frac{dT}{d\theta}\right) \equiv \nu(\nu+1) \ . \tag{B-5}$$

Expression (B-5) can be decomposed into r-dependent and θ-dependent differential equations as

$$\frac{d}{dr}\left(r^2\frac{dR}{dr}\right)+\left[k^2r^2-\nu(\nu+1)\right]R=0\,, \tag{B-6a}$$

and

$$\frac{1}{\sin\theta}\frac{d}{d\theta}\left(\sin\theta\frac{dT}{d\theta}\right)+\nu(\nu+1)T=0\,. \tag{B-6b}$$

The solution of equation (B-6a) is given by

$$R(r)=A\,h_\nu^{(1)}(kr)+B\,h_\nu^{(2)}(kr)\,, \tag{B-7}$$

where $h_\nu^{(1)}(kr)$ and $h_\nu^{(2)}(kr)$ are the spherical Hankel functions of the first and second kinds, respectively, of order ν, and A and B are arbitrary constants. The spherical Hankel functions are expressed in terms of the cylindrical Hankel functions as (reference 24)

$$h_\nu^{(n)}(kr)=\sqrt{\frac{\pi}{2kr}}\,H_{\nu+1/2}^{(n)}(kr)\,,\quad n=1,2\,. \tag{B-8}$$

The solution of (B-6b) is given as follows:

$$T(\theta)=C\,P_\nu(-\cos\theta)+D\,Q_\nu(-\cos\theta)\,, \tag{B-9}$$

where P_ν and Q_ν are Legendre functions of the first and second kinds, respectively, of degree ν and order zero. It should be noted that P_ν is singular when its argument is -1 ($\theta=0$), while Q_ν is singular when its argument is ±1 ($\theta=0,\,\pi$). The minus sign has been included in the argument so that P_ν is singular at $\theta=0$.

For the three radiating sources under consideration in this report, the EM fields are finite everywhere except at the source location ($r=r_s$, $\theta=0$). Therefore, Q_ν is not an acceptable solution of equation (B-6b) and $D=0$. Thus, the substitution of formulas (B-7) and (B-9) into (B-3) yields

$$\Psi(r,\theta)=\left[A\,h_\nu^{(1)}(kr)+B\,h_\nu^{(2)}(kr)\right]P_\nu(-\cos\theta)\,. \tag{B-10}$$

Two of the three constants A, B, and ν are determined from the boundary conditions at the inner ($r=a$) and outer ($r=a+h$) surfaces.

APPENDIX C
TRANSVERSE MAGNETIC (TM) AND TRANSVERSE ELECTRIC (TE) MODAL EXPANSIONS IN A SPHERICAL WAVEGUIDE

Consider the spherical earth-ionosphere waveguide described in figure 1-1. The main interest of this report is the determination of the electromagnetic (EM) fields radiated in the waveguide ($a = r = a + h$) by a dipole source located along the north pole ($\theta = 0$) of the spherical coordinate system. The waveguide is filled with air and has a permittivity $\varepsilon_o = 8.854 \times 10^{-12}$ F/m, a permeability $\mu_o = 4\pi \times 10^{-7}$ H/m, and an intrinsic wave number of $k_o = \omega\sqrt{\mu_o \varepsilon_o}$, where ω is the angular frequency in radians per second (rad/s). The spherical waveguide boundaries along the earth ($r = a$) and the ionosphere ($r = a + h$) are characterized by scalar surface impedances. These impedances are approximations of the general tensor surface impedances that are more representative of these boundaries. However, the scalar impedances allow for tractable solutions of the field equations.

In this appendix, the transverse magnetic (TM) and transverse electric (TE) modes that radiate in a spherical earth-ionosphere waveguide are derived under the assumption that the fields are axisymmetric. The axisymmetric TM modes are launched by a vertical electric dipole (VED) located along the north pole of the waveguide. Similarly, the axisymmetric TE modes are launched by a vertical magnetic dipole (VMD) located in the waveguide along the north pole. As shown in appendix H, the HED fields involve the superposition of both the TM and TE modes.

C.1 TM MODES

In appendix A, it is shown that the TM fields with respect to the radial direction can be obtained from the radial component of the electric-Hertz vector $\boldsymbol{\pi}^e$. Under axisymmetric conditions ($?/?\varphi = 0$), the EM fields are obtained from equations (A-31) and are expressed as

$$E_r = \left(\frac{\partial^2}{\partial r^2} + k_o^2\right)(r\Psi^e) = -\frac{1}{r\sin\theta}\frac{\partial}{\partial\theta}\left(\sin\theta\frac{\partial\Psi^e}{\partial\theta}\right), \tag{C-1a}$$

$$E_\theta = \frac{1}{r}\frac{\partial^2(r\Psi^e)}{\partial r\partial\theta}, \tag{C-1b}$$

and

$$H_\varphi = -j\omega\varepsilon_o \frac{\partial \Psi^e}{\partial \theta} \ . \tag{C-1c}$$

Note that the three remaining field components vanish, namely $E_\varphi = H_r = H_\theta = 0$. In the above formulas, the scalar function Ψ^e is a Debye potential and is related to π_r^e as

$$\Psi^e = \frac{\pi_r^e}{r} , \tag{C-2}$$

where Ψ^e is a solution of the scalar Helmholtz equation given by (A-30a). The solution of the Helmholtz equation is derived in appendix B and is given by expression (B-10). This solution can be rewritten as follows:

$$\Psi^e = \left[h_\nu^{(1)}(k_o r) + B_\nu^e h_\nu^{(2)}(k_o r) \right] P_\nu(-\cos\theta) , \tag{C-3}$$

where B_ν^e and ν are constants. The constants B_ν^e and ν are determined from the boundary conditions at the inner and outer boundaries of the waveguide that are given below. In expression (C-3), note that a constant multiplying $h_\nu^{(1)}(k_o r)$ has not been included because it is unnecessary in satisfying the boundary conditions.

Under the assumptions of a homogeneous, isotropic earth (inner sphere) and a homogeneous, isotropic ionosphere (outer region) of constant height h, the surface EM fields satisfy the following boundary conditions:

$$Z_g = -\left. \frac{E_\theta}{H_\varphi} \right|_{r=a} , \tag{C-4a}$$

and

$$Z_e = \left. \frac{E_\theta}{H_\varphi} \right|_{r=a+h} , \tag{C-4b}$$

where Z_g and Z_e denote the surface impedances along the air-earth and air-ionosphere interfaces, respectively. The substitution of the field component expressions (C-1b) and (C-1c) into the boundary conditions (C-4a) and (C-4b) yields

$$\frac{1}{a} \left. \frac{\partial^2 (r\Psi^e)}{\partial r \partial \theta} \right|_{r=a} = j\omega\varepsilon_o Z_g \left. \frac{\partial \Psi^e}{\partial \theta} \right|_{r=a} , \tag{C-5a}$$

and

$$\frac{1}{(a+h)}\left.\frac{\partial^2(r\Psi^e)}{\partial r\partial\theta}\right|_{r=a+h} = -j\omega\varepsilon_o Z_e \left.\frac{\partial\Psi^e}{\partial\theta}\right|_{r=a+h}. \tag{C-5b}$$

Note that the θ derivatives in the above boundary conditions are continuous across each interface. In addition, the surface impedances Z_g and Z_e are each constant along the surfaces $r = a$ and $r = a + h$, respectively. Therefore, the boundary conditions (C-5a) and (C-5b) reduce to

$$\frac{1}{k_o a}\left.\frac{\partial(r\Psi^e)}{\partial r}\right|_{r=a} = j\Delta_g \Psi^e\Big|_{r=a}, \tag{C-6a}$$

and

$$\frac{1}{k_o(a+h)}\left.\frac{\partial(r\Psi^e)}{\partial r}\right|_{r=a+h} = -j\Delta_e \Psi^e\Big|_{r=a+h}, \tag{C-6b}$$

where $\Delta_g = Z_g/\eta_o$ and $\Delta_e = Z_e/\eta_o$ denote the normalized surface impedances of the inner and outer boundaries, respectively, and $\eta_o = \sqrt{\mu_o/\varepsilon_o}$ is the intrinsic impedance of free space.

The substitution of expression (C-3) for Ψ^e into the boundary condition (C-6a) can be solved for B_ν^e to yield

$$B_\nu^e = -\frac{\left\{\frac{1}{u_g}\left.\frac{\partial\left[uh_\nu^{(1)}(u)\right]}{\partial u}\right|_{u=u_g} - j\Delta_g h_\nu^{(1)}(u_g)\right\}}{\left\{\frac{1}{u_g}\left.\frac{\partial\left[uh_\nu^{(2)}(u)\right]}{\partial u}\right|_{u=u_g} - j\Delta_g h_\nu^{(2)}(u_g)\right\}}, \tag{C-7a}$$

where $u = k_o r$ and $u_g = k_o a$. Following a similar procedure, the substitution of expression (C-3) for Ψ^e into the boundary condition (C-6b) can be solved for B_ν^e to yield

$$B_\nu^e = -\frac{\left\{\frac{1}{u_i}\left.\frac{\partial\left[uh_\nu^{(1)}(u)\right]}{\partial u}\right|_{u=u_i} + j\Delta_e h_\nu^{(1)}(u_i)\right\}}{\left\{\frac{1}{u_i}\left.\frac{\partial\left[uh_\nu^{(2)}(u)\right]}{\partial u}\right|_{u=u_i} + j\Delta_e h_\nu^{(2)}(u_i)\right\}}, \tag{C-7b}$$

where $u_i = k_o(a + h)$. The TM field components must satisfy the boundary conditions (C-4a) and (C-4b) simultaneously. Therefore, the constant B_ν^e in expression (C-7a) is set equal to (C-7b) and yields

$$\frac{\left\{\frac{1}{u_g}\left.\frac{\partial\left[uh_\nu^{(2)}(u)\right]}{\partial u}\right|_{u=u_g} - j\Delta_g h_\nu^{(2)}(u_g)\right\}}{\left\{\frac{1}{u_g}\left.\frac{\partial\left[uh_\nu^{(1)}(u)\right]}{\partial u}\right|_{u=u_g} - j\Delta_g h_\nu^{(1)}(u_g)\right\}} \frac{\left\{\frac{1}{u_i}\left.\frac{\partial\left[uh_\nu^{(1)}(u)\right]}{\partial u}\right|_{u=u_i} + j\Delta_e h_\nu^{(1)}(u_i)\right\}}{\left\{\frac{1}{u_i}\left.\frac{\partial\left[uh_\nu^{(2)}(u)\right]}{\partial u}\right|_{u=u_i} + j\Delta_e h_\nu^{(2)}(u_i)\right\}} = 1 . \quad \text{(C-8)}$$

The above expression denotes the characteristic or modal equation for the TM modes in a spherical earth-ionosphere waveguide. The solution of expression (C-8) yields a discrete set of eigenvalues ν_n, where n denotes an integer index and corresponds to a particular mode.

Given the infinite number of discrete eigenvalues that satisfy the characteristic equation (C-8), Ψ^e can be expressed in terms of a modal expansion as

$$\Psi^e = \sum_{n=0}^{\infty} \Psi_{\nu_n}^e(r,\theta) = \sum_{n=0}^{\infty} A_{\nu_n}^e R_{\nu_n}^e(u) P_{\nu_n}(-\cos\theta) , \quad \text{(C-9)}$$

where $R_{\nu_n}^e$ is defined as

$$R_{\nu_n}^e(u) \equiv h_{\nu_n}^{(1)}(u) + B_{\nu_n}^e h_{\nu_n}^{(2)}(u) . \quad \text{(C-10)}$$

In addition, $A_{\nu_n}^e$ is referred to here as the modal excitation coefficient and depends on the source strength. The modal indices n in expression (C-9) correspond to the TM mode indices for the parallel-plate waveguide model as defined in section 2.1. Expressions for the modal expansions of the TM fields are determined through the substitution of the formula (C-9) into equations (C-1) and are given as follows:

$$E_r = \frac{k_o}{u} \sum_{n=0}^{\infty} A_{\nu_n}^e \nu_n(\nu_n + 1) R_{\nu_n}^e(u) P_{\nu_n}(-\cos\theta) , \quad \text{(C-11a)}$$

$$E_\theta = \frac{k_o}{u} \sum_{n=0}^{\infty} A_{\nu_n}^e \frac{\partial}{\partial u}\left[uR_{\nu_n}^e(u)\right] \frac{\partial}{\partial\theta} P_{\nu_n}(-\cos\theta) , \quad \text{(C-11b)}$$

and

$$H_{\varphi} = -j\omega\varepsilon_o \sum_{n=0}^{\infty} A^e_{\nu_n} R^e_{\nu_n}(u) \frac{\partial}{\partial\theta} P_{\nu_n}(-\cos\theta) \ . \qquad \text{(C-11c)}$$

The expression for E_r was obtained through use of the relation

$$\left(\frac{d^2}{dr^2} + k_o^2\right)\left[rh_\nu^{(m)}(k_o r)\right] = \frac{\nu(\nu+1)}{r} h_\nu^{(m)}(k_o r) \ , \ m = 1, 2 \ . \qquad \text{(C-12)}$$

The above formula can be obtained from expression (B-6a) through the following equivalence:

$$\frac{d}{dr}\left[r^2 \frac{d}{dr} h_\nu^{(m)}(k_o r)\right] = r \frac{d^2}{dr^2}\left[rh_\nu^{(m)}(k_o r)\right], \ m = 1, 2 \ . \qquad \text{(C-13)}$$

C.2 TE MODES

In appendix A, it is shown that the TE fields with respect to the radial direction can be obtained from the radial component of the magnetic Hertz vector $\boldsymbol{\pi}^h$. Under axisymmetric conditions ($?/?\varphi = 0$), the EM fields are obtained from equations (A-31) and are expressed as

$$H_r = \left(\frac{\partial^2}{\partial r^2} + k_o^2\right)(r\Psi^h) = -\frac{1}{r\sin\theta} \frac{\partial}{\partial\theta}\left(\sin\theta \frac{\partial\Psi^h}{\partial\theta}\right), \qquad \text{(C-14a)}$$

$$H_\theta = \frac{1}{r} \frac{\partial^2(r\Psi^h)}{\partial r\partial\theta}, \qquad \text{(C-14b)}$$

and

$$E_\varphi = j\omega\mu_o \frac{\partial\Psi^h}{\partial\theta} \ . \qquad \text{(C-14c)}$$

Note that the three remaining field components vanish, namely $H_\varphi = E_r = E_\theta = 0$. In the above formulas, the scalar function Ψ^e is a Debye potential and is related to π_r^h as

$$\Psi^h = \frac{\pi_r^h}{r} \ , \qquad \text{(C-15)}$$

where Ψ^h is a solution of the scalar Helmholtz equation given by (A-30b). The solution of the Helmholtz equation is derived in appendix B and is given by expression (B-10). The application of the solution (B-10) to equation (A-30b) yields

$$\Psi^h = \left[h_\nu^{(1)}(k_o r) + B_\nu^h h_\nu^{(2)}(k_o r)\right] P_\nu(-\cos\theta) \ , \qquad \text{(C-16)}$$

where B_ν^h and ν are constants. The constants B_ν^h and ν are determined from the boundary conditions at the inner and outer waveguide boundaries that are given below. As was previously mentioned for the TM modes, a constant multiplying $h_\nu^{(1)}(k_o r)$ has not been included because it is unnecessary in satisfying the boundary conditions.

Under the assumptions of a homogeneous, isotropic earth (inner sphere) and a homogeneous, isotropic ionosphere (outer region) of constant height h, the TE surface EM fields satisfy the boundary conditions

$$Z_g = \left. \frac{E_\varphi}{H_\theta} \right|_{r=a}, \tag{C-17a}$$

$$Z_h = - \left. \frac{E_\varphi}{H_\theta} \right|_{r=a+h}, \tag{C-17b}$$

where Z_g and Z_h denote the surface impedances along the air-earth and air-ionosphere interfaces, respectively. The surface impedances Z_g and Z_h given above are generally different from those corresponding to the TM modes given in expressions (C-4a) and (C-4b) because of the anisotropy of the earth and ionosphere. In this report, the earth and ionosphere are each represented as a constant surface impedance that is independent of the mode index, with the surface impedance of the ionosphere different for TE and TM modes.

The substitution of the field component expressions (C-14b) and (C-14c) into the boundary conditions (C-17a) and (C-17b) yields

$$j\omega\mu_o \left. \frac{\partial \Psi^h}{\partial \theta} \right|_{r=a} = \frac{Z_g}{a} \left. \frac{\partial^2 (r\Psi^h)}{\partial r \partial \theta} \right|_{r=a}, \tag{C-18a}$$

and

$$j\omega\mu_o \left. \frac{\partial \Psi^h}{\partial \theta} \right|_{r=a+h} = - \frac{Z_h}{(a+h)} \left. \frac{\partial^2 (r\Psi^h)}{\partial r \partial \theta} \right|_{r=a+h}. \tag{C-18b}$$

Note that the θ derivatives in the above boundary conditions are continuous across each interface. In addition, the surface impedances Z_g and Z_h are each constant along the surfaces $r = a$ and $r = a + h$, respectively. Therefore, the boundary conditions (C-18a) and (C-18b) reduce to

$$\frac{j}{\Delta_g}\Psi^h\Big|_{r=a} = \frac{1}{k_o a}\left.\frac{\partial(r\Psi^h)}{\partial r}\right|_{r=a}, \tag{C-19a}$$

and

$$\frac{j}{\Delta_h}\Psi^h\Big|_{r=a+h} = -\frac{1}{k_o(a+h)}\left.\frac{\partial(r\Psi^h)}{\partial r}\right|_{r=a+h}, \tag{C-19b}$$

where Δ_g and $\Delta_h = Z_h/\eta_o$ denote the normalized surface impedances of the inner and outer waveguide boundaries, respectively.

The substitution of expression (C-16) for Ψ^h into the boundary condition (C-19a) can be solved for B_ν^h to yield

$$B_\nu^h = -\frac{\left\{\frac{1}{u_g}\left.\frac{\partial\left[uh_\nu^{(1)}(u)\right]}{\partial u}\right|_{u=u_g} - j\frac{1}{\Delta_g}h_\nu^{(1)}(u_g)\right\}}{\left\{\frac{1}{u_g}\left.\frac{\partial\left[uh_\nu^{(2)}(u)\right]}{\partial u}\right|_{u=u_g} - j\frac{1}{\Delta_g}h_\nu^{(2)}(u_g)\right\}}, \tag{C-20a}$$

where u and u_g were defined in the TM mode derivation. Following a similar procedure, the substitution of expression (C-16) for Ψ^h into the boundary condition (C-19b) can be solved for B_ν^h to yield

$$B_\nu^h = -\frac{\left\{\frac{1}{u_i}\left.\frac{\partial\left[uh_\nu^{(1)}(u)\right]}{\partial u}\right|_{u=u_i} + j\frac{1}{\Delta_h}h_\nu^{(1)}(u_i)\right\}}{\left\{\frac{1}{u_i}\left.\frac{\partial\left[uh_\nu^{(2)}(u)\right]}{\partial u}\right|_{u=u_i} + j\frac{1}{\Delta_h}h_\nu^{(2)}(u_i)\right\}}, \tag{C-20b}$$

where u_i was defined in the TM mode derivation. Note that expression (C-20a) for the TE field amplitude coefficient B_ν^h is equivalent to expression (C-7a) for the TM field amplitude coefficient B_ν^e if Δ_g is replaced by $1/\Delta_g$. Similarly, expression (C-20b) for B_ν^h is equivalent to expression (C-7b) for B_ν^e if Δ_e is replaced by $1/\Delta_h$. Because the TE field components must satisfy the boundary conditions (C-17a) and (C-17b) simultaneously, the constant B_ν^h in expression (C-20a) is set equal to expression (C-20b) and yields

$$\frac{\left\{\frac{1}{u_g}\left.\frac{\partial\left[uh_\nu^{(2)}(u)\right]}{\partial u}\right|_{u=u_g} - j\frac{1}{\Delta_g}h_\nu^{(2)}(u_g)\right\}\left\{\frac{1}{u_i}\left.\frac{\partial\left[uh_\nu^{(1)}(u)\right]}{\partial u}\right|_{u=u_i} + j\frac{1}{\Delta_h}h_\nu^{(1)}(u_i)\right\}}{\left\{\frac{1}{u_g}\left.\frac{\partial\left[uh_\nu^{(1)}(u)\right]}{\partial u}\right|_{u=u_g} - j\frac{1}{\Delta_g}h_\nu^{(1)}(u_g)\right\}\left\{\frac{1}{u_i}\left.\frac{\partial\left[uh_\nu^{(2)}(u)\right]}{\partial u}\right|_{u=u_i} + j\frac{1}{\Delta_h}h_\nu^{(2)}(u_i)\right\}} = 1\,. \quad \text{(C-21)}$$

The above expression denotes the characteristic or modal equation for the TE modes in a spherical earth-ionosphere waveguide. Note that the above TE characteristic equation is equivalent to the TM characteristic equation (C-8) if Δ_g is replaced by $1/\Delta_g$ and Δ_e is replaced by $1/\Delta_h$. The solution of equation (C-21) yields a discrete set of eigenvalues $\bar{\nu}_m$, where m denotes an integer index and corresponds to a particular mode.

Given the infinite number of discrete eigenvalues that satisfy the characteristic equation (C-21), Ψ^h can be expressed in terms of a modal expansion as

$$\Psi^h = \sum_{m=1}^{\infty} \Psi^h_{\bar{\nu}_m}(r,\theta) = \sum_{m=1}^{\infty} A^h_{\bar{\nu}_m} R^h_{\bar{\nu}_m}(u)\, P_{\bar{\nu}_m}(-\cos\theta)\,, \quad \text{(C-22)}$$

where $R^h_{\bar{\nu}_m}(u)$ is defined as

$$R^h_{\bar{\nu}_m}(u) \equiv h^{(1)}_{\bar{\nu}_m}(u) + B^h_{\bar{\nu}_m} h^{(2)}_{\bar{\nu}_m}(u)\,. \quad \text{(C-23)}$$

In formula (C-22), $A^h_{\bar{\nu}_m}$ is the TE mode excitation coefficient and depends on the source strength. The modal indices m in expression (C-22) correspond to the TE mode indices for the parallel-plate waveguide model as defined in section 2.2. Expressions for the modal expansions of the TE fields are determined through the substitution of formula (C-22) into equations (C-14) and are given as

$$H_r = \frac{k_o}{u}\sum_{m=1}^{\infty} A^h_{\bar{\nu}_m}\,\bar{\nu}_m(\bar{\nu}_m+1)\,R^h_{\bar{\nu}_m}(u)\,P_{\bar{\nu}_m}(-\cos\theta)\,, \quad \text{(C-24a)}$$

$$H_\theta = \frac{k_o}{u}\sum_{m=1}^{\infty} A^h_{\bar{\nu}_m}\frac{\partial}{\partial u}\left[uR^e_{\nu_n}(u)\right]\frac{\partial}{\partial\theta}P_{\bar{\nu}_m}(-\cos\theta)\,, \quad \text{(C-24b)}$$

and

$$E_\varphi = j\omega\mu_o\sum_{m=1}^{\infty} A^h_{\bar{\nu}_m} R^h_{\bar{\nu}_m}(u)\frac{\partial}{\partial\theta}P_{\bar{\nu}_m}(-\cos\theta)\,. \quad \text{(C-24c)}$$

Note that the expression for H_r was obtained through use of formula (C-12).

APPENDIX D
PROOF OF ORTHOGONALITY OF RADIAL FUNCTIONS

In appendix A, it is shown that the transverse magnetic (TM) and the transverse electric (TE) fields in a spherical waveguide can be expressed in terms of the Debye potentials Ψ^e and Ψ^h, respectively. In appendix C, it is shown that the radial dependence of each Debye potential is given in terms of a function $R_\nu(u)$, $u = k_o r$, which satisfies the following differential equation:

$$\frac{d}{du}\left(u^2 \frac{dR_\nu}{du}\right) + \left[u^2 - \nu(\nu+1)\right] R_\nu = 0 . \tag{D-1}$$

The above equation may be rewritten as

$$u \frac{d^2}{du^2}\left(u R_\nu\right) + \left[u^2 - \nu(\nu+1)\right] R_\nu = 0 . \tag{D-2}$$

To prove the orthogonality of the TM mode radial functions, consider the radial functions $R^e_\mu(u)$ and $R^e_\nu(u)$ corresponding to two different TM modes that satisfy the following differential equations:

$$u \frac{d^2}{du^2}\left(u R^e_\mu\right) + \left[u^2 - \mu(\mu+1)\right] R^e_\mu = 0 , \tag{D-3a}$$

and

$$u \frac{d^2}{du^2}\left(u R^e_\nu\right) + \left[u^2 - \nu(\nu+1)\right] R^e_\nu = 0 . \tag{D-3b}$$

From formulas (C-6), the boundary conditions satisfied by each TM mode radial function are given as

$$\frac{1}{u_g} \frac{d(uR^e_\eta)}{du}\bigg|_{u=u_g} = j\Delta_g R^e_\eta(u_g) , \tag{D-4a}$$

$$\frac{1}{u_i} \frac{d(uR^e_\eta)}{du}\bigg|_{u=u_i} = -j\Delta_e R^e_\eta(u_i) , \tag{D-4b}$$

where $u_g = k_o a$, $u_i = k_o(a+h)$, η is a complex eigenvalue that satisfies the TM mode characteristic equation (C-8), and Δ_g and Δ_e denote the normalized surface impedances of the

inner and outer boundaries, respectively. If equation (D-3a) is multiplied by $R_\nu^e(u)$ and equation (D-3b) is multiplied by $R_\mu^e(u)$, the difference of the resulting equations yields

$$\left(uR_\mu^e\right)\frac{d^2}{du^2}\left(uR_\nu^e\right)-\left(uR_\nu^e\right)\frac{d^2}{du^2}\left(uR_\mu^e\right)=\left[\nu(\nu+1)-\mu(\mu+1)\right]R_\mu^e R_\nu^e\,. \tag{D-5}$$

If the above formula is integrated over the height of the waveguide followed by integration by parts, the following is obtained:

$$\left(uR_\mu^e\right)\frac{d}{du}\left(uR_\nu^e\right)\Big|_{u=u_g}^{u=u_i}-\left(uR_\nu^e\right)\frac{d}{du}\left(uR_\mu^e\right)\Big|_{u=u_g}^{u=u_i}=\left[\nu(\nu+1)-\mu(\mu+1)\right]\int_{u_g}^{u_i}R_\mu^e(u)\,R_\nu^e(u)\,du\,. \tag{D-6}$$

The application of the boundary conditions (D-4) to the above result yields the following orthogonality relation:

$$\int_{u_g}^{u_i}R_\mu^e(u)\,R_\nu^e(u)\,du=0\;,\;\mu\neq\nu\;. \tag{D-7}$$

Because the above result is independent of θ, the radial functions may be replaced by the corresponding Debye potentials, i.e.,

$$\int_{u_g}^{u_i}\Psi_\mu^e(u,\theta)\,\Psi_\nu^e(u,\theta)\,du=0\;,\;\mu\neq\nu\;. \tag{D-8}$$

To prove the orthogonality of the TE mode radial functions, consider the radial functions $R_\mu^h(u)$ and $R_\nu^h(u)$ corresponding to two different TE modes that satisfy the differential equations (D-3a) and (D-3b), respectively, where the superscript e is replaced by h. From formulas (C-19), the boundary conditions satisfied by each TE mode radial function are given as

$$\frac{1}{u_g}\frac{d(uR_\eta^h)}{du}\Big|_{u=u_g}=\frac{j}{\Delta_g}R_\eta^h(u_g)\,, \tag{D-9a}$$

and

$$\frac{1}{u_i}\frac{d(uR_\eta^h)}{du}\Big|_{u=u_i}=-\frac{j}{\Delta_h}R_\eta^h(u_i)\,, \tag{D-9b}$$

where Δ_h denotes the normalized surface impedance of the outer boundary and η is a complex eigenvalue that satisfies the TE mode characteristic equation (C-21). If the procedure below expressions (D-4) is followed for the two TE radial functions $R_\mu^h(u)$ and $R_\nu^h(u)$, the result obtained is

$$\left(uR_\mu^h\right)\frac{d}{du}\left(uR_\nu^h\right)\Big|_{u=u_g}^{u=u_i} - \left(uR_\nu^h\right)\frac{d}{du}\left(uR_\mu^h\right)\Big|_{u=u_g}^{u=u_i}$$

$$= \left[\nu(\nu+1) - \mu(\mu+1)\right]\int_{u_g}^{u_i} R_\mu^h(u)\, R_\nu^h(u)\, du \ . \qquad \text{(D-10)}$$

The application of the boundary conditions (D-9) to the above result yields the orthogonality relation

$$\int_{u_g}^{u_i} R_\mu^h(u)\, R_\nu^h(u)\, du = 0 \ , \ \mu \neq \nu \ . \qquad \text{(D-11)}$$

Because the above result is independent of θ, the radial functions may be replaced by the corresponding Debye potentials, i.e.,

$$\int_{u_g}^{u_i} \Psi_\mu^h(u,\theta)\, \Psi_\nu^h(u,\theta)\, du = 0 \ , \ \mu \neq \nu \ . \qquad \text{(D-12)}$$

The orthogonality relations (D-7) and (D-11) are valid provided that the surface impedances of the inner and outer boundaries are independent of the mode indices. If the above procedure is applied to two radial functions $R_\mu^e(u)$ and $R_\nu^h(u)$, corresponding to one TM mode and one TE mode, respectively, it is readily seen that these functions are not orthogonal. Therefore, the TM and TE mode Debye potentials are not orthogonal with respect to each other. (The evaluation of the integrals (D-7) and (D-11) for $\mu = \nu$ is presented in appendix I.)

APPENDIX E
EXCITATION COEFFICIENTS FOR TRANSVERSE MAGNETIC (TM) AND TRANSVERSE ELECTRIC (TE) MODES

In the derivation of the modal expansions of the electromagnetic (EM) fields in a spherical waveguide given in appendix C, each term in the expansion includes an excitation coefficient. Each modal excitation coefficient depends on the source strength and provides a measure of the coupling into that mode. In this appendix, the excitation coefficients corresponding to the transverse magnetic (TM) and transverse electric (TE) modes in a spherical waveguide are derived. The excitation coefficients for the TM modes are applied in the derivation of the vertical electric dipole (VED) fields in appendix F. In addition, the excitation coefficients for the TE modes are applied in the derivation of the vertical magnetic dipole (VMD) fields in appendix G.

E.1 TM MODES

Consider a VED of moment $p = I\,dl$ that is located at the radial distance $r_s = a + z_s$ along the $\theta = 0$ axis of the spherical earth-ionosphere waveguide shown in figure 1-1. As shown in appendix F, the differential equation for the electric Debye potential Ψ^e is given by

$$\left(\nabla^2 + k_o^2\right) \Psi^e = -\frac{p}{j\omega\varepsilon_o r_s}\,\delta(\boldsymbol{r} - \boldsymbol{r}_s)\,, \tag{E-1}$$

where δ denotes the Dirac delta function. The solution of the above differential equation at source-free points ($\boldsymbol{r}$? $\boldsymbol{r}_s$) is derived in appendix C, section C.1, and is given in terms of a modal expansion as

$$\Psi^e(r,\theta) = \sum_{n=0}^{\infty} A^e_{\nu_n} R^e_{\nu_n}(u)\, P_{\nu_n}(-\cos\theta)\,, \tag{E-2}$$

where $R^e_{\nu_n}$ has been defined as

$$R^e_{\nu_n}(u) \equiv h^{(1)}_{\nu_n}(u) + B^e_{\nu_n} h^{(2)}_{\nu_n}(u)\ . \tag{E-3}$$

In the above formulas, n denotes the mode index, $u = k_0 r$, $A^e_{\nu_n}$ is the excitation coefficient of the *nth* TM mode, $B^e_{\nu_n}$ is a constant that is given by either expression (C-7a) or (C-7b), $h^{(1)}_{\nu_n}(u)$ and $h^{(2)}_{\nu_n}(u)$ denote the spherical Hankel functions of the first and second kinds, respectively, of order

ν_n, and P_{ν_n} denotes the Legendre function of the first kind of degree ν_n and order zero. The complex constant ν_n is determined from the solution of the characteristic equation (C-8).

From appendix D, the orthogonality condition for the TM mode radial functions is given by

$$\int_{u_g}^{u_i} R^e_{\nu_m}(u)\, R^e_{\nu_n}(u)\, du = \left\| R^e_{\nu_n} \right\|^2 \delta_{mn}\,, \tag{E-4}$$

where $\left\| R^e_{\nu_n} \right\|$ denotes the L_2 norm of $R^e_{\nu_n}$ as defined in appendix F, $u_g = k_o a$, $u_i = k_o(a+h)$, and δ_{mn} is the Kronecker delta defined as

$$\delta_{mn} = \begin{cases} 1\,, & m = n \\ 0\,, & m \neq n \end{cases}\,. \tag{E-5}$$

If each side of expression (E-2) is multiplied by $R^e_{\nu_m}$ and then integrated with respect to u, the application of the orthogonality condition (E-4) to the resulting equation yields an expression for the mode excitation coefficient $A^e_{\nu_n}$, namely

$$A^e_{\nu_n} = \frac{1}{\left\| R^e_{\nu_n} \right\|^2 P_{\nu_n}(-\cos\theta)} \int_{u_g}^{u_i} \Psi^e(r,\theta)\, R^e_{\nu_n}(u)\, du \;,\; n = 0, 1, 2, \ldots\,. \tag{E-6}$$

It is difficult to determine $A^e_{\nu_n}$ from equation (E-6) because $\Psi^e(r, \theta)$ is not known.

To determine the excitation coefficients $A^e_{\nu_n}$ in formula (E-6), let θ approach zero, resulting in

$$A^e_{\nu_n} = \frac{1}{\left\| R^e_{\nu_n} \right\|^2} \frac{\lim\limits_{\theta \to 0} \int_{u_g}^{u_i} \Psi^e(r,\theta)\, R^e_{\nu_n}(u)\, du}{\lim\limits_{\theta \to 0} P_{\nu_n}(-\cos\theta)}\,. \tag{E-7}$$

Because both the numerator and denominator are singular at $\theta = 0$, the above expression is an indeterminate form. Then, from Magnus and Oberhettinger (reference 25),

$$\lim_{\theta \to 0} P_{\nu_n}(-\cos\theta) = \frac{\sin \nu_n \pi}{\pi} \ln \theta^2\,. \tag{E-8}$$

Before proceeding with the evaluation of the numerator, one needs to look more closely at the behavior of the Debye potential in the vicinity of the source.

The Debye potential Ψ^e can be expressed as the sum of a particular solution Ψ_s^e and a homogeneous solution Ψ_h^e of the differential equation (E-1). The particular solution satisfies the inhomogeneous equation (E-1) and the homogeneous solution satisfies the Helmholtz equation $\left(\nabla^2 + k_o^2\right)\Psi_h^e = 0$. The homogenous solution Ψ_h^e is finite for all points within the spherical waveguide and Ψ_s^e is singular at the source point $\boldsymbol{r} = \boldsymbol{r}_s$. Therefore, in the vicinity of the source, the particular solution Ψ_s^e is the primary influence of Ψ^e and, thus,

$$\lim_{r \to r_s} \Psi^e = \lim_{r \to r_s} \Psi_s^e = \lim_{\substack{\theta \to 0 \\ r \to r_s}} \Psi_s^e(r,\theta) . \tag{E-9}$$

For a VED of moment p lying in free space, the solution of equation (E-1) is given by (reference 23)

$$\Psi^e(r,\theta) = \Psi_s^e(r,\theta) = \frac{p}{j4\pi\omega\varepsilon_o r_s} \frac{e^{-jk_o R}}{R} , \tag{E-10}$$

where

$$R = \left|\boldsymbol{r} - \boldsymbol{r}_s\right| = \left[r^2 - 2rr_s \cos\theta + r_s^2\right]^{1/2} . \tag{E-11}$$

From the above formula, it is easy to see that Ψ_s^e is singular at $\boldsymbol{r} = \boldsymbol{r}_s$.

Because the integrand in the numerator of formula (E-7) is finite everywhere except at the source point ($r = r_s$, $\theta = 0$), its only contribution to the integral is from the immediate neighborhood of the source point. Therefore, expression (E-7) can be simplified to

$$A_{\nu_n}^e = \frac{k_o R_{\nu_n}^e(u_s)}{\left\| R_{\nu_n}^e \right\|^2} \frac{\lim_{\theta \to 0} \int_{r_s(1-\varepsilon)}^{r_s(1+\varepsilon)} \Psi_s^e(r,\theta)\, dr}{\lim_{\theta \to 0} P_{\nu_n}(-\cos\theta)} , \tag{E-12}$$

where u has been replaced by $k_o r$ and $\varepsilon \ll 1$. Note that $R_{\nu_n}^e(u)$ has been replaced by $R_{\nu_n}^e(u_s)$ because it is finite at the source point. The substitution of $\Psi_s^e(r,\theta)$ in formula (E-10) into the integral of equation (E-12) yields

$$\lim_{\theta \to 0} \int_{r_s(1-\varepsilon)}^{r_s(1+\varepsilon)} \Psi_s^e(r,\theta)\, dr = \frac{p}{j4\pi\omega\varepsilon_o r_s} \lim_{\theta \to 0} \int_{r_s(1-\varepsilon)}^{r_s(1+\varepsilon)} \frac{e^{-jk_o R}}{R}\, dr . \tag{E-13}$$

From Sommerfeld (reference 26), let

$$r = r_s(1 + \eta) \ . \tag{E-14}$$

where $-\varepsilon < \eta < \varepsilon$, $\varepsilon \ll 1$. The substitution of formula (E-14) into expression (E-11) gives

$$R = r_s\left[1 - 2(1 + \eta)\cos\theta + (1 + \eta)^2\right]^{1/2} \ . \tag{E-15}$$

As $\theta \to 0$, $\cos\theta \cong 1 - \theta^2/2$. Therefore, R may be approximated as

$$R \cong r_s\left[1 - 2(1 + \eta)\,(1 - \theta^2/2) + (1 + \eta)^2\right]^{1/2}$$

$$= r_s\left[\eta^2 + (1 + \eta)\,\theta^2\right]^{1/2} \cong r_s\sqrt{\eta^2 + \theta^2} \ . \tag{E-16}$$

where the last approximation was made because $\eta \ll 1$. Therefore, with the above approximation for R, the numerator of the integrand in expression (E-13) can be approximated as

$$e^{-jk_o R} \cong 1 \ . \tag{E-17}$$

The substitution of formulas (E-14), (E-16), and (E-17) into (E-13) yields

$$\lim_{\theta \to 0} \int_{r_s(1-\varepsilon)}^{r_s(1+\varepsilon)} \Psi_s^e(r,\theta)\, dr = \frac{p}{j4\pi\omega\varepsilon_o r_s} \lim_{\theta \to 0} \int_{-\varepsilon}^{\varepsilon} \frac{d\eta}{\sqrt{\eta^2 + \theta^2}} \ . \tag{E-18}$$

From a table of integrals (reference 27),

$$\int \frac{d\eta}{\sqrt{\eta^2 + \theta^2}} = \ln\left[\eta + \sqrt{\eta^2 + \theta^2}\right] \ . \tag{E-19}$$

The application of formula (E-19) to the integral in (E-18) yields

$$\int_{-\varepsilon}^{\varepsilon} \frac{d\eta}{\sqrt{\eta^2 + \theta^2}} = \ln\left[\varepsilon + \sqrt{\varepsilon^2 + \theta^2}\right] - \ln\left[-\varepsilon + \sqrt{\varepsilon^2 + \theta^2}\right] \ . \tag{E-20}$$

For $\theta \ll \varepsilon$, the following approximation can be made:

$$\sqrt{\varepsilon^2 + \theta^2} = \varepsilon\sqrt{1 + (\theta/\varepsilon)^2} \cong \varepsilon\left[1 + \frac{1}{2}(\theta/\varepsilon)^2\right] = \varepsilon + \frac{\theta^2}{2\varepsilon} \ .$$

Therefore, from the above, the following is obtained:

$$\varepsilon + \sqrt{\varepsilon^2 + \theta^2} \cong 2\varepsilon + \frac{\theta^2}{2\varepsilon}, \tag{E-21a}$$

and

$$-\varepsilon + \sqrt{\varepsilon^2 + \theta^2} \cong \frac{\theta^2}{2\varepsilon}. \tag{E-21b}$$

The substitution of the approximations (E-21a) and (E-21b) into formula (E-20) yields

$$\int_{-\varepsilon}^{\varepsilon} \frac{d\eta}{\sqrt{\eta^2 + \theta^2}} \cong \ln\left(2\varepsilon + \frac{\theta^2}{2\varepsilon}\right) - \ln\left(\frac{\theta^2}{2\varepsilon}\right) = \ln\left(\frac{2\varepsilon + \theta^2/2\varepsilon}{\theta^2/2\varepsilon}\right)$$

$$\cong \ln\left[\frac{(2\varepsilon)^2}{\theta^2}\right] = \ln(2\varepsilon)^2 - \ln\theta^2 . \tag{E-22}$$

If the limit of the above result is taken as $\theta \to 0$ (with ε finite), then

$$\lim_{\theta \to 0} \int_{-\varepsilon}^{\varepsilon} \frac{d\eta}{\sqrt{\eta^2 + \theta^2}} = -\ln\theta^2 . \tag{E-23}$$

The above limit is the same as the one given by Sommerfeld (reference 26), but differs in sign from the one given by Wait (reference 1). The substitution of the above result into formula (E-18) gives

$$\lim_{\theta \to 0} \int_{r_s(1-\varepsilon)}^{r_s(1+\varepsilon)} \Psi_s^e(r,\theta)\, dr = -\frac{p}{j4\pi\omega\varepsilon_o r_s} \ln\theta^2 . \tag{E-24}$$

The modal excitation coefficients $A^e_{\nu_n}$ can now be obtained through substitution of the limiting results (E-8) and (E-24) into expression (E-12), resulting in

$$A^e_{\nu_n} = \frac{j\eta_o p}{4 r_s} \frac{1}{\sin \nu_n \pi} \frac{R^e_{\nu_n}(u_s)}{\left\| R^e_{\nu_n} \right\|^2} , \quad n = 0, 1, 2, \ldots , \tag{E-25}$$

where $\eta_o = \sqrt{\mu_o/\varepsilon_o}$ is the intrinsic impedance of free space. It should be mentioned that the above result differs in sign from the one given by Wait (reference 1).

E.2 TE MODES

Consider a VMD or, equivalently, an infinitesimally small loop of electric current with axis along the radial direction that is located at the radial distance $r_s = a + z_s$ along the $\theta = 0$ axis of the spherical earth-ionosphere waveguide shown in figure 1-1. As is shown in appendix G, the differential equation for the magnetic Debye potential Ψ^h is given by

$$\left(\nabla^2 + k_o^2\right) \Psi^h = -\frac{m}{r_s}\, \delta(\boldsymbol{r} - \boldsymbol{r}_s)\,, \tag{E-26}$$

where m is the current moment of the loop and δ denotes the Dirac delta function. The solution of the above differential equation at source-free points ($\boldsymbol{r}$? $\boldsymbol{r}_s$) is derived in appendix C, section C.2, and is given in terms of a modal expansion as

$$\Psi^h(r,\theta) = \sum_{m=1}^{\infty} A^h_{\bar{\nu}_m}\, R^h_{\bar{\nu}_m}(u)\, P_{\bar{\nu}_m}(-\cos\theta)\,, \tag{E-27}$$

where $R^h_{\bar{\nu}_m}(u)$ is defined as

$$R^h_{\bar{\nu}_m}(u) \equiv h^{(1)}_{\bar{\nu}_m}(u) + B^h_{\bar{\nu}_m}\, h^{(2)}_{\bar{\nu}_m}(u)\,. \tag{E-28}$$

In the above formulas, m denotes the mode index, $A^h_{\bar{\nu}_m}$ is the excitation coefficient of the mth TE mode, and $B^h_{\bar{\nu}_m}$ is a constant that is given by either expression (C-20a) or (C-20b). The complex constant $\bar{\nu}_m$ is determined from the solution of the characteristic equation (C-21).

From appendix D, the orthogonality condition for the TE mode radial functions is given by

$$\int_{u_g}^{u_i} R^h_{\bar{\nu}_m}(u)\, R^h_{\bar{\nu}_n}(u)\, du = \left\| R^h_{\bar{\nu}_m} \right\|^2 \delta_{mn}\,, \tag{E-29}$$

where $\left\| R^h_{\bar{\nu}_m} \right\|$ denotes the L_2 norm of $R^h_{\bar{\nu}_m}$ as defined in appendix G and δ_{mn} is the Kronecker delta defined in expression (E-5). If each side of expression (E-27) is multiplied by $R^h_{\bar{\nu}_n}$ and then integrated with respect to u, the application of the orthogonality condition (E-29) to the resulting equation yields an expression for the mode excitation coefficient $A^h_{\bar{\nu}_m}$, namely

$$A^h_{\bar{\nu}_m} = \frac{1}{\left\| R^h_{\bar{\nu}_m} \right\|^2 P_{\bar{\nu}_m}(-\cos\theta)} \int_{u_g}^{u_i} \Psi^h(r,\theta)\, R^h_{\bar{\nu}_m}(u)\, du\,,\quad m = 1, 2, 3, \ldots\,. \tag{E-30}$$

It is difficult to determine $A^h_{\bar{\nu}_m}$ from equation (E-30) because $\Psi^h(r,\theta)$ is unknown.

To determine the excitation coefficients $A^h_{\bar{\nu}_m}$ in formula (E-30), let $\theta \to 0$. Then,

$$A^h_{\bar{\nu}_m} = \frac{1}{\left\| R^h_{\bar{\nu}_m} \right\|^2} \frac{\lim\limits_{\theta \to 0} \int_{u_g}^{u_i} \Psi^h(r,\theta)\, R^h_{\bar{\nu}_m}(u)\, du}{\lim\limits_{\theta \to 0} P_{\bar{\nu}_m}(-\cos\theta)} . \tag{E-31}$$

Following the same procedure as for the TM mode excitation coefficients, the magnetic Debye potential Ψ^h satisfies the inhomogeneous differential equation (E-26) and can be expressed as the sum of a particular solution Ψ^h_s and a homogeneous solution Ψ^h_h. The term Ψ^h_h is finite for all values of θ and r within the spherical waveguide and Ψ^h_s is singular at the source point $\boldsymbol{r} = \boldsymbol{r_s}$. The particular solution Ψ^h_s of equation (E-26) is the same as the magnetic Debye potential for a VMD in free space and is given by (reference 20)

$$\Psi^h(r,\theta) = \Psi^h_s(r,\theta) = \frac{m}{4\pi r_s} \frac{e^{-jk_o R}}{R} , \tag{E-32}$$

where R is given by expression (E-11).

Because the integrand in the numerator of formula (E-31) is finite everywhere except at the source point ($r = r_s$, $\theta = 0$), its only contribution to the integral is from the immediate neighborhood of the source point. Therefore, expression (E-31) can be simplified to

$$A^h_{\bar{\nu}_m} = \frac{k_o R^h_{\bar{\nu}_m}(u_s)}{\left\| R^h_{\bar{\nu}_m} \right\|^2} \frac{\lim\limits_{\theta \to 0} \int_{r_s(1-\varepsilon)}^{r_s(1+\varepsilon)} \Psi^h_s(r,\theta)\, dr}{\lim\limits_{\theta \to 0} P_{\bar{\nu}_m}(-\cos\theta)} , \tag{E-33}$$

where u has been replaced by $k_o r$ and $\varepsilon \ll 1$. Note that $R^h_{\bar{\nu}_m}(u)$ has been replaced by $R^h_{\bar{\nu}_m}(u_s)$ because it is finite at the source point. If the procedure described in appendix E, section E.1, is followed, the integral in expression (E-33) reduces to

$$\lim_{\theta \to 0} \int_{r_s(1-\varepsilon)}^{r_s(1+\varepsilon)} \Psi^h_s(r,\theta)\, dr = -\frac{m}{4\pi r_s} \ln \theta^2 . \tag{E-34}$$

The modal excitation coefficients $A^h_{\bar{\nu}_m}$ can now be obtained through substitution of the limiting results (E-8) and (E-34) into expression (E-33), resulting in

$$A^h_{\bar{\nu}_m} = -\frac{k_o m}{4 r_s} \frac{1}{\sin \bar{\nu}_m \pi} \frac{R^h_{\bar{\nu}_m}(u_s)}{\left\| R^h_{\bar{\nu}_m} \right\|^2} \quad , \; m = 1, 2, 3, \ldots . \tag{E-35}$$

It should be noted that the above result differs in sign from the one given by Wait (reference 1).

APPENDIX F
DERIVATION OF VERTICAL ELECTRIC DIPOLE (VED) ELECTROMAGNETIC (EM) FIELDS

In this appendix, the electromagnetic (EM) fields radiated by a vertical electric dipole (VED) in a spherical earth-ionosphere waveguide are derived through the use of the spherical wave formulas derived in appendixes A and C. The fields can be expressed in terms of a transverse magnetic (TM) mode expansion.

F.1 MODAL EXPANSIONS OF EM FIELDS

Consider a radially-directed electric dipole of moment $p = I\,dl$ that is located at the radial distance $r_s = a + z_s$ along the $\theta = 0$ axis of the spherical earth-ionosphere waveguide shown in figure 1-1. The electric dipole can be mathematically expressed in terms of the electric current density vector $\boldsymbol{J}$ as

$$\boldsymbol{J} = \hat{\boldsymbol{r}}\, J_r = \hat{\boldsymbol{r}}\, p\, \delta(\boldsymbol{r} - \boldsymbol{r}_s)\,, \tag{F-1}$$

where $\hat{\boldsymbol{r}}$ is the unit radial vector, $\boldsymbol{r}$ and $\boldsymbol{r}_s$ denote the position vectors of the observation and source points, respectively, and δ denotes the Dirac delta function. The function $\delta(\boldsymbol{r} - \boldsymbol{r}_s)$ has the SI units of m^{-3} and can be represented in spherical coordinates as

$$\delta(\boldsymbol{r} - \boldsymbol{r}_s) = \frac{\delta(r - r_s)\,\delta(\theta)}{2\pi r^2 \sin\theta}\,. \tag{F-2}$$

The spherical coordinate system is illustrated in figure 4-1. Note that

$$\iiint \delta(\boldsymbol{r} - \boldsymbol{r}_s)\, dv = 1\,, \tag{F-3}$$

where the integration domain extends over all space.

To determine the expressions for the EM fields radiated by the VED, one must first obtain the differential equation for the electric Debye potential Ψ^e within the spherical waveguide (defined by the region $a < r < a+h$) with an excitation current given by expression (F-1). From equation (A-6), appendix A, the differential equation for the magnetic vector potential $\boldsymbol{A}$ is given by

$$\nabla \times \nabla \times \boldsymbol{A} - k_o^2 \boldsymbol{A} = -\,j\omega\mu_o\varepsilon_o \nabla \Phi^e + \mu_o \boldsymbol{J}\,, \tag{F-4}$$

where μ_o is the permeability of free space, ε_o is the permittivity of free space, $k_o = \omega\sqrt{\mu_o \varepsilon_o}$ is the wave number in free space, and Φ^e is the electric scalar potential. Following the procedure shown in appendix A, section A.1, if one sets $\boldsymbol{A} = \hat{\boldsymbol{r}} A_r$ and applies the gauge condition given in expression (A-18), the differential equation for $\boldsymbol{A}$ reduces to

$$\left(\nabla^2 + k_o^2\right) \frac{A_r}{r} = -\mu_o \frac{J_r}{r}, \tag{F-5}$$

where ∇^2 is the Laplacian operator. It should be mentioned that with the gauge condition (A-18) chosen and with only a radial component of electric current, the θ and φ components vanish on each side of equation (F-4). From the definition (A-26a), the magnetic vector potential component A_r can be expressed in terms of the radial component of the electric Hertz vector π_r^e as

$$A_r = j\omega\mu_o\varepsilon_o\pi_r^e \ . \tag{F-6}$$

From the definition (A-29a), the electric Debye potential Ψ^e is expressed in terms of π_r^e as

$$\Psi^e = \frac{\pi_r^e}{r} \ . \tag{F-7}$$

The substitution of formulas (F-6) and (F-7) into (F-5) yields

$$\left(\nabla^2 + k_o^2\right) \Psi^e = -\frac{1}{j\omega\varepsilon_o} \frac{J_r}{r} \ . \tag{F-8}$$

For the VED excitation with current density given by (F-1), the differential equation (F-8) becomes

$$\left(\nabla^2 + k_o^2\right) \Psi^e = -\frac{p}{j\omega\varepsilon_o r_s} \delta(\boldsymbol{r} - \boldsymbol{r}_s) \ . \tag{F-9}$$

It should be noted that on the right side of the above equation, r has been replaced by r_s because the expression vanishes everywhere except at $r = r_s$. The solution of the above differential equation at source-free points ($\boldsymbol{r} \neq \boldsymbol{r_s}$) is derived in appendix C, section C.1, and is given in terms of a modal expansion as

$$\Psi^e(r,\theta) = \sum_{n=0}^{\infty} A_{\nu_n}^e R_{\nu_n}^e(u) P_{\nu_n}(-\cos\theta), \tag{F-10}$$

where n denotes the mode index, $R_{\nu_n}^e$ is defined in formula (C-10), $u = k_o r$, $A_{\nu_n}^e$ is the excitation coefficient of the *nth* TM mode, $B_{\nu_n}^e$ is a constant that is given by either expression (C-7a) or (C-

7b), $h^{(1)}_{\nu_n}(u)$ and $h^{(2)}_{\nu_n}(u)$ denote the spherical Hankel functions of the first and second kinds respectively, of order ν_n, and P_{ν_n} denotes the Legendre function of the first kind of degree ν_n and order zero. The complex constant ν_n is determined from the solution of the characteristic equation (C-8). The modal excitation coefficients $A^e_{\nu_n}$ depend on the source strength $p/\omega\varepsilon_0 r_s$. The term $A^e_{\nu_n}$ is derived in appendix E, section E.1, and is given by

$$A^e_{\nu_n} = \frac{j\eta_o p}{4 r_s} \frac{1}{\sin \nu_n \pi} \frac{R^e_{\nu_n}(u_s)}{\left\| R^e_{\nu_n} \right\|^2} \ , \ n = 0, 1, 2, \ldots , \tag{F-11}$$

where $\eta_0 = \sqrt{\mu_o/\varepsilon_o}$ is the intrinsic impedance of the free space. In expression (F-11), $\left\| R^e_{\nu_n} \right\|$ denotes the L_2 norm of $R^e_{\nu_n}$ and is defined as

$$\left\| R^e_{\nu_n} \right\| \equiv \sqrt{\int_{u_g}^{u_i} \left[R^e_{\nu_n}(u) \right]^2 du} \ , \ n = 0, 1, 2, \ldots , \tag{F-12}$$

where $u_g = k_0 a$ and $u_i = k_0(a+h)$.

The EM fields radiated by a VED are given in formulas (C-11) with modal excitation coefficients given by expression (F-11). Therefore, the VED EM field components in spherical coordinates are given as

$$E^{ve}_r = \frac{j\omega\mu_o p}{4 r_s u} \sum_{n=0}^{\infty} \frac{\nu_n(\nu_n + 1)}{\sin \nu_n \pi} \frac{R^e_{\nu_n}(u_s)}{\left\| R^e_{\nu_n} \right\|^2} R^e_{\nu_n}(u) \, P_{\nu_n}(-\cos\theta) \ , \tag{F-13a}$$

$$E^{ve}_\theta = \frac{j\omega\mu_o p}{4 r_s u} \sum_{n=0}^{\infty} \frac{1}{\sin \nu_n \pi} \frac{R^e_{\nu_n}(u_s)}{\left\| R^e_{\nu_n} \right\|^2} \frac{\partial}{\partial u}\left[u R^e_{\nu_n}(u) \right] \frac{\partial}{\partial \theta} P_{\nu_n}(-\cos\theta) , \tag{F-13b}$$

and

$$H^{ve}_\varphi = \frac{k_o p}{4 r_s} \sum_{n=0}^{\infty} \frac{1}{\sin \nu_n \pi} \frac{R^e_{\nu_n}(u_s)}{\left\| R^e_{\nu_n} \right\|^2} R^e_{\nu_n}(u) \frac{\partial}{\partial \theta} P_{\nu_n}(-\cos\theta) \ . \tag{F-13c}$$

In the above formulas, the superscript *ve* refers to a VED source.

Following Wait (reference 1), the effectiveness of a source can be characterized by an excitation factor Λ^e_n and the height variation of the fields by the height-gain function $G^e_n(z)$. These quantities are defined as follows:

$$\Lambda_n^e \equiv \frac{k_o h}{2} \frac{\left[R_{\nu_n}^e(u_g)\right]^2}{\left\| R_{\nu_n}^e \right\|^2} \ , \ n = 0, 1, 2, \ldots , \tag{F-14}$$

and

$$G_n^e(z) \equiv \frac{R_{\nu_n}^e(u)}{R_{\nu_n}^e(u_g)} \ , \ n = 0, 1, 2, \ldots , \tag{F-15}$$

where $z = r - a$ is the radial distance measured from the surface of the spherical earth (see figure 1-1). Following Galejs (reference 2), a z-dependent normalized impedance is defined as

$$\Delta_n^e(z) \equiv \frac{1}{\eta_o} \frac{E_\theta^{ve}}{H_\varphi^{ve}}\bigg|_{mode\ n} = j \frac{\frac{\partial}{\partial u}\left[u R_{\nu_n}^e(u)\right]}{u R_{\nu_n}^e(u)} \ , \ n = 0, 1, 2, \ldots . \tag{F-16}$$

The application of the definitions (F-14) to (F-16) to the VED formulas (F-13) yields

$$E_r^{ve} = \frac{j\eta_o p}{2hr_s u} \sum_{n=0}^{\infty} \frac{\nu_n(\nu_n + 1)}{\sin \nu_n \pi} \Lambda_n^e \, G_n^e(z_s) \, G_n^e(z) \, P_{\nu_n}(-\cos\theta) , \tag{F-17a}$$

$$E_\theta^{ve} = \frac{\eta_o p}{2hr_s} \sum_{n=0}^{\infty} \frac{1}{\sin \nu_n \pi} \Lambda_n^e \, \Delta_n^e(z) \, G_n^e(z_s) \, G_n^e(z) \frac{\partial}{\partial\theta} P_{\nu_n}(-\cos\theta) , \tag{F-17b}$$

and

$$H_\varphi^{ve} = \frac{p}{2r_s h} \sum_{n=0}^{\infty} \frac{1}{\sin \nu_n \pi} \Lambda_n^e \, G_n^e(z_s) \, G_n^e(z) \frac{\partial}{\partial\theta} P_{\nu_n}(-\cos\theta) \ . \tag{F-17c}$$

The above expressions are similar to those given by Wait (reference 1) and Galejs (reference 2). The radial variations in the formulas for each of the above field components may be approximated in order to make them suitable for numerical computation.

If the VED and the field point are each located on the inner boundary of the waveguide (earth's surface), then $z_s = z = 0$ or, equivalently, $r_s = r = a$. Thus,

$$G_n^e(z_s) = G_n^e(z) = G_n^e(0) = 1 \ , \ n = 0, 1, 2, \ldots . \tag{F-18}$$

In addition, from equation (C-6a), the z-dependent normalized impedance $\Delta_n^e(z)$ defined in expression (F-16) reduces to

$$\Delta_n^e(z) = \Delta_n^e(0) = -\Delta_g \ , \ n = 0, 1, 2, \ldots , \tag{F-19}$$

where $\Delta_g = Z_g/\eta_o$ denotes the normalized surface impedance of the inner boundary. The substitution of the above simplifications into the VED field expressions (F-17) gives

$$E_r^{ve} = \frac{j\eta_o p}{2hau_g} \sum_{n=0}^{\infty} \frac{\nu_n(\nu_n+1)}{\sin \nu_n \pi} \Lambda_n^e P_{\nu_n}(-\cos\theta), \tag{F-20a}$$

$$E_\theta^{ve} = -\frac{\eta_o p \Delta_g}{2ha} \sum_{n=0}^{\infty} \frac{1}{\sin \nu_n \pi} \Lambda_n^e \frac{\partial}{\partial\theta} P_{\nu_n}(-\cos\theta), \tag{F-20b}$$

and

$$H_\varphi^{ve} = \frac{p}{2ha} \sum_{n=0}^{\infty} \frac{1}{\sin \nu_n \pi} \Lambda_n^e \frac{\partial}{\partial\theta} P_{\nu_n}(-\cos\theta) \ . \tag{F-20c}$$

F.2 QUASI-TEM FIELDS

The tables of section 4.1 show that in the ELF band, all modes are nonpropagating except the $n = 0$ mode. This mode is often referred to as the quasi-transverse EM, or quasi-TEM, mode. If only the quasi-TEM mode is considered, the VED fields for a source and receiver each located at the surface of the inner sphere (earth) are given as

$$E_r^{ve} = \frac{j\eta_o p}{2hau_g} \frac{\nu_o(\nu_o+1)}{\sin \nu_o \pi} \Lambda_o^e P_{\nu_o}(-\cos\theta), \tag{F-21a}$$

$$E_\theta^{ve} = -\frac{\eta_o p \Delta_g}{2ha} \frac{1}{\sin \nu_o \pi} \Lambda_o^e \frac{\partial}{\partial\theta} P_{\nu_o}(-\cos\theta) \ , \tag{F-21b}$$

and

$$H_\varphi^{ve} = \frac{p}{2ha} \frac{1}{\sin \nu_o \pi} \Lambda_o^e \frac{\partial}{\partial\theta} P_{\nu_o}(-\cos\theta) \ . \tag{F-21c}$$

The above field expressions are of primary interest in this report.

APPENDIX G
DERIVATION OF VERTICAL MAGNETIC DIPOLE (VMD) ELECTROMAGNETIC (EM) FIELDS

In this appendix, the electromagnetic (EM) fields radiated by a vertical magnetic dipole (VMD) in a spherical earth-ionosphere waveguide are derived through the use of the formulas derived in appendixes A and C. The fields can be expressed in terms of a TE mode expansion.

Consider a radially-directed magnetic dipole of moment $K\,dl$ that is located at the radial distance $r_s = a + z_s$ along the $\theta = 0$ axis of the spherical earth-ionosphere waveguide shown in figure 1-1. The magnetic dipole can be mathematically expressed in terms of the magnetic current density vector $\boldsymbol{M}$ as

$$\boldsymbol{M} = \hat{\boldsymbol{r}}\, M_r = \hat{\boldsymbol{r}}\, K dl\, \delta(\boldsymbol{r} - \boldsymbol{r}_s)\ , \tag{G-1}$$

where $\hat{\boldsymbol{r}}$ is the unit radial vector, $\boldsymbol{r}$ and $\boldsymbol{r}_s$ denote the position vectors of the observation and source points, respectively, K denotes the magnetic current, and δ denotes the Dirac delta function. Because an infinitesimal dipole of magnetic current is equivalent to an infinitesimal loop of electric current (where the loop and dipole axes are parallel) through the relation $K\,dl = j\omega\mu_0\, I\, da$ (references 19 and 20), where I is the loop current and da is the differential area enclosed by the loop, equation (G-1) may also be written as

$$\boldsymbol{M} = \hat{\boldsymbol{r}}\, j\omega\mu_o m\, \delta(\boldsymbol{r} - \boldsymbol{r}_s)\,, \tag{G-2}$$

where $m = I\,da$ is the current moment of the loop.

To determine the expressions for the EM field radiated by the VMD, one first needs to obtain the differential equation for the magnetic Debye potential Ψ^h within the spherical waveguide (defined by the region $a < r < a+h$) with an excitation current given by expression (G-2). From equation (A-11), the differential equation for the electric vector potential $\boldsymbol{F}$ is given by

$$\nabla \times \nabla \times \boldsymbol{F} - k_o^2 \boldsymbol{F} = -\, j\omega\mu_o\varepsilon_o \nabla \Phi^h + \varepsilon_o \boldsymbol{M}\,, \tag{G-3}$$

where Φ^h is the magnetic scalar potential. Following the procedure shown in appendix A, section A.1, by setting $\boldsymbol{F} = \hat{\boldsymbol{r}}\, F_r$ and applying the gauge condition (A-24), the differential equation for $\boldsymbol{F}$ reduces to

$$\left(\nabla^2 + k_o^2\right) \frac{F_r}{r} = -\varepsilon_o \frac{M_r}{r} \ . \tag{G-4}$$

It should be mentioned that with the gauge condition (A-24) chosen and with only a radial component of magnetic current, the θ and φ components vanish on each side of equation (G-3). From the definition (A-26b), the electric vector potential component F_r can be expressed in terms of the radial component of the magnetic Hertz vector π_r^h as

$$F_r = j\omega\mu_o\varepsilon_o\pi_r^h \ . \tag{G-5}$$

From the definition (A-29b), the magnetic Debye potential Ψ^h is expressed in terms of π_r^h as

$$\Psi^h = \frac{\pi_r^h}{r} . \tag{G-6}$$

The substitution of formulas (G-5) and (G-6) into (G-4) yields

$$\left(\nabla^2 + k_o^2\right) \Psi^h = -\frac{1}{j\omega\mu_o} \frac{M_r}{r} \ . \tag{G-7}$$

For the VMD excitation with current density given by expression (G-2), the differential equation (G-7) becomes

$$\left(\nabla^2 + k_o^2\right) \Psi^h = -\frac{m}{r_s} \delta(\boldsymbol{r} - \boldsymbol{r_s}) \ . \tag{G-8}$$

It should be noted that on the right side of equation (G-8), r has been replaced by r_s because the expression vanishes everywhere except at $r = r_s$. The solution of the above differential equation at source-free points ($\boldsymbol{r}$? $\boldsymbol{r_s}$) is derived in appendix C, section C.2, and is given in terms of a modal expansion as

$$\Psi^h(r,\theta) = \sum_{m=1}^{\infty} A_{\bar{\nu}_m}^h R_{\bar{\nu}_m}^h(u) \, P_{\bar{\nu}_m}(-\cos\theta) , \tag{G-9}$$

where m denotes the mode index, $R_{\bar{\nu}_m}^h$ is defined in formula (C-23), $A_{\bar{\nu}_m}^h$ is the excitation coefficient of the *mth* TE mode, $B_{\bar{\nu}_m}^h$ is a constant that is given by either expression (C-20a) or (C-20b), and the complex constant $\bar{\nu}_m$ is determined from the solution of the characteristic equation (C-21). The modal excitation coefficients $A_{\bar{\nu}_m}^h$ depend on the source strength m/r_s. The term $A_{\bar{\nu}_m}^h$ is derived in appendix E, section E.2, and is given by

$$A^h_{\bar{\nu}_m} = -\frac{k_o m}{4 r_s} \frac{1}{\sin \bar{\nu}_m \pi} \frac{R^h_{\bar{\nu}_m}(u_s)}{\left\| R^h_{\bar{\nu}_m} \right\|^2} \ , \ m = 1, 2, 3, \ldots . \tag{G-10}$$

In the above expression, $\left\| R^h_{\bar{\nu}_m} \right\|$ denotes the L_2 norm of $R^h_{\bar{\nu}_m}$ and is defined as

$$\left\| R^h_{\bar{\nu}_m} \right\| \equiv \sqrt{\int_{u_g}^{u_i} \left[R^h_{\bar{\nu}_m} \right]^2 du} \ , \tag{G-11}$$

where $u_g = k_o a$ and $u_i = k_o(a+h)$.

The EM fields radiated by a VMD are given in formulas (C-24) with modal excitation coefficients given by expression (G-10). Therefore, the VMD EM field components in spherical coordinates are given as

$$H_r^{vm} = -\frac{k_o^2 m}{4 r_s u} \sum_{m=1}^{\infty} \frac{\bar{\nu}_m(\bar{\nu}_m + 1)}{\sin \bar{\nu}_m \pi} \frac{R^h_{\bar{\nu}_m}(u_s)}{\left\| R^h_{\bar{\nu}_m} \right\|^2} R^h_{\bar{\nu}_m}(u) \, P_{\bar{\nu}_m}(-\cos\theta) , \tag{G-12a}$$

$$H_\theta^{vm} = -\frac{k_o^2 m}{4 r_s u} \sum_{m=1}^{\infty} \frac{1}{\sin \bar{\nu}_m \pi} \frac{R^h_{\bar{\nu}_m}(u_s)}{\left\| R^h_{\bar{\nu}_m} \right\|^2} \frac{\partial}{\partial u}\left[u R^h_{\bar{\nu}_m}(u) \right] \frac{\partial}{\partial \theta} P_{\bar{\nu}_m}(-\cos\theta) , \tag{G-12b}$$

and

$$E_\varphi^{vm} = -\frac{j\eta_o k_o^2 m}{4 r_s} \sum_{m=1}^{\infty} \frac{1}{\sin \bar{\nu}_m \pi} \frac{R^h_{\bar{\nu}_m}(u_s)}{\left\| R^h_{\bar{\nu}_m} \right\|^2} R^h_{\bar{\nu}_m}(u) \frac{\partial}{\partial \theta} P_{\bar{\nu}_m}(-\cos\theta) \ . \tag{G-12c}$$

In the formulas (G-12), the superscript *vm* refers to a VMD source. Following Wait (reference 1) and Galejs (reference 2), the excitation factor Λ^h_m, height-gain function $G^h_m(z)$, and z-dependent normalized impedance $\Delta^h_m(z)$ for TE modes are defined as

$$\Lambda^h_m \equiv \frac{k_o h}{2} \frac{\left[R^h_{\bar{\nu}_m}(u_g) \right]^2}{\left\| R^h_{\bar{\nu}_m} \right\|^2} \ , \ m = 1, 2, 3, \ldots , \tag{G-13}$$

$$G^h_m(z) \equiv \frac{R^h_{\bar{\nu}_m}(u)}{R^h_{\bar{\nu}_m}(u_g)} \ , \ m = 1, 2, 3, \ldots , \tag{G-14}$$

and

$$\Delta_m^h(z) \equiv -\frac{1}{\eta_o}\left.\frac{E_\varphi^{vm}}{H_\theta^{vm}}\right|_{mode\ m} = -j\frac{uR_{\bar{\nu}_m}^h(u)}{\frac{\partial}{\partial u}\left[uR_{\bar{\nu}_m}^h(u)\right]},\ m = 1, 2, 3, \ldots . \tag{G-15}$$

The application of the definitions (G-13) to (G-15) to the VMD formulas (G-12) yields

$$H_r^{vm} = -\frac{k_o m}{2hr_s u}\sum_{m=1}^{\infty}\frac{\bar{\nu}_m(\bar{\nu}_m+1)}{\sin\bar{\nu}_m\pi}\Lambda_m^h\, G_m^h(z_s)\, G_m^h(z)\, P_{\bar{\nu}_m}(-\cos\theta), \tag{G-16a}$$

$$H_\theta^{vm} = \frac{jk_o m}{2hr_s}\sum_{m=1}^{\infty}\frac{1}{\sin\bar{\nu}_m\pi}\frac{\Lambda_m^h}{\Delta_m^h(z)}\, G_m^h(z_s)\, G_m^h(z)\,\frac{\partial}{\partial\theta}P_{\bar{\nu}_m}(-\cos\theta), \tag{G-16b}$$

and

$$E_\varphi^{vm} = -\frac{j\eta_o k_o m}{2r_s h}\sum_{m=1}^{\infty}\frac{1}{\sin\bar{\nu}_m\pi}\Lambda_m^h\, G_m^h(z_s)\, G_m^h(z)\,\frac{\partial}{\partial\theta}P_{\bar{\nu}_m}(-\cos\theta). \tag{G-16c}$$

The above expressions are similar to those given by Wait (reference 1) and Galejs (reference 2). The radial variations in the formulas for each of the above field components may be approximated in order to make them suitable for numerical computation.

If the VMD and the field point are each located on the inner boundary of the waveguide (earth), then $z_s = z = 0$ or, equivalently, $r_s = r = a$. Thus,

$$G_m^h(z_s) = G_m^h(z) = G_m^h(0) = 1\ ,\ m = 1, 2, 3, \ldots , \tag{G-17}$$

and the z-dependent normalized impedance $\Delta_m^h(z)$ reduces to

$$\Delta_m^h(z) = \Delta_m^h(0) = -\Delta_g\ ,\ m = 1, 2, 3, \ldots . \tag{G-18}$$

The substitution of the above simplifications into the VMD field expressions (G-16) gives

$$H_r^{vm} = -\frac{k_o m}{2hau_g}\sum_{m=1}^{\infty}\frac{\bar{\nu}_m(\bar{\nu}_m+1)}{\sin\bar{\nu}_m\pi}\Lambda_m^h\, P_{\bar{\nu}_m}(-\cos\theta), \tag{G-19a}$$

$$H_\theta^{vm} = -\frac{jk_o m}{2ha\Delta_g}\sum_{m=1}^{\infty}\frac{1}{\sin\bar{\nu}_m\pi}\Lambda_m^h\,\frac{\partial}{\partial\theta}P_{\bar{\nu}_m}(-\cos\theta)\ , \tag{G-19b}$$

and

$$E_\varphi^{vm} = -\frac{j\eta_o k_o m}{2ah}\sum_{m=1}^{\infty}\frac{1}{\sin\bar{\nu}_m\pi}\Lambda_m^h\,\frac{\partial}{\partial\theta}P_{\bar{\nu}_m}(-\cos\theta)\ . \tag{G-19c}$$

The above field expressions are of primary interest in this report.

APPENDIX H
DERIVATION OF HORIZONTAL ELECTRIC DIPOLE (HED) ELECTROMAGNETIC (EM) FIELDS

In this appendix, the electromagnetic (EM) fields radiated by a horizontal electric dipole (HED) in a spherical earth-ionosphere waveguide are derived from the vertical electric dipole (VED) and vertical magnetic dipole (VMD) fields through the use of the reciprocity theorem. The expressions for the nonradial field components involve both TM and TE mode expansions.

H.1 MODAL EXPANSIONS OF EM FIELDS

The Lorentz reciprocity theorem (references 19 and 20) relates a response at one source due to a second source to the response at the second source due to the first source. Consider two sets of impressed line-current sources (I_1, K_1) and (I_2, K_2) excited at the same frequency f, where I and K refer to electric and magnetic line currents, respectively. The EM fields produced by (I_1, K_1) are ($\boldsymbol{E}_1$, $\boldsymbol{H}_1$) and the fields produced by (I_2, K_2) are ($\boldsymbol{E}_2$, $\boldsymbol{H}_2$). If the line currents lie in a linear, reciprocal medium, the reciprocity theorem applies and is given as

$$\int \left(\boldsymbol{E}_1 \cdot I_2 \boldsymbol{dl}_2 - \boldsymbol{H}_1 \cdot K_2 \boldsymbol{dl}_2 \right) = \int \left(\boldsymbol{E}_2 \cdot I_1 \boldsymbol{dl}_1 - \boldsymbol{H}_2 \cdot K_1 \boldsymbol{dl}_1 \right), \tag{H-1}$$

where $\boldsymbol{dl}_1$ and $\boldsymbol{dl}_2$ denote the differential length vectors along line current sets one and two, respectively.

To derive the fields produced by a HED, consider the two coordinate systems defined in figure H-1. In this illustration, the coordinates (x, y, z) refer to those of the HED, and the primed coordinates (x', y', z') refer to those of the VED (case 1) and VMD (case 2). The origin of each coordinate system lies at a point on the earth's surface, with the x-y and x'-y' planes each lying on the tangent plane defined at their respective origins. The distance $a\theta$ is the great-circle path length between the origins of the two coordinate systems, where θ is the polar angle defined in figure 1-1. The reciprocity theorem is applied for two different cases. In case 1, an x-directed HED with electric dipole moment $I_1\, dl_1$ is located at coordinates (x, y, z) = (0, 0, z_r) and a z'-directed VED with electric dipole moment $I_2\, dl_2$ is located at coordinates (x', y', z') = (0, 0, z_s). In case 2, an x-directed HED with electric dipole moment $I_1\, dl_1$ is located at coordinates (x, y, z) = (0, 0, z_r) and a z'-directed VMD with magnetic dipole moment $K_2\, dl_2$ is located at coordinates (x', y', z') =

$(0, 0, z_s)$. The radial component of electric field E_r^{he} produced by the HED is determined from reciprocity in case 1 and the radial component of magnetic field H_r^{he} produced by the HED is obtained from reciprocity in case 2, where the superscript *he* refers to a HED source.

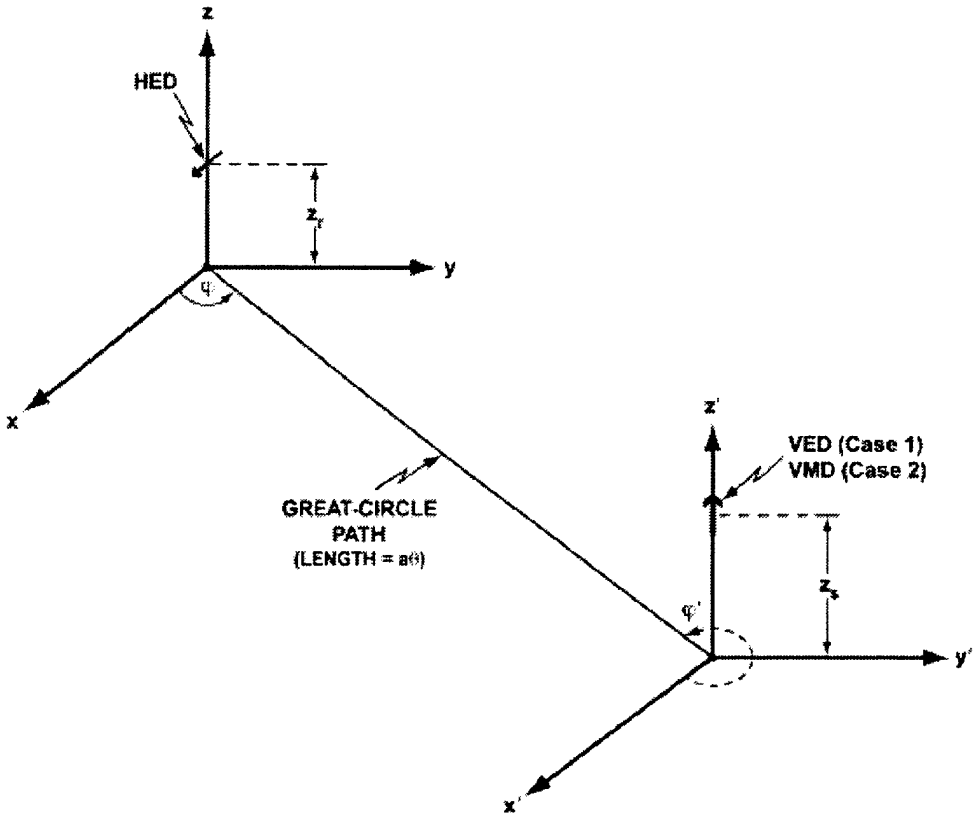

Figure H-1. Coordinate Systems Defined in the Application of the Reciprocity Theorem for Determination of the HED Fields

To determine E_r^{he}, consider case 1 in figure H-1. The application of the reciprocity theorem (H-1) to the HED and VED sources yields

$$E_{1z'}^{he}(x' = 0, y' = 0, z' = z_s)\, I_2\, dl_2 = E_{2x}^{ve}(x = 0, y = 0, z = z_r)\, I_1\, dl_1\,, \qquad \text{(H-2)}$$

where $E_{1z'}^{he}(x' = 0, y' = 0, z' = z_s)$ is the vertical (radial) component of electric field from the HED evaluated at the VED location and $E_{2x}^{ve}(x = 0, y = 0, z = z_r)$ is the x component of electric field from the VED evaluated at the HED location. Setting $I_1\, dl_1 = I_2\, dl_2$, expression (H-2) reduces to

$$E_{1z'}^{he}(x' = 0, y' = 0, z' = z_s) = E_{2x}^{ve}(x = 0, y = 0, z = z_r)\,. \qquad \text{(H-3)}$$

The left side of equation (H-3) can be expressed in spherical coordinates as $E_{1r}^{he}(r = r_s, \theta, \varphi)$, where the spherical coordinates of the source point are $(r, \theta) = (r_r, 0)$ and the spherical coordinates associated with the field point are (r_s, θ, φ). Similarly, the right side of equation (H-3) can be expressed in spherical coordinates as $-E_{2\theta'}^{ve}(r = r_r, \theta') \cos\varphi$, where the spherical coordinates of the source point are $(r, \theta') = (r_s, 0)$ and the spherical coordinates associated with the field point are (r_s, θ', φ'), where $\theta' = \theta$ and $\hat{\theta}' = -\hat{\theta}$. The projection of $E_{2\theta'}^{ve}$ onto the x axis is illustrated in figure H-2. Note that the azimuthal dependence is missing as an argument of $E_{2\theta'}^{ve}$ because the VED fields are axisymmetric.

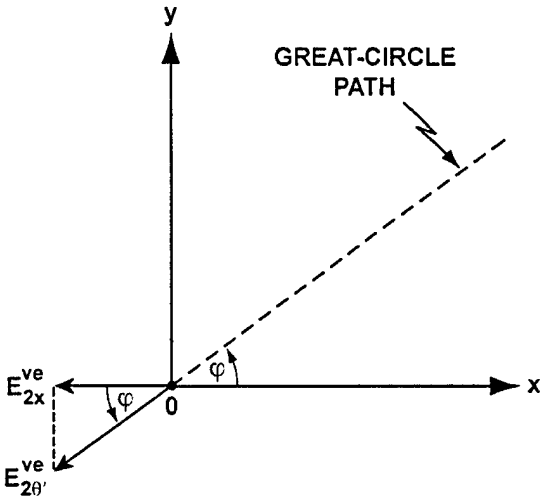

Figure H-2. Electric Field Component $E_{2\theta'}^{ve}$ Radiated by a VED (Source 2) Projected onto the x-Axis at the HED (Source 1) Location

If the above spherical coordinate substitutions are applied to equation (H-3), then

$$E_r^{he}(r_s, \theta, \varphi) = -E_{\theta'}^{ve}(r_r, \theta') \cos\varphi, \tag{H-4}$$

where the source numbers have been dropped. With the radial coordinate of the VED given by $r = r_s$ and the coordinates of the field point given by (r_r, θ'), from formula (F-15), $E_{\theta'}^{ve}$ is expressed as

$$E_{\theta'}^{ve}(r_r, \theta') = \frac{j\omega\mu_o p}{4 r_s u_r} \sum_{n=0}^{\infty} \frac{1}{\sin \nu_n \pi} \frac{R_{\nu_n}^e(u_s)}{\left|R_{\nu_n}^e\right|^2} \frac{\partial}{\partial u}\left[u R_{\nu_n}^e(u)\right]\Big|_{u=u_r} \frac{\partial}{\partial \theta'} P_{\nu_n}(-\cos\theta'), \tag{H-5}$$

where $u_r = k_o r_r$. The substitution of expression (H-5) into (H-4) yields

$$E_r^{he}(r_s, \theta, \varphi) = -\frac{j\omega\mu_o p}{4 r_s u_r} \cos\varphi \sum_{n=0}^{\infty} \frac{1}{\sin \nu_n \pi} \frac{R_{\nu_n}^e(u_s)}{\left|R_{\nu_n}^e\right|^2} \frac{\partial}{\partial u}\left[u R_{\nu_n}^e(u)\right]\Big|_{u=u_r} \frac{\partial}{\partial \theta'} P_{\nu_n}(-\cos\theta') \,. \quad \text{(H-6)}$$

The above formula applies for an x-directed HED located at $(r, \theta) = (r_r, 0)$ and the field point at (r_s, θ, φ). If the HED is located at $(r, \theta) = (r_s, 0)$ and the field point coordinates are (r, θ, φ), then r_s is replaced by r and r_r is replaced by r_s in expression (H-6), resulting in

$$E_r^{he}(r, \theta, \varphi) = \frac{j\omega\mu_o p}{4 r_s u} \cos\varphi \sum_{n=0}^{\infty} \frac{1}{\sin \nu_n \pi} \frac{\frac{\partial}{\partial u}\left[u R_{\nu_n}^e(u)\right]\Big|_{u=u_s}}{\left|R_{\nu_n}^e\right|^2} R_{\nu_n}^e(u) \frac{\partial}{\partial \theta} P_{\nu_n}(-\cos\theta) \,, \quad \text{(H-7)}$$

where $\theta' = \theta$ and $\partial/\partial\theta' = -\partial/\partial\theta$.

To determine H_r^{he}, consider case 2 in figure H-1. The application of the reciprocity theorem (H-1) to the HED and VMD sources yields

$$H_{1z'}^{he}(x' = 0, y' = 0, z' = z_s) = -E_{2x}^{vm}(x = 0, y = 0, z = z_r) \frac{I_1 \, dl_1}{K_2 \, dl_2} \,, \quad \text{(H-8)}$$

where $H_{1z'}^{he}(x' = 0, y' = 0, z' = z_s)$ is the vertical (radial) component of magnetic field from the HED evaluated at the VMD location and $E_{2x}^{vm}(x = 0, y = 0, z = z_r)$ is the x component of electric field from the VMD evaluated at the HED location. The left side of equation (H-8) can be expressed in spherical coordinates as $H_{1r}^{he}(r = r_s, \theta, \varphi)$, where the spherical coordinates of the source point are $(r, \theta) = (r_r, 0)$ and the spherical coordinates associated with the field point are (r_s, θ, φ). Similarly, the right side of equation (H-3) can be expressed in spherical coordinates as $E_{2\varphi'}^{vm}(r = r_r, \theta') \sin\varphi$, where the spherical coordinates of the source point are $(r, \theta') = (r_s, 0)$ and the spherical coordinates associated with the field point are (r_s, θ', φ'), where $\theta' = \theta$ and $\hat{\varphi}' = -\hat{\varphi}$. The projection of $E_{2\varphi'}^{vm}$ onto the x axis is illustrated in figure H-3. Note that the azimuthal dependence is missing as an argument of $E_{2\varphi'}^{vm}$ because the VMD fields are axisymmetric.

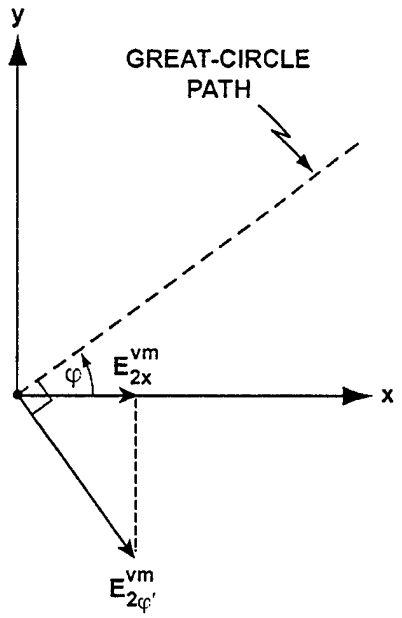

Figure H-3. Electric Field Component $E_{2\varphi'}^{vm}$ Radiated by a VMD (Source 2) Projected onto the x-Axis at the HED (Source 1) Location

If the above spherical coordinate substitutions are applied to equation (H-8), then

$$H_{1r}^{he}(r_s, \theta, \varphi) = -\frac{1}{j\omega\mu_o}\frac{I_1\, dl_1}{I_2\, da_2} E_{2\varphi'}^{vm}(r_r, \theta') \sin\varphi \ , \qquad \text{(H-9)}$$

where the magnetic dipole has been replaced by the equivalent infinitesimal electric current loop of moment $I_2\, da_2$, where $K_2\, dl_2 = j\omega\mu_o\, I_2\, da_2$. With the radial coordinate of the VMD given by $r = r_s$ and the coordinates of the field point given by (r_r, θ'), from formula (G-12c), $E_{2\varphi'}^{vm}$ is expressed as

$$E_{2\varphi'}^{vm}(r_r, \theta') = -\frac{j\eta_o k_o^2 I_2 da_2}{4\, r_s} \sum_{m=1}^{\infty} \frac{1}{\sin \tilde{\nu}_m \pi} \frac{R_{\tilde{\nu}_m}^h(u_s)}{\left| R_{\tilde{\nu}_m}^h \right|^2} R_{\tilde{\nu}_m}^h(u_r) \frac{\partial}{\partial\theta'} P_{\tilde{\nu}_m}(-\cos\theta') \ . \qquad \text{(H-10)}$$

The substitution of expression (H-10) into (H-9) yields

$$H_{1r}^{he}(r_s, \theta, \varphi) = \frac{p_1 k_o}{4\, r_s} \sin\varphi \sum_{m=1}^{\infty} \frac{1}{\sin \tilde{\nu}_m \pi} \frac{R_{\tilde{\nu}_m}^h(u_s)}{\left| R_{\tilde{\nu}_m}^h \right|^2} R_{\tilde{\nu}_m}^h(u_r) \frac{\partial}{\partial\theta'} P_{\tilde{\nu}_m}(-\cos\theta') , \qquad \text{(H-11)}$$

where $p_1 = I_1\, dl_1$. The above formula applies for an x-directed HED located at $(r, \theta) = (r_r, 0)$ and the field point at (r_s, θ, φ). If the HED is located at $(r, \theta) = (r_s, 0)$ and the field point coordinates are (r, θ, φ), then r_s is replaced by r and r_r is replaced by r_s in expression (H-11), resulting in

$$H_r^{he}(r, \theta, \varphi) = -\frac{k_o p}{4r} \sin\varphi \sum_{m=1}^{\infty} \frac{1}{\sin \tilde{\nu}_m \pi} \frac{R_{\tilde{\nu}_m}^h(u_s)}{\left| R_{\tilde{\nu}_m}^h \right|^2} R_{\tilde{\nu}_m}^h(u) \frac{\partial}{\partial\theta} P_{\tilde{\nu}_m}(-\cos\theta), \tag{H-12}$$

where $\theta' = \theta$ and $\partial/\partial\theta' = -\partial/\partial\theta$, and the subscript 1 has been removed.

The remaining field components for a HED source can be determined from the Debye potentials as given by equations (A-31). Because the Debye potentials for a HED have not yet been determined, they must be derived from the radial field components given by expressions (H-7) and (H-12). From equations (A-31a) and (A-31d), the radial field components are expressed in terms of the Debye potentials as

$$E_r^{he} = \left(\frac{\partial^2}{\partial r^2} + k_o^2 \right) (r\Psi^e), \tag{H-13a}$$

and

$$H_r^{he} = \left(\frac{\partial^2}{\partial r^2} + k_o^2 \right) (r\Psi^h), \tag{H-13b}$$

where Ψ^e and Ψ^h denote the electric and magnetic Debye potentials, respectively. Given the expressions for E_r^{he} and H_r^{he} in formulas (H-7) and (H-12), respectively, suitable forms for Ψ^e and Ψ^h are as follows:

$$\Psi^e = \cos\varphi \sum_{n=0}^{\infty} A_{\nu_n}^e R_{\nu_n}^e(u) \frac{\partial}{\partial\theta} P_{\nu_n}(-\cos\theta), \tag{H-14a}$$

and

$$\Psi^h = \sin\varphi \sum_{m=1}^{\infty} A_{\tilde{\nu}_m}^h R_{\tilde{\nu}_m}^h(u) \frac{\partial}{\partial\theta} P_{\tilde{\nu}_m}(-\cos\theta), \tag{H-14b}$$

where $A_{\nu_n}^e$ and $A_{\tilde{\nu}_m}^h$ denote the TM and TE mode expansion coefficients, respectively.

From the relation (C-12),

$$\left(\frac{d^2}{dr^2}+k_o^2\right)\left[rR^e_{\nu_n}(u)\right]=\frac{\nu_n(\nu_n+1)}{r}R^e_{\nu_n}(u)\ ,\ n=0,1,2,\ldots, \tag{H-15a}$$

and

$$\left(\frac{d^2}{dr^2}+k_o^2\right)\left[rR^h_{\bar{\nu}_m}(u)\right]=\frac{\bar{\nu}_m(\bar{\nu}_m+1)}{r}R^h_{\bar{\nu}_m}(u)\ ,\ m=1,2,3,\ldots. \tag{H-15b}$$

The substitution of expressions (H-15a) and (H-15b) into (H-14a) and (H-14b), respectively, yields

$$E^{he}_r=\frac{k_o}{u}\cos\varphi\sum_{n=0}^{\infty}A^e_{\nu_n}\,\nu_n(\nu_n+1)\,R^e_{\nu_n}(u)\,\frac{\partial}{\partial\theta}P_{\nu_n}(-\cos\theta)\ , \tag{H-16a}$$

and

$$H^{he}_r=\frac{k_o}{u}\sin\varphi\sum_{m=1}^{\infty}A^h_{\bar{\nu}_m}\,\bar{\nu}_m(\bar{\nu}_m+1)\,R^h_{\bar{\nu}_m}(u)\,\frac{\partial}{\partial\theta}P_{\bar{\nu}_m}(-\cos\theta)\ . \tag{H-16b}$$

A comparison of formulas (H-7) and (H-16a) shows that

$$A^e_{\nu_n}=\frac{j\omega\mu_o p}{4u_s}\,\frac{1}{\nu_n(\nu_n+1)}\,\frac{1}{\sin\nu_n\pi}\,\frac{\left.\frac{\partial}{\partial u}\left[uR^e_{\nu_n}(u)\right]\right|_{u=u_s}}{\left\|R^e_{\nu_n}\right\|^2}\ ,\ n=0,1,2,\ldots. \tag{H-17a}$$

Similarly, a comparison of formulas (H-12) and (H-16b) yields

$$A^h_{\bar{\nu}_m}=-\frac{k_o p}{4}\,\frac{1}{\bar{\nu}_m(\bar{\nu}_m+1)}\,\frac{1}{\sin\bar{\nu}_m\pi}\,\frac{R^h_{\bar{\nu}_m}(u_s)}{\left\|R^h_{\bar{\nu}_m}\right\|^2}\ ,\ m=1,2,3,\ldots. \tag{H-17b}$$

The substitution of expressions (H-17a) and (H-17b) into (H-14a) and (H-14b), respectively, yields

$$\Psi^e=\frac{j\omega\mu_o p}{4u_s}\cos\varphi\sum_{n=0}^{\infty}\left\{\frac{1}{\nu_n(\nu_n+1)}\,\frac{1}{\sin\nu_n\pi}\,\frac{\left.\frac{\partial}{\partial u}\left[uR^e_{\nu_n}(u)\right]\right|_{u=u_s}}{\left\|R^e_{\nu_n}\right\|^2}\right.$$

$$\left.R^e_{\nu_n}(u)\,\frac{\partial}{\partial\theta}P_{\nu_n}(-\cos\theta)\right\}\ , \tag{H-18a}$$

and

$$\Psi^h = -\frac{k_o p}{4}\sin\varphi \sum_{m=1}^{\infty} \frac{1}{\bar{\nu}_m(\bar{\nu}_m+1)} \frac{1}{\sin \bar{\nu}_m \pi} \frac{R^h_{\bar{\nu}_m}(u_s)}{\left\| R^h_{\bar{\nu}_m} \right\|^2} R^h_{\bar{\nu}_m}(u) \frac{\partial}{\partial\theta} P_{\bar{\nu}_m}(-\cos\theta) \ . \qquad \text{(H-18b)}$$

From formulas (A-31), the remaining HED field components are given in terms of the Debye potentials as

$$E^{he}_{\theta} = \frac{1}{r}\frac{\partial^2(r\Psi^e)}{\partial r \partial\theta} - \frac{j\omega\mu_o}{\sin\theta}\frac{\partial\Psi^h}{\partial\varphi} \ , \qquad \text{(H-19a)}$$

$$E^{he}_{\varphi} = \frac{1}{r\sin\theta}\frac{\partial^2(r\Psi^e)}{\partial r \partial\varphi} + j\omega\mu_o\frac{\partial\Psi^h}{\partial\theta} \ , \qquad \text{(H-19b)}$$

$$H^{he}_{\theta} = \frac{j\omega\varepsilon_o}{\sin\theta}\frac{\partial\Psi^e}{\partial\varphi} + \frac{1}{r}\frac{\partial^2(r\Psi^h)}{\partial r\partial\theta} \ , \qquad \text{(H-19c)}$$

and

$$H^{he}_{\varphi} = -j\omega\varepsilon_o\frac{\partial\Psi^e}{\partial\theta} + \frac{1}{r\sin\theta}\frac{\partial^2(r\Psi^h)}{\partial r\partial\varphi} \ . \qquad \text{(H-19d)}$$

The substitution of the Debye potential expressions (H-18) into the HED field formulas given above yields

$$E^{he}_{\theta} = \frac{jk_o^2\eta_o p\cos\varphi}{4u_s u}\sum_{n=0}^{\infty}\frac{1}{\nu_n(\nu_n+1)}\frac{1}{\sin\nu_n\pi}\frac{\frac{\partial}{\partial u}\left[uR^e_{\nu_n}(u)\right]\Big|_{u=u_s}}{\left\|R^e_{\nu_n}\right\|^2}\frac{\partial}{\partial u}\left[uR^e_{\nu_n}(u)\right]\frac{\partial^2}{\partial\theta^2}P_{\nu_n}(-\cos\theta)$$

$$+\frac{j\omega\mu_o k_o p\cos\varphi}{4\sin\theta}\sum_{m=1}^{\infty}\frac{1}{\bar{\nu}_m(\bar{\nu}_m+1)}\frac{1}{\sin\bar{\nu}_m\pi}\frac{R^h_{\bar{\nu}_m}(u_s)}{\left\|R^h_{\bar{\nu}_m}\right\|^2}R^h_{\bar{\nu}_m}(u)\frac{\partial}{\partial\theta}P_{\bar{\nu}_m}(-\cos\theta) \ , \qquad \text{(H-20a)}$$

$$E^{he}_{\varphi} = -\frac{j\omega\mu_o p\sin\varphi}{4r_s u\sin\theta}\sum_{n=0}^{\infty}\frac{1}{\nu_n(\nu_n+1)}\frac{1}{\sin\nu_n\pi}\frac{\frac{\partial}{\partial u}\left[uR^e_{\nu_n}(u)\right]\Big|_{u=u_s}}{\left\|R^e_{\nu_n}\right\|^2}\frac{\partial}{\partial u}\left[uR^e_{\nu_n}(u)\right]\frac{\partial}{\partial\theta}P_{\nu_n}(-\cos\theta)$$

$$-\frac{j\omega\mu_o k_o p\sin\varphi}{4}\sum_{m=1}^{\infty}\frac{1}{\bar{\nu}_m(\bar{\nu}_m+1)}\frac{1}{\sin\bar{\nu}_m\pi}\frac{R^h_{\bar{\nu}_m}(u_s)}{\left\|R^h_{\bar{\nu}_m}\right\|^2}R^h_{\bar{\nu}_m}(u)\frac{\partial^2}{\partial\theta^2}P_{\bar{\nu}_m}(-\cos\theta) \ , \qquad \text{(H-20b)}$$

$$H_\theta^{he} = \frac{k_o p \sin\varphi}{4r_s \sin\theta} \sum_{n=0}^{\infty} \frac{1}{\nu_n(\nu_n+1)} \frac{1}{\sin \nu_n \pi} \frac{\left.\frac{\partial}{\partial u}\left[uR_{\nu_n}^e(u)\right]\right|_{u=u_s}}{\left\|R_{\nu_n}^e\right\|^2} R_{\nu_n}^e(u) \frac{\partial}{\partial\theta} P_{\nu_n}(-\cos\theta)$$

$$- \frac{k_o p \sin\varphi}{4r} \sum_{m=1}^{\infty} \frac{1}{\bar{\nu}_m(\bar{\nu}_m+1)} \frac{1}{\sin \bar{\nu}_m \pi} \frac{R_{\bar{\nu}_m}^h(u_s)}{\left\|R_{\bar{\nu}_m}^h\right\|^2} \frac{\partial}{\partial u}\left[uR_{\bar{\nu}_m}^h(u)\right] \frac{\partial^2}{\partial\theta^2} P_{\bar{\nu}_m}(-\cos\theta), \qquad \text{(H-20c)}$$

and

$$H_\varphi^{he} = \frac{k_o p \cos\varphi}{4r_s} \sum_{n=0}^{\infty} \frac{1}{\nu_n(\nu_n+1)} \frac{1}{\sin \nu_n \pi} \frac{\left.\frac{\partial}{\partial u}\left[uR_{\nu_n}^e(u)\right]\right|_{u=u_s}}{\left\|R_{\nu_n}^e\right\|^2} R_{\nu_n}^e(u) \frac{\partial^2}{\partial\theta^2} P_{\nu_n}(-\cos\theta)$$

$$- \frac{k_o p \cos\varphi}{4r \sin\theta} \sum_{m=1}^{\infty} \frac{1}{\bar{\nu}_m(\bar{\nu}_m+1)} \frac{1}{\sin \bar{\nu}_m \pi} \frac{R_{\bar{\nu}_m}^h(u_s)}{\left\|R_{\bar{\nu}_m}^h\right\|^2} \frac{\partial}{\partial u}\left[uR_{\bar{\nu}_m}^h(u)\right] \frac{\partial}{\partial\theta} P_{\bar{\nu}_m}(-\cos\theta) \; . \qquad \text{(H-20d)}$$

Formulas (H-20) show that, unlike the VED and VMD fields, four of the six HED field components involve the superposition of both TM and TE modes.

Following Wait (reference 1) and Galejs (reference 2), the HED formulas can be expressed in terms of the excitation factor, height-gain function, and normalized impedance defined in expressions (F-14) to (F-16) and (G-13) to (G-15). The application of these functions to the HED formulas (H-7), (H-12), and (H-20) yields

$$E_r^{he} = \frac{\eta_o p}{2hr} \cos\varphi \sum_{n=0}^{\infty} \frac{1}{\sin \nu_n \pi} \Lambda_n^e \Delta_n^e(z_s) G_n^e(z_s) G_n^e(z) \frac{\partial}{\partial\theta} P_{\nu_n}(-\cos\theta) \quad , \qquad \text{(H-21a)}$$

$$E_\theta^{he} = - \frac{jk_o \eta_o p \cos\varphi}{2h} \sum_{n=0}^{\infty} \frac{1}{\nu_n(\nu_n+1)} \frac{1}{\sin \nu_n \pi} \Lambda_n^e \Delta_n^e(z_s) \Delta_n^e(z) G_n^e(z_s) G_n^e(z) \frac{\partial^2}{\partial\theta^2} P_{\nu_n}(-\cos\theta)$$

$$+ \frac{j\eta_o k_o p \cos\varphi}{2h \sin\theta} \sum_{m=1}^{\infty} \frac{1}{\bar{\nu}_m(\bar{\nu}_m+1)} \frac{1}{\sin \bar{\nu}_m \pi} \Lambda_m^h G_m^h(z_s) G_m^h(z) \frac{\partial}{\partial\theta} P_{\bar{\nu}_m}(-\cos\theta), \qquad \text{(H-21b)}$$

$$E_{\varphi}^{he} = \frac{j\omega\mu_o p \sin\varphi}{2h \sin\theta} \sum_{n=0}^{\infty} \frac{1}{\nu_n(\nu_n+1)} \frac{1}{\sin \nu_n \pi} \Lambda_n^e \, \Delta_n^e(z_s) \, \Delta_n^e(z) \, G_n^e(z_s) \, G_n^e(z) \frac{\partial}{\partial\theta} P_{\nu_n}(-\cos\theta)$$

$$- \frac{j\eta_o k_o p \sin\varphi}{2h} \sum_{m=1}^{\infty} \frac{1}{\bar{\nu}_m(\bar{\nu}_m+1)} \frac{1}{\sin \bar{\nu}_m \pi} \Lambda_m^h \, G_m^h(z_s) \, G_m^h(z) \frac{\partial^2}{\partial\theta^2} P_{\bar{\nu}_m}(-\cos\theta) \,, \qquad \text{(H-21c)}$$

$$H_r^{he} = -\frac{p}{2hr} \sin\varphi \sum_{m=1}^{\infty} \frac{1}{\sin \bar{\nu}_m \pi} \Lambda_m^h \, G_m^h(z_s) \, G_m^h(z) \frac{\partial}{\partial\theta} P_{\bar{\nu}_m}(-\cos\theta) \qquad , \qquad \text{(H-21d)}$$

$$H_{\theta}^{he} = -\frac{jk_o p \sin\varphi}{2h \sin\theta} \sum_{n=0}^{\infty} \frac{1}{\nu_n(\nu_n+1)} \frac{1}{\sin \nu_n \pi} \Lambda_n^e \, \Delta_n^e(z_s) \, G_n^e(z_s) \, G_n^e(z) \frac{\partial}{\partial\theta} P_{\nu_n}(-\cos\theta)$$

$$+ \frac{jk_o p \sin\varphi}{2h} \sum_{m=1}^{\infty} \frac{1}{\bar{\nu}_m(\bar{\nu}_m+1)} \frac{1}{\sin \bar{\nu}_m \pi} \Lambda_m^h \frac{1}{\Delta_m^h(z)} G_m^h(z_s) \, G_m^h(z) \frac{\partial^2}{\partial\theta^2} P_{\bar{\nu}_m}(-\cos\theta) \,, \qquad \text{(H-21e)}$$

$$H_{\varphi}^{he} = -\frac{jk_o p \cos\varphi}{2h} \sum_{n=0}^{\infty} \frac{1}{\nu_n(\nu_n+1)} \frac{1}{\sin \nu_n \pi} \Lambda_n^e \, \Delta_n^e(z_s) \, G_n^e(z_s) \, G_n^e(z) \frac{\partial^2}{\partial\theta^2} P_{\nu_n}(-\cos\theta)$$

$$+ \frac{jk_o p \cos\varphi}{2h \sin\theta} \sum_{m=1}^{\infty} \frac{1}{\bar{\nu}_m(\bar{\nu}_m+1)} \frac{1}{\sin \bar{\nu}_m \pi} \Lambda_m^h \frac{1}{\Delta_m^h(z)} G_m^h(z_s) \, G_m^h(z) \frac{\partial}{\partial\theta} P_{\bar{\nu}_m}(-\cos\theta) \,. \qquad \text{(H-21f)}$$

The above expressions are similar to those given by Wait (reference 1) and Galejs (reference 2). The radial variations in the formulas for each of the above field components may be approximated in order to make them suitable for numerical computation.

If the HED and the field point are each located on the earth's surface, then $z_s = z = 0$. Therefore, the height-gain functions reduce to

$$G_n^e(z_s) = G_n^e(z) = G_n^e(0) = 1 \,, \quad n = 0, 1, 2, \ldots \,, \qquad \text{(H-22a)}$$

and

$$G_m^h(z_s) = G_m^h(z) = G_m^h(0) = 1 \,, \quad m = 1, 2, 3, \ldots . \qquad \text{(H-22b)}$$

In addition, the z-dependent normalized impedances $\Delta_n^e(z)$ and $\Delta_m^h(z)$ defined in expressions (F-16) and (G-15), respectively, reduce to

$$\Delta_n^e(z) = \Delta_n^e(0) = -\Delta_g\,,\ n\ = 0,\ 1,\ 2,\ \ldots\,, \tag{H-23a}$$

and

$$\Delta_m^h(z) = \Delta_m^h(0) = -\Delta_g\,,\ m\ = 1,\ 2,\ 3,\ \ldots\,. \tag{H-23b}$$

The substitution of the above simplifications into the HED formulas (H-21) gives the following:

$$E_r^{he} = -\frac{\eta_o \Delta_g p}{2ha}\cos\varphi \sum_{n=0}^{\infty} \frac{1}{\sin \nu_n \pi}\, \Lambda_n^e\, \frac{\partial}{\partial\theta} P_{\nu_n}(-\cos\theta)\,, \tag{H-24a}$$

$$E_\theta^{he} = -\frac{jk_o\eta_o\Delta_g^2 p\cos\varphi}{2h} \sum_{n=0}^{\infty} \frac{1}{\nu_n(\nu_n+1)}\,\frac{1}{\sin\nu_n\pi}\,\Lambda_n^e\,\frac{\partial^2}{\partial\theta^2} P_{\nu_n}(-\cos\theta)$$

$$+\frac{j\eta_o k_o p\cos\varphi}{2h\sin\theta} \sum_{m=1}^{\infty} \frac{1}{\bar{\nu}_m(\bar{\nu}_m+1)}\,\frac{1}{\sin\bar{\nu}_m\pi}\,\Lambda_m^h\,\frac{\partial}{\partial\theta} P_{\bar{\nu}_m}(-\cos\theta)\,, \tag{H-24b}$$

$$E_\varphi^{he} = \frac{j\omega\mu_o\Delta_g^2 p\sin\varphi}{2h\sin\theta} \sum_{n=0}^{\infty} \frac{1}{\nu_n(\nu_n+1)}\,\frac{1}{\sin\nu_n\pi}\,\Lambda_n^e\,\frac{\partial}{\partial\theta} P_{\nu_n}(-\cos\theta)$$

$$-\frac{j\eta_o k_o p\sin\varphi}{2h} \sum_{m=1}^{\infty} \frac{1}{\bar{\nu}_m(\bar{\nu}_m+1)}\,\frac{1}{\sin\bar{\nu}_m\pi}\,\Lambda_m^h\,\frac{\partial^2}{\partial\theta^2} P_{\bar{\nu}_m}(-\cos\theta)\,, \tag{H-24c}$$

$$H_r^{he} = -\frac{p}{2ha}\sin\varphi \sum_{m=1}^{\infty} \frac{1}{\sin\bar{\nu}_m\pi}\,\Lambda_m^h\,\frac{\partial}{\partial\theta} P_{\bar{\nu}_m}(-\cos\theta)\,, \tag{H-24d}$$

$$H_\theta^{he} = \frac{jk_o\Delta_g p\sin\varphi}{2h\sin\theta} \sum_{n=0}^{\infty} \frac{1}{\nu_n(\nu_n+1)}\,\frac{1}{\sin\nu_n\pi}\,\Lambda_n^e\,\frac{\partial}{\partial\theta} P_{\nu_n}(-\cos\theta)$$

$$-\frac{jk_o p\sin\varphi}{2h\Delta_g} \sum_{m=1}^{\infty} \frac{1}{\bar{\nu}_m(\bar{\nu}_m+1)}\,\frac{1}{\sin\bar{\nu}_m\pi}\,\Lambda_m^h\,\frac{\partial^2}{\partial\theta^2} P_{\bar{\nu}_m}(-\cos\theta)\,, \tag{H-24e}$$

and

$$H_\varphi^{he} = \frac{jk_o\Delta_g p\cos\varphi}{2h} \sum_{n=0}^{\infty} \frac{1}{\nu_n(\nu_n+1)}\,\frac{1}{\sin\nu_n\pi}\,\Lambda_n^e\,\frac{\partial^2}{\partial\theta^2} P_{\nu_n}(-\cos\theta)$$

$$-\frac{jk_o p\cos\varphi}{2h\Delta_g\sin\theta} \sum_{m=1}^{\infty} \frac{1}{\bar{\nu}_m(\bar{\nu}_m+1)}\,\frac{1}{\sin\bar{\nu}_m\pi}\,\Lambda_m^h\,\frac{\partial}{\partial\theta} P_{\bar{\nu}_m}(-\cos\theta)\,. \tag{H-24f}$$

H.2 QUASI-TEM FIELDS

The tables of section 4.1 showed that in the ELF band, all modes are nonpropagating except the $n = 0$ TM mode. This mode is often referred to as the quasi-transverse EM, or quasi-TEM mode. If only the quasi-TEM mode is considered, the HED fields for a source and receiver each located at the surface of the earth are given as

$$E_r^{he} = -\frac{\eta_o \Delta_g p \Lambda_o^e}{2ha} \frac{1}{\sin \nu_o \pi} \frac{\partial}{\partial \theta} P_{\nu_o}(-\cos\theta) \cos\varphi, \tag{H-25a}$$

$$E_\theta^{he} = -\frac{jk_o \eta_o \Delta_g^2 p \Lambda_o^e}{2h} \frac{1}{\nu_o(\nu_o+1)} \frac{1}{\sin \nu_o \pi} \frac{\partial^2}{\partial \theta^2} P_{\nu_o}(-\cos\theta) \cos\varphi, \tag{H-25b}$$

$$E_\varphi^{he} = \frac{j\omega\mu_o \Delta_g^2 p \Lambda_o^e}{2h} \frac{1}{\nu_o(\nu_o+1)} \frac{1}{\sin \nu_o \pi} \frac{1}{\sin\theta} \frac{\partial}{\partial \theta} P_{\nu_o}(-\cos\theta) \sin\varphi, \tag{H-25c}$$

$$H_\theta^{he} = \frac{jk_o \Delta_g p \Lambda_o^e}{2h} \frac{1}{\nu_o(\nu_o+1)} \frac{1}{\sin \nu_o \pi} \frac{1}{\sin\theta} \frac{\partial}{\partial \theta} P_{\nu_o}(-\cos\theta) \sin\varphi, \tag{H-25d}$$

and

$$H_\varphi^{he} = \frac{jk_o \Delta_g p \Lambda_o^e}{2h} \frac{1}{\nu_o(\nu_o+1)} \frac{1}{\sin \nu_o \pi} \frac{\partial^2}{\partial \theta^2} P_{\nu_o}(-\cos\theta) \cos\varphi \ . \tag{H-25e}$$

Note that the radial magnetic field component H_r^{he} is not listed above because it is expressed only in terms of TE modes.

APPENDIX I
THIN-SHELL APPROXIMATION TO THE RADIAL DEPENDENCE OF THE FIELDS

The spherical waveguide formulas derived in appendices F, G, and H involve the Legendre function of the first kind for the θ dependence and the spherical Bessel functions for the r (radial) dependence, where each function is of complex order. Exact and approximate representations for the Legendre function are presented in appendices J and K. Galejs (reference 2) has presented an approximate formula for the radial variation of the fields under the condition $h/r \ll 1$. This approximation, referred to as the thin-shell approximation, is suitable in the extremely low frequency (ELF) band and provides results of qualitative accuracy in the very low frequency (VLF) band. In this appendix, a derivation of the thin-shell approximation is presented and applied to obtain approximate solutions of the transverse magnetic (TM) and transverse electric (TE) mode characteristic equations. Thin-shell approximations for the mode excitation factors, the height-gain functions, and the z-dependent normalized impedances are also presented.

I.1 APPROXIMATE SOLUTION OF THE RADIAL DIFFERENTIAL EQUATION

In appendix B, it is shown that the radial dependence of each Debye potential is given in terms of a function $R_\nu(u)$, $u = k_o r$, which satisfies the following differential equation:

$$\frac{d}{dr}\left(r^2 \frac{dR_\nu}{dr}\right) + \left[(k_o r)^2 - \nu(\nu+1)\right] R_\nu = 0 \ . \tag{I-1}$$

As shown in appendix B, two linearly independent solutions of the above differential equation are given by the spherical Hankel functions of the first and second kinds, $h_\nu^{(1)}(u)$ and $h_\nu^{(2)}(u)$, respectively. Consider the following function:

$$W_\nu(r) \equiv r\, R_\nu(k_o r) \ . \tag{I-2}$$

The substitution of the above function into equation (I-1) yields the following differential equation for $W_\nu(r)$:

$$W_\nu''(r) + \left[k_o^2 - \frac{\nu(\nu+1)}{r^2}\right] W_\nu(r) = 0 \ . \tag{I-3}$$

For $r \to 8$ or for fields in a thin shell of $h/r \ll 1$, the radial variable r that appears in brackets in the above equation may be approximated by its average value $\tilde{r}$ in the shell that is given by

$$r \cong \tilde{r} = a + \varepsilon , \tag{I-4}$$

where $\varepsilon = h/a \ll 1$. The application of the above approximation into the differential equation (I-3) yields

$$W_\nu''(r) + k_{r\nu}^2 W_\nu(r) \cong 0 , \tag{I-5}$$

where

$$k_{r\nu}^2 \equiv k_o^2 - \frac{\nu(\nu+1)}{\tilde{r}^2} \quad . \tag{I-6}$$

If $|\nu| \gg 1$, then from formulas (K-26) and (K-27),

$$\nu(\nu+1) \cong (ka)^2 , \tag{I-7}$$

where k is the wave number in the θ direction. From the approximations (I-4) and (I-7), $k_{r\nu}$ in formula (I-6) is approximated as

$$k_{r\nu}^2 \cong k_o^2 - \frac{k^2}{\left(1+\frac{\varepsilon}{a}\right)^2} \cong k_o^2 - k^2\left(1 - \frac{2\varepsilon}{a}\right) \cong k_o^2 - k^2 , \ \varepsilon/a \ll 1 . \tag{I-8}$$

From the final expression in the above approximation, $k_{r\nu}$ can be interpreted as the wave number in the radial direction. Also note that the above approximation slightly underestimates the radial wave number for all values of r.

The solution of equation (I-5) is given by

$$W_\nu(r) = A\, e^{jk_{r\nu}r} + B\, e^{-jk_{r\nu}r} , \tag{I-9}$$

where A and B are arbitrary constants. From definition (I-2), R_ν is approximated as

$$R_\nu \cong \frac{W_\nu(r)}{\tilde{r}} \cong A\,\frac{e^{jk_{r\nu}r}}{\tilde{r}} + B\,\frac{e^{-jk_{r\nu}r}}{\tilde{r}} \quad . \tag{I-10}$$

A comparison of the exact solution (B-7) for R_ν with the approximation given above yields

$$h_\nu^{(1)}(u) \cong \frac{e^{jk_{r\nu}r}}{\tilde{r}} , \tag{I-11a}$$

and

$$h_\nu^{(2)}(u) \cong \frac{e^{-jk_{r\nu}r}}{\tilde{r}} \ . \tag{I-11b}$$

The above approximations are used to solve the TM and TE mode characteristic equations that are derived in appendix C.

I.2 APPLICATION OF THIN-SHELL APPROXIMATION TO TM MODES

Consider the characteristic equation for the TM modes given in expression (C-8). The application of the thin-shell approximation (I-11a) to the derivative terms in formula (C-8) that involve $h_\nu^{(1)}(u)$ yields the following:

$$h_\nu^{(1)'}(u) \cong \frac{1}{k_o}\frac{d}{dr}\left(\frac{e^{jk_{r\nu}r}}{\tilde{r}}\right) = \frac{jk_{r\nu}}{k_o}\frac{e^{jk_{r\nu}r}}{\tilde{r}}, \tag{I-12}$$

and

$$\frac{d\left[uh_\nu^{(1)}(u)\right]}{du} = h_\nu^{(1)}(u) + u\,h_\nu^{(1)'}(u) \cong \left(1 + jk_{r\nu}r\right)\frac{e^{jk_{r\nu}r}}{\tilde{r}} \ . \tag{I-13}$$

Following a similar procedure for $h_\nu^{(2)}(u)$, from approximation (I-11b), gives

$$\frac{d\left[uh_\nu^{(2)}(u)\right]}{du} \cong \left(1 - jk_{r\nu}r\right)\frac{e^{-jk_{r\nu}r}}{\tilde{r}} \ . \tag{I-14}$$

The substitutions of the thin-shell approximations (I-11), (I-13), and (I-14) into the quotients in equation (C-8) yields

$$\frac{\left\{\frac{1}{u_g}\left.\frac{\partial\left[uh_\nu^{(2)}(u)\right]}{\partial u}\right|_{u=u_g} - j\Delta_g h_\nu^{(2)}(u_g)\right\}}{\left\{\frac{1}{u_g}\left.\frac{\partial\left[uh_\nu^{(1)}(u)\right]}{\partial u}\right|_{u=u_g} - j\Delta_g h_\nu^{(1)}(u_g)\right\}} \cong \left[\frac{\frac{1}{a} - j(k_{r\nu} + \Delta_g k_o)}{\frac{1}{a} + j(k_{r\nu} - \Delta_g k_o)}\right] e^{-j2k_{r\nu}a}$$

$$\cong -\left(\frac{k_{r\nu} + \Delta_g k_o}{k_{r\nu} - \Delta_g k_o}\right) e^{-j2k_{r\nu}a}, \tag{I-15a}$$

and

$$\frac{\left\{\frac{1}{u_i}\left.\frac{\partial\left[uh_\nu^{(1)}(u)\right]}{\partial u}\right|_{u=u_i} + j\Delta_e h_\nu^{(1)}(u_i)\right\}}{\left\{\frac{1}{u_i}\left.\frac{\partial\left[uh_\nu^{(2)}(u)\right]}{\partial u}\right|_{u=u_i} + j\Delta_e h_\nu^{(2)}(u_i)\right\}} \cong \left[\frac{\frac{1}{(a+h)} + j(k_{r\nu} + \Delta_e k_o)}{\frac{1}{(a+h)} - j(k_{r\nu} - \Delta_e k_o)}\right] e^{j2k_{r\nu}(a+h)}$$

$$\cong -\left(\frac{k_{r\nu} + \Delta_e k_o}{k_{r\nu} - \Delta_e k_o}\right) e^{j2k_{r\nu}(a+h)} \quad . \tag{I-15b}$$

The final forms of approximations (I-15a) and (I-15b) are suitable because $1/a \ll 1$. The substitution of the above quotients into the TM mode characteristic equation (C-8) yields

$$\left(\frac{k_{r\nu_n} + \Delta_g k_o}{k_{r\nu_n} - \Delta_g k_o}\right)\left(\frac{k_{r\nu_n} + \Delta_e k_o}{k_{r\nu_n} - \Delta_e k_o}\right) e^{j2k_{r\nu_n}h} \cong 1 = e^{j2n\pi} \quad , \; n = 0, 1, 2, \ldots . \tag{I-16}$$

In the above equation, the index n corresponds to the order of the TM mode. Note that there are an infinite number of solutions to the above equation.

The TM mode characteristic equation (I-16) may be rewritten as

$$\left(\frac{1+\kappa_n}{1-\kappa_n}\right)\left(\frac{1+\zeta_n}{1-\zeta_n}\right) = e^{-j2(k_{r\nu_n}h - n\pi)} \quad , \; n = 0, 1, 2, \ldots , \tag{I-17}$$

where κ_n and ζ_n are defined as

$$\kappa_n \equiv \frac{\Delta_g k_o}{k_{r\nu_n}} , \tag{I-18}$$

$$\zeta_n \equiv \frac{\Delta_e k_o}{k_{r\nu_n}} \quad . \tag{I-19}$$

In the above expressions, note that a subscript has been added to the radial wave number to indicate the mode index. The natural logarithm of equation (I-17) yields

$$\ln\left(\frac{1+\kappa_n}{1-\kappa_n}\right) + \ln\left(\frac{1+\zeta_n}{1-\zeta_n}\right) = -j2\left(k_{r\nu_n}h - n\pi\right) \quad , \; n = 0, 1, 2, \ldots . \tag{I-20}$$

In the ELF band, the spherical waveguide boundaries appear as nearly perfect electric conductors. Therefore, $|\Delta_g| \ll 1$ and $|\Delta_e| \ll 1$ and the following conditions are valid:

$$|\kappa_n| \ll 1, \ |\zeta_n| \ll 1 \ . \tag{I-21}$$

From reference 27,

$$\ln\left(\frac{1+x}{1-x}\right) = 2\left(x + \frac{x^3}{3} + \frac{x^5}{5} + \ldots\right) \cong 2\left(x + \frac{x^3}{3}\right), \ |x| \ll 1 \ . \tag{I-22}$$

The application of the approximations (I-21) and (I-22) into the TM mode characteristic equation (I-20) results in

$$\kappa_n + \frac{\kappa_n^3}{3} + \zeta_n + \frac{\zeta_n^3}{3} \cong -j\left(k_{rv_n} h - n\pi\right) \ , \ n = 0, 1, 2, \ldots . \tag{I-23}$$

The substitution of the variable definitions (I-18) and (I-19) into the above equation yields the following quartic equation for k_{rv_n}:

$$k_{rv_n}^4 - \frac{n\pi}{h} k_{rv_n}^3 - \left[\frac{j(\Delta_g + \Delta_e) k_o}{h}\right] k_{rv_n}^2 - \left[\frac{j(\Delta_g^3 + \Delta_e^3) k_o^3}{3h}\right] = 0 \ , \ n = 0, 1, 2, \ldots . \tag{I-24}$$

Approximate solutions of the above equation for the quasi-TEM mode ($n = 0$) will be determined separately from the higher-order TM modes.

From the parallel-plate waveguide results given in section 2, it is known that the quasi-TEM mode ($n = 0$) is the only propagating mode over most of the ELF band. If $n = 0$, the quartic equation for k_{rv_n} given above reduces to the following quadratic equation for $k_{rv_o}^2$:

$$k_{rv_o}^4 - \left[\frac{j(\Delta_g + \Delta_e) k_o}{h}\right] k_{rv_o}^2 - \left[\frac{j(\Delta_g^3 + \Delta_e^3) k_o^3}{3h}\right] = 0 \ . \tag{I-25}$$

A solution of the above equation is

$$k_{rv_o}^2 = \frac{j(\Delta_g + \Delta_e) k_o}{2h} \left\{1 + \left[1 - \frac{j4k_o h}{3} \frac{(\Delta_g^3 + \Delta_e^3)}{(\Delta_g + \Delta_e)^2}\right]^{1/2}\right\} \ . \tag{I-26}$$

Because the earth is more highly conducting than the ionosphere, the following simplification is allowed:

$$\frac{(\Delta_g^3 + \Delta_e^3)}{(\Delta_g + \Delta_e)^2} = \Delta_g + \Delta_e - \frac{3\Delta_g\Delta_e}{\Delta_g + \Delta_e} \cong \Delta_e - 2\Delta_g \,, \quad |\Delta_g| \ll |\Delta_e| \,. \tag{I-27}$$

The substitution of the above approximation to the solution (I-26) yields

$$k_{rv_o}^2 \cong \frac{j(\Delta_g + \Delta_e)k_o}{2h}\left\{1 + \left[1 - \frac{j4k_o h}{3}(\Delta_e - 2\Delta_g)\right]^{1/2}\right\}$$

$$\cong \frac{j(\Delta_g + \Delta_e)k_o}{h} \,, \quad |\Delta_e k_o h| \ll 1 \,. \tag{I-28}$$

The above result corresponds with expression (87) on page 89 of Galejs (reference 2). Note that as $\Delta_g \to 0$ and $\Delta_e \to 0$, corresponding to perfectly conducting boundaries, then $k_{rv_o} \to 0$ and $k \cong k_o$, resulting in a purely TEM mode as described in section 2.

For the higher-order TM modes ($n \neq 0$), if only the first-order term in the series expansion (I-22) is applied to the TM mode characteristic equation (I-20), the following quadratic equation for k_{rv_n} is obtained:

$$k_{rv_n}^2 - \frac{n\pi}{h}k_{rv_n} - \left[\frac{j(\Delta_g + \Delta_e)k_o}{h}\right] = 0 \,, \quad n = 1, 2, 3, \ldots . \tag{I-29}$$

Note that a factor of $k_{rv_n}^2$ has been removed from the original quartic equation because this yields the trivial solution $k_{rv_n} = 0$. A solution of equation (I-29) is given by

$$k_{rv_n} = \frac{n\pi}{2h}\left\{1 + \left[1 + \frac{j4(\Delta_g + \Delta_e)k_o h}{(n\pi)^2}\right]^{1/2}\right\}$$

$$\cong \frac{n\pi}{h} + \frac{j(\Delta_g + \Delta_e)k_o}{n\pi} \,, \quad |\Delta_e k_o h| \ll 1 \,; \; n = 1, 2, 3, \ldots . \tag{I-30}$$

The above result corresponds with expression (88) on page 90 of Galejs (reference 2). Note that the first term in the above expression corresponds to the cutoff wave number for the TM modes in the parallel-plate waveguide with perfectly conducting walls as given in formula (2-15).

To determine the thin-shell approximations for the excitation factor Λ_n^e, the height-gain function $G_n^e(z)$, and the z-dependent normalized impedance $\Delta_n^e(z)$ for the TM modes as defined in expressions (F-14), (F-15), and (F-16), respectively, one must first obtain the thin-shell approximation for the constant $B_{\nu_n}^e$ that appears in the radial function $R_{\nu_n}^e$ that is defined in formula (C-10). The constant $B_{\nu_n}^e$ is given by either formula (C-7a) or (C-7b). The substitution of the thin-shell approximations (I-11), (I-13), and (I-14) into formula (C-7a) yields

$$B_{\nu_n}^e \cong -\left[\frac{1+j\left(k_{r\nu_n}a-\Delta_g k_o a\right)}{1-j\left(k_{r\nu_n}a+\Delta_g k_o a\right)}\right] e^{j2k_{r\nu_n}a} \ , \ n=0,\,1,\,2,\,\ldots\,. \tag{I-31}$$

Therefore, the thin-shell approximation to the radial function $R_{\nu_n}^e$ is

$$R_{\nu_n}^e(u) \cong \frac{e^{jk_{r\nu_n}r}}{\tilde{r}} - \left[\frac{1+j\left(k_{r\nu_n}a-\Delta_g k_o a\right)}{1-j\left(k_{r\nu_n}a+\Delta_g k_o a\right)}\right] \frac{e^{-jk_{r\nu_n}(r-2a)}}{\tilde{r}} \ , \ n=0,\,1,\,2,\,\ldots\,. \tag{I-32}$$

The thin-shell approximation for the height-gain function $G_n^e(z)$ is obtained through substitution of the approximation (I-32) into (F-15) and is given by

$$G_n^e(z) \cong \cos k_{r\nu_n}z - \left(\frac{1}{k_{r\nu_n}a} - j\frac{\Delta_g k_o}{k_{r\nu_n}}\right)\sin k_{r\nu_n}z \ , \ n=0,\,1,\,2,\,\ldots\,. \tag{I-33}$$

Note that in the above expression, $r-a$ has been replaced by z, the vertical distance above the earth. At ELF, the second term in the above expression is much less than the first term, resulting in the following:

$$G_n^e(z) \cong \cos k_{r\nu_n}z + j\frac{\Delta_g k_o}{k_{r\nu_n}}\sin k_{r\nu_n}z \ , \ n=0,\,1,\,2,\,\ldots\,. \tag{I-34}$$

The above result corresponds with expression (93) on page 93 of Galejs (reference 2).

The thin-shell approximation for the square of the L_2 norm of $R_{\nu_n}^e$, $\left\|R_{\nu_n}^e\right\|^2$, is obtained through substitution of the approximation (I-32) into the definition (F-12) and is given by

$$\left\| R^e_{\nu_n} \right\|^2 \cong k_o \int_a^{a+h} \left\{ \frac{e^{jk_{r\nu_n} r}}{\tilde{r}} - \left[\frac{1 + j\left(k_{r\nu_n} a - \Delta_g k_o a\right)}{1 - j\left(k_{r\nu_n} a + \Delta_g k_o a\right)} \right] \frac{e^{-jk_{r\nu_n}(r-2a)}}{\tilde{r}} \right\}^2 dr$$

$$= \frac{k_o}{\tilde{r}^2} e^{j2k_{r\nu_n} a} \left\{ -\frac{j}{2k_{r\nu_n}} \left(e^{j2k_{r\nu_n} h} - 1 \right) - 2h \left[\frac{1 + j\left(k_{r\nu_n} a - \Delta_g k_o a\right)}{1 - j\left(k_{r\nu_n} a + \Delta_g k_o a\right)} \right] \right.$$

$$\left. + \frac{j}{2k_{r\nu_n}} \left[\frac{1 + j\left(k_{r\nu_n} a - \Delta_g k_o a\right)}{1 - j\left(k_{r\nu_n} a + \Delta_g k_o a\right)} \right]^2 \left(e^{-j2k_{r\nu_n} h} - 1 \right) \right\} , \quad n = 0, 1, 2, \ldots . \tag{I-35}$$

If the square of approximation (I-32) is evaluated at $r = a$, then

$$\left[R^e_{\nu_n}(u_g) \right]^2 \cong \frac{e^{j2k_{r\nu_n} a}}{\tilde{r}^2} \left\{ 1 - 2 \left[\frac{1 + j\left(k_{r\nu_n} a - \Delta_g k_o a\right)}{1 - j\left(k_{r\nu_n} a + \Delta_g k_o a\right)} \right] + \left[\frac{1 + j\left(k_{r\nu_n} a - \Delta_g k_o a\right)}{1 - j\left(k_{r\nu_n} a + \Delta_g k_o a\right)} \right]^2 \right\}$$

$$n = 0, 1, 2, \ldots . \tag{I-36}$$

The thin-shell approximation for the TM mode excitation factor Λ^e_n is found through the substitution of approximations (I-35) and (I-36) into the definition (F-14), resulting in

$$\Lambda^e_n \cong \left\{ 1 + \frac{\sin 2k_{r\nu_n} h}{2k_{r\nu_n} h} + \left(\frac{\sin 2k_{r\nu_n} h}{2k_{r\nu_n} h} - 1 \right) \left[\left(\frac{\Delta_g k_o}{k_{r\nu_n}} \right)^2 - \frac{1}{\left(k_{r\nu_n} a\right)^2} + \frac{j2\Delta_g k_o}{k^2_{r\nu_n} a} \right] \right.$$

$$\left. + \left(1 - \cos 2k_{r\nu_n} h \right) \left[-\frac{1}{\left(k_{r\nu_n} a\right)\left(k_{r\nu_n} h\right)} + \frac{j\Delta_g k_o}{k^2_{r\nu_n} h} \right] \right\}^{-1} , \quad n = 0, 1, 2, \ldots . \tag{I-37}$$

Note that in the ELF band, $k_{r\nu_n} h \to 0$, $|\Delta_g| \ll 1$, and $|\Delta_e| \ll 1$, and, therefore, the above result reduces to $\Lambda_n^e \cong 0.5$.

The z-dependent normalized impedance for TM modes, $\Delta_n^e(z)$, has been defined in formula (F-16). The substitution of definition (C-10) and the thin-shell approximations (I-13), (I-14), and (I-31) into the numerator of formula (F-16), in appendix F, yields

$$\frac{\partial}{\partial u}\left[uR_{\nu_n}^e(u)\right] \cong \left(1 + jk_{r\nu} r\right) \frac{e^{jk_{r\nu_n} r}}{\tilde{r}} - \left[\frac{1 + j\left(k_{r\nu_n} a - \Delta_g k_o a\right)}{1 - j\left(k_{r\nu_n} a + \Delta_g k_o a\right)}\right] \left(1 - jk_{r\nu} r\right) \frac{e^{-jk_{r\nu_n}(r-2a)}}{\tilde{r}}. \quad \text{(I-38)}$$

The substitution of approximations (I-32) and (I-38) into expression (F-16) gives

$$\Delta_n^e(z) \cong \frac{-k_{r\nu_n}\left[(z+a)\,\Delta_g k_o a + jz\right] \cos k_{r\nu_n} z - j\left[1 + \left(k_{r\nu_n}(z+a)\right)\left(k_{r\nu_n} a\right) - j\Delta_g k_o a\right] \sin k_{r\nu_n} z}{k_o(z+a)\left[k_{r\nu_n} a \cos k_{r\nu_n} z - \left(1 - j\Delta_g k_o a\right) \sin k_{r\nu_n} z\right]},$$

$$n = 0, 1, 2, \ldots. \quad \text{(I-39)}$$

Note that for points on the surface of the earth, $z = 0$, the normalized impedance reduces to $\Delta_n^e(0) = -\Delta_g$.

I.3 APPLICATION OF THIN-SHELL APPROXIMATION TO TE MODES

Consider the characteristic equation for the TE modes as given in expression (C-21). As mentioned in appendix C, the TE characteristic equation is equivalent to the TM characteristic equation (C-8) if Δ_g is replaced by $1/\Delta_g$ and Δ_e is replaced by $1/\Delta_h$. Therefore, with the appropriate substitutions applied to the approximate TM mode characteristic equation (I-16), the TE mode characteristic equation is given by

$$\left(\frac{k_{r\bar{\nu}_m}\Delta_g + k_o}{k_{r\bar{\nu}_m}\Delta_g - k_o}\right)\left(\frac{k_{r\bar{\nu}_m}\Delta_h + k_o}{k_{r\bar{\nu}_m}\Delta_h - k_o}\right) e^{j2k_{r\bar{\nu}_m} h} \cong 1 = e^{j2m\pi}, \quad m = 1, 2, 3, \ldots. \quad \text{(I-40)}$$

In the above equation, the index m corresponds to the order of the TE mode. Note that there are an infinite number of solutions to the above equation.

The TE mode characteristic equation (I-40) may be rewritten as

$$\left(\frac{1+\bar{\kappa}_m}{1-\bar{\kappa}_m}\right)\left(\frac{1+\bar{\xi}_m}{1-\bar{\xi}_m}\right) = e^{-j2(k_{r\bar{\nu}_m}h - m\pi)}, \quad m = 1, 2, 3, \ldots, \tag{I-41}$$

where $\bar{\kappa}_m$ and $\bar{\xi}_m$ are defined as

$$\bar{\kappa}_m \equiv \frac{k_{r\bar{\nu}_m}\Delta_g}{k_o}, \tag{I-42}$$

and

$$\bar{\xi}_m \equiv \frac{k_{r\bar{\nu}_m}\Delta_h}{k_o}. \tag{I-43}$$

In the above expressions, note that a subscript has been added to the radial wave number to indicate the mode index. The natural logarithm of equation (I-41) yields the following:

$$\ln\left(\frac{1+\bar{\kappa}_m}{1-\bar{\kappa}_m}\right) + \ln\left(\frac{1+\bar{\xi}_m}{1-\bar{\xi}_m}\right) = -j2\left(k_{r\bar{\nu}_m}h - m\pi\right), \quad m = 1, 2, 3, \ldots. \tag{I-44}$$

In the ELF band, because the spherical waveguide boundaries appear as nearly perfect electric conductors, then $|\Delta_g| \ll 1$ and $|\Delta_h| \ll 1$, resulting in the following conditions:

$$\left|\bar{\kappa}_m\right| \ll 1, \quad \left|\bar{\xi}_m\right| \ll 1. \tag{I-45}$$

The application of the approximations (I-22) and (I-45) into the TE mode characteristic equation (I-44) results in

$$\bar{\kappa}_m + \frac{\bar{\kappa}_m^3}{3} + \bar{\xi}_m + \frac{\bar{\xi}_m^3}{3} \cong -j\left(k_{r\bar{\nu}_m}h - m\pi\right), \quad m = 1, 2, 3, \ldots. \tag{I-46}$$

The substitution of the variable definitions (I-42) and (I- 43) into the approximate TE mode characteristic equation (I-46) yields the following cubic equation for $k_{r\bar{\nu}_m}$:

$$\left[\frac{(\Delta_g^3 + \Delta_h^3)}{3k_o^3}\right]k_{r\bar{\nu}_m}^3 + \left[\frac{(\Delta_g + \Delta_h)}{k_o} + jh\right]k_{r\bar{\nu}_m} = jm\pi, \quad m = 1, 2, 3, \ldots. \tag{I-47}$$

The application of the conditions (I-45) to the above equation results in a negligible cubic term in

$k_{r\bar{\nu}_m}$ resulting in the following approximate solution:

$$k_{r\bar{\nu}_m} \cong \frac{m\pi}{h}\left[1 - \frac{j(\Delta_g + \Delta_h)}{k_o h}\right]^{-1}, \quad m = 1, 2, 3, \ldots . \tag{I-48}$$

The above result corresponds with expression (90) on page 90 of Galejs (reference 2). Note that as $\Delta_g \to 0$ and $\Delta_h \to 0$, then $k_{r\bar{\nu}_m} \to m\pi/h$, corresponding to the cutoff wave number for the TE modes in the parallel-plate waveguide with perfectly conducting walls as given in formula (2-32). Also note that if $m = 0$, then $k_{r\bar{\nu}_m} = 0$ and the TE fields are not excited.

To determine the thin-shell approximations for the excitation factor Λ_m^h, the height-gain function $G_m^h(z)$, and the z-dependent normalized impedance $\Delta_m^h(z)$ for the TE modes as defined in expressions (G-13), (G-14), and (G-15), respectively, one must first obtain the thin-shell approximation for the constant $B_{\bar{\nu}_m}^h$ that appears in the radial function $R_{\bar{\nu}_m}^h$ that is defined in formula (C-23). $B_{\bar{\nu}_m}^h$ is given by either formula (C-20a) or (C-20b). The substitution of the thin-shell approximations (I-11), (I-13), and (I-14) into formula (C-20a) yields the following:

$$B_{\bar{\nu}_m}^h = -\left[\frac{\Delta_g + j\left(k_{r\bar{\nu}_m} a\Delta_g - k_o a\right)}{\Delta_g - j\left(k_{r\bar{\nu}_m} a\Delta_g + k_o a\right)}\right] e^{j2k_{r\bar{\nu}_m} a}, \quad m = 1, 2, 3, \ldots . \tag{I-49}$$

Therefore, the thin-shell approximation to the radial function $R_{\bar{\nu}_m}^h$ is

$$R_{\bar{\nu}_m}^h(u) \cong \frac{e^{jk_{r\bar{\nu}_m} r}}{\tilde{r}} - \left[\frac{\Delta_g + j\left(k_{r\bar{\nu}_m} a\Delta_g - k_o a\right)}{\Delta_g - j\left(k_{r\bar{\nu}_m} a\Delta_g + k_o a\right)}\right] \frac{e^{-jk_{r\bar{\nu}_m}(r-2a)}}{\tilde{r}}, \quad m = 1, 2, 3, \ldots . \tag{I-50}$$

The thin-shell approximation for the height-gain function $G_m^h(z)$ follows directly from $G_n^e(z)$ with Δ_g replaced by $1/\Delta_g$. Therefore, from formula (I-34),

$$G_m^h(z) \cong \cos k_{r\bar{\nu}_m} z + j\frac{k_o}{\Delta_g k_{r\bar{\nu}_m}} \sin k_{r\bar{\nu}_m} z, \quad m = 1, 2, 3, \ldots . \tag{I-51}$$

The above result is applicable at ELF and corresponds with expression (99) on page 94 of Galejs (reference 2).

The thin-shell approximation for the TE mode excitation factor Λ_m^h follows directly from Λ_n^e with Δ_g is replaced by $1/\Delta_g$. Therefore, from formula (I-37),

$$\Lambda_m^h \cong -\left(\frac{\Delta_g k_{r\bar{\nu}_m}}{k_o}\right)^2 \left\{ \left(1 - \frac{\sin 2k_{r\bar{\nu}_m} h}{2k_{r\bar{\nu}_m} h}\right)\left[1 - \left(\frac{\Delta_g}{k_o a}\right)^2 + \frac{j2\Delta_g}{k_o a}\right] - \left(\frac{\Delta_g k_{r\bar{\nu}_m}}{k_o}\right)^2 \left(1 + \frac{\sin 2k_{r\bar{\nu}_m} h}{2k_{r\bar{\nu}_m} h}\right) \right.$$
$$\left. - \left(\frac{j\Delta_g}{k_o h}\right)\left(1 + \frac{j\Delta_g}{k_o a}\right)\left(1 - \cos 2k_{r\bar{\nu}_m} h\right) \right\}^{-1}, \quad m = 1, 2, 3, \ldots . \tag{I-52}$$

Note that in the ELF band, $k_{r\bar{\nu}_m} h \to 0$ and with the conditions (I-45), then $\Lambda_m^h \to 0$. Therefore, the TE modes are weakly excited in the ELF band. The z-dependent normalized impedance for the TE modes, $\Delta_m^h(z)$, is obtained through inversion of the formula (I-39) for $\Delta_n^e(z)$ and with Δ_g replaced by $1/\Delta_g$ and is given as follows:

$$\Delta_m^h(z) \cong \frac{-k_o(z+a)\left[\Delta_g k_{r\bar{\nu}_m} a \cos k_{r\bar{\nu}_m} z - \left(\Delta_g - jk_o a\right)\sin k_{r\bar{\nu}_m} z\right]}{k_{r\bar{\nu}_m}\left[(z+a)k_o a + jz\Delta_g\right]\cos k_{r\bar{\nu}_m} z + j\left[\Delta_g + \Delta_g\left(k_{r\bar{\nu}_m}(z+a)\right)\left(k_{r\bar{\nu}_m} a\right) - jk_o a\right]\sin k_{r\bar{\nu}_m} z}$$

$$m = 1, 2, 3, \ldots . \tag{I-53}$$

Note that for points on the surface of the earth, $z = 0$, the normalized impedance reduces to $\Delta_m^h(0) = -\Delta_g$.

APPENDIX J
LEGENDRE FUNCTION $P_\nu(-\cos\theta)$ AND ITS DERIVATIVES

The range dependencies of the spherical wave propagation formulas derived in this report involve the Legendre function of the first kind P_ν and its first two derivatives. In this appendix, both exact and approximate formulas for P_ν are presented. The exact formula is expressed in terms of an infinite series. The approximate formulas for P_ν are restricted to particular ranges of the argument. Comparisons of the exact and approximate formulas for P_ν are given for several values of ν that correspond to particular propagation conditions.

J.1 ASYMPTOTIC APPROXIMATION

A traveling wave representation of the spherical wave formulas derived in this report is obtained from the first term in the asymptotic series for $P_\nu(-\cos\theta)$. From Erdelyi (reference 28), if $|\nu| \gg 1$, $\mathrm{Im}\{\nu\} > 0$, and θ is not near 0 or π, a suitable asymptotic approximation for $P_\nu(-\cos\theta)$ is

$$P_\nu(-\cos\theta) \sim \left[\frac{2}{\pi(\nu+1/2)\sin\theta}\right]^{1/2} \cos\left[(\nu+1/2)(\pi-\theta)-\pi/4\right] . \tag{J-1}$$

If the cosine is expressed as the sum of two complex exponentials, the above approximation becomes

$$P_\nu(-\cos\theta) \sim \left[\frac{1}{2\pi(\nu+1/2)\sin\theta}\right]^{1/2} \left\{\exp\left[j(\nu+1/2)(\pi-\theta)-j\pi/4\right] + \exp\left[-j(\nu+1/2)(\pi-\theta)+j\pi/4\right]\right\} . \tag{J-2}$$

The asymptotic formula (J-2) may be rewritten as the superposition of two waves traveling in opposite directions as

$$P_\nu(-\cos\theta) \sim \left[\frac{1}{j2\pi ka\sin\theta}\right]^{1/2} e^{jka\pi}\left[e^{-jk\rho} + j\,e^{-jk\rho_i}\right] , \tag{J-3}$$

where

$$k \equiv \beta - j\alpha = \frac{\nu+1/2}{a} . \tag{J-4}$$

In the above formulas, k is the wave number in the earth-ionosphere waveguide, $\beta = 2\pi/\lambda$ and α are the phase and attenuation constants, respectively, and λ is the wavelength. In addition, $\rho = a\theta$ and $\rho_i = 2\pi a - \rho$ are the direct and indirect great-circle path distances from the source to the receiver, respectively, as shown in figure 4. Note that there is a 90° phase advance acquired by the indirect great-circle path wave as it passes through the antipode ($\theta = \pi$).

As shown in appendices F, G, and H, the range dependencies of many of the field expressions involve either the first or the second derivative of $P_\nu(-\cos\theta)$ with respect to θ. From equation (J-3), the asymptotic formulas for the first and second derivatives of $P_\nu(-\cos\theta)$ with respect to θ are

$$\frac{d}{d\theta} P_\nu(-\cos\theta) \sim -\left[\frac{jka}{2\pi \sin\theta}\right]^{1/2} e^{jka\pi}\left[e^{-jk\rho} - j e^{-jk\rho_i}\right], \tag{J-5}$$

and

$$\frac{d^2}{d\theta^2} P_\nu(-\cos\theta) \sim -\left[\frac{1}{2j\pi \sin\theta}\right]^{1/2} (ka)^{3/2} e^{jka\pi}\left[e^{-jk\rho} + j e^{-jk\rho_i}\right]. \tag{J-6}$$

The above formulas are based on taking only the derivative of the exponential sum in expression (J-3) because this is the dominant spatially varying part of the asymptotic formula for $P_\nu(-\cos\theta)$. Note that there is a 90° phase advance in the indirect wave in the first derivative formula and a 90° phase decrease in the indirect wave in the second derivative formula.

The asymptotic formulas (J-3), (J-5), and (J-6) are useful in the determination of the relative phase differences between the direct and indirect great-circle path fields. For ELF propagation formulas based on the earth-flattening approximation, each indirect great-circle path field component is obtained from the corresponding direct great-circle path component through replacement of ρ by ρ_i and with an appropriate phase adjustment as obtained from the asymptotic formulas (J-3), (J-5), and (J-6). From these asymptotic formulas, the phase adjustments for the indirect great-circle path fields are given in the table J-1. Note that the spherical components r and θ of the fields are replaced by the equivalent cylindrical components z and ρ, respectively. This replacement is made because table J-1 is applied to the formulas based on the earth-flattening approximation that are presented in cylindrical coordinates in section 3.

Table J-1. Phase Adjustment Terms for the Indirect Great-Circle Path Fields

Source	Field Component(s)	Primary Range Dependence	Phase Adjustment Term
VED	E_z	$P_\nu(-\cos\theta)$	j
	E_ρ, H_φ	$\frac{d}{d\theta} P_\nu(-\cos\theta)$	$-j$
HED	E_z, E_φ, H_ρ	$\frac{d}{d\theta} P_\nu(-\cos\theta)$	$-j$
	E_ρ, H_φ	$\frac{d^2}{d\theta^2} P_\nu(-\cos\theta)$	j

J.2 APPROXIMATE SERIES FORMULA SUITABLE IN THE VICINITY OF THE ANTIPODE

In the previous section, the asymptotic formulas for $P_\nu(-\cos\theta)$ and its first two derivatives are not valid for θ near 0 or π (i.e., for field points located near the source or the antipode). Therefore, these formulas are not suitable for observation points lying in the vicinity of the antipode. MacDonald (reference 29) has derived an approximate formula for P_ν that is valid when its argument is at or close to one and is, therefore, valid in the vicinity of the antipode. MacDonald's formula for $P_\nu(-\cos\theta)$ is given as

$$P_\nu(-\cos\theta) = J_0(\eta) + \sin^2\left(\frac{\pi-\theta}{2}\right)\left[\frac{1}{2\eta} J_1(\eta) - J_2(\eta) + \frac{\eta}{6} J_3(\eta)\right] + O\left[\sin^4\left(\frac{\pi-\theta}{2}\right)\right], \quad \text{(J-7)}$$

where

$$\eta = 2(\nu + 1/2)\sin\left(\frac{\pi-\theta}{2}\right) = 2ka\sin\left(\frac{\pi-\theta}{2}\right). \quad \text{(J-8)}$$

In expression (J-7), J_n denotes the Bessel function of the first kind and order n. Note that formula (J-4) is applied in expression (J-8). Expression (J-7) can be simplified through the use of the following recurrence relation (reference 24)

$$J_{n+1}(z) = \frac{2n}{z} J_n(z) - J_{n-1}(z), \quad \text{(J-9)}$$

where n is a positive integer or zero, and z is an arbitrary complex constant. The application of the above relation to the first bracketed term in formula (J-7) yields

$$\frac{1}{2\eta} J_1(\eta) - J_2(\eta) + \frac{\eta}{6} J_3(\eta) = \frac{1}{3} J_0(\eta) - \frac{1}{6\eta}\left(1 + \eta^2\right) J_1(\eta) \ . \tag{J-10}$$

For observation points in the vicinity of the antipode, $(\pi - \theta)/2 \ll 1$ and

$$\sin\left(\frac{\pi - \theta}{2}\right) \cong \frac{\pi - \theta}{2} \ . \tag{J-11}$$

As a result, η can be approximated as

$$\eta \cong k\rho_a \ , \quad \left(\frac{\pi - \theta}{2}\right) \ll 1 \ , \tag{J-12}$$

where $\rho_a = a(\pi - \theta)$ is the great-circle path distance from the antipode to the field point (figure 4). The substitution of expression (J-10) and approximations (J-11) and (J-12) to the two leading terms in the series (J-7) yields

$$P_v(-\cos\theta) \cong J_0(k\rho_a)\left[1 + \frac{1}{12}\left(\frac{\rho_a}{a}\right)^2\right] - \frac{\rho_a/a}{24ka}\left[1 + (k\rho_a)^2\right] J_1(k\rho_a) \ , \quad \rho_a \ll 1 \ . \tag{J-13}$$

For field points in the vicinity of the antipode, the first term in the series (J-13) is dominant. Therefore, for small ρ_a, consider only the leading term of the above series, i.e.,

$$P_v(-\cos\theta) \cong J_0(k\rho_a)\left[1 + \frac{1}{12}\left(\frac{\rho_a}{a}\right)^2\right] . \tag{J-14}$$

In the above approximation, the second term within the brackets accounts for the curvature of the earth as ρ_a/a increases. From Wait (reference 1), the bracketed term in formula (J-14) can be approximated as

$$\left[1 + \frac{1}{12}\left(\frac{\rho_a}{a}\right)^2\right] \cong \left[\frac{\rho_a/a}{\sin \rho_a/a}\right]^{1/2} , \tag{J-15}$$

where the error in the in the above approximation is $O[(\rho_a/a)^4]$. The substitution of the above approximation into formula (J-14) yields

$$P_v(-\cos\theta) \cong J_0(k\rho_a)\left[\frac{\rho_a/a}{\sin \rho_a/a}\right]^{1/2} . \tag{J-16}$$

In the above formula, $J_0(k\rho_a)$ corresponds to the range dependence for a flat earth and the square-root term accounts for the curvature. Therefore, formula (J-16) is an earth-flattening approximation to $P_\nu(-\cos\theta)$ that accounts for curvature and is valid for field points located in the vicinity of the antipode.

The approximation (J-16) has been applied in the development of some antipode-centered ELF propagation formulas that were previously derived by the author (reference 7). From formula (J-16), the first and second derivatives of $P_\nu(-\cos\theta)$ with respect to θ are

$$\frac{d}{d\theta} P_\nu(-\cos\theta) \cong ka\, J_1(k\rho_a) \left[\frac{\rho_a/a}{\sin \rho_a/a}\right]^{1/2}, \tag{J-17}$$

and

$$\frac{d^2}{d\theta^2} P_\nu(-\cos\theta) \cong -(ka)^2 \left[J_0(k\rho_a) - \frac{1}{k\rho_a} J_1(k\rho_a)\right] \left[\frac{\rho_a/a}{\sin \rho_a/a}\right]^{1/2}. \tag{J-18}$$

The approximate formulas for $P_\nu(-\cos\theta)$ and its first two derivatives as given in expressions (J-16), (J-17), and (J-18) are required in order to reduce the vertical electric dipole (VED) and horizontal electric dipole (HED) spherical waveguide formulas to the corresponding antipode-centered ELF propagation formulas presented in section 4.3.

J.3 INFINITE SERIES FORMULA

The Legendre function of the first kind and degree ν and order zero, P_ν, is related to the hypergeometric series F as (reference 24)

$$P_\nu(z) = F\left(-\nu, \nu+1; 1; \frac{1-z}{2}\right), \tag{J-19}$$

where F is given as

$$F(a, b; c; z) = \sum_{n=0}^{\infty} \frac{(a)_n (b)_n}{(c)_n} \frac{z^n}{n!} = \frac{\Gamma(c)}{\Gamma(a)\,\Gamma(b)} \sum_{n=0}^{\infty} \frac{\Gamma(a+n)\,\Gamma(b+n)}{\Gamma(c+n)} \frac{z^n}{n!}. \tag{J-20}$$

In the above series, Γ denotes the gamma function and $(\cdot)_n$ denotes Pochhammer's symbol defined as

$$(z)_n = \begin{cases} 1\,, & n = 0 \\ z(z+1)(z+2)\ \ldots\ (z+n-1)\,, & n = 1, 2, 3, \ldots \end{cases} \quad . \tag{J-21}$$

With the recurrence formula for the gamma function given by $\Gamma(z+1) = z\,\Gamma(z)$, Pochhammer's symbol can be expressed in terms of the gamma function as

$$(z)_n = \frac{\Gamma(z+n)}{\Gamma(z)}\,, \quad n = 0, 1, 2, \ldots . \tag{J-22}$$

According to Abramowitz and Stegun (reference 24), the hypergeometric series (J-20) converges for $|z| < 1$. From expressions (J-19) and (J-20), $P_\nu(-\cos\theta)$ is given by

$$P_\nu(-\cos\theta) = F\left(-\nu, \nu+1; 1; \frac{1+\cos\theta}{2}\right) = \sum_{n=0}^{\infty} \frac{(-\nu)_n\,(\nu+1)_n\,(1+\cos\theta)^n}{2^n\,(n!)^2}\,. \tag{J-23}$$

Therefore, in the evaluation of $P_\nu(-\cos\theta)$, the hypergeometric series (J-23) converges for $0 < \theta = \pi$.

The derivative of $P_\nu(-\cos\theta)$ with respect to θ is given as

$$\frac{d}{d\theta} P_\nu(-\cos\theta) = P_\nu'(-\cos\theta)\,\frac{d(-\cos\theta)}{d\theta} = P_\nu'(-\cos\theta)\,\sin\theta\,, \tag{J-24}$$

where the prime denotes the derivative with respect to the argument $-\cos\theta$. From equation (J-24), the second derivative of $P_\nu(-\cos\theta)$ with respect to θ is given as

$$\frac{d^2}{d\theta^2} P_\nu(-\cos\theta) = \frac{d}{d\theta}\left[P_\nu'(-\cos\theta)\,\sin\theta\right] = P_\nu'(-\cos\theta)\,\cos\theta + \sin\theta\,\frac{d}{d\theta} P_\nu'(-\cos\theta)$$

$$= P_\nu'(-\cos\theta)\,\cos\theta + P_\nu''(-\cos\theta)\,\sin^2\theta\,. \tag{J-25}$$

From the series formula (J-20), the first and second derivatives of the hypergeometric series are

$$\frac{d}{dz} F(a, b; c; z) = \frac{ab}{c}\,F(a+1, b+1; c+1; z)\,, \tag{J-26}$$

and

$$\frac{d^2}{dz^2} F(a, b; c; z) = \frac{(a)_2(b)_2}{(c)_2}\,F(a+2, b+2; c+2; z)\,. \tag{J-27}$$

From equations (J-19), (J-26), and (J-27), the first and second derivatives of $P_\nu(-\cos\theta)$ with respect to the argument $-\cos\theta$ are given as

$$P'_\nu(-\cos\theta) = \frac{\nu(\nu+1)}{2} F\left(-\nu+1, \nu+2; 2; \frac{1+\cos\theta}{2}\right), \tag{J-28}$$

and

$$P''_\nu(-\cos\theta) = \frac{(-\nu)_2 (\nu+1)_2}{8} F\left(-\nu+2, \nu+3; 3; \frac{1+\cos\theta}{2}\right) . \tag{J-29}$$

The substitution of equations (J-20) and (J-28) into (J-24) yields

$$\frac{d}{d\theta} P_\nu(-\cos\theta) = \frac{\nu(\nu+1)}{2} \sin\theta \sum_{n=0}^{\infty} \frac{(-\nu+1)_n (\nu+2)_n (1+\cos\theta)^n}{2^n\, n!\, (n+1)!} . \tag{J-30}$$

Similarly, the substitution of equations (J-20), (J-28), and (J-29) into (J-25) yields

$$\frac{d^2}{d\theta^2} P_\nu(-\cos\theta) = \frac{\nu(\nu+1)}{2} \cos\theta \sum_{n=0}^{\infty} \frac{(-\nu+1)_n (\nu+2)_n (1+\cos\theta)^n}{2^n\, n!\, (n+1)!}$$

$$+ \frac{(-\nu)_2 (\nu+1)_2}{4} \sin^2\theta \sum_{n=0}^{\infty} \frac{(-\nu+2)_n (\nu+3)_n (1+\cos\theta)^n}{2^n\, n!\, (n+2)!} . \tag{J-31}$$

In the evaluation of the spherical wave propagation formulas derived in this report, the Legendre function and its first two derivatives are computed from formulas (J-23), (J-30), and (J-31).

Before computing the Legendre function and its first two derivatives from the series formulas given above, a discussion of numerical convergence is in order. As an example, consider the propagation parameters for the quasi-TEM mode at 76 Hz that are given in table 5-1. Under daytime conditions, $\nu = 11.7 + j\ 0.880$. Table J-2 provides a listing of the number of iterations required for the series formulas to convergence to 15 decimal places for various values of θ. The table shows that the number of iterations required for each function to converge increases with distance from the antipode ($\theta = \pi$). As $\theta \to 0$ (source point), the number of required iterations increases rapidly. This behavior is expected because formulas (J-23), (J-30), and (J-31) are ascending series in the argument $(1 + \cos\theta)$. In summary, for θ not too close to zero, not much CPU time is required in order for these series formulas to converge.

Table J-2. Number of Iterations Required for the Infinite Series Formulas for $P_\nu(-\cos\theta)$ and its First Two Derivatives to Converge to 15 Decimal Places with $\nu = 11.7 + j\,0.880$

θ (deg)	$P_\nu(-\cos\theta)$	$\frac{d}{d\theta} P_\nu(-\cos\theta)$	$\frac{d^2}{d\theta^2} P_\nu(-\cos\theta)$
10	3414	3827	4240
30	423	454	486
50	160	168	176
70	84	87	89
90	51	52	53
110	34	34	35
130	24	24	23
150	17	16	16
170	11	10	10

The series formulas for the Legendre function and its first two derivatives can be used to check the accuracies of the approximate formulas (J-16), (J-17), and (J-18). Figures J-1 show plots of the real and imaginary parts of the Legendre function and its first two derivatives as computed by the series and approximate formulas given as functions of the polar angle θ_a measured from the antipode, where $\theta_a = \pi - \theta$.

The ranges of validity of the approximate formulas for the Legendre function and its first two θ derivatives as given in expressions (J-16), (J-17), and (J-18) can be determined through comparison with the infinite series (exact) formulas. Figures J-1a and J-1b show comparisons of the magnitude and phase, respectively, of the exact and approximate formulas for $P_\nu(-\cos\theta)$ as a function of θ_a for $\nu = 4.75 - j\,0.440$. This value of ν corresponds to typical daytime propagation conditions at 30 Hz as given in table 5-1. Figures J-2 and J-3 show similar comparisons for $dP_\nu(-\cos\theta)/d\theta$ and $d^2P_\nu(-\cos\theta)/d\theta^2$, respectively. The plots show that the exact and approximate formulas are in excellent agreement out to $\theta_a \cong 45°$. Beyond this angle, the approximate formula for the second derivative starts to slowly depart from the exact formula. For example, at $\theta_a = 45.1°$, the approximate formula for the second derivative differs by 0.067 dB in magnitude and 0.95° in phase with the exact formula. In comparison, at $\theta_a = 90°$, the approximate formula for the second derivative differs by 0.46 dB in magnitude and 8.32° in phase with the exact formula. At $\theta_a = 170.1°$, the approximate formula for the second derivative differs by 2.18 dB in magnitude and 69.6° in phase with the exact formula. The approximate

formula for $dP_\nu(-\cos\theta)/d\theta$ shows better agreement with the exact formula than the second derivative and the approximate formula for $P_\nu(-\cos\theta)$ shows an even better agreement. This observation is attributed to the fact that each successive derivative of the approximate formula for $P_\nu(-\cos\theta)$ introduces additional error into the result. The approximate formula for $P_\nu(-\cos\theta)$ does not start to noticeably depart from the exact formula until $\theta_a \cong 150°$, where the formulas differ by 0.14 dB in magnitude and 2.26° in phase.

Comparison plots of the exact and approximate formulas for $P_\nu(-\cos\theta)$, $dP_\nu(-\cos\theta)/d\theta$, and $d^2P_\nu(-\cos\theta)/d\theta^2$ as a function of θ_a are given in figures J-4, J-5, and J-6, respectively, for $\nu = 15.9 - j\,1.32$. This value of ν corresponds to daytime propagation conditions at 100 Hz as given in table 5-2. In these plots, the oscillations near the antipode are considerably damped because of the larger attenuation at this higher frequency. Each of these plots show a noticeable improvement in agreement as compared to the previous value of ν. For example, at $\theta_a = 90°$, the approximate formula for the second derivative differs by 0.012 dB in magnitude and 1.88° in phase with the exact formula; and at $\theta_a = 150°$, the approximate formula for the second derivative differs by 0.065 dB in magnitude and 6.47° in phase with the exact formula. As in the previous set of plots, the approximate formula for $dP_\nu(-\cos\theta)/d\theta$ shows better agreement with the exact formula than the second derivative, and the approximate formula for $P_\nu(-\cos\theta)$ shows an even better agreement. Further examination of the approximate formulas at other ELF frequencies indicates that the accuracies of the approximate formulas for $P_\nu(-\cos\theta)$ and its derivatives improve with increasing frequency.

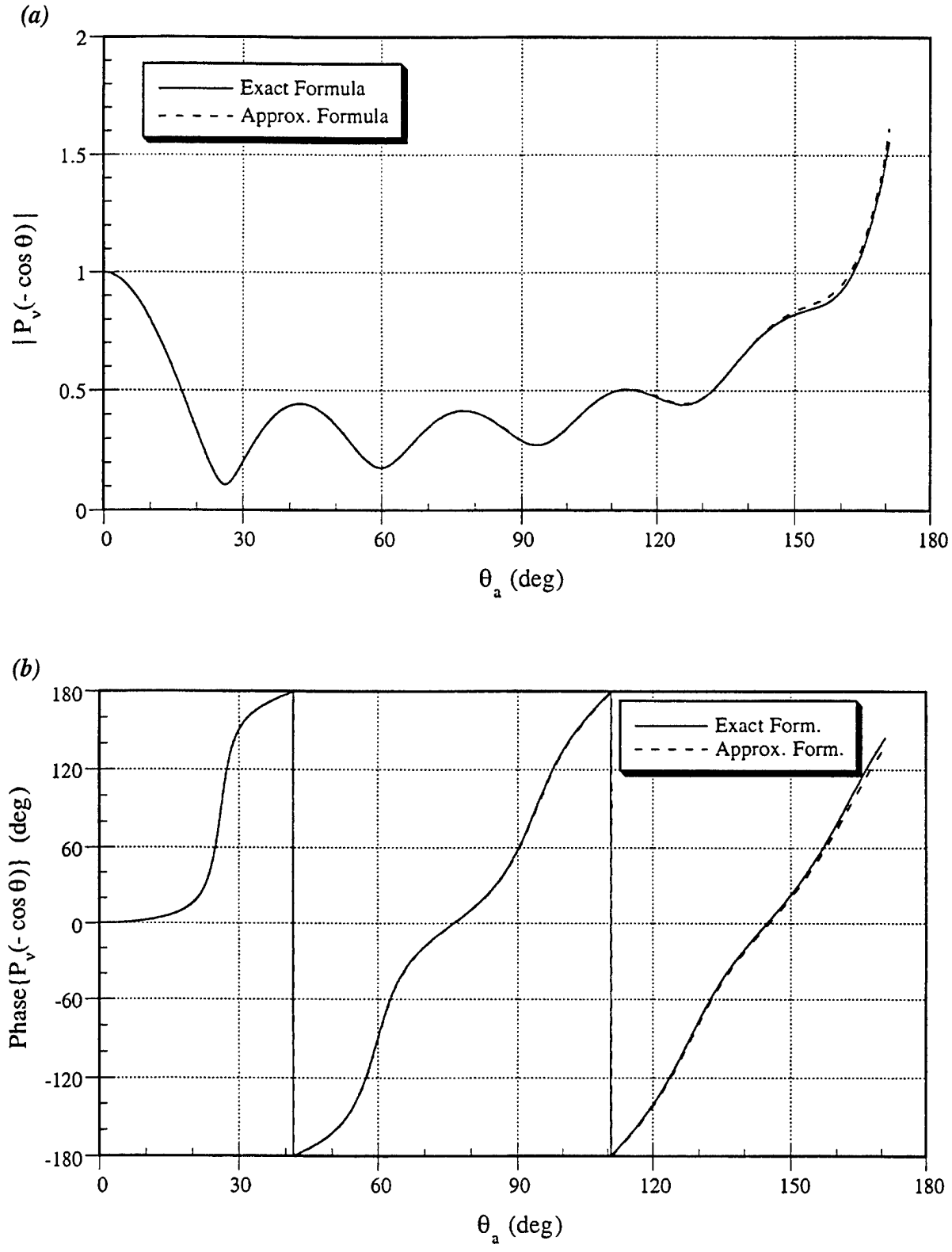

Figure J-1. Comparison of the Infinite Series (Exact) and Approximate Formulas for $P_\nu(-\cos\theta)$ for $\nu = 4.75 - j\,0.440$; (a) Magnitude; (b) Phase

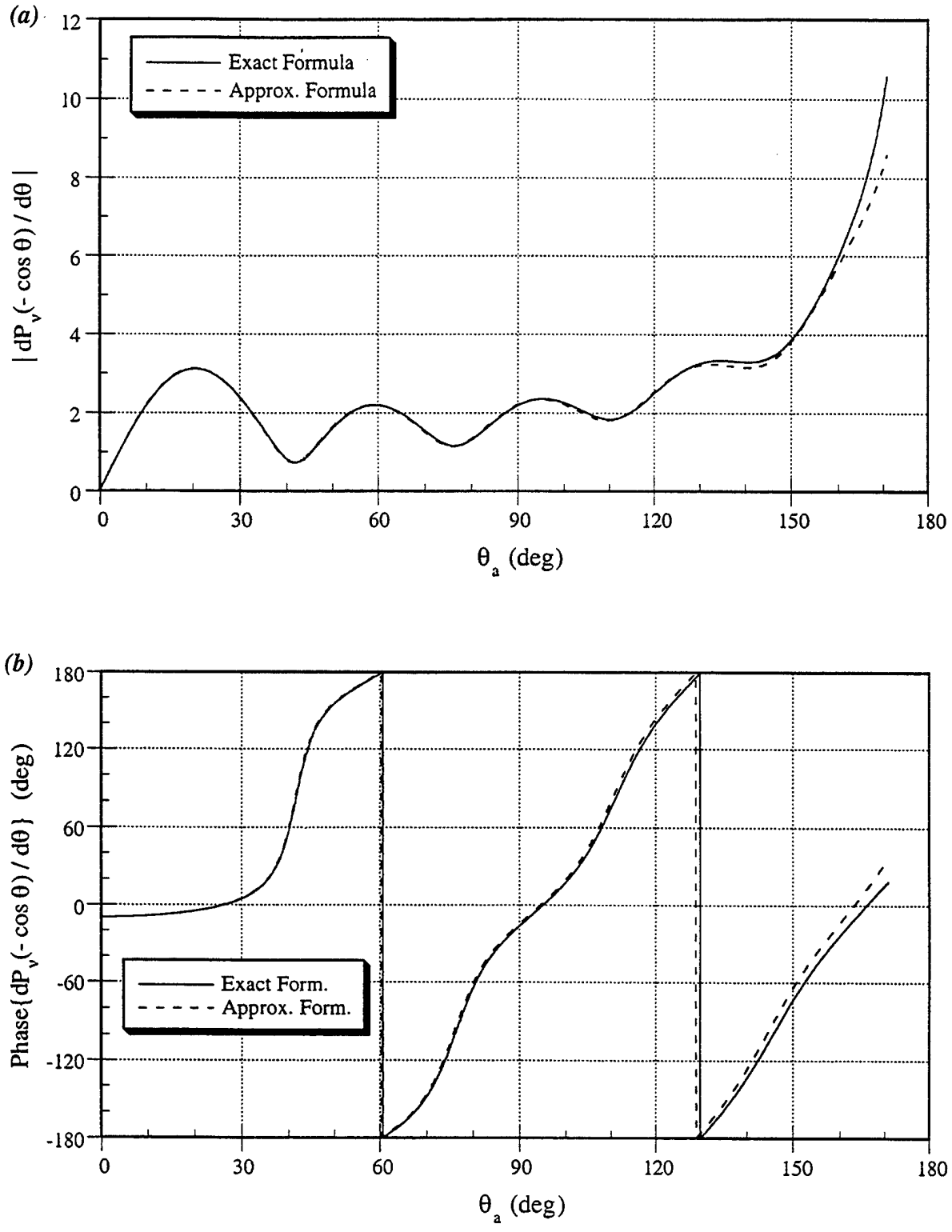

Figure J-2. Comparison of the Infinite Series (Exact) and Approximate Formulas for $dP_\nu(-\cos\theta)/d\theta$ for $\nu = 4.75 - j\,0.440$; (a) Magnitude; (b) Phase

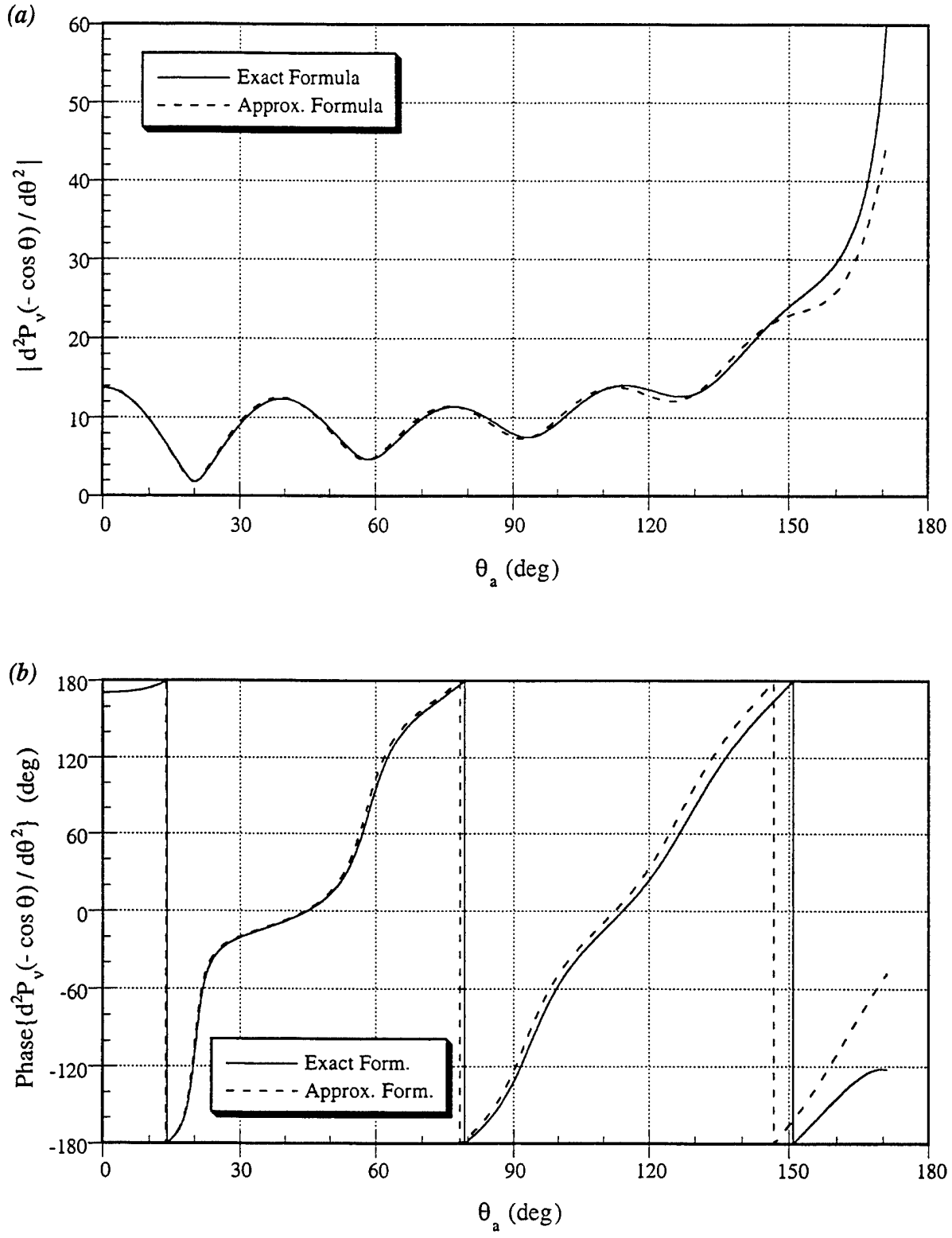

Figure J-3. Comparison of the Infinite Series (Exact) and Approximate Formulas for $d^2P_\nu(-\cos\theta)/d\theta^2$ for $\nu = 4.75 - j\,0.440$; (a) Magnitude; (b) Phase

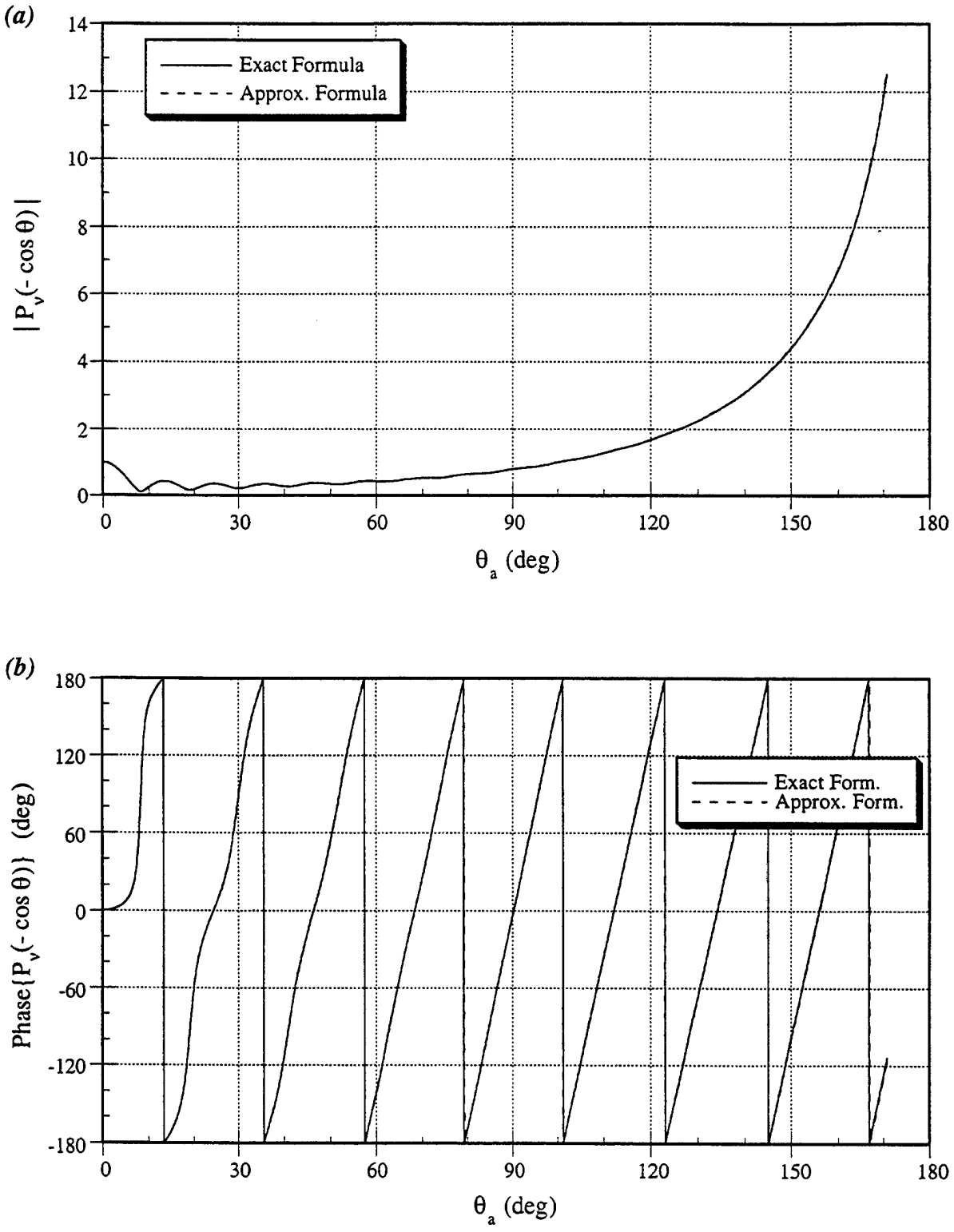

Figure J-4. Comparison of the Infinite Series (Exact) and Approximate Formulas for $P_\nu(-\cos\theta)$ for $\nu = 15.9 - j\,1.32$; (a) Magnitude; (b) Phase

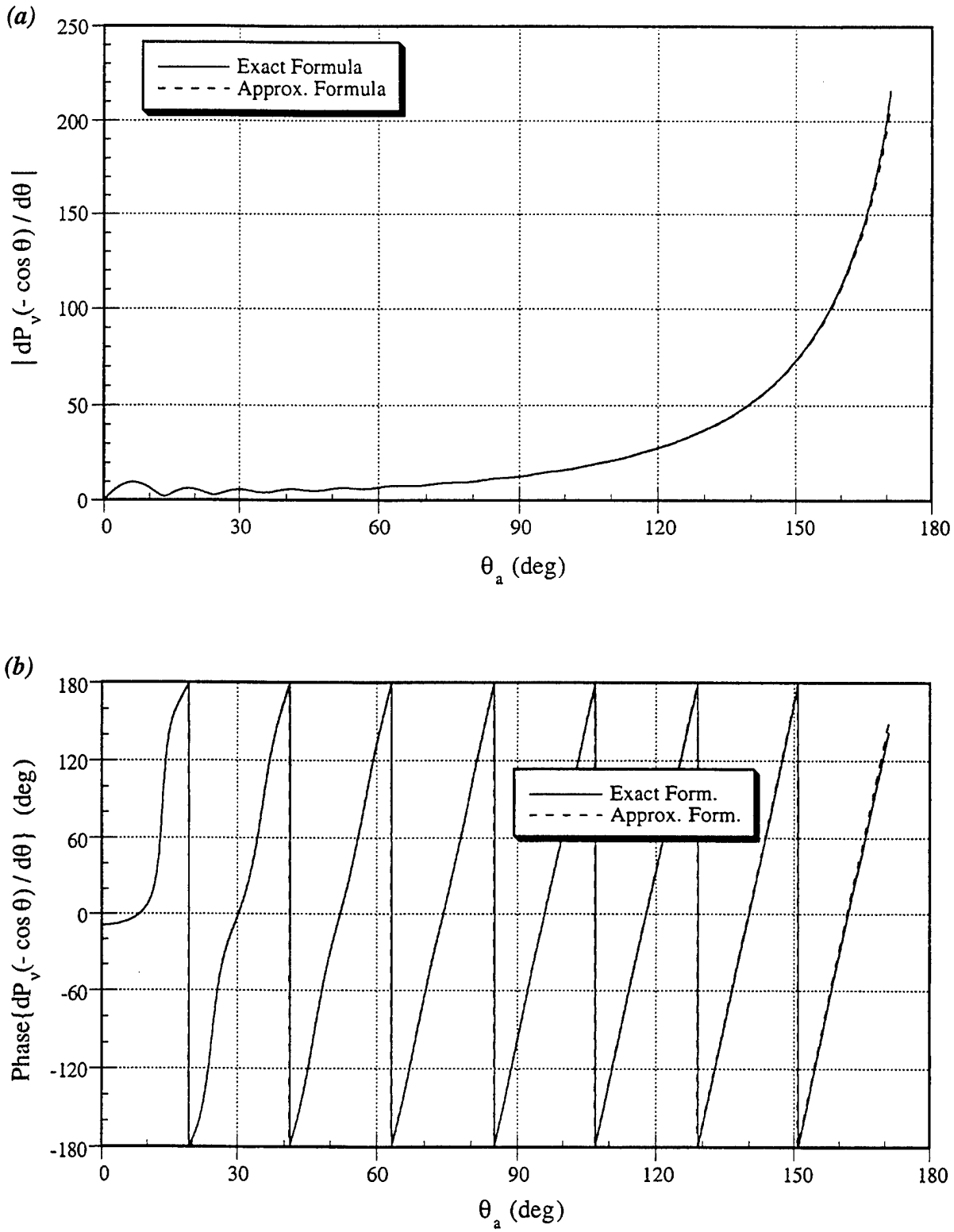

Figure J-5. Comparison of the Infinite Series (Exact) and Approximate Formulas for $dP_\nu(-\cos\theta)/d\theta$ for $\nu = 15.9 - j\,1.32$; (a) Magnitude; (b) Phase

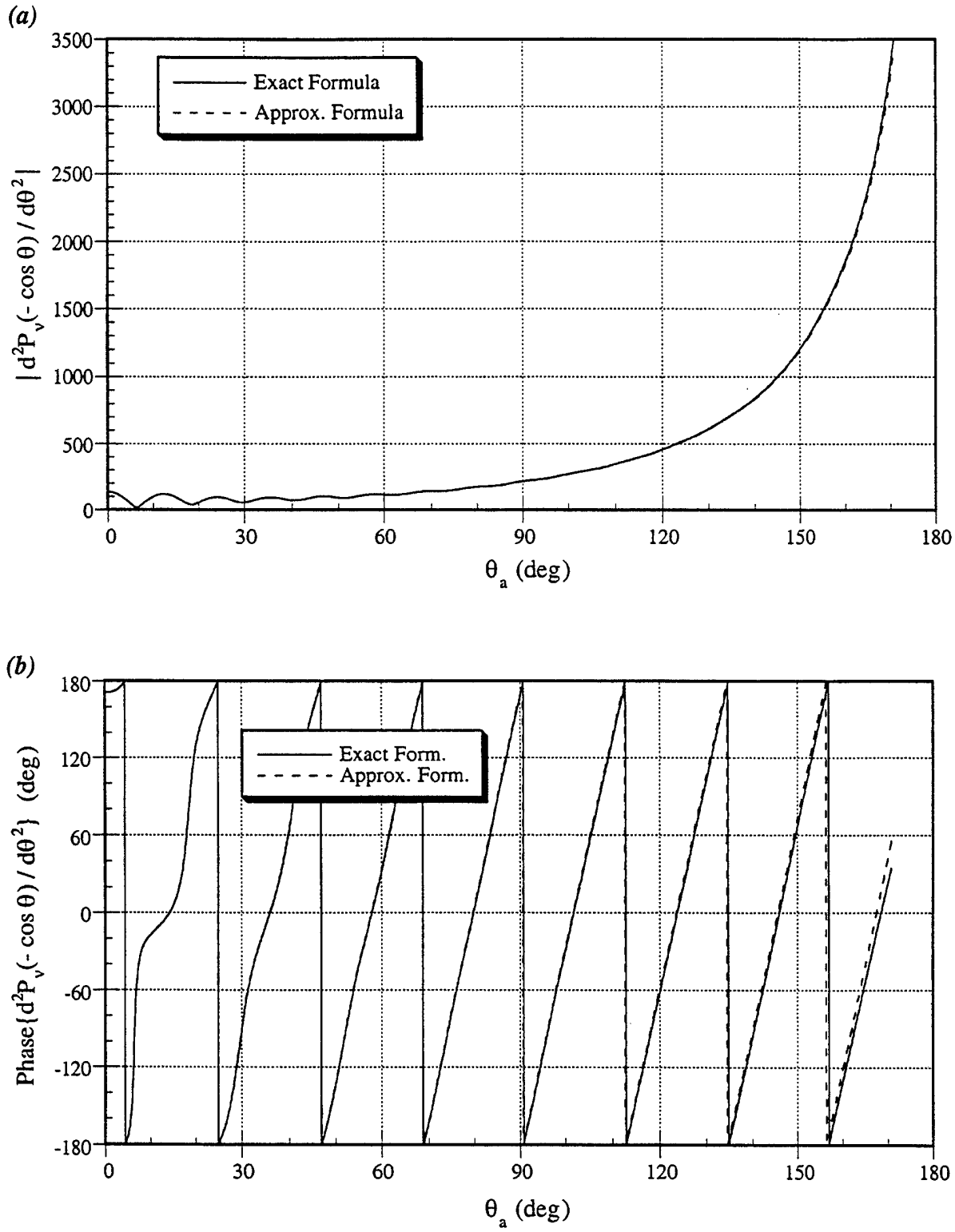

Figure J-6. Comparison of the Infinite Series (Exact) and Approximate Formulas for $d^2P_\nu(-\cos\theta)/d\theta^2$ for $\nu = 15.9 - j\,1.32$; (a) Magnitude; (b) Phase

APPENDIX K
EARTH-FLATTENING APPROXIMATION

As shown in appendix A, the electromagnetic (EM) fields in a spherical earth-ionosphere waveguide can be expressed in terms of two Debye potentials. At a source-free point, each of these potentials satisfies the scalar Helmholtz equation. As shown in appendix B, the Helmholtz equation can be solved in spherical coordinates by the separation of variables method in which the range or θ dependence is expressed in terms of a function $T(\theta)$, which satisfies the following differential equation:

$$\frac{d^2T}{d\theta^2} + \cot\theta \frac{dT}{d\theta} + \nu(\nu+1)T = 0 \ . \tag{K-1}$$

In equation (K-1), $\nu(\nu+1)$ is the separation constant. As shown in appendix B, for a source located at $\theta = 0$, the solution of equation (K-1) that is finite at the antipode ($\theta = \pi$) is given by

$$T(\theta) = C P_\nu(-\cos\theta) \ , \tag{K-2}$$

where P_ν is the Legendre function of the first degree ν and order zero, and C is an arbitrary constant. Both exact and approximate formulas for $P_\nu(-\cos\theta)$ are given in appendix J.

In the earth-flattening approximation, the polar angle θ in equation (K-1) is replaced by the range variable ρ, where $\rho = a\theta$ and a is the radius of the earth. Note that ρ is the direct great-circle path distance along the spherical earth that connects the source and the field points (see figure 3-2). The replacement of θ by ρ/a in equation (K-1) yields

$$\frac{d^2T}{d\rho^2} + \frac{1}{a}\cot\left(\frac{\rho}{a}\right)\frac{dT}{d\rho} + s^2 T = 0 \ , \tag{K-3}$$

where the constant s is defined as

$$s^2 \equiv \frac{\nu(\nu+1)}{a^2} \ . \tag{K-4}$$

In his estimation of the error involved in the earth-flattening approximation, Pekeris (reference 12) assumed that $T(\theta)$ can be expanded in the following asymptotic series:

$$T(\theta) = T(\rho/a) = \sum_{n=0}^{\infty} (as)^{-2n} T_{2n}(\rho) = T_o(\rho) + (as)^{-2} T_2(\rho) + (as)^{-4} T_4(\rho) + \ldots . \tag{K-5}$$

The series expansion of $\cot(\rho/a)$ is given by (reference 27)

$$\cot\left(\frac{\rho}{a}\right) = \left(\frac{\rho}{a}\right)^{-1} - \frac{1}{3}\left(\frac{\rho}{a}\right) - \frac{1}{45}\left(\frac{\rho}{a}\right)^{3} - \frac{2}{945}\left(\frac{\rho}{a}\right)^{5} - \ldots \ . \tag{K-6}$$

The substitution of the series expansions (K-5) and (K-6) into the differential equation (K-3) followed by the multiplication of s^{-2} yields

$$\left[\frac{d^2T_o}{dx^2} + (as)^{-2}\frac{d^2T_2}{dx^2} + (as)^{-4}\frac{d^2T_4}{dx^2} + \ldots\right]$$

$$+\left[\frac{1}{x} - \frac{1}{3}\frac{x}{(as)^2} - \frac{1}{45}\frac{x^3}{(as)^4} - \ldots\right]\left[\frac{dT_o}{dx} + (as)^{-2}\frac{dT_2}{dx} + (as)^{-4}\frac{dT_4}{dx} + \ldots\right]$$

$$+\left[T_o + (as)^{-2}T_2 + (as)^{-4}T_4 + \ldots\right] = 0 \ , \tag{K-7}$$

where $x = s\rho$. Following Pekeris (reference 12), the coefficients of like powers of $(as)^{-2}$ are equated to obtain a system of simultaneous differential equations. The first three equations are given as

$$L(T_o) = 0 \ , \tag{K-8a}$$

$$L(T_2) = \frac{x}{3}\frac{dT_o}{dx} \ , \tag{K-8b}$$

and

$$L(T_4) = \frac{x^3}{45}\frac{dT_o}{dx} + \frac{x}{3}\frac{dT_2}{dx} \ , \tag{K-8c}$$

where the differential operator L is given as

$$L = \frac{d^2}{dx^2} + \frac{1}{x}\frac{d}{dx} + 1 \ . \tag{K-9}$$

The solution of equation (K-8a) is

$$T_o(\rho) = H_o^{(2)}(s\rho) \ . \tag{K-10}$$

The above formula gives the range dependence for a planar earth (with a source located at $\rho = 0$) and represents the earth-flattening approximation. To obtain the solution of equation (K-8b), let

us consider the following differential equation that is valid for any cylindrical Bessel function $Z_n(x)$ of arbitrary order n:

$$L\left[x^n Z_n(x)\right] = \frac{2n}{x}\frac{d}{dx}\left[x^n Z_n(x)\right] . \qquad \text{(K-11)}$$

The above result was obtained from Koo and Katzin (reference 13). Note that $Z_n(x)$ refers to the Bessel function of the first kind $J_n(x)$, the Bessel function of the second kind $Y_n(x)$, the Hankel function of the first kind $H_n^{(1)}(x)$, or the Hankel function of the second kind $H_n^{(2)}(x)$. With the assumed time-harmonic dependence of $e^{j\omega t}$ and an outward propagating wave from the source, $Z_n(x) = H_n^{(2)}(x)$ in the present application.

The substitution of $Z_n(x) = H_n^{(2)}(x)$ and $n = 2$ into formula (K-11) yields

$$L\left[x^2 H_2^{(2)}(x)\right] = \frac{4}{x}\frac{d}{dx}\left[x^2 H_2^{(2)}(x)\right] . \qquad \text{(K-12)}$$

The derivative of $x^2 H_2^{(2)}(x)$ is given by

$$\frac{d}{dx}\left[x^2 H_2^{(2)}(x)\right] = x^2 H_2^{(2)'}(x) + 2x H_2^{(2)}(x) , \qquad \text{(K-13)}$$

where the prime denotes the derivative with respect to the argument. The substitution of the recurrence relation (reference 24)

$$H_2^{(2)'}(x) = H_1^{(2)}(x) - \frac{2}{x} H_2^{(2)}(x) ,$$

into equation (K-13) yields

$$\frac{d}{dx}\left[x^2 H_2^{(2)}(x)\right] = x^2 H_1^{(2)}(x) = -x^2 H_0^{(2)'}(x) . \qquad \text{(K-14)}$$

The substitution of the above result into expression (K-12) gives

$$L\left[x^2 H_2^{(2)}(x)\right] = -4x H_0^{(2)'}(x) . \qquad \text{(K-15)}$$

If $H_0^{(2)}(x)$ is replaced by $T_o(\rho)$, formula (K-15) may be rewritten as

$$L\left[-\frac{1}{12} x^2 H_2^{(2)}(x)\right] = \frac{x}{3}\frac{dT_o}{dx} . \qquad \text{(K-16)}$$

A comparison of expressions (K-8b) and (K-16) shows that

$$T_2(\rho) = -\frac{1}{12}(s\rho)^2 H_2^{(2)}(s\rho)\,, \tag{K-17}$$

where x has been replaced by $s\rho$.

The substitution of formulas (K-10) and (K-17) into the asymptotic series (K-5) yields

$$T(\rho/a) \cong H_o^{(2)}(s\rho) - \frac{1}{12}\left(\frac{\rho}{a}\right)^2 H_2^{(2)}(s\rho) + O\left(\frac{\rho}{a}\right)^4 . \tag{K-18}$$

In the above equation, the first term corresponds to the model of a flat earth and the remaining terms are corrections for curvature. Therefore, the earth-flattening approximation is given by

$$T(\rho/a) \cong H_o^{(2)}(s\rho) \ . \tag{K-19}$$

The earth-flattening approximation is valid when the great-circle path distance ρ is small compared with the earth's radius a. In particular, Pekeris (reference 12) found that the earth-flattening approximation is correct to within 2% of the exact value for ranges out to about half the radius of the earth. It should be noted that this result is independent of the frequency.

Next one needs to determine the constant C in formula (K-2) so that $T(\theta)$ can be related to $P_\nu(-\cos\theta)$. To obtain C, let $\theta \to 0$ on each side of expression (K-2), giving

$$\lim_{\theta \to 0} T(\theta) = C \lim_{\theta \to 0} P_\nu(-\cos\theta) \ . \tag{K-20}$$

From equation (K-18),

$$\lim_{\theta \to 0} T(\theta) = \lim_{\rho \to 0} T(\rho/a) = \lim_{\rho \to 0} H_o^{(2)}(s\rho) \ . \tag{K-21}$$

From Abramowitz and Stegun (reference 24),

$$\lim_{\rho \to 0} H_o^{(2)}(s\rho) = -j\frac{2}{\pi}\ln(s\rho) \to -j\frac{2}{\pi}\ln\rho \ . \tag{K-22}$$

From appendix E, formula (E-8),

$$\lim_{\theta \to 0} P_\nu(-\cos\theta) = \frac{\sin\nu\pi}{\pi}\ln\theta^2 = \frac{2\sin\nu\pi}{\pi}\ln\left(\frac{\rho}{a}\right) \to \frac{2\sin\nu\pi}{\pi}\ln\rho \ . \tag{K-23}$$

The substitution of the limits (K-21), (K-22), and (K-23) into expression (K-20) gives

$$C = \frac{1}{j \sin \nu\pi} \ . \tag{K-24}$$

From expressions (K-2), (K-18), and (K-24),

$$\frac{P_\nu(-\cos\theta)}{j \sin \nu\pi} = T(\theta) = T\left(\frac{\rho}{a}\right) \cong H_o^{(2)}(s\rho) - \frac{1}{12}\left(\frac{\rho}{a}\right)^2 H_2^{(2)}(s\rho) \ , \tag{K-25}$$

where the error in the above approximation is $O(\rho/a)^4$. From formula (J-4), the wave number k in the earth-ionosphere waveguide is given by

$$k \equiv \beta - j\alpha = \frac{\nu + 1/2}{a} \ . \tag{K-26}$$

If $|\nu| \gg 1$, then

$$(\nu + 1/2)^2 \cong \nu(\nu + 1) \ . \tag{K-27}$$

The above result is generally valid in the ELF band. The application of the above approximation to definitions (K-4) and (K-26) results in the following approximation:

$$s \cong k \ , \ |\nu| \gg 1 \ . \tag{K-28}$$

Therefore, expression (K-25) can be approximated out to order $(\rho/a)^2$ as

$$\frac{P_\nu(-\cos\theta)}{j \sin \nu\pi} \cong H_o^{(2)}(k\rho) - \frac{1}{12}\left(\frac{\rho}{a}\right)^2 H_2^{(2)}(k\rho) \ , \ |\nu| \gg 1 \ . \tag{K-29}$$

The above formula is similar to the one applied by Wait (reference 1) in his development of ELF propagation formulas. The formulas differ by a factor of j.

For $|k\rho| \gg 1$, the Hankel functions in expression (K-29) can be replaced by the first term of their respective asymptotic expansions:

$$H_o^{(2)}(k\rho) \sim \sqrt{\frac{2}{\pi k\rho}}\ e^{-j(k\rho - \pi/4)} \ , \tag{K-30a}$$

and

$$H_2^{(2)}(k\rho) \sim \sqrt{\frac{2}{\pi k\rho}}\ e^{-j(k\rho - 5\pi/4)} \ . \tag{K-30b}$$

The substitution of the above approximations into formula (K-29) yields

$$\frac{P_\nu(-\cos\theta)}{j\sin\nu\pi} \cong \sqrt{\frac{2}{\pi k\rho}}\, e^{-j(k\rho-\pi/4)}\left[1+\frac{1}{12}\left(\frac{\rho}{a}\right)^2\right],\ |\nu|\gg 1, |k\rho|\gg 1\ . \tag{K-31}$$

From Wait (reference 1),

$$\sqrt{\frac{\theta}{\sin\theta}} \cong 1+\frac{\theta^2}{12}\,, \tag{K-32}$$

where the error in the above approximation is $O(\theta^4)$. The application of the above approximation to expression (K-31) results in

$$\frac{P_\nu(-\cos\theta)}{j\sin\nu\pi} \cong H_o^{(2)}(k\rho)\sqrt{\frac{\rho/a}{\sin\rho/a}}\ ,\ |\nu|\gg 1, |k\rho|\gg 1\,, \tag{K-33}$$

where the asymptotic approximation in expression (K-30a) has been replaced by $H_o^{(2)}(k\rho)$. In the above approximation (K-33) for $P_\nu(-\cos\theta)$, $H_o^{(2)}(k\rho)$ corresponds to the range dependence for a flat earth and the square-root term is the correction for curvature. As was noted following approximation (K-29), expression (K-33) also differs with the one derived by Wait (reference 1) by a factor of j. Formula (K-33) is referred to as the earth-flattening approximation with curvature correction for $P_\nu(-\cos\theta)$.

REFERENCES

1. J. R. Wait, *Electromagnetic Waves in Stratified Media*, Classic Reissue Edition, IEEE Press, Piscataway, NJ, 1996, Chs. 6, 10.

2. J. Galejs, *Terrestrial Propagation of Long Electromagnetic Waves*, Pergamon Press, Oxford, England, 1972, Ch. 4.

3. P. R. Bannister, "Simplified Formulas for ELF Propagation at Shorter Distances," *Radio Science*, vol. 21, no. 3, May-June 1986, pp. 529-537.

4. E. A. Wolkoff and W. A. Kraimer, "Pattern Measurements of U.S. Navy ELF Antennas," *AGARD Conference Proceedings 529*, ELF/VLF/LF Radio Propagation and Systems Aspects, North Atlantic Treaty Organization, 1993, pp. 26-1-26-10.

5. E. A. Wolkoff and W. A. Kraimer, "ELF Radio Source Location," NUSC Technical Memorandum 901262, Naval Underwater Systems Center, New London, CT, 31 January 1991.

6. J. P. Casey, "Extremely Low Frequency (ELF) Propagation Formulas for an Anisotropic Earth Conductivity," NUWC-NPT Technical Memorandum 00-056, Naval Undersea Warfare Center Division, Newport, RI, 26 April 2000.

7. J. P. Casey, "Antipode-Centered ELF Propagation Formulas," NUWC-NPT Technical Memorandum 00-031, Naval Undersea Warfare Center Division, Newport, RI, 16 February 2000.

8. M. L. Burrows, *ELF Communications Antennas*, Peter Peregrinus Ltd., Stevanage, England, 1978, Ch. 2.

9. K. G. Budden, *The Wave-Guide Mode Theory of Wave Propagation*, Prentice-Hall, Englewood Cliffs, NJ, 1961.

10. R. E. Collin, *Field Theory of Guided Waves*, Second Edition, IEEE Press, Piscataway, NJ, 1991, pp. 30-34, 173-178.

11. M. H. L. Pryce, "The Diffraction of Radio Waves by the Curvature of the Earth," *Advances in Physics*, vol. 2, 1953, p. 67.

12. C. L. Pekeris, "Accuracy of the Earth-Flattening Approximation in the Theory of Microwave Propagation," *Physical Review*, vol. 70, nos. 7 and 8, 1 and 15 October 1946, pp. 518-522.

13. B. Y.-C. Koo and M. Katzin, "An Exact Earth-Flattening Procedure in Propagation Around a Sphere," *Journal of Research of the National Bureau of Standards*, vol. 64D, no. 1, January-February 1960, pp. 61-64.

14. P. R. Bannister, "Quasi-Static Fields of Dipole Antennas at the Earth's Surface," *Radio Science*, vol. 1, no. 11, November 1966, pp. 1321-1330.

15. E. A. Wolkoff and J. P. Casey, "Extremely Low Frequency (ELF) Mixed-Path Propagation Model - Technical Description," NUWC-NPT Technical Report (in preparation), Naval Undersea Warfare Center Division, Newport, RI.

16. P. R. Bannister, Sebastian, FL, Private Communication, 21 December 2001.

17. P. R. Bannister, "The Determination of Representative Ionospheric Conductivity Parameters for ELF Propagation in the Earth-Ionosphere Waveguide," *Radio Science*, vol. 20, no. 4, July-August 1985, pp. 977-984.

18. E. A. Wolkoff, Science Applications International Corporation, Mystic, CT, Private Communication, 11 January 2000.

19. R. F. Harrington, *Time-Harmonic Electromagnetic Fields*, McGraw-Hill, New York, 1961, pp. 1-19, 100, 116-120.

20. J. R. Wait, *Electromagnetic Wave Theory*, Harper & Row Publishers, New York, 1985, pp. 120-123, 229-233, 265-267.

21. J. A. Stratton, *Electromagnetic Theory*, McGraw-Hill, New York, 1941, Ch. 1.

22. G. Arfken, *Mathematical Methods for Physicists*, Third Edition, Academic Press, San Diego, CA, 1985, pp. 78-79.

23. J. A. Kong, *Electromagnetic Wave Theory*, Second Edition, John Wiley & Sons, New York, 1990, pp. 331 - 332, 432, 493 - 494.

24. M. Abramowitz and I. A. Stegun, eds., *Handbook of Mathematical Functions*, National Bureau of Standards, AMS 55, U.S. Dept. of Commerce, Washington, DC, 1964, Chs. 9, 15.

25. W. Magnus, F. Oberhettinger, and R. P. Soni, *Formulas and Theorems for the Special Functions of Mathematical Physics*, Third Edition, Springer-Verlag, New York, 1966, p. 197.

26. A. Sommerfeld, *Partial Differential Equations in Mathematical Physics*, Academic Press, New York, 1949, pp. 157, 214-224, 279-289.

27. W. H. Beyer, ed., *CRC Standard Mathematical Tables*, 28th Edition, CRC Press, Boca Raton, FL, 1987.

28. A. Erdelyi (ed.), *Higher Transcendental Functions*, Volume 1, McGraw-Hill, New York, 1953, p. 162.

29. H. M. MacDonald, "Formulae for the Spherical Harmonic $P_n^{-m}(-\mu)$, when $1-\mu$ is a Small Quantity," Proceedings of the London Mathematical Society, vol. 13, 12 February 1914, pp. 220-221.

INITIAL DISTRIBUTION LIST

Addressee	No. of Copies
Space and Naval Warfare Systems Command (P. Singer, S. Little, L. Isorena, R. Youngs-Lew, LCDR D. Moore)	5
Space and Naval Warfare Systems Center, San Diego (P. Hansen, R. Dinger)	
Office of Naval Research (ONR-313: W. Stachnik, D. Crowder, D. McGregor)	3
Science Applications International Corporation (R. Ingram, D. Miller, E. Wolkoff)	3
Harvard University (R. W. P. King)	1
Stanford University (A. Fraser-Smith)	1
University of Connecticut (R. Bansal)	1
University of London, King's College, UK (D. L. Jones)	1
University of Rhode Island (S. Mitra, C. Polk, D. Tufts)	3
P. Bannister, Sebastian, FL	1
Defense Technical Information Center	2
Center for Naval Analyses	1